Loughborough University

Application of process analytical technology (PAT) tools for the better understanding and control of the crystallization of polymorphic and impure systems

---

by

Elena Simone

A Doctoral Thesis submitted in partial fulfilment of the requirements for the award of the degree of Doctor of Philosophy in Chemical Engineering

December 2015

Certificate of originality

This is to certify that I am responsible for the work submitted in this thesis, that the original work is my own except as specified in acknowledgments or in footnotes, and that neither the thesis nor the original work contained therein has been submitted to this or any other institution for a degree.

Abstract

This work presents a comprehensive study on the application of PAT tools to study, monitor and control polymorphism during batch cooling crystallization process. For the first time, the same techniques were used to control and adjust polymorphic purity of the solid phase but also to investigate the relation between chemical equilibrium in solution and polymorphic outcome of cooling crystallization.

Crystallization is an important unit operation used as separation and purification technique. It is widely employed in the pharmaceutical, chemical, agrochemical, food and cosmetics industries but also in the electronic, metallurgic and material industries. More than 90% of the APIs on the market are produced by crystallization, therefore, monitoring and control this process is fundamental to ensure the quality of the final product. The implementation of process analytical technology (PAT) tools during the development stage of APIs has largely helped in better understanding and optimizing both batch and, more recently, continuous crystallization.

Polymorphism is the capacity of a compound to crystallize in more than one different crystalline structure, which can have different properties such as density, melting point, bioavailability and solubility. The choice of solvent, pH, kinetic conditions and presence of impurities has very strong effect on the polymorphic outcome of a cooling crystallization in solution. Understanding this phenomenon as well as being able to monitor and control it during industrial crystallization is one the biggest challenges for pharmaceutical industries.

The correct interpretation of signals from PAT tools and the development of efficient calibration functions is very important in order to have a good understanding of the process monitored and to avoid mistakes during the manufacturing stage that can lead to failed batches. For this reason a good calibration practice procedure (GCPP) for Raman spectroscopy was developed in this thesis for the quantitative determination of polymorphic purity in solid slurries. Despite being developed for the application of Raman spectroscopy for crystallization monitoring, the GCPP is a general procedure that can be applied to any other spectroscopic technique and for the study of several other processes. Additionally, the concept of composite sensor array (CSA) is experimentally tested for the first time in this thesis: signals from multiple PAT tools during a polymorphic transformation are collected and processed using a dimension reduction technique (principal component analysis, PCA) for an easier and quicker monitoring of the process.

In fact, the application of PCA reduces the amount of signals that have to be monitored to two or three main principal components that contains and summarize all the information from the PAT tools used.

In this work, polymorphic purity of the solid phase during a cooling crystallization was controlled using a simple feedback control strategy (active polymorphic feedback control, APFC) that combines Raman and ATR-UV/Vis spectroscopy to select and grow the stable polymorph after nucleation of a mixture or erroneous seeding was developed; that was the first example of integration of signal for feedback control of the crystallization of polymorphic systems. A model-based APFC was also developed to control crystal purity and also maximise the size distribution at the end of the batch crystallization process.

The second part of this thesis is dedicated to understand the phenomenon of polymorphism and, in particular, the effect of solvent and additives on the polymorphic outcome of cooling crystallization processes. A good knowledge of these effects can help in the correct design of the crystallization conditions to ensure the quality of the final product. A strong relationship between chemical equilibrium in solution and polymorphic form nucleated was found using ATR-UV/Vis and Raman spectroscopy for a zwitterionic compound (OABA). Furthermore, polymorphism of OABA was successfully tailored using combinations of solvents and different amounts of a structurally related additive.

In the last chapters of this work the crystallization of a biopharmaceutical compound (vitamin B12) was investigated using PAT tools. The compound was donated by Hebei Welcome Pharmaceutical Co., LTD (China) and it is normally commercialised as nutritional supplement. This vitamin is produced mainly by fermentation and presents a high amount of impurities to eliminate. Impurities were found to strongly inhibit growth of the compound and greatly decrease the quality of the final crystal size distribution. Several feedback control strategies using FBRM and ATR-UV/Vis spectroscopy were tested on the batch crystallization of vitamin B12 in order to improve purity and crystal size distribution at the end of the process.

Acknowledgements

I am grateful to my supervisor Professor Zoltan K. Nagy for giving me the opportunity to work with him and his group. I really appreciate the time that he spent with me in our never-ending meetings, all his suggestions and also his sincere criticism. He encouraged me to work hard but he also allowed me to participate to conferences and schools around the world. He is probably the best supervisor a PhD student can have!

A special thank goes to Professor Gerald Steele who helped me a lot with all my "chemistry issues" and to Mrs Wei Zhang for giving me the opportunity to work on vitamin B12.

I would also like to thank my colleagues Ali, Akos, Keddon and Iyke for their help and support in the laboratory and in the office: we had our hard times but it was also a good fun! Thanks a lot also to all the technicians and my friends in the department, they made my work much easier and enjoyable.

I also acknowledge the European Research Council (grant no. 280106-CrySys) for the financial support during these three years.

Finally, a big Italian GRAZIE to my family who always believe in me and support all my decisions (also the stupid ones!). This thesis is dedicated to them.

Table of contents

List of figures

List of Tables

List of abbreviations

API Active pharmaceutical ingredient

ADNC Automated direct nucleation control

APFC Active polymorphic feedback control

API Active pharmaceutical ingredient

ATR Attenuated total reflection

BA Benzoic acid

CLD Chord length distribution

CryPRINS Crystallization process informatics system

CSA Composite sensor array

CSD Crystal size distribution

DoE Design of experiments

DSC Differential scanning calorimetry

FBRM Focused beam reflectance measurement

FDA Food and drug administration

FT-IR Fourier transform infra-red

GCPP Good calibration practice procedure

IPA Iso propyl alcohol

MSZ Metastable zone

MSZW Metastable zone width

NIR Near infra-red

NMR Nuclear magnetic resonance

OABA Ortho aminobenzoic acid

PAT Process analytical technology

PBE Population balance equation

PCA Principal component analysis

PCR Principal component regression

PLSR Partial least squares regression

PVM Particle vision and measurement

QBD Quality by design

RMSEC Root mean squared error of calibration

RMSECV Root mean squared error of cross validation

RMSEP Root mean squared error of prediction

SEM-Scanning electron microscope

SNV Standard normal variate

SSC Supersaturation control

SWCLD Square weighted chord length distribution

UV/Vis Ultra violet visible

XRD X-ray diffraction

XRPD X-ray powder diffraction

1 Introduction

1.1 Background

Crystallization is one of the oldest unit operations in the chemical industry that can be carried out in several ways (Mullin 2001). Crystallization from solution or by evaporation are widely used in the pharmaceutical, chemical, agrochemical, food and cosmetics industries while melt crystallization is mainly exploited in the electronic, metallurgic and material industries. Pharmaceutical tablets are made of small crystals, as well as fertilizers and daily use products such as cooking salt, sugar and chocolate. Solar panels are instead produced by cutting in slices huge silicon monocrystals and turbines blades for the aeronautical industries are also constituted by a big single crystal of a superalloy. Although the widespread use of this process some of its aspects are still not completely understood, especially regarding crystallization from solutions. The presence of the solvent and the chemical equilibrium between solvent and solute molecules greatly influence the crystals produced and make the process quite complex to understand. Mixing also has a strong effect on cooling crystallization as well as the rate of cooling and the interaction with a second solvent for antisolvent crystallizations. Additionally, the presence of impurities or additives can complicate the process even further.

A large portion of literature is dedicated to understanding nucleation from solution, in particular how solute molecules self-assembly during, or just before nucleation, what is the exact mechanism and kinetics of nucleation and how solvent or external particles can affect it (Davey et al. 2002a; Davey et al. 2002b; Davey et al. 2013; Davey and Garside 2000; Threlfall 2000; Kulkarni et al. 2014; Vekilov 2010; Sullivan et al. 2014; Yani et al. 2012). Growth and its possible mechanisms are also largely studied in order to have a better control over the shape and size of crystals during the manufacturing process (Acevedo and Nagy 2014; Ma and Wang 2012; Kubota 2001; Borsos et al. 2014; Nagy et al. 2011; Aamir et al. 2010). The choice of solvent, the temperature profile, the mixing conditions and the presence of impurities or additives can change the growth kinetics of the crystals and affect the efficiency of the downstream operations as well as the overall quality of the final product. Several studies are currently being conducted on growth and shape control, using both experiments and modelling techniques (Borsos et al. 2014;

Majumder and Nagy 2013c; Ilevbare et al. 2012a; Larsen et al 2006; Acevedo et al. 2015; Braatz et al. 2012, Saleemi 2011).

Another important challenge for crystal engineers and crystallographers is to better understand the ability of many compounds to nucleate with different crystal structures (polymorphism). Polymorphs of the same compound can have very different properties (solubility, bioavailability, melting point, density) and the quality of the final product is deeply dependent on the polymorphic form of the crystals produced. After many famous accidents caused by this problem, screening for polymorphs is now a routine procedure during the development of a new drug in pharmaceutical industries.

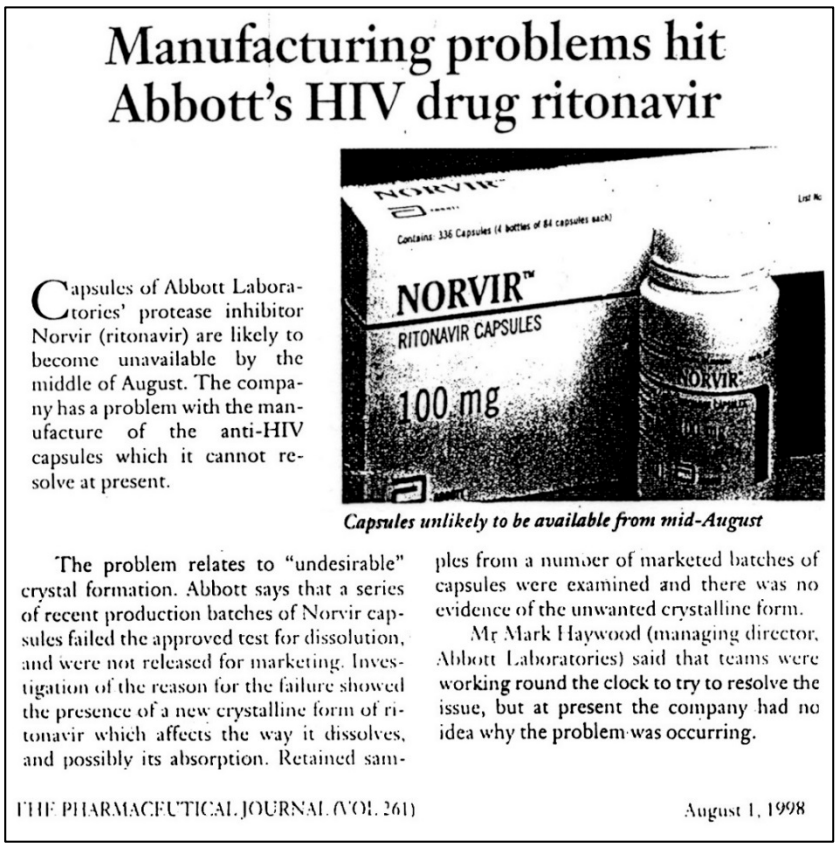

Manufacturing problems hit Abbott's HIV drug ritonavir

Capsules of Abbott Laboratories' protease inhibitor Norvir (ritonavir) are likely to become unavailable by the middle of August. The company has a problem with the manufacture of the anti-HIV capsules which it cannot resolve at present.

Capsules unlikely to be available from mid-August

The problem relates to "undesirable" crystal formation. Abbott says that a series of recent production batches of Norvir capsules failed the approved test for dissolution, and were not released for marketing. Investigation of the reason for the failure showed the presence of a new crystalline form of ritonavir which affects the way it dissolves, and possibly its absorption. Retained samples from a number of marketed batches of capsules were examined and there was no evidence of the unwanted crystalline form.

Mr Mark Haywood (managing director, Abbott Laboratories) said that teams were working round the clock to try to resolve the issue, but at present the company had no idea why the problem was occurring.

THE PHARMACEUTICAL JOURNAL (VOL. 261) August 1, 1998

Figure 1.1: The Ritonavir case was one of the first issue with polymorphism occurred in a pharmaceutical industry. Article from the Pharmaceutical Journal (vol. 261).

The first major issue with polymorphs is the Ritonavir case: this anti-HIV Abbott drug started being commercialized in the early nineties but it had to be withdrawn in 1998 because of the appearance of a more stable, and therefore less soluble, polymorphic form. The new form was failing the dissolution tests and was not effective for the treatment of the disease. Abbott had to reformulate the drug and the losses were estimated in about 250

million dollars (Chemburkar et al. 2000). Eventually other three polymorphic forms of Ritonavir were discovered for a total of five polymorphs for this compound (Morissette et al. 2003). In more recent years, a skin's patch (the Rotigotine produced by Aderis Pharmaceuticals) for the treatment of the symptoms of early Parkinson disease had to be recalled from the market because of the crystallization of a less soluble crystalline structure on the patch surface. The new polymorph had a reduced solubility that caused it to remain in the patch and decreased the amount of the active ingredient available for release (Cajigal 2008).

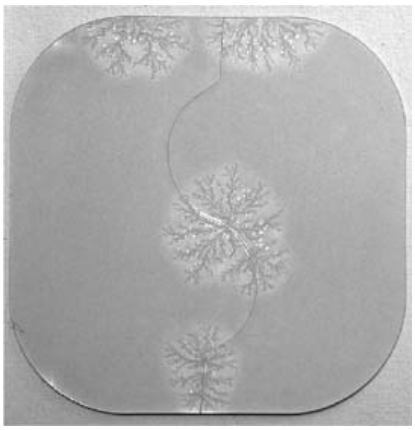

Figure 1.2: the Rotigotine patch and the crystals nucleated on it. Image from Neurology Today: 17 April 2008 - Volume 8 - Issue 8 - pp 1,8.

Polymorphism and pseudo polymorphism (co-crystals, solvates and hydrates) have being extensively studied especially in the last twenty years in order to determine the factors affecting this phenomenon and to be able to control it (Bernstein 2011; Chieng et al. 2011; Mangin, et al. 2009; Kitamura 2002). Understanding the main phenomena related to solution crystallization is not the only topic of interest for crystallization scientists; the development and application of new technologies to control the crystallization process and the quality of the crystals is also essential. Off-line, at-line and in situ techniques that can give information on the nucleation time and temperature, solute concentration, crystalline structure, size and shape of the crystals in slurry are being explored and new manual and automatic control strategies are being developed. Process analytical technologies (PAT) tools started being used for in situ monitoring and control of batch crystallization through several feedback strategies. Up to date, they have been used for in situ control over the size and number of particles, their shape and polymorphic form. PAT tools are also very useful in extracting information on the kinetics of nucleation, growth, agglomeration and

breakage and determine more sophisticated control strategies using modelling techniques (Nagy et al. 2013; Samad et al. 2013; Braatz et al. 2012).

1.2 Research aims

The aims of this thesis work can be summarized in:

- Analysing, comparing, and combining the signals of several PAT tools for getting both qualitative and quantitative information during crystallization processes in the presence of multiple polymorphs. Solute concentration and solid composition are the most important parameters to measure during a crystallization process with polymorphic transformation: opportune experiments can be designed and chemometrics can be used to determine calibration functions that can predict those parameters. Alternatively, chemometrics can be used to merge the data from multiple PAT tools and get information that can be immediately and more easily interpreted.
- Studying Raman spectroscopy and its features and exploring its use for polymorph control during batch crystallization processes. In particular, developing a feedback control strategy for the selection of the right polymorph after nucleation of a mixture of polymorphs or erroneous seeding.
- Modelling and optimizing a system with different polymorphs in slurry using population balance equations solved with the method of moments. That requires estimation of the kinetics parameters through specifically designed experiments and development of a model in Matlab.
- Examining in details the effect of solvent composition and additives on the polymorphic outcome of cooling crystallization processes. In particular, trying to get a better understanding of the relation between the crystal structure of the different polymorph nucleated and the physical-chemical properties of solvent and additives.
- Appling PAT tools and feedback control strategies for the study and optimization of the crystallization process of a biopharmaceutical compound. Substances produced by fermentation are usually more impure than chemically synthetized compounds and, therefore, crystallization has to be carefully designed and control in order to obtain the required quality of the crystals.

1.3 Research contribution

The main contributions of this thesis are:

a) The determination of a good calibration practice procedure for the application of quantitative Raman spectroscopy for monitoring polymorphic transformations. For the first time, a complete study on the effect of the different properties of the analysed sample on the Raman signal has been performed and used, together with design of experiments, to develop a calibration strategy for polymorphic form determination in slurries.

b) A comparison of several PAT tools for obtaining quantitative information on solute concentration and polymorphic ratio of slurries. Different chemometrics techniques were applied and the characteristics of each signal for the specific system used studied.

c) The development of a novel active polymorphic feedback control (APFC) that combines Raman and ATR-UV/Vis spectroscopy for the selection and growth of the stable form of an organic compound after nucleation of a mixture of polymorphs or erroneous seeding. Raman spectroscopy can detect the undesired polymorphs and triggers a heating cycle that dissolves it. After elimination of the metastable form supersaturation control using ATR-UV/Vis can grow the stable form. Both a model-free (experimental) and a model–based APFC were developed in this thesis.

d) A first example of composite sensor array is presented in this work. Different combinations of PAT tools were used to monitor a polymorphic transformation: the signals were merged together and analysed using principal component analysis in order to obtain more immediate and easy to interpret information. A selection criterion using rotated loadings was also proposed for the selection or the best combination of sensors for the study of a specific system.

e) A comprehensive study on polymorphism of a zwitterionic compound in different solvents and with the addition of a structurally related additive. Cooling crystallizations of anthranilic acid were performed in different combinations of solvents and additive: specific relations between the polymorphic form nucleated and the chemical interactions between additive-solute and solvent-solute were found.

1.4 Thesis structure

Chapter 2 presents a literature review which includes the fundamentals of solubility, crystal nucleation, growth and polymorphism. It also shortly describes the population balance equations and the methods of moments for modelling and optimization of crystallization processes. The definition of PAT tools is also given, together with a description of their use and importance in both pharmaceutical and biopharmaceutical industries. The different tools used in the experimental work are described in detail together with further analytical techniques used. Basics of chemometrics applied to spectroscopic data are also discussed in this chapter. Finally the last section of the literature review is dedicated to feedback control strategies for polymorph control.

Chapter 3 is the methodology chapter. All the materials and instrumentation used during this work are presented in it. The final section shows the rig used in the experiments.

Chapter 4 describes a good calibration practice procedure for extracting quantitative information about the polymorphic state of slurries using Raman spectroscopy. The first part is dedicated to the study of Raman signal and the possible parameters that can influence it during a crystallization experiment, while the second part shows the results of a systematic calibration conducted with design of experiments.

In **Chapter 5** several spectroscopic techniques are analysed, calibrated and compared for the quantitative estimation of solute concentration and polymorphic ratio of a slurry during a crystallization process. A general experimental procedure is described as well as the chemometrics techniques used for the data manipulation.

Chapter 6 presents the concept of active polymorphic feedback control (APFC): a feedback strategy that uses a combination of Raman and ATR-UV/Vis spectroscopy in order to obtain the desired polymorphic form of anthranilic acid (OABA) during batch crystallization processes.

A model-based approach of the APFC is described in **Chapter 7**. The kinetics parameters of the studied system are estimated using a specific design of experiments and then applied to model and optimize the APFC using the population balance equations solved with the method of moments.

Chapter 8 presents the concept of composite sensor array (CSA). A polymorphic transformation is studied using multiple PAT tools and combining all the signals together through chemometrics techniques in order to simplify and extract more useful and understandable information.

Chapter 9 shows a study on the solvent effect on polymorphism of a zwitterionic compound, anthranilic acid (OABA). ATR-UV/Vis and Raman spectroscopy are used to study the effect of different mixtures of water and an organic solvent on the polymorphic outcome of cooling crystallization processes.

In **Chapter 10** the effects of combinations of solvents and a structurally related additive on the cooling crystallization of anthranilic acid are studied. The changes induced on nucleation kinetics, growth, agglomeration and polymorphism of anthranilic acid are examined.

Chapter 11 shows the effect of impurities on the crystallization of a biopharmaceutical compound (vitamin B12) and demonstrate the efficacy of PAT tools in understanding and controlling the crystallization process of a the studied compound.

In **Chapter 12** several feedback control strategies exploiting PAT tools are tested for the crystallization of impure vitamin B12. The effect of direct nucleation control, simple slow linear cooling, temperature cycling and supersaturation control on crystal size distribution and purity of vitamin B12 were analysed.

The final **Chapter 13** shows the main conclusions of this works and gives some recommendations for future work.

2 Literature review

During crystallization an ensemble of randomly organized molecules, ions or atoms in a fluid come together to create an ordered and regular three-dimensional structure that is called crystal. The crystallization process can be seen as a purification technique, a separation process or a branch of particle technology (Mullin 2001).

2.1 Solutions and solubility

A solution is a homogenous mixture of two or more substances. It can be in a gaseous, liquid or solid state and its constituent are called solvent (the continuous phase) and solute (the dispersed phase). Water is the most used solvent for the industrial crystallization of inorganic substances because it can dissolve many compounds; it is readily available, cheap and innocuous. For organic chemicals in industrial applications, when water cannot be used, solvents are chosen from the following categories: acetic acid and its esters, lower alcohols and ketones, ethers, chlorinated hydrocarbons, benzene homologues and light petroleum fractions (Mullin 2001). The solubility of a solute represents the maximum concentration that can be dissolved in a specific solvent at any temperature. Because this parameter is usually strongly affected by temperature solubility curves are built, which report the solubility as a function of temperature. Figure 2.1 shows a hypothetical solubility curve: if the concentration is below the solubility curve the solution is undersaturated and existing crystals dissolve.

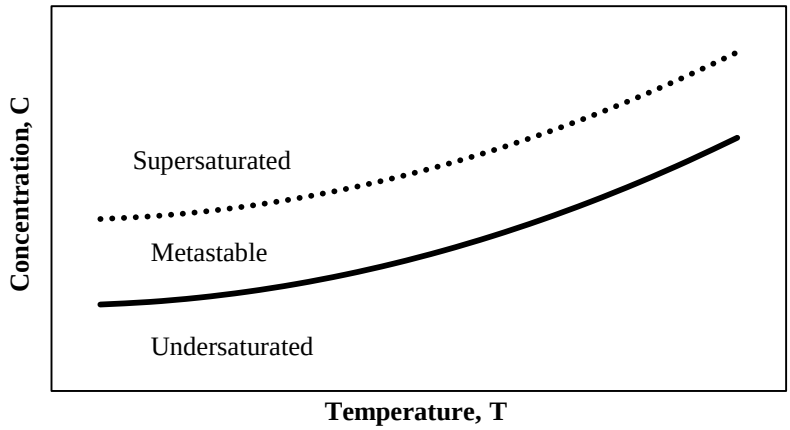

Figure 2.1: Solubility/ supersolubility diagram.

A solution above the solubility curve is called supersaturated, in there crystals can nucleate and grow. However, at low supersaturations, existing crystals grow but the formation of new crystals is difficult. Nucleation usually requires a critical level of supersaturation to happen. The region between equilibrium and the supersaturation level necessary to induce nucleation is called metastable zone. The width of this zone depends both on kinetics and thermodynamic factors (Davey and Garside 2000). Supersaturation is, therefore, the driving force for nucleation and growth. It is defined as the difference between the chemical potential of the solute molecules in the supersaturated (μ_{ss}) and saturated (μ_{eq}) state respectively (Mangin et al. 2009).

The expression of supersaturation σ can be written as:

$$\sigma = \frac{\mu_{ss} - \mu_{eq}}{kT}, \tag{2.1}$$

where k is the Boltzmann constant and T is the temperature.

Using the Gibbs-Duhem equation the chemical potentials can be related to the activities, which, for ideal solutions, are independent from concentration:

$$\sigma = ln\left(\frac{a_{ss}}{a_{eq}}\right) \rightarrow ln\left(\frac{x_{ss}}{x_{eq}}\right) \approx \frac{x_{ss} - x_{eq}}{x_{eq}}. \tag{2.2}$$

The letter x refers to the molar fractions of solute in the supersaturated and saturated solution.

In industrial applications the supersaturation is more commonly defined as:

$$\Delta C = C_{ss} - C_{eq}, \tag{2.3}$$

where C is the concentration of solute, ΔC is usually called “concentration driving force” and is more suitable than the chemical potential for engineering applications.

2.2 Crystallization techniques

Crystallization usually takes place in a solution or in an impure liquid above its melting point. This situation has led to the development of two major crystallization techniques (Davey 2003):

- Suspension crystallization (solution mediated crystallization)

- Solidification of melts

Suspension crystallization can be realized by cooling, solvent evaporation or by antisolvent addiction. The aim is the same: creating a supersaturated solution that allows nucleation and/or growth of the crystals. Evaporation is used with substances whose solubility is slightly dependent on temperature.

In some applications the solution can be sprayed from the top of a tower in form of drops that cool below their melting point as they fall and solidify in form of crystals. Progressive freezing is another possibility: a cooling surface (at a temperature below the melting point of the liquid) is placed in contact with the melt and a layer of solid will form at the surface. This layer will grow while heat is removed at the surface.

2.3 Nucleation

Supersaturation is not sufficient for a system to begin to crystallize. Some nuclei or seeds must be present in the solution to act as centres of crystallization.

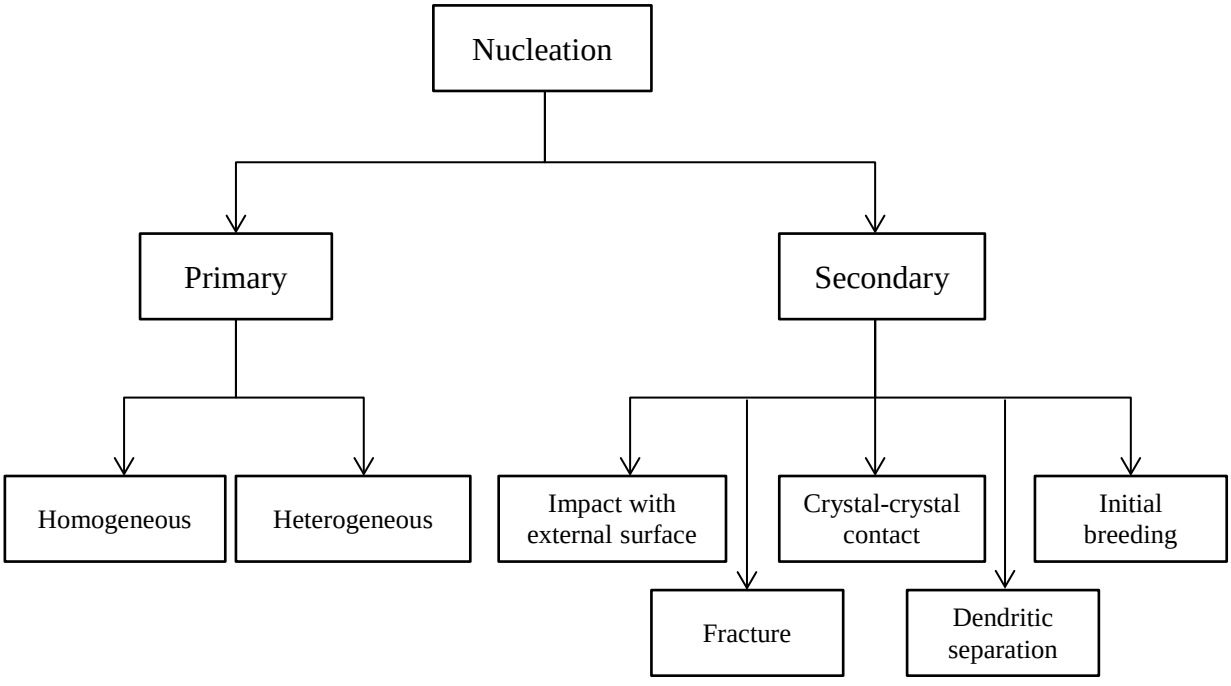

Figure 2.2: Nucleation mechanisms (Rawlings, J. 1993).

Nucleation can occur spontaneously or it may be induced artificially. It can also be triggered by agitation, mechanical shock, friction and pressure within solutions or melts (Mullin 2001). Nucleation that happens in systems which do not contain crystals is defined as "primary". If the nuclei appear in the vicinity of other crystals in a supersaturated solution the process is then called "secondary" nucleation. Primary nucleation can be homogeneous if it happens spontaneously in the solution or heterogeneous if it is induced by foreign particles. A schematic summary of the principal types of nucleation is shown in Figure 2.2.

2.3.1 Primary nucleation: homogeneous

There are two opposite theories used to describe homogeneous nucleation:

- The classical nucleation theory (CNT);
- The two-step nucleation theory.

According to the CNT, nucleation is a first-order phase transition that requires energy to happen. The thermodynamic explanation of this phenomenon was given by Gibbs in the 19th century. The free energy change for the formation of a stable cluster that can grow is the sum of the free energy required for the phase transformation (ΔG_V), which is proportional to the volume of the nucleus, and the free energy to form a surface (ΔG_S), which is proportional to the surface of the cluster itself. In a supersaturated solution the solid state is more stable than the solution so ΔG_V is a negative term and tends to decrease the barrier energy for nucleation. The ΔG_s instead is associated with the presence of a discontinuity of concentration at the solution-crystal boundary, thus is positive and tends to increase the total ΔG_V as shown in Figure 2.3 (Erdemir et al. 2009). In the CNT the activation energy for the nucleation is related to the size of the cluster: a group of molecules becomes stable and can grow when it reaches a critical size. Below that the molecules tend to dissolve again in the solution (Davey and Garside 2000). Clusters of this critical size are called critical nuclei and the chance of forming nuclei of this size will depend on the height of the free energy barrier. As the supersaturation increases, both the height of the barrier and the value of the critical size decrease. The rate of nucleation for the CNT is defined as the rate at which cluster grow through this critical size and become a crystal. A simple, semi empirical equation can be derived from an energy balance on a critical nucleus and is reported below (Mullin 2001):

$$J = A\ exp\left[-\frac{16\pi\gamma^3\nu^2}{3k^3T^2(ln\,S)^2}\right]. \quad (2.4)$$

The equation has the typical Arrhenius form where: T is the temperature, S the supersaturation, k the Boltzmann constant, γ is the interfacial tension on the surface of the cluster and ν the molecular volume.

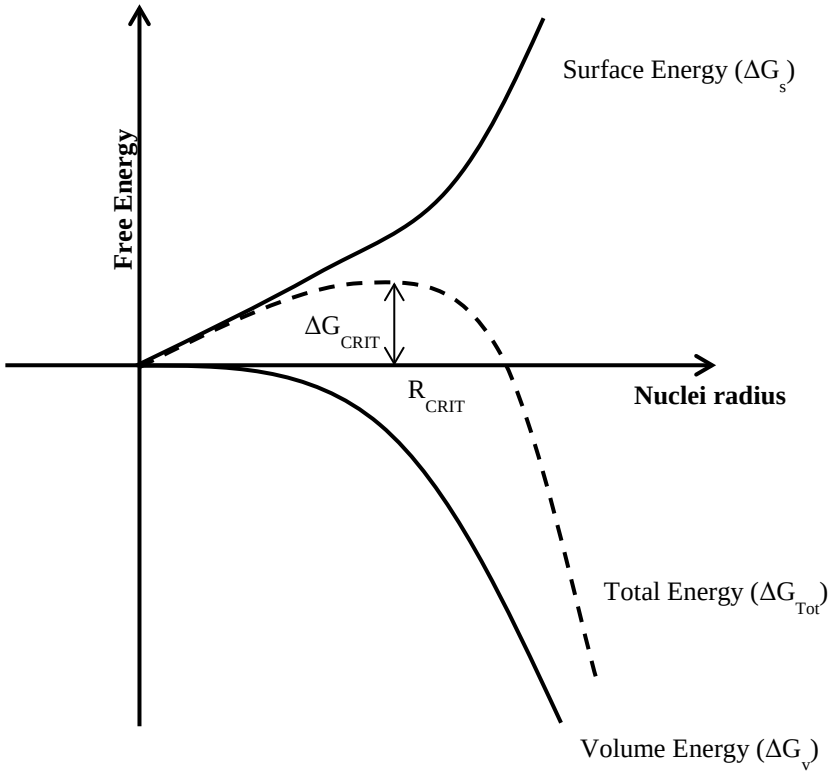

Figure 2.3: Free energy diagram of nucleation.

The CNT approach was found not to perfectly work for some proteins and few organic and inorganic molecules, for which the two-step theory seems to work better (Vekilov 2010). According to this theory the formation of a nucleus is preceded by the formation of a stable liquid cluster at higher density than the solution. The high concentration of molecules in this cluster favours the formation of the solid nuclei which then can grow in ordered crystalline structures (Davey et al. 2013). Both the theories imply the formation of clusters in the liquid phase where molecules are connected to each other by weak forces (polar, hydrogen bonding ect.). The difference is that for the CNT clusters are metastable, while for the two step nucleation theory clusters represent a distinct, stable phase. The type of interactions at the cluster level is very important in the determination of the polymorphic form of the nucleated crystals (Davey et al. 2013; Vekilov 2010; Bernstein

2011). For this reason, many researchers are currently trying to understand how the nature of the chemical bonding before nucleation affects the polymorphic form nucleated (Davey et al. 2001; Chiarella et al. 2007; Parveen et al. 2005; Davey et al. 2006; Kulkarni et al. 2012). The most used technique to detect changes in the liquid state just before nucleation is ATR-FTIR although Kulkarni has successfully used Raman to understand the type of bonding between molecules of isonicotinamide in different solvents.

2.3.2 Secondary nucleation

Secondary nucleation happens in the presence of other crystals and it can be affected by many parameters. It can be expressed empirically by a power law function:

$$B = k_B M_T^j N^k \Delta C^b; \tag{2.5}$$

where B is the secondary nucleation rate, N is a measure of the fluid mechanics interactions and of the power inputs (a stirrer or a pump impeller), ΔC is the supersaturation and M_T is the concentration of crystals in the solution. k_B, j, k and b can be predicted by semi-empirical models of contact nucleation in crystallizers (Davey and Garside 2000).

2.4 Crystal growth

The growth of a crystal is a combination of two stages in series: diffusion and reaction. The molecules must diffuse from the bulk to the surface of the nuclei where they can attach. Therefore, two resistances in series are present: diffusion ($^1/_{k_d}$) and particle integration on the surface ($^1/_{k_r}$). The expressions of the mass flux to the crystal surface for the two mechanisms are reported below (Mullin 2001):

$$\frac{dm}{dt} = k_d A(c - c_i), \tag{2.6}$$

for diffusion,

$$\frac{\mathrm{dm}}{\mathrm{dt}} = \mathrm{k_r A(c_i - c^*)}, \tag{2.7}$$

for reaction.

Figure 2.4 is a schematic picture of the diffusion-reaction model. It is possible to identify in the figure: (i) the crystal surface, (ii) the absorption layer where the solids in suspension come in contact with the crystal (iii) the stagnant film where the diffusion takes place and (iv) the bulk at constant concentration.

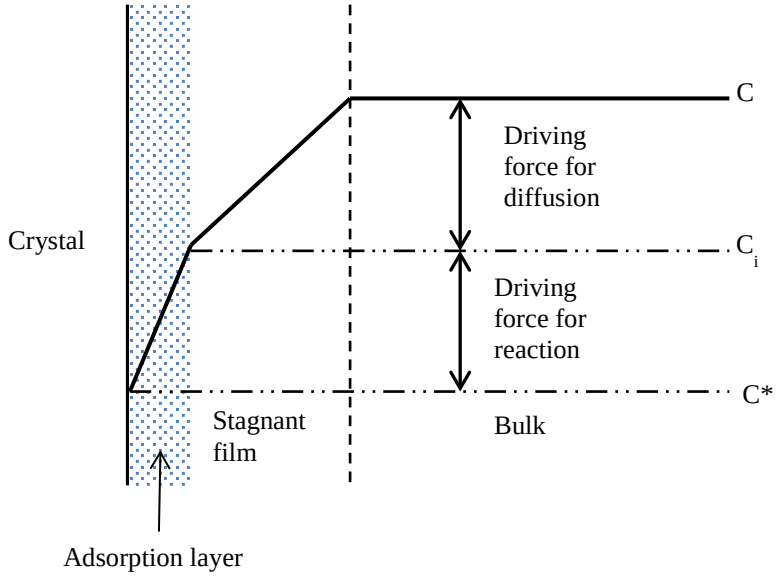

Figure 2.4: Concentration driving forces in crystallization from solution according to the simple diffusion-reaction model (Mullin 2001).

Because of the difficulty in measuring the interface concentration C_i the two equations are normally combined together as follows:

$$\frac{dm}{dt} = K_G A(c - c^*)^g, \tag{2.8}$$

where K_G is the overall crystal growth coefficient and g is the order of the overall crystal growth process. If g=1 then:

$$\frac{1}{K_G} = \frac{1}{k_r} + \frac{1}{k_d}. \tag{2.9}$$

A system can have a diffusion controlled growth kinetics if $k_r \gg k_d$ or a integration controlled growth kinetic if $k_d \gg k_r$.

2.5 Polymorphism

The capacity of a substance to exist in two or more different crystalline structures is called polymorphism. The first definition of polymorphic form was given by Mitscherlinch in 1821, in relation to arsenates, phosphates and sulphur while, in 1832, Wöhler and Liebig discovered the first example of polymorphism in an organic substance. In 1899, Ostwald concluded that almost every substance could exist in two or more solid phases (Davey and Garside 2000). Polymorphism can be considered the rule rather than an exception as also stated by Walter McCrone who, in 1965, wrote: "Every compound has different polymorphic forms, and, in general, the number of forms known for a given compound is proportional to the time and money spent in research on that compound"(McCrone 1965). The nucleation of a certain polymorph and the transition between one form to another is an important issue in industry because different polymorphs have different chemical and physical properties. A polymorphic transformation occurs in response to changes in pressure, temperature, composition, pH ect; therefore, it can happen in several stages of tablet manufacturing, from the crystallization stage, to drying, milling granulation or storage. There are four possible polymorphic transformations: solid state, solution mediated, melt mediated and interface mediated. From a kinetic point of view the solid state transformation occurs much slower than the other three since it requires larger activation energy (Sato 1993).

The solution mediated transformation is among the most interesting because the solvent can have a strong influence both on the thermodynamic and the kinetic parameters. Besides, crystallization from solutions is widely used in pharmaceutical, food and agrochemical industries and the interest in understanding and controlling this mechanism is very high. For all these reasons, in this section of the literature review, a brief description of solvent-mediated polymorphic transformation is presented.

In a dimorphic system constituted by form I and II, at specific temperature and pressure, the more stable form (II for example) has the lower free energy:

$$G_{II} < G_I, \tag{2.10}$$

which is, in terms of chemical potentials can be written as:

$$\mu_{II,solid} < \mu_{I,solid}. \tag{2.11}$$

At equilibrium the solution and the solids have the same chemical potential, thus:

$$\mu_{I,solid} = \mu_{I,solution} = \mu_0 + RT\, ln\, a_{I,solution}, \quad (2.12)$$

$$\mu_{II,solid} = \mu_{II,solution} = \mu_0 + RT\, ln\, a_{II,solution}, \quad (2.13)$$

where μ_0 is the standard chemical potential and $a_{I,solution}$ and $a_{II,solution}$ the solution activities. Combining the last three equations it can be inferred:

$$a_{II} < a_I. \quad (2.14)$$

Because the activities are proportional to the equilibrium concentration of the polymorph in solution, it can be written (Mangin et al. 2009):

$$C_{II} < C_I. \quad (2.15)$$

In conclusion the most stable form will always be the more soluble in every solvent at given temperature and pressure. There are two possible situations for a dimorphic system:

- The system is considered enantiotropic if the solubility curves cross each other at a lower temperature (called transition temperature) than the melting points of both form I and II. See Figure 2.5 (a).
- The system is considered monotropic if the solubility curves do not cross each other in solution. See Figure 2.5 (b).

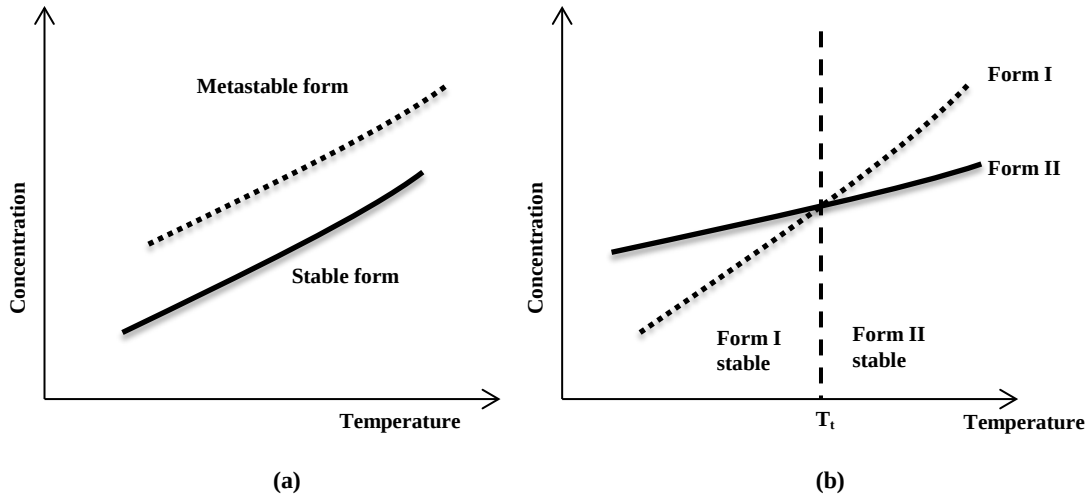

Figure 2.5: Monotropic system (a) and enantiotropic (b).

The less stable form is called “metastable” and it can nucleate for kinetic reasons but it will always tend to transform into the thermodynamically stable polymorph. The classical nucleation theory is usually good enough to describe the nucleation of many organic molecules included polymorphs remembering that the competitive nucleation between them can generate a very complex system. Solvent was proved to have a strong effect on the nucleation of one polymorph or another because of the kind of bonds that can form in the clusters (Bernstein 2011). Also the level of supersaturation affects the polymorph nucleated: generally, high supersaturation favours the nucleation of the metastable form. Additives can also direct the nucleation towards a specific polymorph rather than others. In chapter 9 and 10 of this thesis a more detailed study on the effect of solvent, additives and kinetic conditions on the nucleation of an organic polymorphic compound will be presented. The polymorphic transformation from a metastable to a stable structure is the result of a combined effect of competitive nucleation and crystal growth of the two different polymorphs as shown in the schematic of Figure 2.6.

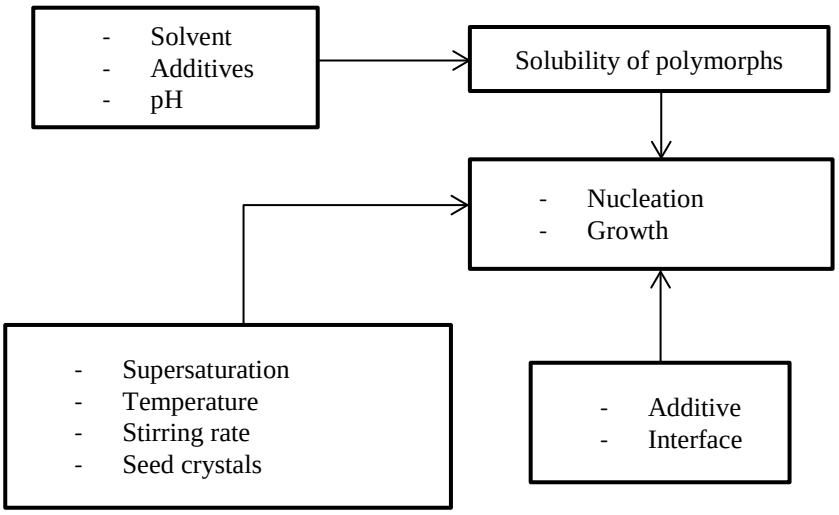

Figure 2.6: Schematic of controlling factors in crystallization of polymorphs (Kitamura, Mitsutaka 2002).

During the polymorphic transformation the metastable form dissolves in the solution while the stable form nucleates. The difference in solubility is the driving force of the process but the rate of transformation depends on many different factors such as temperature, solvent, crystal size, stirring rate, impurities etc. (Kitamura 2002). The solute concentration changes in time according to the relative speed of the processes of dissolution of the metastable form and nucleation and growth of the stable one (Cardew

and Davey 1985). If the dissolution of the metastable form is considerably slower than growth and nucleation of the stable one the process is defined dissolution-controlled. On the contrary, if growth of the stable form is the limiting factor the transformation is called growth-controlled. Figure 2.7 shows the trend of supersaturation for the two limiting and an intermediate case. If nucleation and growth of the stable form are significantly slower than the dissolution of the metastable form, the supersaturation remains constant for a long time since the dissolution process is able to sustain the growth one. When all the metastable form is dissolved the supersaturation rapidly drops down and the solubility of the solution reaches the one of the stable form. In the opposite case, if dissolution is slower, the supersaturation falls rapidly from the initial value to a very low one (solubility close to the equilibrium of the stable polymorph) because of the nucleation and growth of the stable form and then slowly goes to zero as dissolution of the metastable polymorph proceeds. If there is not a controlling factor the supersaturation profile is intermediate between the two limiting case (Cardew and Davey 1985; Davey and Cardew 1986).

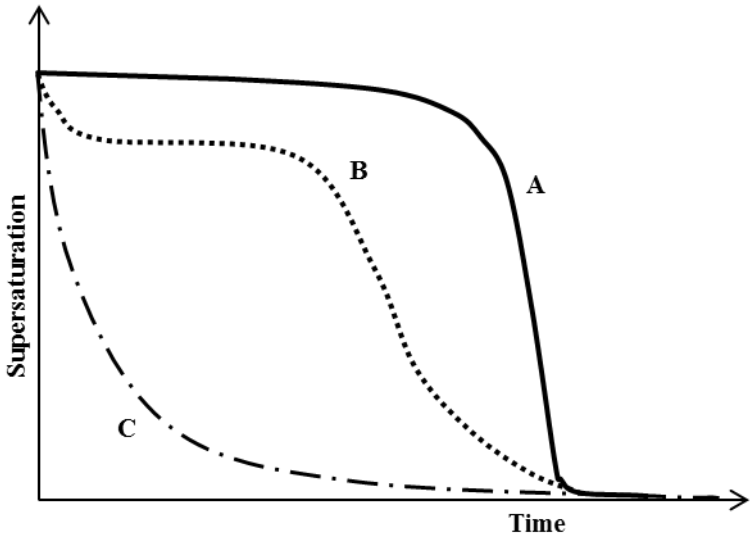

Figure 2.7: Supersaturation profile in the case (a) growth-limited (b) intermediate case (c) dissolution-limited.

Growth controlled kinetics is usually more common for organic compounds than dissolution controlled: piracetam, carbamazepine and glutamic acid present this type of kinetic (Scholl et al. 2006; Maher et al. 2012; Tian et al. 2006; O'Brien et al. 2004).

2.6 Impurities effect

Impurities in a crystallizer can have an incredibly large effect on the properties of the crystals produced in term of size distribution, shape and aspect ratio, polymorphic form and purity. They can inhibit crystal growth and delay nucleation as well as induce the nucleation of a different polymorphic form. A common model to describe the rate of crystal growth in solution in the presence of impurities was proposed in the late nineties by Kubota and Mullin (Kubota 2001; Kubota et al. 2000; Kubota et al. 1997; Kubota and Mullin 1995). The equations are based on the pinning mechanism of Cabrera and Vermilyea for the inhibition of step advancement considering one-dimensional adsorption of the impurities on the step lines. Besides, the impurities adsorption is assumed to obey the Langmuir adsorption isotherm. According to the pinning mechanism the step displacements (where growth normally proceeds) are stopped by impurities adsorbed on the crystal and, therefore, are forced to curve as shown in Figure 2.8 (Sangwal 1996; van Enckevort et al. 1996).

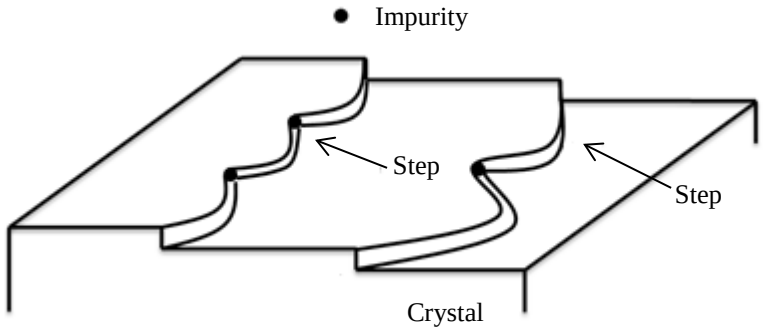

Figure 2.8: Model of impurity adsorption. Impurity are adsorbed on the step lines at kink sites ant retard the advancement of the step.

The step-advancement velocity can be written as:

$$\frac{v}{v_0} = 1 - \alpha\theta_{eq}, \tag{2.16}$$

and

$$\frac{v}{v_0} = 0 \; for \; \alpha\theta_{eq} > 1 \, , \tag{2.17}$$

where ν is the step-advancement velocity in the presence of impurities, ν_0 the step-advancement velocity for the pure system, α the impurity effectiveness factor and θ_{eq} the surface coverage of active sites on the crystal surface by impurities adsorption. The impurity effectiveness is related to the surface area of the crystal per growth unit a, the edge free energy γ, the Boltzmann constant k, the average distance between active sites L, the compound supersaturation σ and the temperature T with the equation:

$$\alpha = \frac{\gamma a}{kT\sigma L}, \tag{2.18}$$

while the equilibrium surface coverage can be calculated using the Langmuir adsorption with first order kinetics:

$$\theta_{eq} = \frac{Kc}{1+Kc}, \tag{2.19}$$

where c is the concentration of impurity and K is the Langmuir constant. The step advancement can be replaced by the crystal growth rate if it is assumed to be proportional to ν:

$$\frac{G}{G_0} = 1 - \left(\frac{\gamma a}{kT\sigma L}\right)\left(\frac{Kc}{1+Kc}\right), \tag{2.20}$$

It is clear that supersaturation strongly affect the growth in presence of impurities. From the growth kinetics equation it is possible to calculate a critical supersaturation below which growth can't happen ($G = 0$):

$$\frac{G}{G_0} = 1 - \left(\frac{\sigma}{\sigma_c}\right)^{-1} for\ \sigma_c < \sigma \ll 1, \tag{2.21}$$

$$\sigma_c = \frac{\gamma a K c}{kTL(1+Kc)}. \tag{2.22}$$

This mathematical model is well validated and the crystals' growth rate as a function of the concentration and the type of impurities has been largely studied both from a qualitative and a quantitative point of view (Tanoury et al. 2002; Wood 2001). The effect of impurities on nucleation, however, is still not completely clear (Anwar et al. 2009). A delay in nucleation is often observed, that generates crystals at higher supersaturation and therefore affects the size of the particles produced and, sometimes, the polymorphic outcome of the crystallization. This delay can be related to a change in solubility or to chemical interactions between solute, solvent and impurity just before nucleation (Fevotte

et al. 2013). Recently, the nucleation and growth rates of several drugs were studied in the presence of polymeric additives such as HPMC, PEG, PVP, PAA etc. For example, Vetter et al. (2011) studied the effect of a surfactant (Pluronic F127) on the growth kinetics of ibuprofen and modelled it using population balance equations. Similar investigations were performed by Alonzo et al. (2012) and Oucherif et al. (2013) who studied and modelled the growth and nucleation kinetics of felopidine in the presence of HPMC. The same research group also analysed the effect of HPMC and several other polymeric additives on flutamide (Trasi and Taylor 2012) and ritonavir (Ilevbare et al. 2012b; Ilevbare et al. 2012a). Polymers have also been shown to affect the growth and nucleation of inorganic compounds; in particular, a very small amount of a polymeric additive (ethylene dinitrotetraacetic acid disodium salt, EDTA) could accelerate the growth of potassium dihydrogen phosphate (KDP) crystals by forming molecular complexes with adventitious impurities in solution and eliminating the inhibiting effect which was observed at higher concentration of the polymer (Kuznetsov et al. 1998).

If impurities are added deliberately to the solution they are called additives and they can be used to control the shape of the final crystals (Poornachary et al. 2008b; Poornachary at al. 2008a; Majumder and Nagy 2013; Clydesdale et al. 1994; Poornachary et al. 2008c), their size (Reis et al. 2014; Saleemi et al. 2013; Hendriksen et al. 1998; Garnier et al. 2002) and polymorphic form (Price et al. 2005; Weissbuch et al. 1995). The molecular structure of an additive or a specific substrate (templates characterized by a film of adsorbed molecules are often used) can influence the polymorphic form nucleated: a correspondence between the molecular lattice of the substrate/impurity and the target polymorph usually facilitates its nucleation, the presence of opportune functionality group in the substrate can also cause the nucleation of a specific polymorphic form (Hiremath et al. 2005; Bonafede and Ward 1995; Chadwick et al. 2011; Di Profio et al. 2012; Kulkarni et al. 2014; Lang et al. 1999). Structurally related additives can inhibit the nucleation or the growth of a certain polymorph stabilizing another form (Gu et al. 2002; Mukuta et al. 2005a; Tian et al. 2009; He et al. 2001; Davey et al. 2002; Mo et al. 2011; Mukuta et al. 2005b), whereby they can be incorporated in the crystal lattice and slow down nucleation or growth of the stable polymorph favouring the metastable, and more soluble form (Mo et al. 2011; Mukuta et al. 2005b).

2.7 Population balance equations and solution

Every time a certain number of particles is present in a continuous system, the concept of population can be applied. Particles are in an innumerable variety of systems: solid-liquid (such as in crystallization), liquid-liquid and gas-liquid dispersions. Population balance equations are widely used to describe the particles behaviour in the continuous media and therefore they can be a useful tool in the prediction and design of specific systems (Ramakrishna 2000). The basic parameter in population balance is the average number density function defined in the particle state space:

$$E[n(x,r,t)] = f_1(x,r,t), \tag{2.23}$$

$$x \in \Omega_x, \tag{2.24}$$

$$r \in \Omega_r, \tag{2.25}$$

In the equation, n is the actual number density as a function of time t, external coordinates r (in the domain Ω_r) and internal coordinates x (in the domain Ω_x), while f_1 is the average number density function. The total number of particle per unit of spatial volume with an internal volume V_x can be calculated with the equation:

$$N(r,t) = \int_{\Omega_x} dV_x f_1(x,r,t). \tag{2.26}$$

In order to define the population balance equations it is convenient to define a particle space continuum that pervades the space of internal, x, and external, r, coordinates. This continuum is deforming in space and time in accordance with the field relative to fixed coordinates (Ramakrishna 2000):

$$\frac{dX}{dt} = \dot{X}(X,R,Y,t), \tag{2.27}$$

$$\frac{dR}{dt} = \dot{R}(X,R,Y,t), \tag{2.28}$$

where Y is defined as the continuous phase vector, which is a function only of the external coordinates $r$and time t. Using the Reynolds transport theorem it is possible to write a balance equation for f_1 (Bird et al. 1960):

$$\frac{\partial}{\partial t} f_1 + \nabla_x \cdot \dot{X} f_1 + \nabla_r \cdot \dot{R} f_1 = h, \tag{2.29}$$

where h is the particle generation rate that can be represented by different models.

The general equation can be simplified. In the case of homogeneity in space (i.e. CSTR reactor) the equation can be written as:

$$\frac{\partial}{\partial t} f_1 + \nabla_x \cdot \dot{X} f_1 = h + \frac{1}{\theta}\left(f_{1,in} - f_1\right), \tag{2.30}$$

Where θ is the resident time in the reactor and $f_{1,in}$ is the particle density function associated with the inlet stream. For a batch system at constant volume instead the equation becomes:

$$\frac{\partial}{\partial t} f_1 + \nabla_x \cdot \dot{X} f_1 = h, \tag{2.31}$$

There are many ways to reformulate the population balance model into computationally more affordable forms. For example, one of the most commonly used approaches is the method of moments (Ramakrishna 2000). The j^{th} moment of distribution f_1 is defined by:

$$\mu_j(t) = \int_0^\infty r^j f_1(r, x, t) dr, \tag{2.32}$$

when crystals are characterized by only one length $r = L$ and x is constant in time and space:

$$\mu_j(t) = \int_0^\infty L^j f_1(L, t) dL. \tag{2.33}$$

The method of moments is the simplest way to express the PBEs; more sophisticated techniques (i.e. finite elements) can be used but they require a higher computational effort to solve the optimization problem.

The moments have physical meaning. The zeroth moment is related to the total number of particles, μ_1/μ_0 with the average length of the crystals, μ_2/μ_0 is proportional to the surface area and $\mu_3$to the total volume of particles in the system. Assuming the initial nuclei have zero size the general equation 2.31 can be substituted to a system of equation containing the moments:

$$\frac{d\mu_0(t)}{dt} = h(t)V, \tag{2.34}$$

$$\frac{d\mu_j(t)}{dt} = j\mu_{j-1}(t)G(t), \tag{2.35}$$

where $G(t)$ is the growth rate of the crystals:

$$G(t) = \frac{dL}{dt} \equiv \frac{dR}{dt}. \tag{2.36}$$

PBEs can be used also to predict and simulate polymorphic transformations. In that case, one general equation for each polymorph must be considered. Three main mechanisms are involved in polymorphic transformations: the nucleation and growth of the more stable form and the dissolution of the less stable polymorph. Indicating with the index *m* the parameters of the metastable form, and with *s* the ones of the stable one the PBEs for a polymorphic system can be written as (Hermanto et al. 2007):

$$\frac{\partial f_m}{\partial t} - \frac{\partial (D_m f_m)}{\partial L} = 0, \tag{2.37}$$

$$\frac{\partial f_s}{\partial t} + \frac{\partial (G_s f_s)}{\partial L} = B_s \delta(L - L_0), \tag{2.38}$$

With initial conditions:

$$f_m^0(L) = f_m(L, 0), \tag{2.39}$$

$$f_s^0(L) = 0, \tag{2.40}$$

And where:

$$D_m = k_{d,m}(C - C_{sat,m}) \tag{2.41}$$

is the dissolution rate of the metastable form,

$$G_s = k_{g,s}(C - C_{sat,s})^n \tag{2.42}$$

is the growth rate of the stable form, and

$$B_s = K_{b1} S_s exp(\frac{-K_{b2}}{(\ln S_s)^2}) \tag{2.43}$$

is a common form to express the secondary nucleation rate of the stable form. In terms of moments the PBEs of a polymorphic system can be expressed as:

$$\frac{d\mu_{0s}}{dt} = B_s \tag{2.44}$$

$$\frac{d\mu_{i,s}}{dt} = iG_s\mu_{i-1,s} \; with \; i = 1,2 \ldots n \tag{2.45}$$

$$\frac{d\mu_{0,m}}{dt} = 0 \tag{2.46}$$

$$\frac{d\mu_{i,m}}{dt} = -iD_m\mu_{i-1,m}\ with\ i = 1,2 \dots n \tag{2.47}$$

A mass balance equation has to be included to solve the system:

$$\frac{dC_{liq}}{dt} = 3k_v\rho_c(-G_s\mu_{2,s} + D_m\mu_{2,m}) \tag{2.48}$$

where C_{liq} is the solute concentration, ρ_c is the crystal density and k_v is the shape factor of the crystals.

Experiments are necessary to measure and calculate the principal parameters related to crystallization mechanisms (Flood and Wantha 2012). Parameter estimation and modelling of polymorphic transformation have rarely been performed because of the complexity of the phenomenon. A first example of population balance applied to a polymorphic transformation was the study of the conversion of citric acid from anhydrate to its monohydrate form (Fevotte et al. 2007). Raman and image analysis were used to derive solute concentration, crystal size distribution and polymorphic ratio while the finite elements method was used to solve the PBEs (using the software FEMLAB). Many different algorithms were used to solve the PBEs for the polymorphic transformation of glutamic acid: moving pivot technique (Cornel et al. 2009), finite volume method in gPROMS (Ono et al. 2004), and the method of moments (Hermanto et al. 2007; Sheikholeslamzadeh and Rohani 2013; Kobari et al. 2014; Qamar et al. 2010). The method of moments was also used for the modelling of the solution-mediated transformation of DL-methionine polymorphs (Wantha and Flood 2013). Models can include or not primary nucleation of both the stable and the metastable form (unseeded or seeded hypothesis) but all of them include secondary nucleation of the stable form. Only one theoretical study also considered the presence of secondary nucleation for the metastable form and analysed its effect on the transformation time and the concentration profile (Kobari et al. 2014). After the estimation of the kinetic parameters, a good way to check the reliability of the model is determining the 95% interval of confidence, which is the range of values in which the estimated parameters are likely to be (with a 95% probability). Given the estimated parameter, the 95% confidence interval is given by:

$$CI = P \pm 1.96\frac{s}{\sqrt{n}} \tag{2.49}$$

where P is the parameter, s is the standard deviation of the samples and n is the total number of samples.

2.8 Optimization of batch crystallization (constrained optimization problems)

Crystallization is among the unit operations which are less easy to control. The main reason to estimate the kinetics parameters for growth, dissolution and nucleation is to be able to better understand this process and to improve it through simulations, optimization and model-based control. Crystallization optimization has been the subject of numerous studies because of the complexity of the mathematics behind it (Lang et al. 1999; Choong and Smith 2004; Abbas and Romagnoli 2007; Worlitschek and Mazzotti 2004). Optimizing a batch crystallization process can require the minimization of a system of non-linear ordinary equations (when the PBEs equations are expressed as a function of moments) that can have several local solutions and, therefore, might not easily converge to the global minimum. Different techniques were formulated in order to improve the convergence of the optimization and reduce the dependence of the solution on the initial guess (Choong and Smith 2004; Nowee et al. 2007).

Two parameters are normally optimized for a cooling crystallization: the seeding conditions (seed load and CSD) and the temperature profile. The time of batch is usually fixed as well as the initial conditions (temperature and concentration for the seeding optimization, seeds CSD for the temperature optimization). If the temperature profile has to be optimized, the problem to solve can be formulated in this way:

$$\min_{T(k)}\left(-\bar{L}_{l,end}\right) \tag{2.50}$$

Subject to the following conditions:

$$r_{min} \leq \frac{dT}{dt} \leq r_{max} \tag{2.51}$$

$$T_{min} \leq T \leq T_{max} \tag{2.52}$$

$$C_{end} \leq C_{max,end} \tag{2.53}$$

T is the vector of unknown variables (crystallizer temperatures at different times) formed by k elements and the higher is k the more difficult is the convergence of the optimization. $-\bar{L}_{I,end}$ is the parameter that has to be minimized (called objective function) and it is usually related to the final size of the particles. In normal applications it is desired to have large particles at the end of the batch that can be more easily filtrated; so the objective function can be expressed as:

$$\bar{L}_{I,end} = \frac{\mu_{1,end}}{\mu_{0,end}} \tag{2.54}$$

where $\mu_{1,end}$ is the value of the first moment at the end of the batch and $\mu_{0,end}$ the value of the zeroth moment. Their ratio is called the number mean diameter and it is related to the average size of the crystal produced. (Sanzida 2013; Sanzida and Nagy 2013)

Most of the optimization problems for batch crystallization in the literature do not include dissolution of the crystallized form and the optimal profile calculated is usually an only cooling profile that tends to keep the concentration close to the metastable zone limit to avoid nucleation, but high enough to allow growth of the crystals. Furthermore, dissolution can't be easily handled with the method of moments and it often requires the application of other techniques to represent the PBEs. More recently, some optimizations studies included dissolution in the PBEs and obtained more complex temperature profiles that included heating cycles in order to dissolve undesired fine particles present in the solution (Majumder and Nagy 2013a; Qamar et al. 2010; Yeom et al. 2013; Sanzida and Nagy 2013). These optimal profiles are in accordance with the experimental results for the application of crystallization strategies that use dissolution cycles such as temperature cycling (Abu Bakar et al. 2010; Abu Bakar 2010; Abu Bakar et al. 2009) and direct nucleation control (Saleemi et al. 2012a; Saleemi et al. 2012b; Saleemi et al. 2012; Abu Bakar et al. 2008).

2.9 Process analytical technology (PAT)

The term process analytical technology (PAT) became widely popular in 2004 when the Food and Drug Administration published the "Guidance for industry". A process analytical technology is there describe as a tool that "enable process understanding for scientific, risk-managed pharmaceutical development, manufacture, and quality assurance" (U.S.

Department of Health and Human Services 2004). These tools can provide effective and efficient means for acquiring information to facilitate process understanding, continuous improvement, and development of risk-mitigation strategies.

Four categories of PAT tools exist:

- Multivariate tools for design, data acquisition and analysis,
- Process analysers,
- Process control tools,
- Continuous improvement and knowledge management tools.

The first category include the use of multivariate mathematical approaches (statistical design of experiments, response surface methodologies, process simulation, and pattern recognition tools) to understand multi-factorial relationships between process, formulation and quality. Statistical evaluation of model predictions can assess mathematical expressions and models that describe the studied relationship (U.S. Department of Health and Human Services 2004). Process analysers and instrumentation include on- and in-line equipment. Those allow obtaining instant measurements avoiding the time delay typical of off-line analysis. The measured properties can be univariate (scalar) quantities or multivariate (vector and matrix). In the last decades advanced spectroscopic instrumentation progressed tremendously: UV-Visible, near- and mid-infrared and Raman spectroscopy are studied and began to be implemented in manufacturing (Chew and Sharrat 2010). The formulation of a specific control strategy must take into account the attributes of input materials, the characteristics of process analysers and the achievement of process end points in order to ensure the desired quality of the out materials and final product. The typical steps to follow to identify a good control strategy with the aid of PAT are:

- Identify a particular variable or variables in the process related to product quality,
- Design a process measurement system to monitor it or them,
- Design process controls that provide adjustments to the system in order to control the critical variables.

The implementation of PAT tools is a key element in the “Quality by Design” (QbD) approach that allows obtaining the desired quality of the product by the correct design of the manufacturing process. With the QbD implementation it is possible to control the

quality of the product by controlling the process itself avoiding any product waste due to mistakes in the manufacturing process (Rathore and Winkle 2009; Rathore et al. 2010).

Table 2.1: Summary of recent studies conducted using PAT tools for polymorph screening and transformation monitoring

Techniques	Process studied	Reference
Mid-IR	Discrimination between polymorphic forms of solids	Van Eerdenbrugh and Taylor 2011; Wartewig, and Neubert 2005
ATR-UV/Vis	Solvent-mediated polymorphic transformation monitoring in batch crystallization (changes in solute concentration)	Abu Bakar et al. 2009; Howard et al. 2009b; Abu Bakar et al. 2011; Howard et al. 2009a
NIR	Determination the polymorphic ratio of solid mixtures	Gimet and Luong 1987; Aaltonen et al. 2003; Patel et al. 2000
NIR	Solvent-mediated polymorphic transformation monitoring	Aaltonen et al. 2003; Wang et al. 2011
Raman	Determination the polymorphic ratio of solid mixtures	Tudor et al. 1993; Deeley et al. 1991; Strachan et al. 2007; Langkilde et al. 1997; Campbell Roberts et al. 2002
FT-Raman, FTIR	Comparison between the two techniques in determining the polymorphic ration of solid mixtures	Al-Zoubi et al. 2002; Hennigan and Ryder 2013
Raman	Cocrystallization of carbamazepine and nicotinamide monitoring	Rodriguez-Hornedo et al. 2006
Raman	Solvent-mediated polymorphic transformation monitoring	Herman et al. 2012; Barrett et al. 2011
Raman, FBRM, PVM	Study on the impact of operating parameters on polymorphic transformation of D-mannitol	Su et al. 2010
Raman	Measurement of the total solid concentration in a polymorphic system	Caillet et al. 2006; Caillet et al. 2007; Caillet et al. 2007; Caillet et al. 2008
Raman	Measurement of solute concentration in a polymorphic system	Cornel et al. 2008; Qu et al. 2008
FBRM	Solvent-mediated polymorphic transformation monitoring	Barthe et al. 2008; Zhao et al. 2013; Sathe et al. 2010; Liu et al. 2011;Simon et al. 2009; Simon, et al. 2011
Raman, NIR ,UV-Vis	Solvent-mediated polymorphic transformation monitoring	Helmdach et al. 2013; Helmdach et al. 2013; Kadam et al. 2012
Raman, FBRM, FTIR	Solvent-mediated polymorphic transformation monitoring	Yang et al. 2013

For the crystallization process, PATs have been widely used recently, in particular focused beam reflectance measurement (FBRM) (Yang and Nagy 2014), particle vision and measurement (PVM), attenuated total reflectance (ATR)-UV/Vis, ATR-FTIR and Raman spectroscopy. Near-infrared (NIR) and mid-infrared (mid-IR) have been used both with ATR probes for solute concentration measurement (Freitas et al. 2005; Kadam et al. 2010) and without ATR for the analysis of solid powders and tablets (Berntsson et al. 2000). PAT tools were used for monitoring both batch and continuous crystallization (Powell et al. 2015).

For polymorphic transformations normally NIR and Raman are the preferred tools. Mid-IR was also used with some systems but the differences between polymorphs are less visible with this technique (Van Eerdenbrugh and Taylor 2011; Wartewig and Neubert 2005). ATR-UV/Vis could also be a good tool for understanding polymorphic transformation as it can measure the changes in solute concentration and therefore detect the formation of a polymorphic form with a different solubility (Howard et al. 2009b; Abu Bakar et al. 2011). In Table 2.1 a brief summary of the most common PAT tools used in polymorph screening and transformation monitoring in recent years is shown.

A more detailed description of the PAT tools used in this thesis work is presented in the following sections, together with a brief literature review on how these techniques have been used for crystallization.

2.9.1 Focused beam reflectance measurement (FBRM)

FBRM is an in situ sensor used for real-time analysis in the pharmaceutical industry. It can give a particle size characterization using the principle of laser backscattering. The variable measured is the chord length, which is related to the particle size and shape. FBRM uses a high velocity scanning infrared laser beam that emanates trough the probe window inserted in the crystallizer (Braatz et al. 2012); the laser beam hits a particle and then it is reflected back to the probe. The chord length is calculated multiplying the length of time for which a continuous signal is reflected back to the probe by the velocity of the laser beam. The chord length distribution (CLD) is different from the crystal size distribution (CSD) but they are related. However, the calculation of CSD from FBRM measurement is not always straightforward. A schematic of an FBRM probe is shown in Figure 2.9. Many authors have used FBRM to infer information on the CSD or to detect primary or secondary nucleation and dissolution of crystals through changes in the particle

counts (Braatz et al. 2012). FBRM is not usually the preferred technique to monitor polymorphic transitions but an interesting study was performed by Barthe et al.: the system analysed was paracetamol in ethanol and the CLD evolution was monitored during polymorphic change. The paper shows how FBRM can track a polymorphic transition without the help of other tools (Barthe et al. 2008). A similar approach was also used by other researchers (Liu et al.2009; Zhao et al. 2013; Sathe et al. 2010; Liu et al. 2013). It must be notice that FBRM can be used if there is a significant difference in shape between the polymorphic forms otherwise it is not easy to distinguish polymorphs just looking at the CLD. A useful study on the interpretation of FBRM data for needle-shaped particle was performed by Leyssens et al. (2011): opportune statistics were chosen and used to describe the nucleation and growth of a hydrated sulphate salt of CDP323-2, a drug used in the treatment of multiple sclerosis.

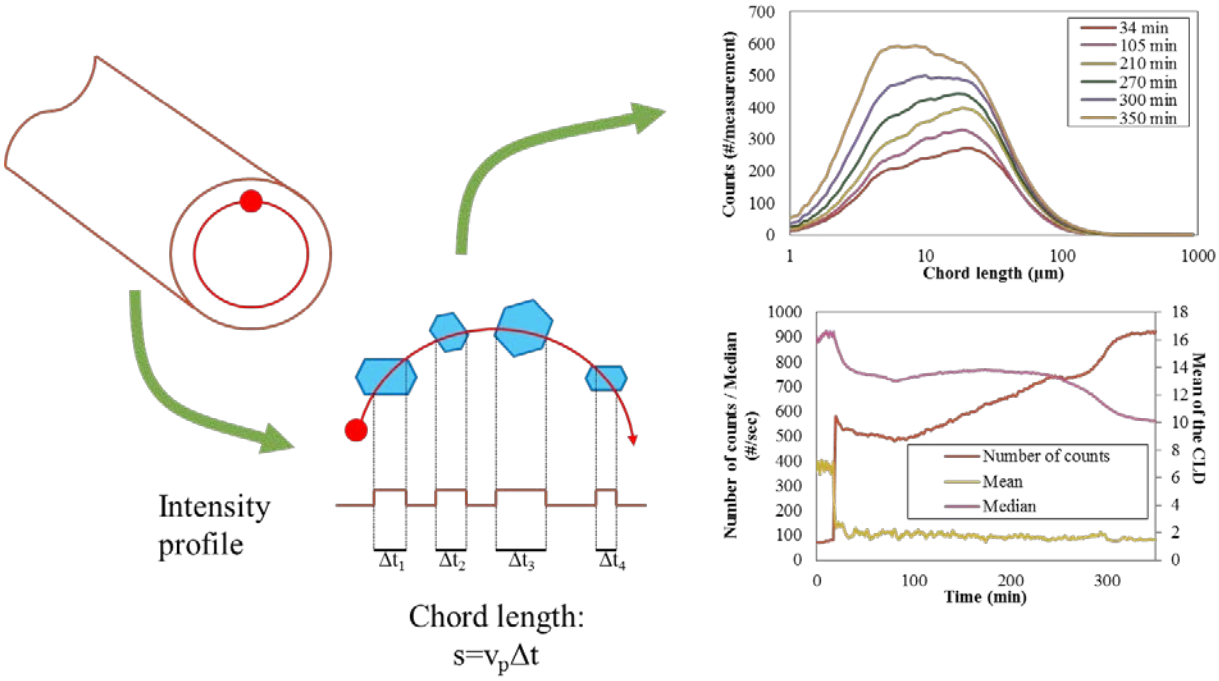

Figure 2.9: Schematic of the mode of operation of an FBRM probe.

FBRM was also compared to other techniques that can give information closer to the actual CSD such as laser diffraction, dynamic image analysis or PVM (Hamilton et al. 2012; Boxall et al. 2010).

2.9.2 Particle Vision Measurement (PVM)

This tool provides real-time information of the crystals shape, size and whether the crystals are aggregating or breaking during crystallization. It is a simple in-process video microscopy probe that can be inserted in the reactor to have images of the crystallization process. Quantitative information can be extracted by PVM images (equivalent diameter, aspect ratio, total count) even if the quality is not as good as off-line microscopic images (Braatz et al. 2012). Image analysis is a potentially great tool for kinetic parameters determination since it takes into account both crystal shape and size. However, extracting quantitative information from images can be very challenging and many studies are focused on the optimization of this technique (Wang et al. 2005; Ma, Wang 2012a; Ma, Wang 2012b). Image analysis and PVM can be used also to monitor polymorphic transformations (De Anda et al. 2005) if there is a considerable difference in shape between the two polymorphs (as for FBRM). In general, the use of FBRM or PVM should be always matched with Raman or NIR spectroscopy in order to avoid confusing two different polymorphs and two crystals with different morphology but same crystalline structure.

2.9.3 Attenuated total reflection – UV/Vis

ATR-UV/Vis is a spectroscopic technique that uses UV/Vis wavelength (200-900 nm). The measured variable is absorbance, which is related to the concentration of a certain species trough the Lambert-Beer law:

$$A = \varepsilon \lambda c, \tag{2.55}$$

where ε is the molar absorption coefficient, λ is the path length of the absorbing solution, and c is the concentration of the absorbing species. The presence of the ATR crystal allows measuring only the sample that is in close contact to the probe since the laser beam has a penetration depth of only a few microns. In the case of a crystallization process only the liquid phase is analysed. This tool has been widely used to measure the concentration of the dissolved solute during crystallization. A schematic representation of an ATR is shown in Figure 2.10.

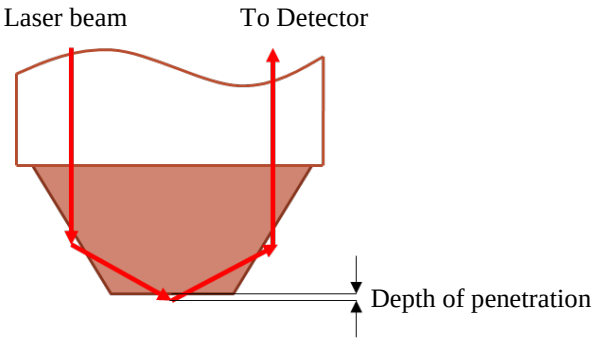

Figure 2.10: schematic of an ATR probe.

2.9.4 Raman spectroscopy

Raman spectroscopy is a form of vibrational spectroscopy, very much like infrared. The difference in the two techniques is the fact that IR bands arise from a change in the dipole moment of the molecule while Raman bands arise from a change in its polarizability. This spectroscopic technique is, precisely, based on inelastic scattering of monochromatic light, usually from a laser source. This phenomenon is known as Raman radiation and was first observed by Raman and Krishnan in 1928 (Vankeirsbilck et al. 2002). Photons of the laser beam are absorbed by the sample and then reemitted with a different frequency (that is why this type of scattering is called inelastic). The shifting of the frequency is the so called Raman Effect which provides information about vibrational, rotational and other low frequency transitions in molecules. When a substance is irradiated with monochromatic light, most of the scattered energy comprises radiation of the incident frequency (Raylight scattering) while only a very small quantity of photons (about 0.0001%) are scattered at a smaller frequency (Stokes Raman scattering). In the case a photon hits a molecule which has already been excited the scattered signal will have a larger frequency (anti- Stokes Raman scattering) (Verpoort at al. 2002). The possible energy transitions for vibrational spectroscopy are shown in Figure 2.11. Raman spectroscopy can be used to study solid, liquid and gaseous samples. This technique is a potential tool to monitor and control crystallization processes since it enables in situ, non-destructive and fast quantitative measurements of solid samples without specific sample preparation. In particular, it can be used to distinguish between different polymorphic forms of both inorganic and organic compounds (Févotte 2007). It was defined, in recent years, as “one of the fastest, most reliable and most suitable techniques to identify crystals forms in drug products and can be easily exploited routinely for monitoring phase change in drug products and quality control

assays" (Auer et al. 2003). Most organic molecules present clear and resolved peaks in Raman spectra, offering the possibility to do both quantitative and qualitative analysis without any specific sample preparation. Some disadvantages of Raman spectroscopy are the fluorescence and photobleaching phenomena that can disturb the measurements. Furthermore, the high temperature induced by the laser beam can destroy part of the analysed sample and the spectra of organic solvent can completely cover the sample's signal (Fevotte et al. 2007). Raman spectroscopy can be directly and quickly used in the qualitative identification of polymorphs in dry powders and slurries but quantitative studies have also been carried out as shown in Table 2.2.

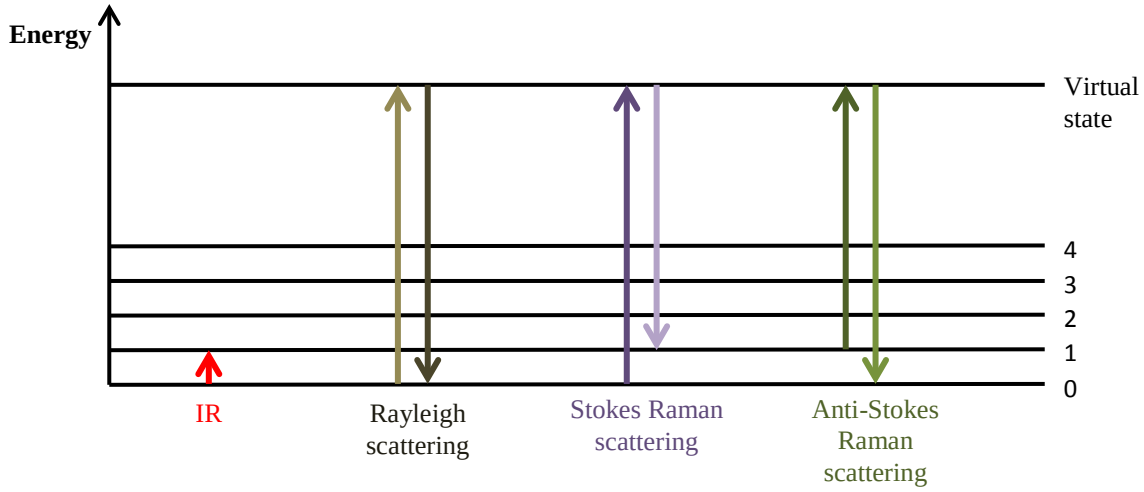

Figure 2.11: Schematic representation of energy transition in Raman and IR spectroscopy. Absorption of IR radiation and Stokes and Anti- Stokes Raman scattering. The mechanism of elastic scattering (Rayleigh) is also shown.

The potentiality of Raman spectroscopy to quantitatively determine polymorphic forms' concentration in slurries or dry solid mixtures depends on the possibility of building a good calibration function using a correct experimental approach. Determining a calibration function to predict polymorphic ratio in solid mixtures is relatively simpler than working with slurries or solutions. In general, univariate models seem to be sufficient to analyse solid mixtures whose biggest problem is usually mixing. Obtaining a homogeneous mixture of two or three different powders can be very difficult, so solid vortex mixer devices are often used (Hennigan and Ryder 2013). Dispersing the solid mixtures in water, which has a very weak Raman signal, can also be a solution especially for compounds that are insoluble in water.

Table 2.2: Several applications of Raman spectroscopy for qualitative and quantitative polymorph identification of pharmaceutical compounds

Application of Raman spectroscopy	Reference
Monitoring the cocrystallization of carbamazepine and nicotinamide	Rodriguez-Hornedo et al. 2006
Measuring the transition temperature for an enantiotropic system	Herman et al. 2011
Monitoring the presence of different forms of piracetam in ethanol as a function of operating conditions during batch cooling crystallization	Barrett et al. 2011
Quantitative determination of polymorphic ratio in solid mixtures	Deeley et al. 1991; Tudor et al. 1993; Strachan et al. 2007; Langkilde et al. 1997; Campbell Roberts et al. 2002
FT-Raman and FTIR spectroscopy were compared in the quantification of orthorhombic and monoclinic forms of paracetamol in solid samples	Al-Zoubi et al. 2002
Comparison between backscattered and transmission Raman spectroscopy in calibrating tablets made by two polymorphic forms of piracetam	Hennigan and Ryder 2013
Determination of the polymorphic composition of dry solid samples (univariate and multivariate calibration functions)	Wang et al. 2000; Német et al. 2009; Kachrimanis et al. 2007; Ono et al. 2004; Alatalo et al. 2010; Alatalo et al. 2008; Qu et al. 2009; Braun et al. 2010; Qu et al. 2008; O'Brien et al. 2004; Salameh, Taylor 2006; Agarwal, Berglund 2003; Strachan et al. 2004
Identifying impurities in solid samples	Hargreaves et al. 2011; Li et al. 2011; Pratiwi et al. 2002
Determination of the polymorphic composition of slurries in water at constant temperature (multivariate calibration functions)	Hu et al. 2005; Wikstrom et al. 2005; Caillet et al. 2007; Caillet et al. 2008; Caillet et al. 2006; Tian et al. 2006; De Beer et al. 2006; Cornel et al. 2008; Falcon, Berglund 2004
Determination of the polymorphic composition of slurries in organic solvents at constant temperature (multivariate calibration functions)	O'Sullivan et al. 2003; Zhao et al. 2012; Su et al. 2010; Starbuck, C. et al. 2002 Falcon, Berglund 2004; De Spiegeleer et al. 2005; Kobayashi et al. 2006
Study on the crystallization of Carvedilol at different temperatures and mixtures of solvents	Pataki et al. 2012a; Pataki et al. 2012b
Quantitative determination of both total solid concentration and solid composition	Caillet et al. 2006; Chen et al. 2008
Quantitative determination of liquid concentration	Qu et al. 2008; Hu et al. 2005; Cornel et al. 2008

Many factors can affect Raman spectroscopy other than the polymorphic composition and they have to be taken into account when developing a calibration function: temperature, solid density of the slurry, crystal size and shape and solute concentration (in the case of suspensions or slurries) are the most important. The effect of temperature on calibration was only briefly studied (Fevotte et al. 2007; Wong et al. 2007) and most of the experiments were actually performed in isothermal conditions or neglecting the effect of temperature on the calibration curve. The effect of crystal size, solution density and sample position on Raman spectra are very similar and it is often a change in intensity that can partly be compensated using pre-processing (Vankeirsbilck et al. 2002). A different approach to calibration, considering particle size effect on spectra was conducted by both Hu et al. (2006) and Chen et al. (2012). It is interesting to notice that Hu et al. found that increasing particle size generates a decrease in the Raman intensity while Chen et al. observed exactly the opposite trend. An attempt to introduce other parameters in a Raman calibration model was done by Wong et al. (Wong et al. 2007; Wong et al. 2008). They simply included temperature and slurry density in a PLS model which was then validated with a cooling crystallization experiment. The results for validation were greatly improved by the introduction of these two parameters. However, a good calibration procedure, using design of experiment, could lead to good results even without explicitly introducing additional variables in the calibration function because their effect is already included in the spectra of the calibration set (Chen et al. 2011; Wulfert et al. 2000; Wulfert et al. 1998). A more complete analysis of the parameters affecting Raman spectra was performed by Cornel et al. (2008) for the study of the polymorphic transformation of L-glutamic acid. Cornel et al. studied the effect of temperature, crystal size, solute concentration and solid concentration and then planned a set of calibration experiment that leaded to a final error in polymorphic ratio estimation of about 3%. A similar approach will be used in this thesis but with the help of design of experiment in order to reduce the number of calibration experiments needed.

2.9.5 Near-infrared (NIR) spectroscopy

Near infrared spectroscopy is a vibrational spectroscopy technique. The sample is irradiated with NIR light (4000-12000 cm^{-1}) which is partially absorbed by the molecules bringing them to a higher vibrational state. Only vibrations resulting in changes in the dipole moment of a molecule can absorb NIR radiation. R-H groups have very high dipole moment so they have the strongest overtone. Also O-H, N-H, C-H, S-H bonds strongly

absorb in NIR. There are two types of vibration for these groups: stretching and bending. The low molar absorptivity of absorption bands in the NIR regions allows using the reflection mode, in which the light reflected by the sample is measured so no specific preparation is required (De Beer et al. 2011).

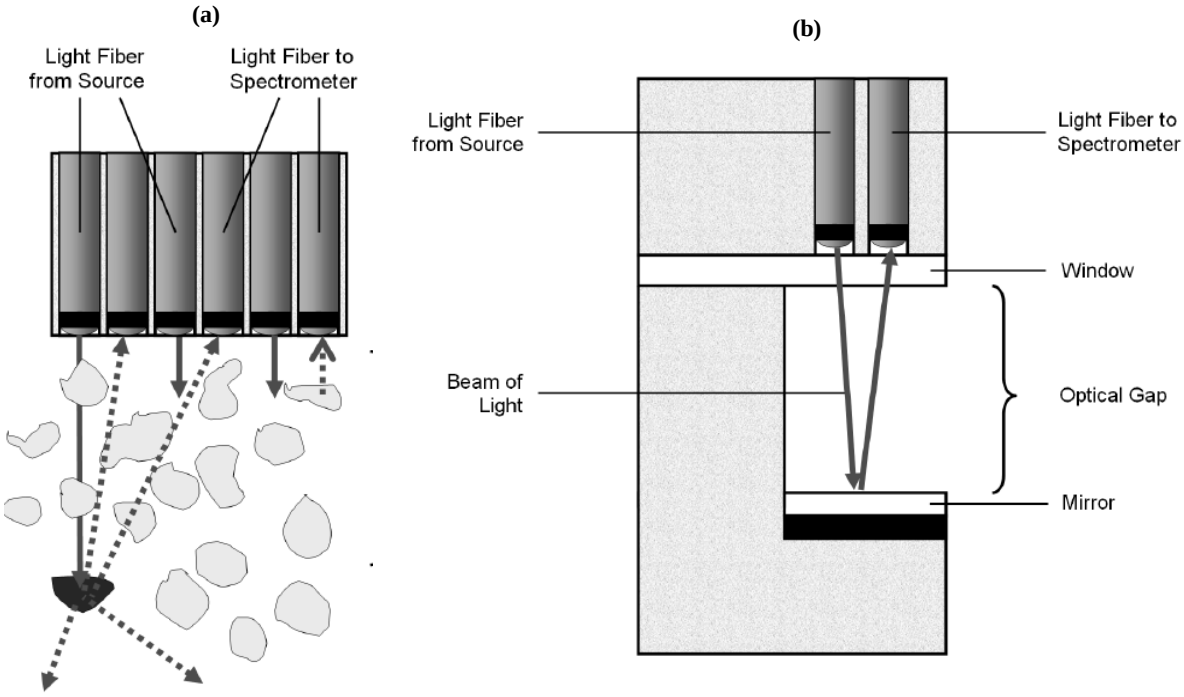

Figure 2.12: (a) NIR reflectance probe (b) NIR transflectance probe.

Different types of NIR immersion probes can be used for solid analysis:

- *Reflection probe* (Figure 2.12a): it is formed by several light fibres that both irradiate the sample and collect the reflected light (diffuse reflection). This type of probe is not suitable for liquid analysis.
- *Transflection probe* (Figure 2.12b): it is formed by two fibres, one to irradiate the sample and one to collect both the diffuse reflected signal and the signal reflected in a mirror placed opposite the source (transmission mode). The possibility to work both in transmission and reflectance makes this type of probe suitable for more applications than the reflectance probe. Unfortunately the optical gap is strongly affected to fouling in the presence of solids.

A third type of NIR immersion probe exists, the transmission type which is suitable mainly for analysis of liquid samples and was not used in the experiments performed for this thesis.

2.9.6 Mid-infrared (mid-IR) spectroscopy

Mid-IR is very similar to NIR spectroscopy. The light region is at a lower wavelength (400-4000 cm^{-1}) but it is still a vibrational technique that excites dipoles. Compared to NIR it is characterized by a higher degree of excitation that generates sharper absorption peaks at higher intensity. Because of the strongest absorption in mid-IR, working in reflectance mode is more difficult because the reflected signal is less intense. A disadvantage of both NIR and mid-IR is the strong absorption of water. The peak of water is usually very intense and broad and can cover useful information of the solid studied (Wartewig and Neubert 2005). Helmdach et al. recently demonstrated how ATR-midIR can be used to speed up and optimize the scale up of crystallization processes using paracetamol as model compound (Helmdach et al. 2013).

2.10 Application of PAT tools for the crystallization of biopharmaceutical compounds

The term biopharmaceutical refers to pharmaceuticals that are manufactured using living organisms, and therefore, are inherently biological. Proteins, antibodies, vaccines, blood and plasma products, cultured cellular and tissue products are all biopharmaceutical compounds (Rader 2007). The birth of biopharmaceutical industry dates back to the early 70s when the first DNA technology experiment was performed. A decade later, in 1982, recombinant human insulin was approved and then introduced to the market (European commission Enterprise and Industry 2009) and in 2011 three of the top ten blockbuster drugs were produced biologically (Humira, Enbrel and Remicade, all used for the treatment of rheumatoid arthritis). The US biopharmaceutical industry is estimated to support more than 810,000 direct jobs (and nearly 3.4 million total jobs) and to generate nearly $789 billion of economic output (The Pharmaceutical Research and Munufacturers of America (PhRMA), Bettelle 2014). The biopharmaceutical industry is among the most innovative industries if measured by R&D investment, IP generation, venture capital and share of total R&D employment in manufacturing industries; in 2011 the total expenditure for R&D across all biopharmaceutical industries in the US was of $41.1 billion (against the

$7.6 billion invested in aerospace industry, $11.7 billion in automotive and $22.9 billion in the semiconductor and electronic component industry). The number of patent applications in the same year was 6,777 with 4,405 of them awarded (The Pharmaceutical Research and Munufacturers of America (PhRMA), Bettelle 2014). Clearly, this is an industry where incremental process improvements can have high economic and societal impact.

The QbD approach has been successfully implemented in the pharmaceutical industries and in recent years it has also been considered for the biopharmaceutical industry (Read et al. 2010; Glassey et al. 2011). Biotech products and biopharmaceuticals are a result of biological processes that are more difficult to control than standard chemical operations, since more variables are involved and their interactions have to be taken into account. Nevertheless, PAT tools such as NIR and Raman spectroscopy, HPLC and image analysis were recently used to control biological processes (Ündey et al. 2010; Bhambure et al. 2011; Smith 2014).

Crystallization is not a common process for the production of biopharmaceuticals since, normally, higher purity can be reach with other techniques such as chromatography or membrane filtration. However, many studies are currently being conducted in order to test this simple and cost-effective process for the purification of biopharmaceutical, proteins in particular (Gavira et al. 2014; McPherson and Gavira 2014).

2.11 Further solid and liquid state analysis

2.11.1 Differential scanning calorimetry (DSC)

Differential Scanning Calorimetry (DSC) is a thermal technique that allows to measure changes in the heat flows associated with transitions in materials as a function of time and temperature. The measurements are taken in a controlled atmosphere (usually nitrogen) and the samples are heated up at a constant rate. These measurements provide quantitative and qualitative information about physical and chemical changes that involve endothermic or exothermic processes, or changes in heat capacity.

DSC can be used to study:

- Glass Transitions,
- Melting and Boiling Points,

- Crystallization time and temperature,
- Percentage of Crystallinity,
- Heats of Fusion and Reactions,
- Specific Heat,
- Oxidative/Thermal Stability,
- Rate and Degree of Cure,
- Reaction Kinetics,
- Purity.

Transformations can be endothermic (like melting or polymorphic transformations) or exothermic (chemical reactions). In a DSC diagram the type of transformation can be recognized by the sign of the heat flow absorbed by the sample. In this thesis it was arbitrarily decided to indicate as positive the endothermic transitions, and the exothermic as negative (see Figure 2.13).

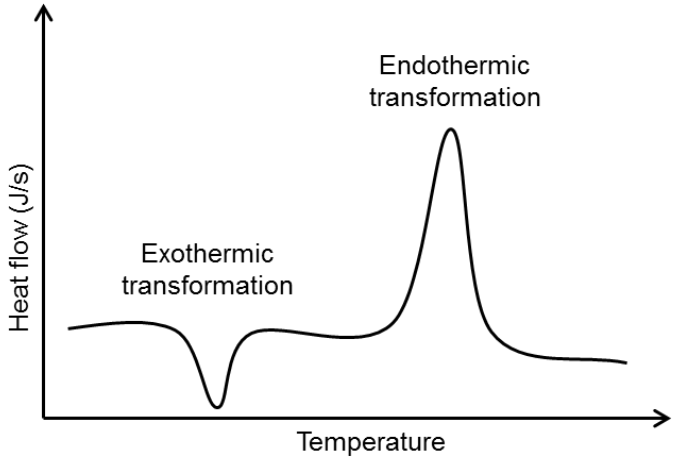

Figure 2.13: DSC diagram example for a polymorphic transition and melting of a sample. In this thesis work the DSC diagrams will be represented with positive endothermic peaks and negative exothermic peaks.

2.11.2 X-Ray diffraction

X-Ray diffraction (XRD) is a rapid and reliable technique widely used for many applications such as:

• Characterization of crystalline materials (discrimination between polymorphs for example);

• Determination of unit cell dimensions;

• Measurement of sample purity;

• Characterization of thin films samples;

• Textural measurements (such as the orientation of grains) in a polycrystalline sample.

An X-ray diffractometer consist in an X-ray cathode tube, a sample holder, and a detector. X-rays are generated by the cathode ray tube, filtered to produce monochromatic radiation, collimated to be concentrated, and then directed towards the sample. X-ray diffraction is based on constructive interference of monochromatic light and the crystalline sample. If the sample generates the conditions to satisfy Bragg's Law, the interaction of the incident rays with the sample will produce a constructive interference and, therefore, a diffracted ray (as shown in Figure 2.14). Bragg's law relates the wavelength of electromagnetic radiation λ to the diffraction angle θ and the lattice spacing d in a crystalline sample (see Figure 2.14):

$$\lambda = 2d\ sin\ \theta \tag{2.56}$$

The diffracted X-rays are detected by the detector and then processed and counted. Because of the random orientation of the powdered material, it is possible to obtain all possible diffraction direction of the crystal lattice by scanning the sample through a range of 2θ angles.

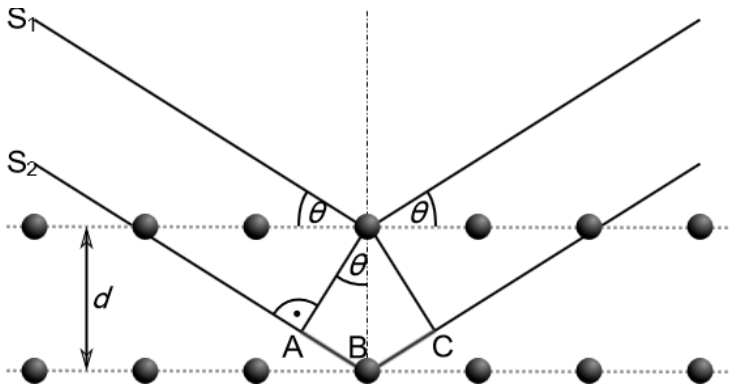

Figure 2.14: X-Ray diffracted by a crystalline lattice following Bragg's law.

2.11.3 Laser diffraction (Malvern Mastersizer)

Laser diffraction is one of the best available techniques to measure particle size of solids, droplets or bubbles (Mullin 2001). It is based on light scattering: the particles passed through a laser beam and scatter light at an angle related to their size. Bigger particles will

scatter light at narrow angle and high intensity while small particles will generate low intensity scattering at wider angles. The combination of two theories, Fraunhofer and Mie, is used to determine the particle size of the sample, measured from the diffraction pattern generated by its particles. The two theories assume that the particles are spherical and the suspension is dilute. Laser diffraction is the working principle of the Malvern Mastersizer which enables to measure particles in the size range of 0.1 to 10000 μm. The disadvantage of the Mastersizer is that it is an offline technique that needs sampling.

2.11.4 High performance liquid chromatography

High performance liquid chromatography (HPLC) is a common technique to analyse liquid samples. It allows separation and both qualitative and quantitative analysis of the components present in the liquid sample. A simple schematic of an HPLC system is shown in Figure 2.15. A solvent is pumped at high pressure inside a column filled with a solid absorbent material (normally silica or polymers) and the sample is injected in the high pressure flow. The sample components will pass through the column at different speeds in relation to the size of their molecules and their level of affinity to the column packing material. A UV detector is placed at the end of the column for the quantification of each component.

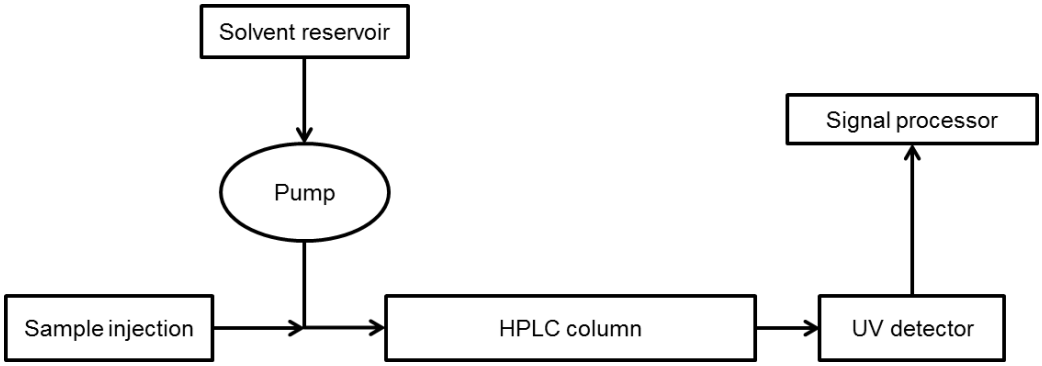

Figure 2.15: Schematic of an HPLC system.

A selected UV wavelength is directed and absorbed by each component going out of the column. The non-absorbed light is then processed in order to quantify the amount of each component of the sample analysed using the Beer and Lambert law. The relative retention times are used to qualitatively identify each component of the sample.

2.12 Chemometrics techniques

Chemometrics is defined as the science of extracting information from series of data. The principal aim of chemometrics is to find a relation between two or more variables. When data is collected as a function of only one variable is called univariate while it is defined multivariate if collected for several variables. With the recent development of PAT tools and the simultaneous use or more than one analysing technique, chemometrics has become very important for the interpretation of complex data and the extrapolation of useful information. Typical multivariate techniques for data analysis are PCA (principal component analysis) and PLSR (partial least squares regression) (Cox 2005).

2.12.1 Principal components analysis

Principal components analysis (PCA) is a dimension reduction technique for quantitative data. Given a set of data in more variables, with PCA it is possible to reduce the dimensions of the problem down to two or three keeping, at the same time, as much information as the inherent variability within the data (Cox 2005; Pratiwi et al. 2004). PCA models all the variations in the data set using orthogonal basis vectors which are called principal components (Gemperline 2006). One of the main goals of this analysis is to eliminate the principal components associated to noise and, therefore, minimize the effects of measurement error. If A is the $n \times m$ matrix of input data (n rows of spectra recorded at m wavelengths for example) a PCA can decompose it in the following linear system:

$$A = CP^T + \varepsilon, \tag{2.57}$$

where C is the $n \times k$ matrix of k principal components' scores and P is the $m \times k$ matrix of the eigenvectors of A. The eigenvectors are called "loadings" in the PCA. ε is a matrix containing the unexplained variance. For each independent source of variation in the data, a principal component is expected in the model. The first principal component is the one with the largest eigenvalue, or, the one that explains the maximum amount of variance in the original data. The second component is associated with the second largest eigenvalue and it explains the maximum amount of variance left in the original data after eliminating the one associated to the first component. The third component corresponds to the third largest eigenvalue and so on. Usually the most important variations in a process are explained in the first few principal components while the rest is just noise.

Loadings and scores for PCA can be used to interpret the data matrix. The scores are usually represented in two-dimensional scatter plots. Often, a very high percentage of variability is gathered in the first few principal components so only a few of these plots are necessary. The scores plots are used to detect similarities, differences or other interesting relationships among samples. Loadings are also presented in two-dimensional scatter plots, but more often they are plotted against the original variables in order to interpret their relationship with the scores. In fact, they can tell which of the variables are most relevant for the different components in the data set and, therefore, what phenomenon is associated to the component itself. If the focus is to find clusters in the data set, loading plots can be useful to identify which variables characterise each different cluster (Næs et al. 2004). In order to interpret in an easier way the loadings, Varimax rotation can be performed on the matrix data loadings using Matlab (function *rotatefactors*). This operation maximizes the sum of the variances of the square loadings: in this way every component is associated to a smaller amount of variables and the determination of the most influent variables on each component is greatly simplified. Considering the matrix of loadings $\mathbf{P} = [p_{j,i}]$ (with dimensions $m \times k$), doing a varimax rotation means maximizing the varimax criterion among all orthogonal rotations of **P**. The varimax criterion is defined by the formula:

$$V(\mathbf{P}) = \sum_i \left(\frac{1}{m} \sum_j p_{j,i}^4 - \left(\frac{1}{m} \sum_j p_{j,i}^2 \right)^2 \right). \tag{2.58}$$

A simple computational method to obtain simultaneously loadings, scores and percentage of variance associated with each PC is the single value decomposition. The input data matrix A is decomposed in:

$$A = USV^T, \tag{2.59}$$

where U is the matrix of the principal component scores, V is the matrix of the loadings and S is a diagonal matrix whose elements are the square roots of the eigenvalues. If normalized to 1, matrix S gives the percent of variance associated with each correspondent component. The SVD is a practical and numerically accurate method to calculate principal components of a data matrix. A function *svd* is also present in Matlab to perform single value decomposition of a matrix automatically.

2.12.2 Regression on Principal components

Principal components can also be used as a multivariate calibration technique. A standard univariate linear calibration model is in the form (Gemperline 2006)):

$$y = b_1 x + e, \tag{2.60}$$

where x is the set of known variables (for example the values of a certain wavelength in a set of spectra) and y is the vector of the correspondent desired dependent value (usually the concentration of a specific compound associated with each spectrum). The vector e represents the error of each calibration experiment $e = y - y_{calculated}$. The value b_1 is calculated by the least-squares procedure (which minimize the sum of square errors $e^T e$) using the formula:

$$b_1 = (x^T x)^{-1} x^T y, \tag{2.61}$$

The same concept can be used in a multivariate calibration. The difference between univariate and multivariate is the number of inputs in the model, which is higher than one for a multivariate technique. That means that x is not a vector anymore but it is a $n \times m$ matrix X where, for example, every raw represent a specific measurement and every column a specific wavelength. Also b_1 is now a vector b calculated as:

$$b = (X^T X)^{-1} X^T y. \tag{2.62}$$

The first step in carrying out a regression using principal components is calculating the scores and loading of the data set matrix X. Then, the scores are treated as any other variable would be in a multiple regression analysis and the calibration model is constructed as:

$$y = a_1 PC_{x1} + a_2 PC_{x2} + \cdots a_p PC_{xp} + c, \tag{2.63}$$

where y is the desired dependent value, a_1 to a_p are a set of regression coefficients fitted by least squares to the PC principal components in the model and c is a constant (Livingstone 2009).

The principal components are calculated by PCA in order or variance explained, but not necessary in the order in which they will appear in the equation (2.61). For example, considering a regression model with 4 components, the equation that fit the dependent variable best does not necessary include PC_1, PC_2, PC_3 and PC_4; but it can include PC_1,

PC_2, PC_3 and PC_5 instead of PC_4. Although PCs are in order of variance explained some of them may not be useful in the description of the dependent variable such as PC_4 in the example given.

2.12.3 Partial least squares regression

The method of partial least square is also a regression technique that uses quantities derived from the set of original data like the principal components. The PCs in the regression models are called latent variables LV (or factors) and the equation is in the form:

$$y = a_1 LV_1 + a_2 LV_2 + \cdots a_p LV_p, \tag{2.64}$$

where y is the dependent variable and a_1 to a_p are a set of regression coefficients fitted by partial least squares procedure. Each latent variable is a linear combination of the independent data set:

$$LV_1 = b_{1,1}x_1 + b_{1,2}x_2 + \cdots b_{1,p}x_p$$

$$LV_2 = b_{2,1}x_1 + b_{2,2}x_2 + \cdots b_{2,p}x_p$$

… … … … … … … … … … … … … … … …

$$LV_q = b_{q,1}x_1 + b_{q,2}x_2 + \cdots b_{q,p}x_p \tag{2.65}$$

As in PCA, PLS will generate as many latent variables (q) as the smaller of P (dimensions) or N (samples). The difference between the two techniques is that PLS procedure calculates the latent variables and the regression coefficients at the same time. The algorithm is actually an iterative procedure that combines the PCA step with the regression step. Latent variables are calculated to explain most of the variance of X while remaining orthogonal to each other. In PLS the LVs are constructed in order to maximize their covariance with the dependent variable. Unlike PCR equations where the PCs are not entered in a particular order the latent variables appear in the PLSR equations in order: the first, LV_1, is the one that explains maximum variance; LV_2 is the second in order of variance explained and so on.

The number of latent variable to use is usually calculated using the leave one out cross validation (or K-fold cross validation in Matlab). In K-fold cross-validation, K-1 folds are used for training and the last fold is used for evaluation. This process is repeated K times, leaving every different fold for evaluation each time. For every left out sample the

prediction error $y_i - y_{i,calculated}$ is determined using the regression function calculated from the rest of the samples. Then the MSECV (mean square error of cross validation) is estimated using the K prediction errors:

$$MSECV = \sum_{i=1}^{K} \left(y_i - y_{i,calculated}\right)^2. \quad (2.66)$$

The MSECV is calculated for different values of the number of latent variables q, and the optimum value is chosen as the one which minimize the MSECV (Livingstone 2009).

2.12.4 Pre-processing techniques

Pre-processing spectra before using PCR or PLS regression can help to eliminate some external effect like fluorescence or to obtain a better signal to noise ratio that allows a better resolution of the peaks. Many techniques can be used, in particular for the instruments used in this work the best options are:

- Autoscaling;
- Smoothing;
- Baseline correction;
- Derivative;
- Multiplicative scatter correction (MSC) and standard normal variate (SNV) transform.

Pre-processing techniques are normally necessary to treat the spectroscopic data before its interpretation. For NIR it usually common to do second derivative, which allows eliminating baseline effect and makes the peaks narrower. It is generally preferred to first derivative because the position of the tracked peak does not change and, compared to the first derivative, even extremely flat structures can be evaluated. For Raman spectra a baseline correction is advisable because it partly eliminates the effect of fluorescence. Generally, Raman's peaks are narrow enough in the raw spectrum but first derivative can be useful especially for quantitative calibration and for dilute slurries.

Autoscaling

This term indicates the procedure of performing both mean centering and variance scaling of the data. Mean centering is performed by calculating the average data vector of all the samples and then subtracting it point by point from each vector in the data set. Graphically, mean centering is just a shift in the origin of the plot. Mean centering must always be

performed before variance scaling which is used to give equal weight to all portions of the experimentally measured data vectors. This can be done by normalizing each column of variables so that the sum of the square values for each of them is equal to 1. Autoscaling should be performed at last, after all the other pre-processing techniques (Gemperline 2006).

Smoothing

Smoothing can improve the signal-to-noise ratio of a signal recorded. The most useful algorithm used is the Savitzky-Golay which essentially fits individual polynomials to windows around each point of the spectrum. It is possible to choose the size of the window (in points) and the order of the polynomial. The larger the window and lower the polynomial order, the more smoothing is done.

Baseline correction

In the simplest kind of baseline correction the spectrum must have a region where the signal is zero. It is possible to calculate then the average signal over this region for each spectrum and subtract it from each wavelength in the respective spectrum (Gemperline 2006). Alternative baseline corrections are possible if the background is a curved signal with multiple valleys. In this case it is possible to fit a polynomial function though the valleys and then subtract it from the spectra to be corrected.

Derivative

This kind of pre-processing technique allows to remove some baseline effect and to have a better resolution of the peaks. It usually accentuates the noise effect so it must be performed together with smoothing. The derivative transformation is linear, so the quantitative aspects of the original spectra are retained (Gemperline 2006).

MSC and SNV

Those two techniques are very similar to each other and normally the one which works better is chosen. They are particularly useful in NIR to eliminate differences due to the particle size in powdered samples (Gemperline 2006).

2.12.5 Model validation

The reliability of a calibration model is estimated using validation. Cross-validation has been explained in the previous paragraphs and it is usually a good choice if the calibration set does not include many samples. However, an external validation is usually preferred. In

this technique a group of known samples are not included in the calculations but they are used to test the estimated calibration function. Usually the root mean squared error of prediction (RMSEP) is calculated in order to have a numeric value that represents the reliability of the model:

$$RMSEP = \sqrt{\frac{\sum_{i=1}^{q}\left(y_{i,P}-y_{i,cal}\right)^2}{q}}, \tag{2.67}$$

where q is the number of validation samples, $y_{i,P}$ is the dependent variable for each of them and $y_{i,cal}$ is the correspondent value calculated with the calibration model. The root mean square error of prediction is usually compared with the root mean square error of calibration (RMSEC):

$$RMSEC = \sqrt{\frac{\sum_{i=1}^{n}\left(y_{i,C}-y_{i,cal}\right)^2}{n}}, \tag{2.68}$$

where n is the number of calibration samples, $y_{i,C}$ is the dependent variable for each of them and $y_{i,cal}$ is the correspondent value calculated with the calibration model. A good calibration model has similar values of RMSEC and RMSEP. A further indication of the reliability of the model and in general, of the linearity of the system is the correlation coefficient (R^2). That is calculated as:

$$R^2 = 1 - \frac{SS_{res}}{SS_{tot}}, \tag{2.69}$$

with the sum of squares of residuals expressed as:

$$SS_{res} = \sum_{i=1}^{n}\left(y_i - y_{i,cal}\right)^2, \tag{2.70}$$

and the total sum of squares as:

$$SS_{tot} = \sum_{i=1}^{n}(y_i - y_{mean})^2, \tag{2.71}$$

where $y_{mean}$is simple the mean value of the set of dependent variables. The more linear is the correlation between y and X and the closer R^2 is to 1.

2.12.6 Calibration free models

Chemometrics is a very useful tool to calculate calibration functions that can predict with high accuracy important parameters of a crystallization system, such as the solute

concentration or the polymorphic ratio. However, the calculation of a good calibration function requires many experiments, time and resources. To avoid waste of time and money many researchers proposed calibration free approaches (Barrett et al. 2010; Hao et al. 2010; Cornel and Mazzotti 2008). In this kind of methodology chemometrics is not used but only simple relationships between some spectroscopic data (peak heights, areas, shifts etc.) and the parameter to control (the solute concentration or the polymorphic ratio for example) are exploited. This kind of approach still requires a set of preliminary experiments to find the best spectroscopic parameter and to analyse its trend during a crystallization process. However, the number of experiments necessary to develop a calibration free control strategy is lower in comparison with the development of a good calibration function.

In 2010 Barrett at al. used the height of a peak in the ART-FTIR spectrum of benzoic acid in a solution of ethanol and water to perform supersaturation control during different crystallization processes. They also combined this strategy with a temperature cycle in order to obtain a better final crystal size distribution. More recently Duffy et al. used the same approach in the antisolvent crystallization of paracetamol in acetone and water (Duffy et al. 2013). Hao et al. monitored the concentration of mannitol during a cooling crystallization using the relative intensities of two Raman peaks (Hao et al. 2010).A more complex approach was ideated by Cornel: Raman was used to monitor solute concentration and polymorphic ratio of L-glutamic acid in a seeded, isothermal transformation (Cornel and Mazzotti 2008). A combination of modelling and multivariate approach was used to determine the calibration function without performing too many experiments. Raman spectra during the polymorphic transition were also simulated using just few initial spectral data. However, this approach implies a good knowledge of the thermodynamic and kinetics of the substance studied for the development of the model which can, sometimes, require a large number of preliminary experiments.

2.12.7 Design of Experiments

Design of experiments is a common practice used to reduce the number of experiments needed for a calibration and, therefore, the time spent in calibrating. It is also a good approach in modelling to optimize the number and combinations of factors to consider in the simulations. A good design of experiments allows having a reliable calibration function with a reasonable number of experiments (Brereton 2003).

This technique is extremely useful in calibrations when multiple factors can affect the instrument response. For example, if ATR-UV/Vis is chosen to measure the concentration of a compound in a specific solvent during a crystallization process, all the factors that may change in the process and that can affect the spectrum, must be considered during calibration. If it is a cooling crystallization temperature will change, and because this parameter affects the UV spectra, the calibration set of experiments will have to include samples at different temperatures.

In order to have a suitable set of calibration samples all the affecting factors must be changed independently in the experiments. Factorial design is the simplest method to plan a set of experiments. In this method a number of levels for each variable must be chosen. The levels are the values of the independents factors that will be analysed. The maximum and minimum levels must be chosen in order to accurately represent the type of experiments where the calibration will be used. Once the number of independent factors, F, is determined and the levels, L, are chosen, the number of experiments required in the factorial design is given by F^L. Factorial design can be very time consuming if the number of independent factors is very high. In that case other approaches can be used, such as Box-Behnken, face-centered cube or central composite design (Brereton 2003).

The Box-Behnken design is an independent quadratic design that requires 3 levels of each factor. In this design the experimental values are at the midpoints of edges of the process space and at the centre as shown in Figure 2.16.

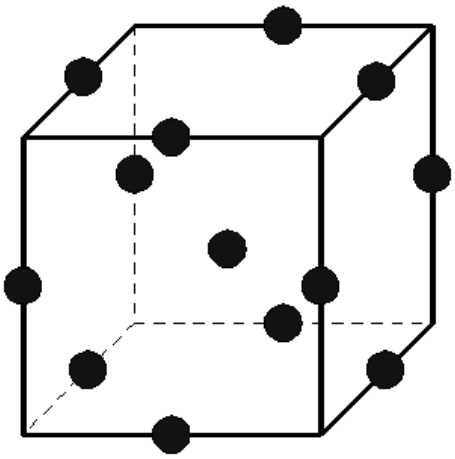

Figure 2.16: A Box-Behnken Design for Three Factors (http://www.itl.nist.gov/).

2.13 Feedback control for polymorphic systems

Chapter 6 of this thesis is focused on the development of a feedback control strategy (called active polymorphic feedback control, APFC) that detects and eliminates an undesired polymorph during batch crystallization processes, allowing the growth of the desired form. This innovative strategy combines Raman and ATR-UV spectroscopy and consist of a dissolution cycle triggered by the Raman signal that eliminates the unwanted form, and then a supersaturation control (using the ATR-UV/Vis signal) over the desired polymorph.

The most common PAT tools used for monitoring polymorphic transformations are near-infrared (NIR) and Raman spectroscopy, although FBRM and ATR-FTIR are also used to indirectly detect a change in the polymorphic form. Recently, new techniques such as ATR-MIR and advanced particle analysing system (APAS) were tested for the crystallization of paracetamol and L-glutamic acid (Helmdach et al. 2013). Raman spectroscopy is particularly sensitive to changes in the polymorphic form and the spectra are not influenced by water. However, for quantitative monitoring of polymorphic crystallization processes calibration experiments are required; the Raman spectrum is influenced by many parameters in addition to the polymorphic form and composition, (e.g. slurry density and particle size) and the calibration of a specific system can be challenging (Helmdach et al. 2013). This is probably the main reason why Raman has not been exploited often as a feedback control tool. One of the first concepts that aimed to use information from the Raman spectroscopy to detect the formation of an unwanted polymorph to change operating condition of a crystallizer was proposed by Pataki et al (2012). In their work Raman spectroscopy was used to detect the presence of the metastable form of carvedilol. In the case of the presence of the undesired form, the solution was heated up until complete dissolution and then cooled down with a different cooling rate to favour the nucleation of the stable polymorph. This approach in principle leads to the adaptive redesign of the operating conditions of the crystallization process by repeated recrystallizations of the product with decreasing cooling rate until the formation of the stable form is detected, and it is not an actual feedback control technique, as it did not attempt to control the crystallization in the phase diagram directly, to avoid the formation of the unwanted form. Seeding with the desired polymorph is used most often in the literature as a way of controlling the polymorphic purity. Most approaches proposed use then in principle trial-and-error approaches, albeit greatly enhanced by the use of PAT

tools, to design the operating trajectory that promotes the formation of the wanted polymorph, and only a few papers apply supersaturation control for direct feedback control. A list of control strategies used by researcher for polymorphic systems is shown in Table 2.3. Most of these studies indicated that supersaturation control is an effective way to control the supersaturation and growth of crystals and reduce spontaneous nucleation in order to reduce the amount of fine crystals or the nucleation of unwanted polymorphs (Saleemi et al. 2012b; Nagy 2012; Nagy et al. 2013), however it does not provide a suitable control approach alone, in the case of contaminated seed crystals or when the nucleation of unwanted polymorphic form does occur during the crystallization. Overall, most of the approaches available in the literature are not applicable in the case of contaminated seed with variable level of polymorphic impurity. In these cases controlled dissolution can be used to eliminate the unwanted polymorph. Controlled dissolution cycles have been used for the control of size distribution (Abu Bakar et al. 2009; Abu Bakar et al. 2010), with the cycles designed using model-based approaches for batch or continuous crystallization systems (Majumder and Nagy 2013b) or using model-free techniques based on direct measurement of particle counts using FBRM, such as the direct nucleation control (DNC) approach (Nagy et al. 2011; Saleemi, et al. 2012a; Saleemi et al. 2012). Abu Bakar et al. used a model-free temperature cycling approach to control simultaneously size uniformity and polymorphic purity of sulfathiazole crystals in batch crystallization (Abu Bakar et al. 2009) by using the DNC approach to eliminate the newly nucleated particles, assuming those consist of unwanted polymorph, and promoting the growth of the seeded crystals. The approach, however, similarly as the other techniques would not work in the case of contaminated seed as the undesired polymorphic form is not directly detected. Generally speaking the control of the desired polymorph can be achieved in different ways: (i) the desired form can be seeded during a cooling crystallization and its growth can be determined by a supersaturation control; or (ii) in the case of unseeded system with the potential nucleation of a mixture of polymorphs, the less stable form can be dissolved by heating the solution and the suspersaturation control can be imposed to let the stable form grow. In both cases, e.g. of seed is contaminated with the unwanted polymorph or a mixture of polymorphs nucleates, the use of a direct detection of the presence of the unwanted polymorph (e.g. by using Raman spectroscopy) and then the trigger of a controlled dissolution cycle can significantly improve the robustness of the control approach. All control strategies proposed in the literature so far either use the Raman system only to detect the formation of the unwanted polymorph as a trigger to

restart the crystallization with a different cooling rate, or use only supersaturation control in conjunction with the suitable seed to drive the system in the phase diagram to obtain the desired polymorphic form. In this thesis for the first time the active polymorphic feedback control (APFC), which is a combined control strategy using directly the Raman signal and the supersaturation feedback control approach for increased robustness, is proposed.

Table 2.3: Control strategy used by researcher to control the crystallization of polymorphic compounds.

Control strategy	Reference
Seeding the desired form between the solubility curve and the metastable limit line in order to avoid the nucleation of the other form and keep cooling until the supersaturation is consumed	Threlfall 2000; Beckmann 2000
Finding the correct amount of seed above which secondary nucleation of the metastable form is suppressed and solution-mediated transformation is avoided in a cooling crystallization.	Doki et al. 2003
Seeding during a cooling crystallization and using focused beam reflectance measurement (FBRM) in combination with ATR-FTIR to check the total counts and the supersaturation in order to reach the desired size of the crystals and eliminate the fines.	Doki et al. 2004
T-control and C-control for the conversion of the metastable form of a polymorph to its stable form (simulation and experimental work)	Hermanto et al. 2007; Kee et al. 2009; Hermanto et al. 2009
Seeding and growth of the metastable form during a cooling crystallization performing supersaturation control	Kee et al. 2009; Chew et al. 2007
Combination of anti-solvent and cooling crystallization was performed to obtain the desired form of indomethacin in acetone	Minamisono and Takiyama 2013
Feedback control of the reactive crystallization of L-glutamic acid in a semi-batch precipitation was conducted using MID-IR or Raman, ATR-FTIR and a pH-meter	Qu et al. 2009; Alatalo et al. 2010

2.14 Conclusions on literature review

This chapter illustrated basics of crystallization, polymorphism, PAT tools and chemometrics. The background covered in the chapter has been used to plan and interpret the experimental and modelling work done in this thesis. PAT tools have been used to study polymorphic transformations during crystallization processes as well as to understand the effect of solvent and additive on polymorphism of ortho-aminobenzoic acid. Chemometrics techniques have been applied to qualitatively and quantitatively determine

the different phenomena during the experiments. A calibration has been performed to determine high quality measurement for solute concentration and polymorphic ratio in the solid phase.

3 Materials and instrumentation

The compounds and solvents used for the experiments are briefly described in this chapter together with the equipment available for the experiments. Different combinations of instruments (PAT tools and offline analysis) were used for the several sets of experiments conducted for this thesis work. The exact setup for each set of experiments will be described in each experimental chapter together with the specific methodology used.

3.1 Materials

3.1.1 Ortho-aminobenzoic acid (OABA)

The main compound used for the experiments is anthranilic acid purchased from Sigma-Aldrich. The material was found to be Form I with purity >98%. Anthranilic acid (2-aminobenzoic acid or ortho-aminobenzoic acid, OABA) is mainly used for the synthesis of benzofused heterocycles and other molecules such as tryptophan, tyrosine or phenylalanine. It is also used as intermediate in the production of dyes and pigments, while its esters can be used to prepare perfumes, pharmaceuticals and UV absorbers. OABA exhibits fluorescence when dissolved in ether, alcohol or glycerol (Susindran et al. 2012). It has three known different polymorphic forms: (i) Form I is the stable form at room temperature and is also the only one that presents zwitterions in the crystal structure, (ii) Form II is the most metastable at low temperature and it is usually obtained by cooling crystallization; it is enantiotropically related to form I (transition temperature around 60°C) and monotropically related to the relatively more stable form III (iii) Form III it is usually very difficult to nucleate during cooling crystallization from solution, it is normally produced by sublimation or by polymorphic transformation of form I at high temperatures. Form I and III are enantiotropically related with a transition temperature around 50°C (Jiang 2009; Jiang et al. 2010b; Jiang et al. 2010a). Figure 3.1a, b and c show the crystal structures of the three polymorphic forms (data from the Cambridge Crystallographic Data centre, WebCSD). Form I crystallizes in solution mainly with a prismatic shape while form II has needle morphology. The crystals of form III looks still prismatic although they are different from form I.

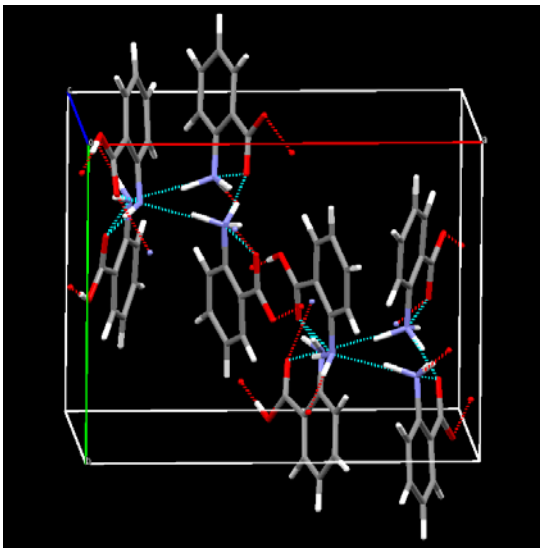

(a) Form I: orthorhombic cell, zwitterions and neutral molecules

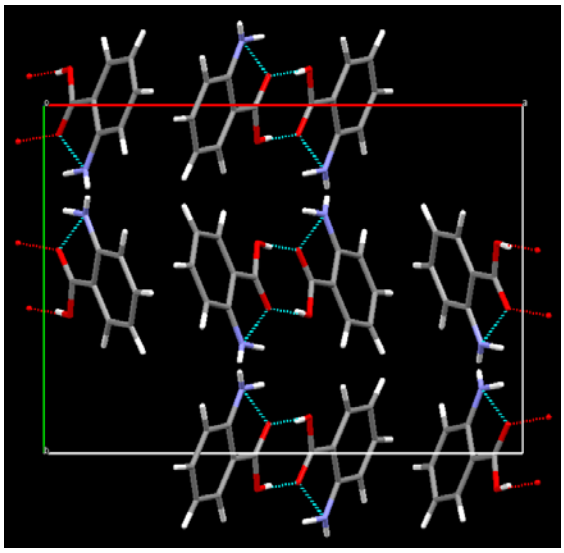

(b) Form II: orthorhombic cell, dimers of neutral molecules

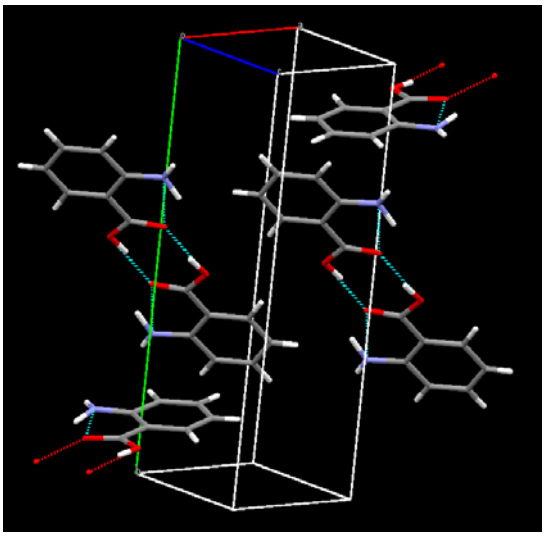

(c) Form III: monoclinic cell, dimers of neutral molecules

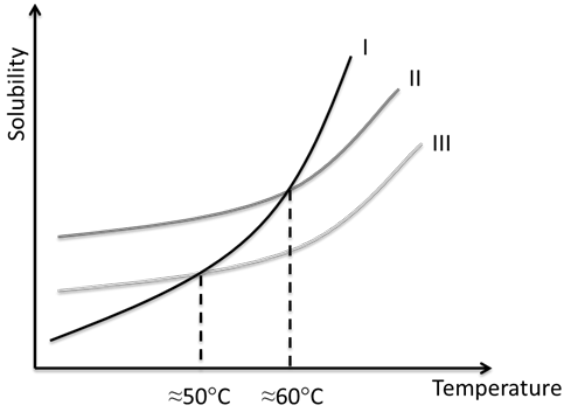

(d) Phase diagram of the three forms

Figure 3.1: (a) Molecular structure of anthranilic acid form I, view down the a-axis (Cambridge crystallographic data centre, reference AMBACO07) (b) Molecular structure of anthranilic acid form II, view down the c-axis (Cambridge crystallographic data centre, reference AMBACO03) (c) Molecular structure of anthranilic acid form III, view down the a-axis (Cambridge crystallographic data centre, reference AMBACO08) (d) Qualitative representation of the phase diagram for the three polymorphic forms.

The morphology of form III was difficult to determine as these crystals were obtained as solid solutions with benzoic acid and tended to agglomerate. Some microscopic pictures of the three forms are shown in Figure 3.2.

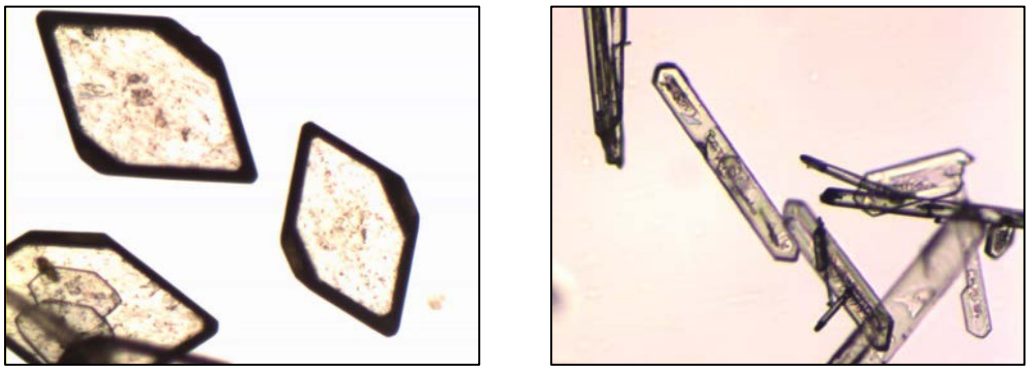

(a) (b)

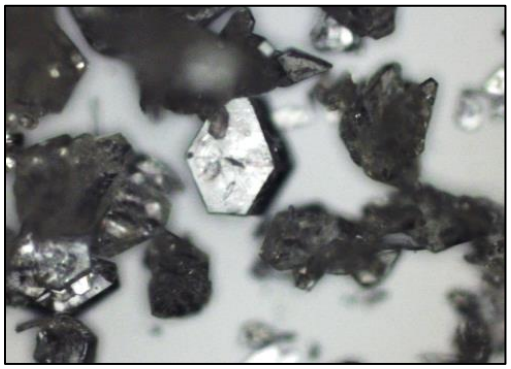

(c)

Figure 3.2: (a) Crystals of form I (b) Crystals of form II (b) Crystals of form III.

In chapter 4 OABA will be used as test compound to evaluate the potentiality of Raman spectroscopy to qualitatively and quantitatively determine the polymorphic composition of solid samples and slurries. In chapter 5 it will be used to prepare slurries and solutions in order to calibrate different PAT tools for the determination of solute concentration and polymorphic ratio in slurries. OABA will be the model compound for the active polymorphic feedback control strategy presented in chapters 6 and 7 and to prove the concept of composite PAT array in chapter 8. Chapter 9 will explore the solvent effect on the polymorphic outcome of OABA in cooling crystallization; and in chapter 10 the interaction with a structurally additive will be studied.

Figure 3.3 and Figure 3.4 show spectra of the solid OABA forms I and II, taken with NIR (Figure 3.3) and Raman (Figure 3.4). NIR spectra of form I and II present few and broad peaks but, nevertheless, discrimination between the two is possible. Figure 3.3a shows form I NIR spectrum while Figure 3.3b shows form II. Form II presents more peaks than form I, in particular in the region between 4000 and 5000 cm^{-1}. Two peaks are present in the region between 6000 and 7000 cm^{-1} for both polymorphs but their intensity is considerably higher for form II.

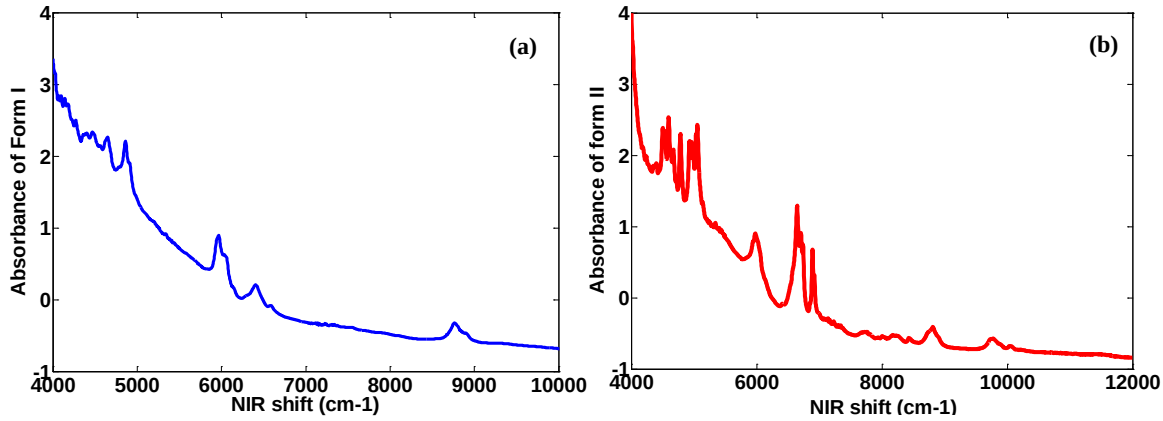

Figure 3.3: NIR spectra of OABA (a) form I and (b) form II. The regions with more differences are 6000-8000 cm^{-1} and 4000-5000 cm^{-1}.

Raman spectra present more peaks compared to NIR and the differences between the two polymorphs are numerous as shown in Figure 3.4a and b. Both OABA form I and II solids have two characteristic peaks in the region 817-786 (peak 1) and 786-755 cm^{-1} (peak 2) (Jiang et al. 2008).

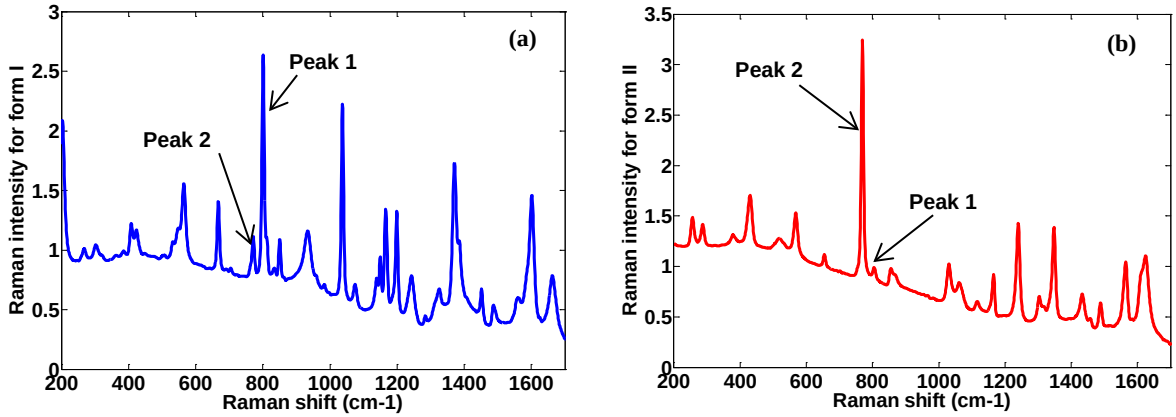

Figure 3.4: Raman spectrum of OABA (a) form I and (b) form II.

The more intense peak for form I is at 817-786 cm^{-1} while for form II is between 786-755 cm^{-1}. Form I also presents strong characteristic peaks at 1038 cm^{-1} and 950 cm^{-1} as shown in Figure 3.4a.). Looking at mixtures at different ratios of form I and II it can be observed that when the ratio of form II increases the intensity of peak 2 increases. At the same time there is a decrease in the intensity of peak 1. So it is possible to differentiate if a solid sample is pure form I, form II or a mixture. This characteristic trend is due to the fact that vibrations of different chemical bonds are affected by the crystalline arrangement. In the case of OABA, the crystal structure of form I allows more easily vibrations in the region

817-786 cm^{-1} while vibrations in the region 786-755 cm^{-1} are not favoured. The structure of form II instead favours vibrations in 786-755 cm^{-1} and partially blocks the ones in 817-786 cm^{-1}. It can be noted that the two studied peaks are both corresponding to ring vibrations of benzene derivatives.

Solubility of the two polymorphic forms of OABA

Three different methods were used to measure the solubility of OABA polymorphs I and II in the chosen solvent (10% w/w IPA and water):

- The Avantium Crystal 16 (turbidity probe);
- A thermogravimetric method;
- A spectroscopic method (ATR-UV/Vis).

Avantium Crystal 16

Vials of about 1 mL volume were filled with the solvent (10/90 w/w solution of IPA and water) and different amount of either form I or II of OABA. The slurries were then inserted in the Crystal 16 (a system of sixteen small stirred reactors with controlled temperature) and a slow heating rate of about 0.1 °C/min was applied. Complete dissolution of the solid was recorded by a turbidity probe and that temperature was taken as the saturation temperature of the sample. Data were processed using the CrystalClear software (Avantium). Results are shown in Figure 3.5.

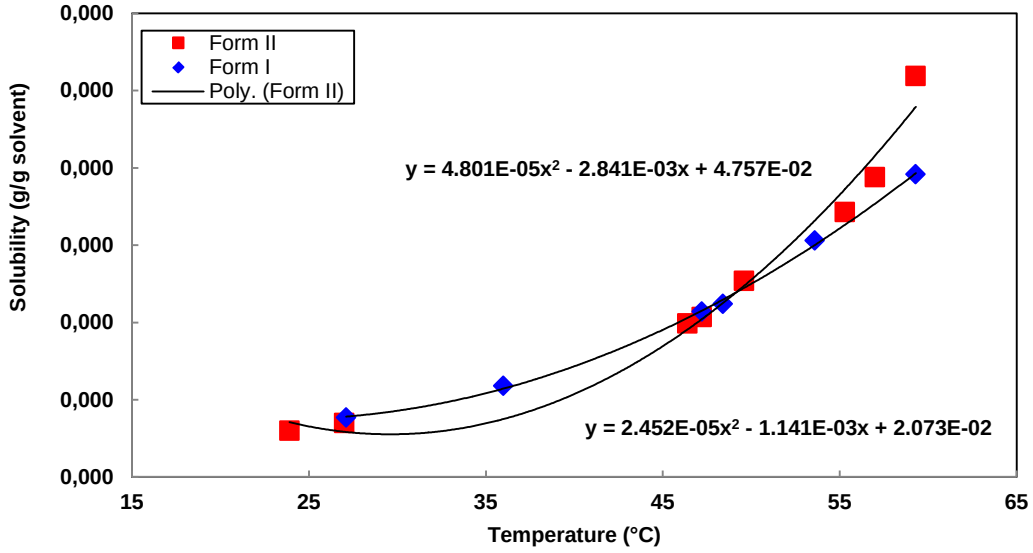

Figure 3.5: Solubility of OABA form I and II in solution 90:10 w/w water:IPA measured with the Crystal16.

Thermogravimetric method

Two suspensions of the OABA polymorphs I and II were prepared in the chosen solvent. Temperature was raised in steps of five degrees from 10 to 50 °C. Each step was 3 hours long for form I and only 1 hour long for form II to avoid polymorphic transformation during the measurement. As temperature got closer to the transition temperature (50 °C), the step time for form I was reduced to one hour, again in the interest of preventing a polymorphic change. For each temperature step three samples were taken, the liquid phase was separated from the solid in suspension though filtration and then left to evaporate at 40 °C for 24 hours. At high temperatures, the pipette and containing dishes were heated to prevent an undesirable rapid nucleation of the sample. The containing dishes were weighed before taking the sample (w_0 empty dish weight), before drying (w_w wet dish weight), and after drying (w_d dry dish weight). Solubility *S* was then obtained using the formula:

$$S = \frac{(w_d - w_0)}{(w_w - w_d)} \tag{3.1}$$

The results of the measurements are shown in Figure 3.6:

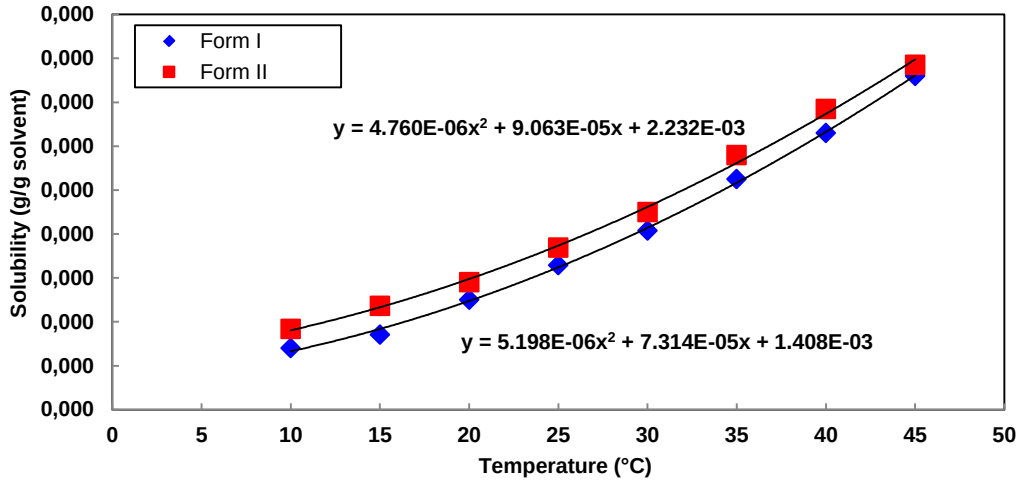

Figure 3.6: Solubility of OABA form I and II in solution 90:10 w/w water:IPA measured with the thermogravimetric method.

Spectroscopic method

A large amount of OABA was added to the solvent and heated up until complete dissolution at around 80°C. The solution was kept as such a high temperature only for 30min in order to avoid decomposition and solvent evaporation. Form II was then nucleated applied a fast cooling rate (-1°C/min) and temperature was dropped to 10°C and

kept for about 1 hour. After that temperature was raised to 20°C and kept for another hour and a similar procedure was done for 30 and 40°C. Concentration at the different temperatures was calculated using the same calibration method exploited for the supersaturation control (SSC) experiments. Excel and Matlab were used for the processing and interpolation of the data. The same procedure was repeated for form I but with a smaller supersaturation and slower cooling rate in order to nucleate form I. Figure 3.7 shows the solubility curves measured with the spectroscopic method. During some preliminary experiments of heating and cooling both form I and II it was found that this method gives the more reliable data. The equations found were successfully implemented in CryPRINS for the supersaturation control of OABA form I in chapter 6.

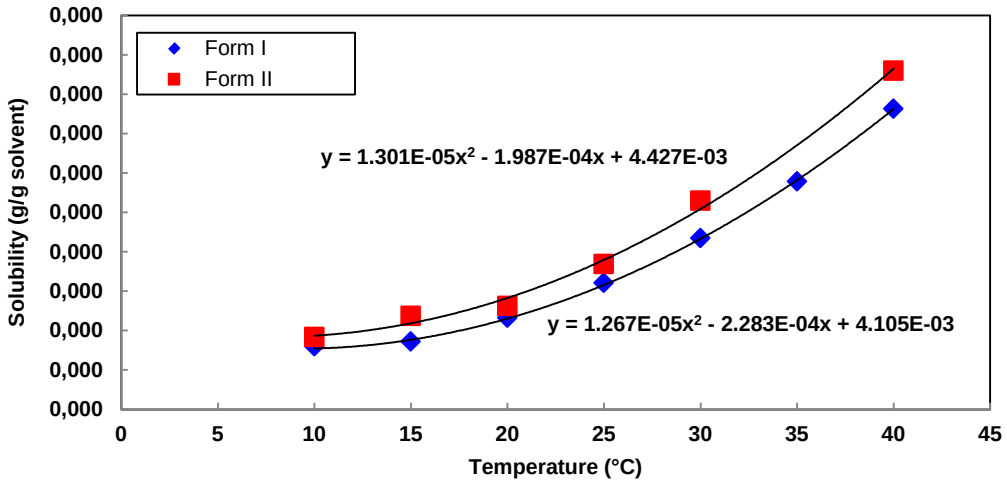

Figure 3.7: Solubility of OABA form I and II in solution 90:10 w/w water:IPA measured with the spectroscopic method.

3.1.2 Vitamin B12

Vitamin B12 (cobalamin) is one of the biggest and most complex vitamins and, in humans, it is required to assist the actions of two enzymes: methionine synthase and (R)-methylmalonyl-CoA mutase. It is commonly used to cure pernicious anaemia and its deficiency determines an increase in homocysteine levels that leads to a major risk for heart disease, stroke, atherosclerosis and vascular diseases. Despite the lack of solid evidences on the importance of vitamin B12 in maintaining normal myelination of nerve cells, its role in preventing many neurological and psychiatric symptoms is becoming clearer and clearer. For these reasons, every year, around 10 tons of the semisynthetic version of vitamin B12 (cyanocobalamin) are produced by biofermentation from several

bacterial species (Martens et al. 2002). A schematic of vitamin B12 molecule is shown in Figure 3.8. The molecule is fairly big and complex and can be divided in three parts: (1) a central corrin ring which contains four ligands for the central cobalt ion, (2) a lower ligand donated by the 5,6-dimethylbenzimidazole (DMBI) and (3) an upper ligand made from either an adenosyl group or a methyl group. Two crystalline forms were discovered by X-ray diffraction: a wet and an air-dried structure (Hodgkin et al. 1956; Hodgkin et al. 1955). The main difference between the two is the presence of water molecules in the crystal lattice that makes the unit cell of the wet form bigger than the air-dried. Cyanocobalamin is mainly produced by biosynthetic fermentation processes although a full chemical synthesis (consisting of 70 steps) was developed in the early 70s (Martens et al. 2002). High levels of impurities are present in the biosynthesized vitamin B12 that can inhibit growth and strongly affect the final crystal size distribution together with the ease of downstream processes (filtration in particular). Vitamin B12 is the biopharmaceutical compound studied in chapter 11 and 12.

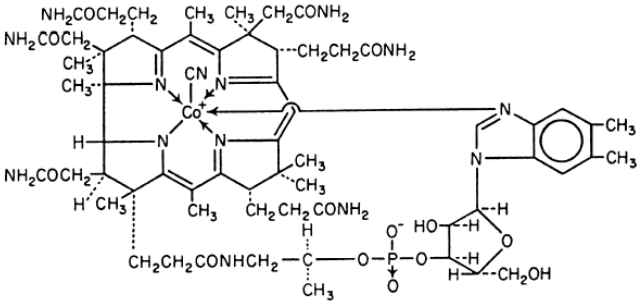

Figure 3.8: Molecular structure of cyanocobalamin. The CN group constitutes the difference from the natural vitamin B12 and it is the results of the extraction procedure by which the compound is removed from bacterial cultures (Martens et al. 2002).

Crude Vitamin B12 produced by fermentation was donated by Hebei Welcome Pharmaceutical Co., LTD (China). The raw material consisted in a dry powder containing around 7% of impurities. Those were mainly byproducts of the fermentation process (e.g. 50-carboxyl cyanocobalamin, 34-methyl cobalamin, 8-epi-cyanocobalamin and cyanocobalaminic lactate) and inert.

3.1.3 Solvents and additives

As solvents isopropyl alcohol (IPA 99.97% grade, Fisher Scientific), and ultrapure water obtained via a Millipore ultra-pure water system were used for the experiments with OABA. Vitamin B12 was crystallized from de-ionized water and mixtures of water and ethanol (purity 99.99%, Fisher Scientific). Benzoic acid purchased by Sigma-Aldrich (purity ≥99.5%) was used as structurally related additive in the experiments of chapter 10. Pure ethanol (Fisher Scientific with purity >95% v/v) was used in the experiments with vitamin B12 (chapters 11 and 12).

3.2 Equipment and rig used during the experiments

A simple schematic representation of the experimental rig used for the experiments of this thesis is shown in Figure 3.9 while a list of the instruments as well as a brief description of their characteristics is reported in Table 3.1. The pre- and post-processing of the data were done with Matlab R2013 and Excel 2010. The signals from FBRM, ATR-UV/Vis and the Huber were transmitted in real-time to the Crystallization process Informatics System (CryPRINS) software. This in-house software CryPRINS provides a communication interface via file transfer, OPC (Object linking and embedding for process control), RS232 or DDE (dynamic data exchange), with a variety of PAT tools and allows real-time monitoring of these signals, as well as setting a desired temperature profile and performing different types of feedback control. In particular, direct nucleation control and supersaturation control were performed with CryPRINS during the experiments performed for this thesis. Raman, NIR and PVM data was collected separately with the software packages of the respective instruments.

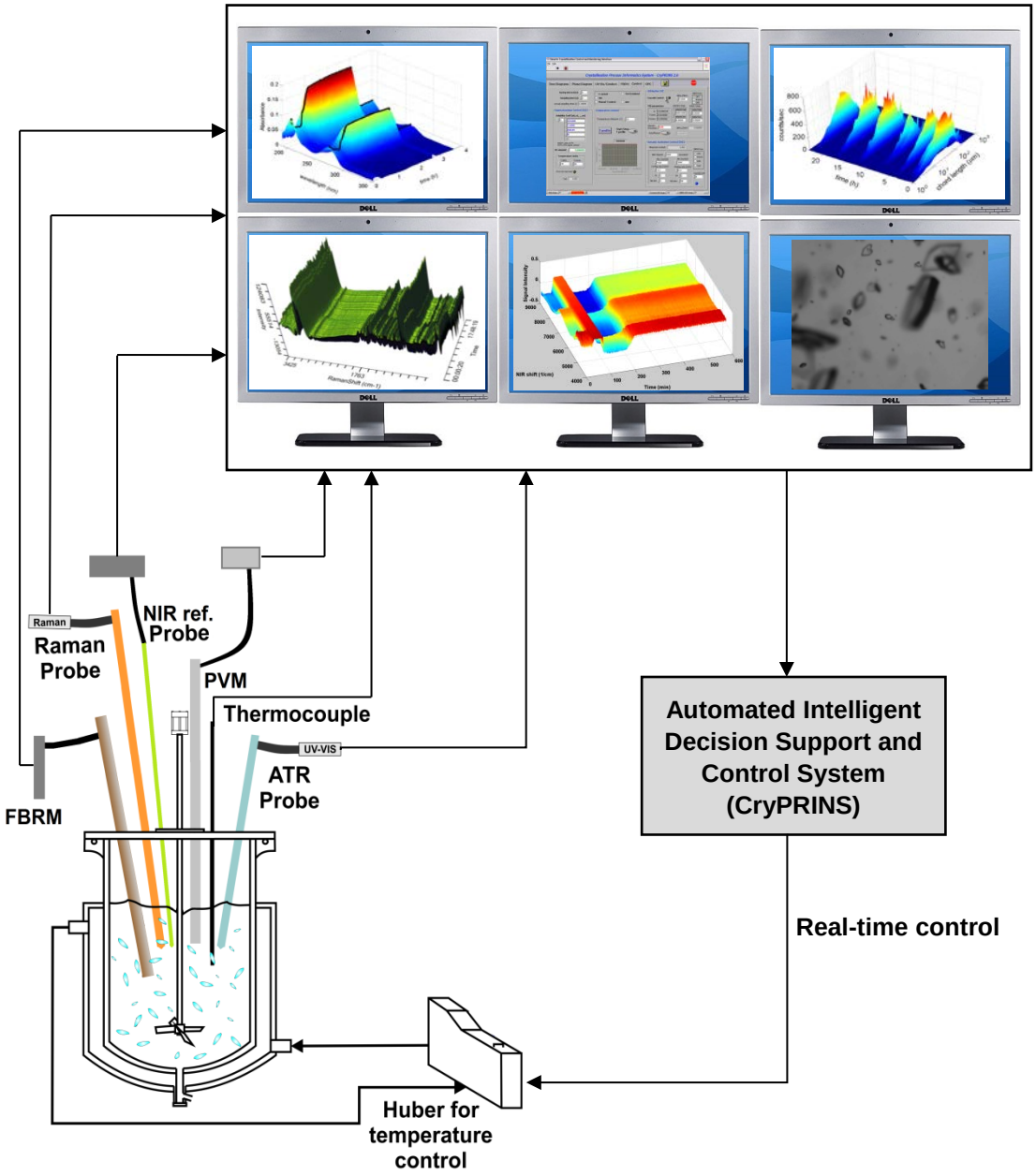

Figure 3.9: Schematic of the rig used during some of the experiments.

Table 3.1: Instruments used for the experiments

Instrument	Characteristics	Chapters in the thesis where the instrument was used
400 ml vessel	Glass jacketed vessel fitted with a retreat curved impeller. The temperature of the jacket was controlled by a temperature probe PT-100 connected to the Huber.	Chapter 4 to Chapter 12
Huber circulation thermostat	Model ministat 230-cc-NR controlled by CryPRINS	Chapter 4 to Chapter 12
Raman spectroscope	RXN1 Raman analyser with immersion and optical probe and 785 nm laser (Kaiser with iC Raman 4.1 software)	Chapter 4 to Chapter 10
NIR spectroscope	Matrix F FT-NIR analyser equipped with an IN268 NIR reflection probe and an IN271P NIR transflection probe (Bruker with OPUS 7.0129)	Chapters 5 and 8
FBRM	D600L Lasentec FBRM probe (Mettler Toledo with FBRM software V 6.7.0) connected to CryPRINS	Chapter 4 to Chapter 12
PVM	PVM V819 probe (Mettler Toledo with PVM on-line image acquisition software version 8.3)	Chapter 5 to Chapter 10
UV/Vis spectroscope	MSC621 Carl Zeiss ATR-UV/Vis analyser (with in-house LabView software) with Helma ATR (type 661.822-UV) probe connected to CryPRINS	Chapter 5 to Chapter 12
DSC analyser	Q10 DSC (Thermo analytics)	Chapter 4 to Chapter 12
X-ray diffractometer	D2-Phaser XRD (Bruker)	Chapters 6 and 10
ATR-FTIR spectroscope	Nicolet is50 ATR-FTIR (Thermo scientific equipped with OMNIC 7 software)	Chapter 10
HPLC analyser	HPLC Agilent 1100 series (Hewlett Packard) with ChemStation software rev. A.09.03[1417]	Chapters 10 to 12
Raman microscope	Model DXR 780nm (thermo Scientific equipped with OMNIC 8 software)	Chapter 4 to 12

3.3 Conclusions

The technical characteristic of the instruments used in this thesis were described in this chapter. In the last section a schematic of the setup is also presented. Additionally, the raw materials and solvents used for the experiments are described. Ortho-aminobenzoic acid

and its polymorphism are explained in detail. The main characteristics of vitamin B12 obtained by fermentation are also listed as well as some additional information on the history of this biomolecule.

4 Application of quantitative Raman spectroscopy for the monitoring of polymorphic transformation in crystallization processes using a good calibration practice (GCP) procedure

A good calibration practice procedure to quantify polymorphic purity of slurries using Raman spectroscopy is described in this chapter. The Raman signal and the possible parameters that can influence it during a cooling crystallization experiment are analysed in the first part of the chapter. The second part of shows the results of a systematic calibration conducted with design of experiments.

4.1 Introduction

Determining and monitoring polymorphic transformations has become very important, especially in the pharmaceutical industry since polymorphs of the same chemical compound can have different physical and chemical properties that can strongly affect the manufacturing process. Significant work has been done for the calibration of Raman spectroscopy to monitor the presence and amount of solid polymorphs in suspensions, as well as the liquid concentration during crystallization processes. Nevertheless, a clear and systematic approach to Raman calibration is missing in the literature. The aim of this chapter is to develop a methodical strategy for Raman calibration for the determination of polymorphic ratio of slurries in cooling crystallization processes. The principal factors that can affect the Raman spectra of a specific compound in solution, such as solid type, solute concentration, temperature, crystal size and solid concentration were taken into account. Furthermore, the effects of those factors have been studied in more details to determine if they can be effectively modelled with a linear calibration approach. Univariate and multivariate calibration techniques were investigated using several pre-processing techniques to optimize the signal. The results are combined in a systematic “good calibration practice (GCP) procedure”, that allows obtaining high quality measurement with a reduced amount of experiments.

4.2 Methodology, materials and equipment

4.2.1 Materials and Equipment

Form I and II of ortho-aminobenzoic acid were used for the experimental work of this chapter. OABA form II was prepared in laboratory by cooling crystallization in the jacketed vessel described in the methodology chapter. Form I of OABA was dissolved in pure isopropyl alcohol and heated up to 60 °C. The temperature was kept constant for 15 min in order to reach a complete dissolution and then dropped to 20°C. Crystals of form II were rapidly filtrated and dried to avoid polymorphic transformation in solution. Differential scanning calorimetry (DSC) and Raman spectroscopy were used to check the purity of form II. Calibrations of slurries were conducted using the same stirred vessel with temperature controlled via the CryPRINS software. The vessel was provided with a condenser to avoid loss of solution via evaporation during the experiments. Raman, PVM and FBRM were used for the experiments.

4.2.2 Effect of solute concentration on the Raman spectra

In order to study the effect of solute concentration on Raman signal a solution of 10% IPA and 90% water (w/w) was prepared and held at 40°C during the experiment. Solid OABA form I was added in steps and dissolved in the solvent (+1.01 g, +1.13 g, +1.25 g, +1.60 g). The maximum concentration reached was below the saturation point; therefore, all the measurements were taken in clear solution. Three Raman spectra were collected for every concentration. A time exposure of 10 s was used and the total number of scansions was 10. For the multivariate analysis K-fold cross validation was performed to choose the correct number of components or factors, which is the one which minimizes the root mean square error of cross validation (RMSECV).

4.2.3 Effect of crystal size on the Raman spectra

Raman spectra are affected by the crystal size as previously demonstrated by Chen et al. (2012). A more detailed study on this phenomenon has been done in this work using OABA form I solid powder with different sizes. Metallic sieves were used to produce four different size fractions: (1) 63-75 µm, (2) 75-125 µm, (3) 125-150 µm, and (4) 150-250 µm. For each solid mixture, three measurements were taken using a non-contact NCO-1.3-VIS/NIR Raman probe at a distance of 2.5 cm from the samples. The exposure time was 10 s and 17 scansions were taken for each measurement. Every sample had the same mass

and approximately the same volume (some mixtures were compressed in order to have always the similar volume); in order to minimize the differences between samples. Multiple series of experiments were conducted to evaluate the consistency of the results. Two further experiments were carried out in slurries to investigate the effect of crystal size on the spectra collected with the immersion probe. A solution of IPA and water (10% w/w IPA) was prepared and OABA form I was added in order to obtain a saturation temperature of about 40 ºC. The temperature was kept at 38 ºC for 30 min, then the solution was cooled down slowly to 33ºC, kept for 1 h, cooled down again to 28°C and kept for an additional hour. The temperature effect on the Raman signal within a range of ten degrees is negligible. The seeds were added at a very low supersaturation so that nucleation was avoided. FBRM was used to check the presence of nucleation and to confirm the growth of the crystals during the experiments.

4.2.4 Effect of solid concentration on the Raman spectra

The experiment was conducted in water at a constant controlled temperature of 20 °C. OABA has very low solubility in those conditions (0.35g OABA/100 g water). Form I was added progressively in the solution and 5 measurements were taken after each addition in order to have Raman spectra at different solid concentration in water.

Table 4.1: Solid added, exposure times and solid concentration during the experiments performed to check the effect of solid density on Raman spectra

Sample	Solid added (g)	Exposure time (s)	Solid concentration (g solid/100 g solution)
1	4.68	10	1.21
2	6.25	10	3.29
3	10.95	5	6.94
4	10.49	5	10.44
5	8.68	4	13.33

For every new addition the time of exposure had to be reduced in order to have a clear Raman spectrum (a larger amount of solids generates a stronger Raman signal with the effect of a possible saturation of the instrument). The number of scansions was adjusted accordingly with the decrease of the exposure time in order to have the same signal to noise ratio in all the measurements. The most important variables of the experiment are shown in Table 4.1: these are amount of solid added in each measurement, exposure time and solid concentration of the suspension.

4.2.5 Effect of temperature on the Raman spectra

The effect of temperature on Raman spectra is more difficult to study because the solubility of OABA varies with this parameter. In the case of suspensions of solids, an increase of the temperature will provoke the dissolution of part of the solids and thus a change in their concentration. Moreover, solids in suspension can grow and nucleation can occur, making even more difficult to distinguish between the effect of temperature and crystal size or suspension density. For these reasons the effect of temperature was studied on clear solutions in the absence of solid particles. Clear solutions at constant concentration of OABA form I in a mixture of ethanol and water (50/50 w/w) were used. The choice of a different solvent was to avoid overlapping peaks with OABA. Ethanol has characteristic peaks which are less overlapping with the typical peaks of OABA compared to IPA. Five measurements were taken for each temperature with 5s time of exposure and 20 scansions. Five temperatures were tested: 20 °C, 30 °C, 40 °C, 50 °C and 60 °C.

4.2.6 Calibration of solid samples of OABA form I and II

The aim of these experiments was to build a calibration model for the quantification of the mass fraction of solid OABA form II using Raman spectroscopy in powder mixtures of both form I and II. Dry mixtures were prepared using different proportions of form I and II (0, 25, 50, 75 and 100%). The crystal size of the two forms was the same 75-150 µm (sieves were used to prepare the samples of each form). Each sample was agitated by hand for 5 min before the first measurement and then agitated again for about 1 min before each other measurement. A Raman non-contact NCO-1.3-VIS/NIR (Kaiser optical systems) probe was used. The samples were put on a paper and arranged in a circular shape of 3 cm of diameter. Five measurements were taken and for each measurement three samples were collected from different points of the samples. A comparison with a NIR Q412/A-Ex

(Bruker) emission probe was also performed to investigate the effect of the slot area and the accuracy of the Raman non-contact probe.

4.2.7 Calibration of solid mixtures of form I and II in suspensions of IPA and water

A Box-Behnken design of experiment approach was used to plan the experiments considering the factors that affect Raman spectra the most and the ones that could be easily controlled: solute concentration, solid concentration and polymorphic ratio.

Table 4.2: Box-Behnken design of experiment for the calibration of polymorphic concentration in solutions of water and IPA

Experiment	Temperature (°C)	Polymorphic ratio (%)	Total solid for 100g solvent (g)
1	10	0	0.775
2	10	100	0.775
3	40	0	0.775
4	40	100	0.775
5	10	50	0.3
6	10	50	1.25
7	40	50	0.3
8	40	50	1.25
9	25	0	0.3
10	25	0	1.25
11	25	100	0.3
12	25	100	1.25
13	25	50	0.775
14	25	50	0.775
15	25	50	0.775

Solute concentration is dependent only on temperature for saturated solutions in the presence of suspended solids so that was considered as the changing factor. This type of design allows considering more factors with a restricted number of experiments. It is a typical three level approach. The upper and lower levels for each factor must be chosen in this approach. Because the calibration is for a cooling crystallization it was decided to work in a range of temperature from 10 to 40 °C, and the maximum solid content was chosen as the amount of solids needed to produce a 40 °C saturated solution. The minimum was chosen arbitrary considering a 10° C saturated solution. Table 4.2 reports the experiment planning. Each experiment was conducted at constant temperature (10, 20, 30 and 40 °C). OABA form I or II was dissolved in the solvent until saturation of the solution and kept for at least 30 min. Then, the other form was added in order to reach the desired polymorph ratios and measurements were rapidly taken (2 samples for each measurement). Each sample was the result of 10 scansions with an exposure time of 10 s.

4.3 Results and discussion

4.3.1 Effect of solute concentration

The effect of solute concentration was studied using both a univariate and multivariate approach. In both cases it was found that the effect of solute itself on Raman is linear, and an increase in concentration generates an increase in the intensity of the characteristic peaks of OABA (as shown in Figure 4.1).

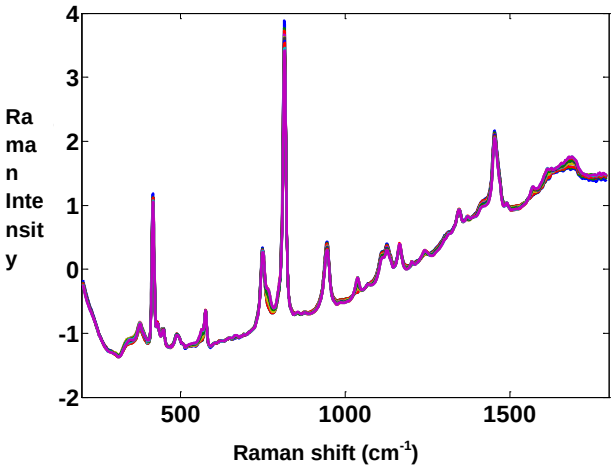

Figure 4.1: Effect of solute concentration of OABA on Raman spectra. The signal of the specific peaks of OABA increases with increase of concentration.

While for some compounds it is possible to find specific peaks for the solute (Hu et al. 2005), for OABA a peak corresponding to the dissolved molecules only was not identified. For the univariate analysis six different peaks were studied as reported in Table 4.3. Second derivative was calculated in order to have narrower peaks and eliminate the baseline shift generated by fluorescence; smoothing was performed using iCRaman. In order to find a correlation between Raman signal and solute concentration the area under the chosen peaks was considered. Results are shown in Table 4.3 and Figure 4.2.

Table 4.3: Raman peaks analysed for the univariate study of solute concentration effect on spectra and results of univariate interpolation performed in Excel. C is the solute concentration while A is the area of each chosen peak

Peak number	Region of the spectrum (cm^{-1})	Linear function of peak area (cm^{-1})	Correlation coefficient
1	1175-1164	C=0.2709A+0.0062	0.9843
2	1046-1025	C=0.6707A-0.0006	0.9967
3	777-759	C=0.7031A-0.0129	0.9975
4	570-556	C=0.6583A-0.012	0.9965
5	1496-1484	C=0.4616A-0.0013	0.9881
6	1573-1561	C=0.4306A-0.0008	0.9884

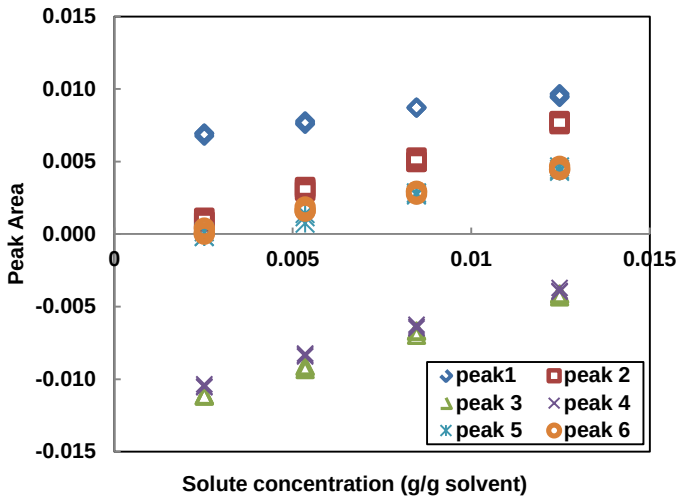

Figure 4.2: Trends of the chosen peak areas as a function of solute concentration (peak specifications shown in Table 4.3).

The trend is linear from the univariate analysis but each peak increases in intensity with a slightly different slope. A multivariate approach was also used considering the region between 200 and 1800 cm^{-1}. Spectra were only smoothed with 11 points windows and a 2^{nd} order polynomial function. Both PCR and PLSR approaches were performed in Matlab 2012, with PLSR giving better results: using 5 factors the correlation coefficient is 1.0000 with root mean square error of calibration (RMSEC) of 2.64E-09 and root mean square error of prediction for the cross validation (RMSECV) of 3.47E-08. With both the univariate and multivariate approaches the effect of solute concentration on the Raman spectra is linear and in particular, increasing the concentration generates an increase in the signal.

4.3.2 Effect of crystal size

Many attempts were conducted to find a correlation between particle size and Raman spectra (Hu et al. 2006; Cornel et al. 2008; Allan et al. 2013). However, a characteristic trend and a clear explanation of this effect has not yet been found, partly due the dependence on the type of probe and the sampling conditions. In this section both the non-contact and the immersion Raman probe were used to analyse how the size of the OABA particles affect the Raman signal. Figure 4.3 shows the spectra for different solid samples after a baseline correction.

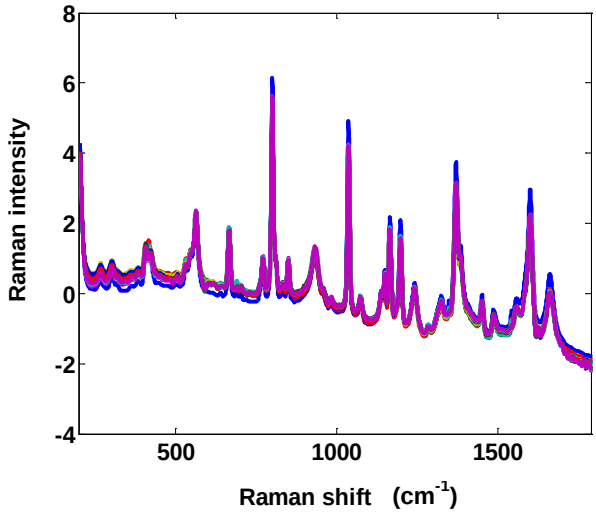

Figure 4.3: Spectra of OABA form I for samples with different size of the crystals (Autoscaled and smoothed).

Two series of experiments were conducted on solid powders but a specific trend between the Raman signal and the mean size of the particles was not found. The difference in intensity in the raw spectra of the several samples is small and it is difficult to understand if the signal increases or decreases with the particle size. The effect of size and packing is not clear from the literature and probably minor differences in the preparation of the sample as well as in the type of probe used can strongly affect the measurement considering the high sensitivity of Raman spectroscopy. However, results indicate that pre-processing can reduce the differences between the spectra of solid samples. Different pre-processing techniques, such as standard normal variate (SNV), normalization, baseline corrections of different orders, 1st and 2nd order derivatives, etc. were evaluated to find the best combination that reduces the effect of crystal size on Raman spectra of solid powders. The combination of SNV, 1st derivative and normalization was found to be the most effective in reducing this effect. Eight peaks were analysed, and the corresponding region of the spectrum are shown in Table 4.4.

Table 4.4: Peaks analysed for the evaluation of the effect of crystal size on Raman spectra.

Peak number	Region of the spectrum (cm^{-1})
1	809-795
2	1700-1625
3	1625-1572
4	1050-1020
5	1381-1050
6	1220-1180
7	1180-1157
8	681-650

The signal intensity of the different peaks, for samples with different particle size, and different pre-processing techniques is shown in Figure 4.4. For the first series of experiments a slight increasing in the signal is associated with the increase in crystal size. The use of SNV correction partially eliminates this trend, as well as the second derivative and the normalization of all the spectra for the same peak at 801 cm^{-1}. The combined used of SNV and derivative for eliminating scattering effect was already tested and known to be effective (Huang et al. 2010). The second series of data still shows a slightly increasing

trend apart from the data at 125 µm. With the same pre-processing techniques, the differences between the samples are almost completely eliminated even for this series of experiments (see Figure 4.5). As shown in Figure 4.4 and Figure 4.5 good pre-processing can eliminate the effect of crystal size in the solid sample using the non-contact probe available.

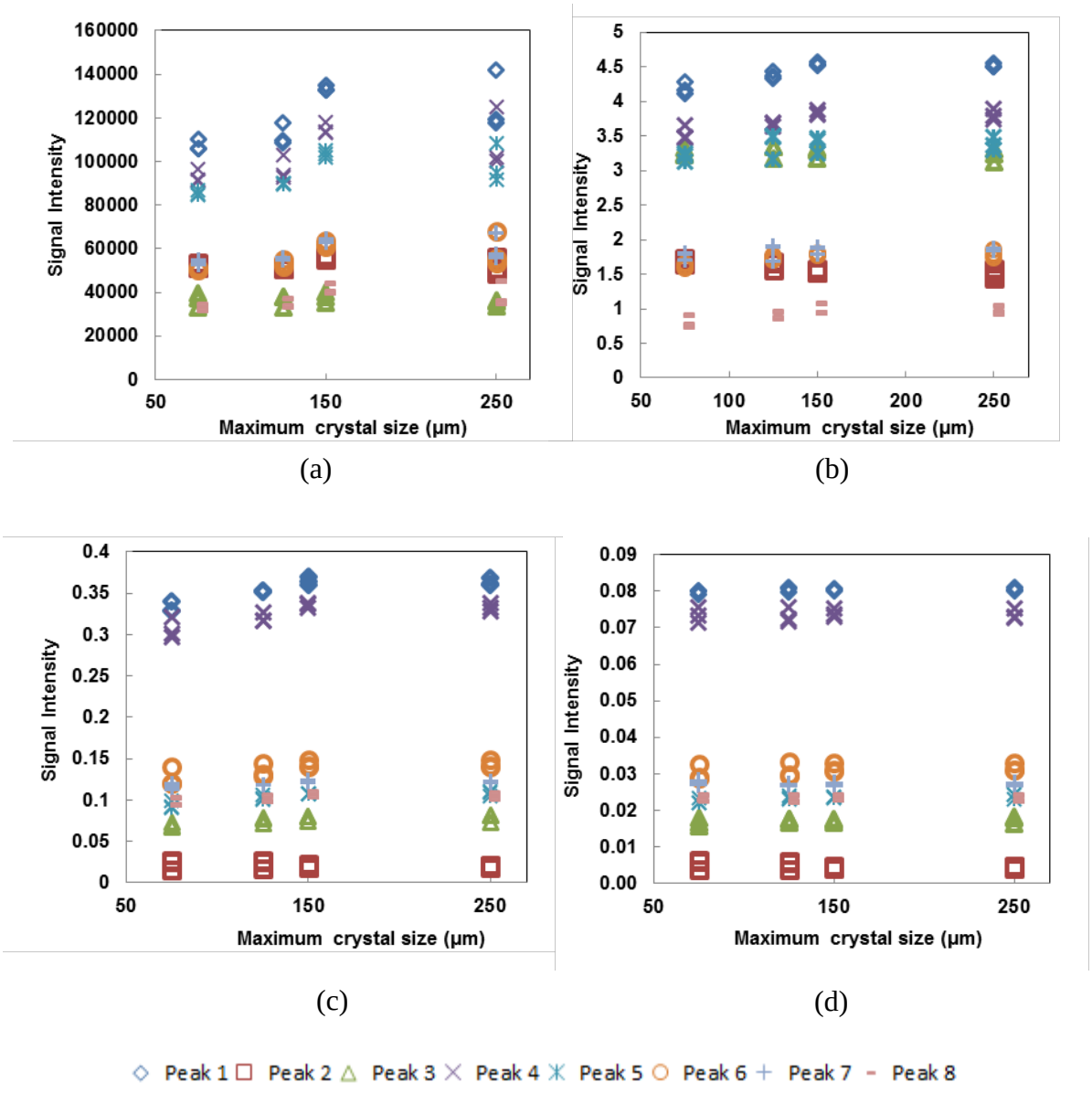

Figure 4.4: Signal intensities of the chosen peaks for the first set of samples at different crystal size (peak specifications in Table 4.4). Pre-processing was performed in iC Raman:(a) 3rd order baseline correction; (b)3rd order baseline correction and SNV; (c)3rd order baseline correction, SNV and 2nd derivative; (d) 3rd order baseline correction, SNV, 2nd derivative and normalization with peak at 801cm^{-1}.

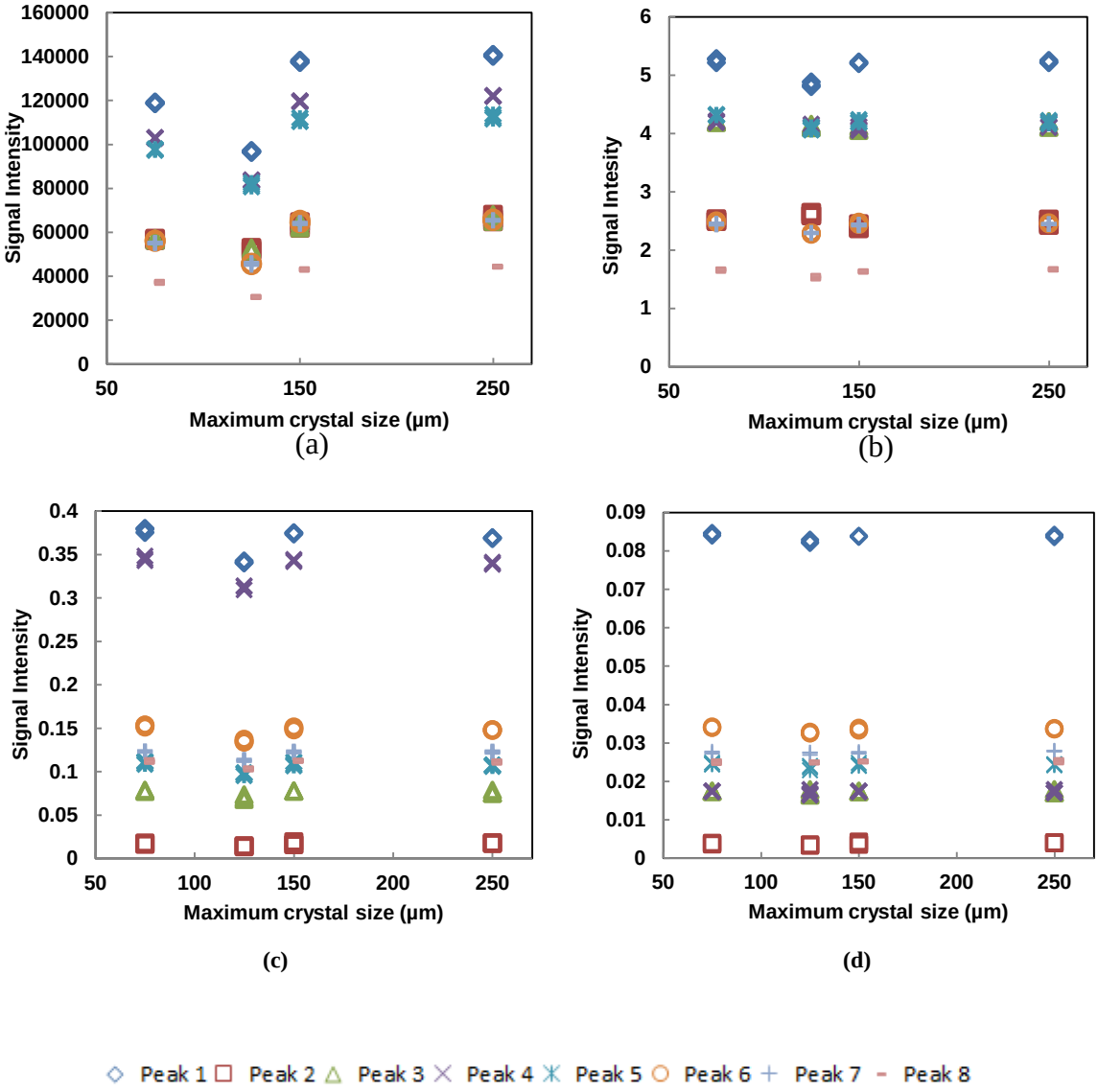

Figure 4.5: Signal intensities of the chosen peaks for the second set of samples at different crystal size (peak specifications in Table 4.4). Pre-processing was performed in iC Raman: (a) 3rd order baseline correction; (b) 3rd order baseline correction and SNV; (c) 3rd order baseline correction, SNV and 2nd derivative; (d) 3rd order baseline correction, SNV, 2nd derivative and normalization at 801cm^{-1}.

A further set of experiments was carried out to investigate the effect of crystal size on the measurements obtained in slurry using the immersion probe. Specific peaks were tracked during the experiments and FBRM and PVM were used to check the crystal growth and nucleation. The material at the beginning and at the end of the experiment was filtered and analysed with an optical microscope to check the increase in size. Two experiments were conducted using similar seeds and seed load but experiment 2 presented agglomeration of

the particles while experiment 1 did not. However, in both cases, the final size of the crystals was considerably higher than the initial one as shown by the chord length distribution measured by FBRM. Figure 4.6 shows the total counts registered by FBRM and the temperature profile for experiment 1.

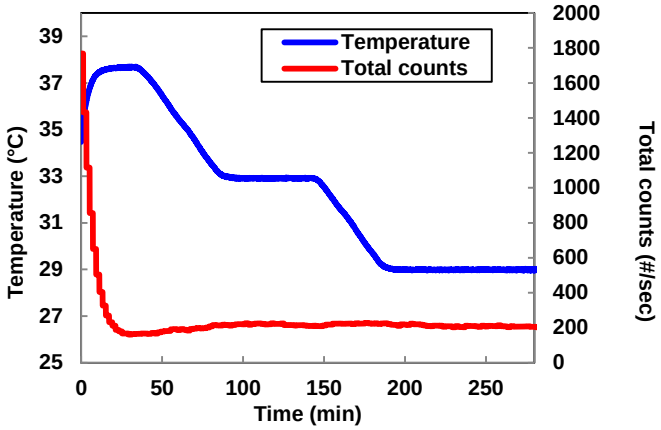

Figure 4.6: Temperature profile and total counts recorded by FBRM during Experiment 1.

The total counts go down rapidly in the first 25 min as the seeds partially dissolved in the solution; then it remains constant for the rest of the experiment. The trend of the total counts shows that during the cooling phase there was no nucleation, so only growth was happening in the system. The growth of the crystals is well visible in the chord length distribution trend recorded by FBRM at different times during the batch (Figure 4.7).

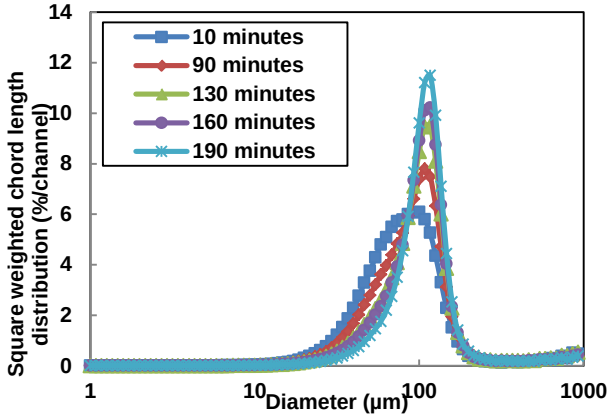

Figure 4.7: Crystal size distribution during Experiment 1 during the study of the effect of crystal size on Raman spectra.

The initial CLD is characterized by a maximum of the square weighted chord length distribution of about 85 µm (in good correlation with the initial sieve fraction of 63-75 µm). During the batch the distribution shifts towards a higher maximum and becomes narrower, as results of the growth of the crystals. The Raman spectra were analysed by tracking different peaks. Figure 4.8 indicates the peaks followed during experiment 1: (i) peak 1 between 1051-1023 cm^{-1}, (ii) peak 2 between 777-760 cm^{-1}, and (iii) peak 3 between 1175-1154 cm^{-1}. The signal is relatively noisy but no significant change in the intensity of all the three peaks can be observed although the change in the crystals size is remarkable.

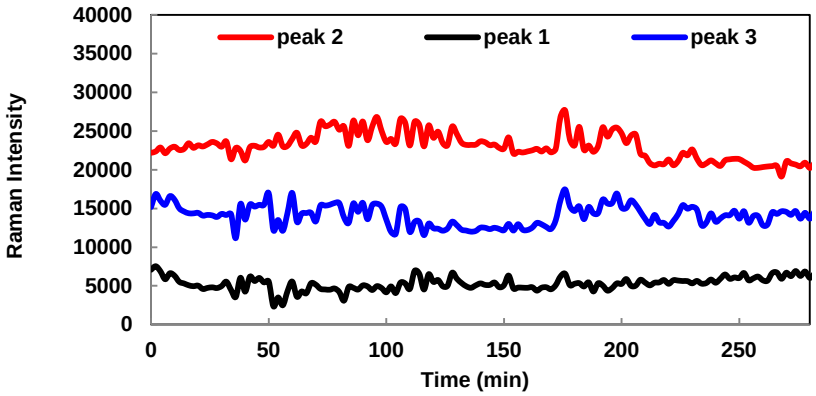

Figure 4.8: Trend of three different Raman peaks of OABA form I during experiment 1. (1) Peak 1: 1051-1023 cm^{-1}. (2) Peak 2: 777-760 cm^{-1}. (3) Peak 3: 1175-1154 cm^{-1}.

A principal component analysis (PCA) was performed on the Raman autoscaled spectra and it was found that the first principal component covers 95.8% of the variance in the signal.

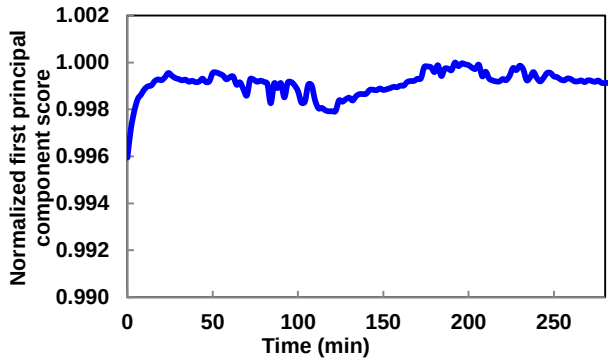

Figure 4.9: Trend of the first principal component (normalized to 1) during experiment 1. PCA performed on smoothed and autoscaled spectra.

For this reason it is the only component shown in this study. Its trend is shown in Figure 4.9: the variations during the whole experiment are minimal and mainly confined during the first 25 min where there was still dissolution of the seeds. A second experiment was conducted using similar conditions. In this case the growth of single crystals is lower but significant agglomeration was observed with PVM and FBRM.

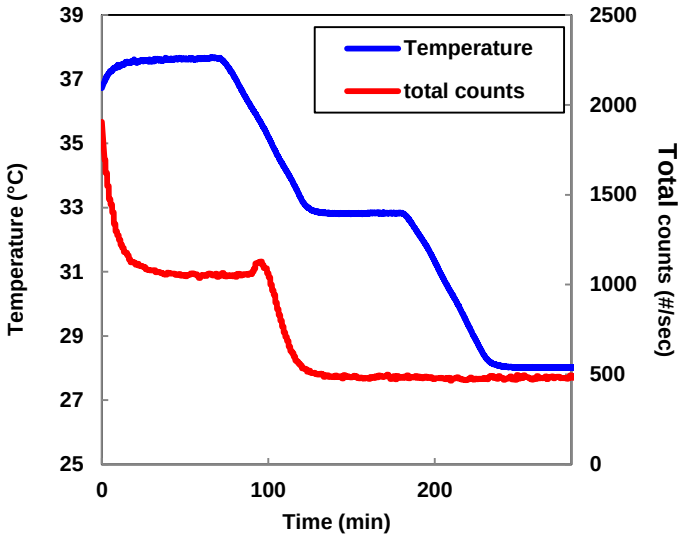

Figure 4.10: Temperature profile and total counts recorded by FBRM during Experiment 2.

Since agglomeration is a competing phenomenon with growth, the final single crystals are smaller than in experiment 1. In fact, part of the supersaturation was used to develop the crystal bonds between the particles in the agglomerates. The FBRM signal is also different from the previous experiment: the total counts/s starts decreasing as the temperature goes down (see Figure 4.10). This decrease is associated to the formation of agglomerates as shown by the PVM images in Figure 4.11. The difference between the two experiments is probably due to a slight difference in the size of the seeds at the beginning of the cooling profile. In fact, despite both seeds were obtained using the same sieves, the particles used for experiment 2 seems to be smaller (see Figure 4.12 the SWCLD at 40 minutes presents a maximum of the square weighted CLD of about 50 μm and also the total counts is higher compared to experiment 1) and therefore, tend to agglomerate more easily. Also, the stirring rate for Experiment 2 was lower compared to experiment 1 (200 rpm instead of 340 rpm), and that might also have affected the tendency of agglomeration together with the initial step of dissolution. The agglomerates in experiment 2 start appearing after the

first cooling step and that is related to the kinetics of agglomeration. In fact, agglomeration depends strongly on the surface of the particles and the probability of collision between each other. The initial suspension is characterized by small particles highly dispersed in the solution.

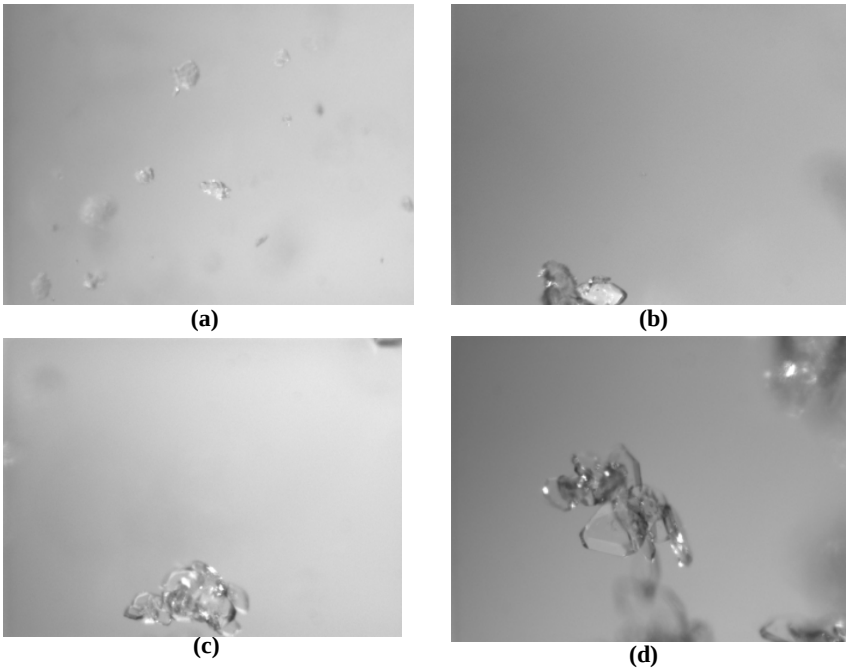

Figure 4.11: PVM images at (a) 10 min (b) 90 min (c) 120 min (d) 172 min during Experiment 2.

These particles tend to agglomerate more easily than big ones because of the higher specific surface energy, but since the particles are dispersed in the solution the probability of collision and the kinetic energy of collisions are lower. During the cooling step supersaturation increases and the particles start to grow. At some point they are large enough to have high probability of collision but still small enough to maintain strong inter-particle forces that generate agglomerates. As a result the total counts decreases and agglomerates start to appear as shown in the PVM images (see Figure 4.11). The formation of agglomerates generates a decrease in the growth of the single crystals. The images with the optical microscope and the PVM confirm that the final size of the crystal is not much different from the initial one. The CLD trend, shown in Figure 4.12, is also different from experiment 1: the maximum of the square weighted CLD increases significantly during the

batch as the number of counts per size bins decreases, also indicating the formation of agglomerates.

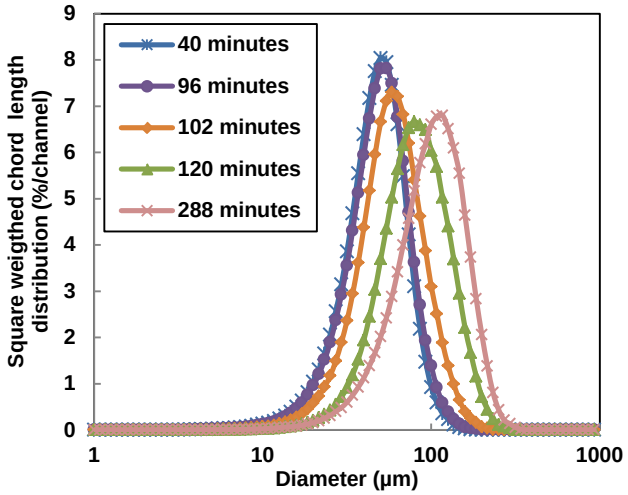

Figure 4.12: Crystal size distribution during Experiment 2 for the determination of the effect of crystal size in solution on the Raman spectra.

Even in this experiment the Raman signal does not change significantly as shown by the principal component analysis (see Figure 4.13).

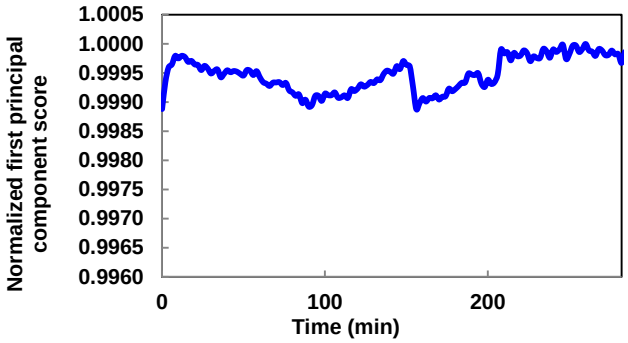

Figure 4.13: Trend of the first principal component (normalized to 1) during experiment 2. PCA performed on smoothed and autoscaled spectra.

The first principal component covers the 96.8% of the variance and it stays relatively constant during the entire experiment showing that agglomeration of crystals, hence significant change in size, does not affect the Raman signal considerably in the case of the immersion probe used in this study.

4.3.3 Effect of solid concentration in slurry

The gradual addition of solid in the solution generates an increase in the intensity of the Raman peaks as shown in Figure 4.14.

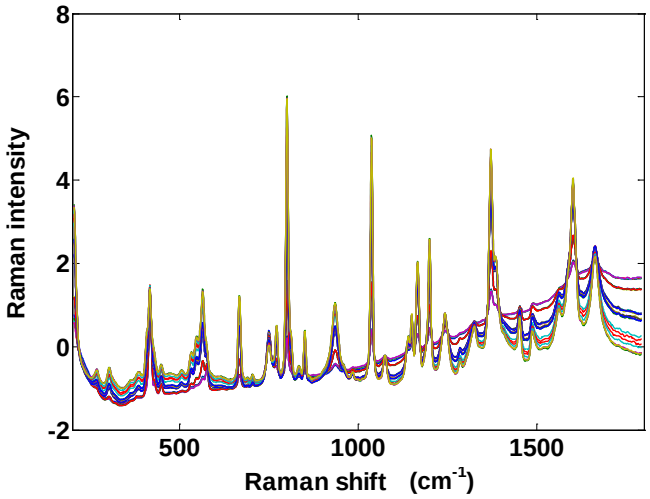

Figure 4.14: Spectra of suspensions of OABA form I in water at different solid concentrations.

The data was analysed with both univariate and multivariate techniques in order to find a correlation between the solid concentration of the slurry and the intensity of specific peaks. Three peaks were analysed (data were slightly smoothed) for the univariate analysis.

Table 4.5: Increase in the signal intensity for three specific Raman peaks of OABA, associated with an increase in the solid concentration by 10 times

Region of the spectrum (cm^{-1})	Increase in the peak intensity
680-650	50%
1059-1000	201.3%
964-900	215%

The rise in the signal compared to the increase in the solid concentration is significant. Table 4.5 indicates the change in the signal intensity of three Raman peaks of OABA when the solid concentration rises of about 10 times; depending on the region the Raman peaks analysed increase between 50 and 215%. The strong dependence of the signal on the solid concentration of the solution requires considering this parameter during the design of the

calibration experiments. The best univariate regression result was obtained using the first derivative spectra of the third peak analysed (964-900 cm^{-1}). A parabolic relation between the peak height and the solid concentration was found; with a correlation coefficient of about 0.96 (see Figure 4.15).

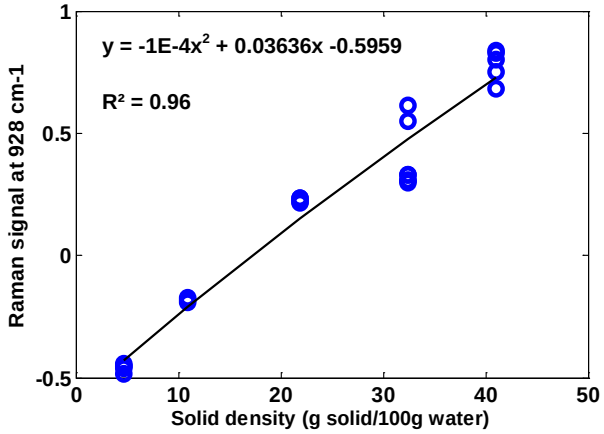

Figure 4.15: Univariate analysis of the effect of solid concentration on the Raman signal.

A linear multivariate approach was also used considering the raw spectrum with linear baseline correction (average in range 4000-0 cm^{-1}) in the regions between 124-117, 575-423, 843-831, 1608-1597, 1671-1656 cm^{-1} and using a PLSR technique with 3 factors. The correlation coefficient was found to be 0.9913 with RMSEC=1.73 g solid/100g water. The calculated versus actual values are shown in Figure 4.16.

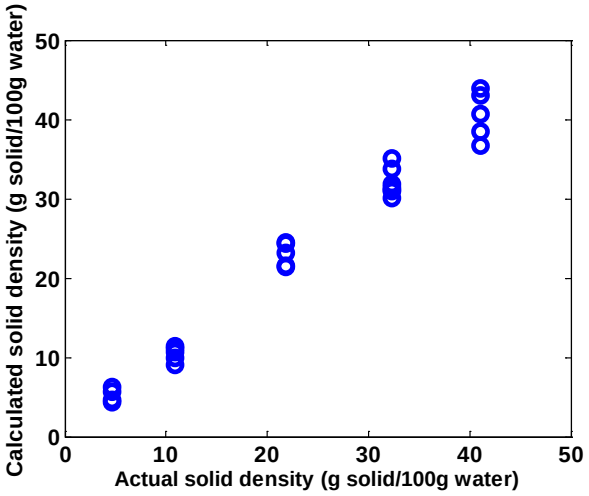

Figure 4.16: Multivariate analysis result for the effect of suspension density on the Raman spectra.

The multivariate approach seems to be the more reliable in considering the effect of solid concentration. In fact, although from the univariate analysis the change in Raman intensity seems to be non-linear, the linear PLSR model can still predict quite well the variation of the spectra. However, an increase in the prediction error at very high solid concentration can be observed, which is due to a non-linearity effect. This indicates that a nonlinear calibration model may be more suitable in the case of calibration with very high solid concentration.

4.3.4 Temperature effect

The effect of temperature on the Raman spectra for both the solvent and the solution was studied. Characteristic peaks were chosen for the solid as well as the solvent and the data were analysed with univariate and multivariate techniques.

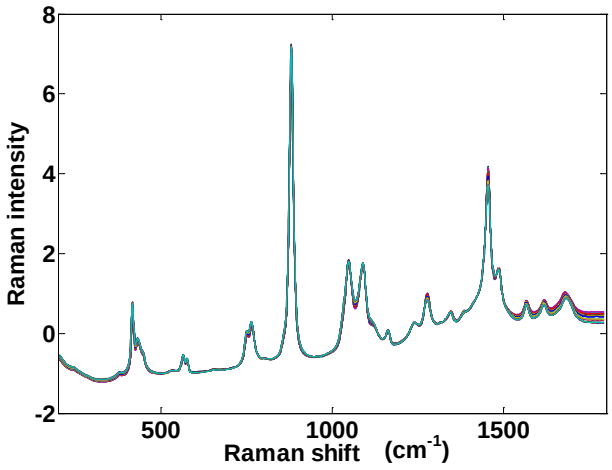

Figure 4.17: Raman spectra of clear solutions of OABA at different temperatures but same concentration.

Figure 4.17 shows the spectra of OABA solutions at different temperatures, from 20 to 60 °C. The difference between the spectra is minimal; temperature does not seem to have a strong effect on the Raman signal. For the univariate analysis of the dissolved solute three regions were chosen, the first derivative was calculated and spectra were smoothed (31 points window). An increase in temperature of 40 °C generates less than 15% decrease in intensity in the 1st derivative Raman spectra for the peaks reported in Table 4.6 (characteristic of the solid form of OABA).

Table 4.6: Decrease in the signal intensity for three specific Raman peaks of OABA, associated with an increase in the temperature of 4 times

Region of spectrum (cm^{-1})	Decrease in intensity of the peaks in first derivative
1190-1148	-13%
1365-1345	-14%
1587-1567	-7.45%

Figure 4.18 shows the trend of the Raman intensity as a function of the temperature.

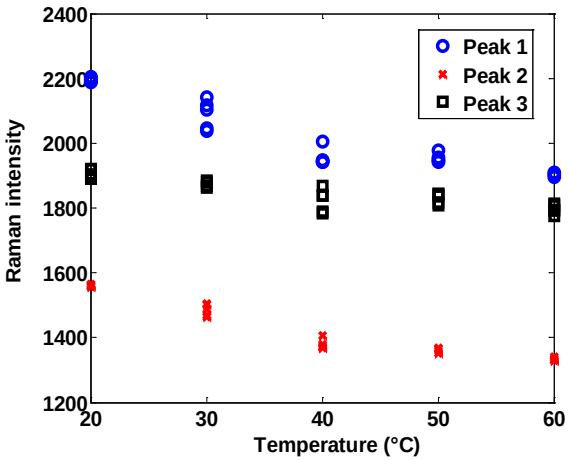

Figure 4.18: Trend of the three chosen peaks for solid OABA in solution as a function of temperature. Peak specifications are shown in Table 4.6.

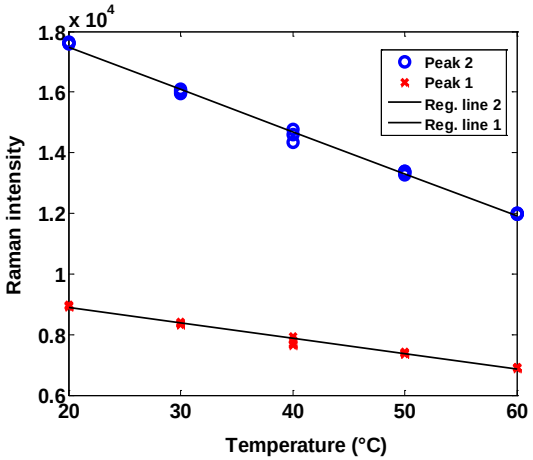

Figure 4.19: Trend of the two chosen peaks for the solvent as a function of the temperature of the solution. Data were pre-processed with a 31 points smoothing and a 3rd order baseline correction.

Temperature seems to have a stronger effect on the peaks of the solvent: the intensity of the first derivative of the characteristic peaks of ethanol decreases of -22% (1479-1444 cm^{-1}) and -19% (1117-1079 cm^{-1}) with an increase in temperature of 40 °C. Results are graphically shown in Figure 4.19. The data of Figure 4.18 and Figure 4.19 were interpolated using a logarithmic (for the solute peaks) and a linear (for the solvent peaks) function in Excel. The results of the interpolation are shown in Table 4.7.

Table 4.7: Univariate analysis results for temperature effect on different peaks of Raman spectra. The variable I represents the peak intensity in the region of spectrum chosen while the variable T represents temperature

Peak	Region of spectrum (cm^{-1})	Interpolating function	Correlation coefficient (R^2)
Peak 1 (OABA)	1190-1148	T=-269.7ln(I)+2995.9	0.917
Peak 2 (OABA)	1365-1345	T=-216.8ln(I)+2208.2	0.951
Peak 3 (OABA)	1587-1567	T=-96.86ln(I)+2196.1	0.769
Peak 1 (Solvent)	1479-1444	T=-50.443I+9894.9	0.987
Peak 2 (Solvent)	1117-1079	T=-139.46I+20270	0.9941

It must be noticed that the trend of each peak is different, both for the solute and for the solvent ones. An equal decrease of temperature generates different changes in intensity for different peaks and while for the solvent the best correlation is linear, for the solute peaks it is logarithmic.

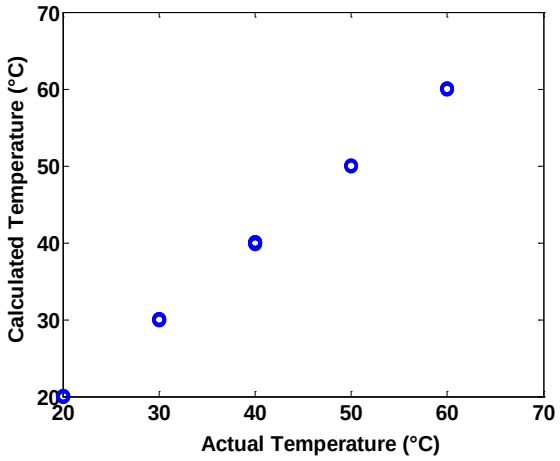

Figure 4.20: Multivariate calibration approach to study the effect of temperature on the Raman spectra: calculated temperatures versus actual.

Thus, considering the peaks ratio to compensate the temperature effect can lead to an error in the calibration. A multivariate approach was also used with PCR and 4 components. The 1st derivative was calculated and a Norris derivative filter was applied to the data (segment length of 7 and gap between segments of 5) in the region 1066-166 cm^{-1}. Temperature was chosen as the variable to be inferred by the spectra, and the resulting function has a correlation coefficient R^2=0.9999 (see Figure 4.20). Similarly to the solid concentration effect, a multivariate regression can capture the variation of Raman spectra due to the change in temperature with reasonable precision although the system appears to be non-linear using a univariate approach.

4.3.5 Calibration of Raman for solid dry mixtures of form I and II

This set of experiments is necessary to confirm that Raman can effectively discriminate between the two polymorphic forms of OABA. A preliminary attempt with solid mixtures should always be done, even if the desired calibration function is in a specific solvent. As described in the previous chapter two characteristic Raman peaks in the region 817-786 (peak 1) and 786-755 (peak 2) cm^{-1} are present in both forms but peak 1 is the most intense for form I while for form II peak 2 is the strongest. Form I also presents strong characteristic peaks at 1038 cm-1 and 950 cm^{-1}. The most significant effect on the accuracy of a calibration model for solid powders is given by the non-homogeneity of the mixtures and the width of the spot area of the measuring probe. A specific procedure described in the methodology section of this chapter was used in order to minimize the effect of bad mixing. A comparison with a NIR optical probe was performed using the same samples and measuring procedure. Both NIR and Raman can discriminate form I and II of OABA but the two probes have different spot areas (a diameter of 100 microns for Raman and 1 cm for the NIR probe). A larger spot area can capture a larger amount of sample so that non homogeneities in the sample have less effect on the measurement. The Thermo Scientific software TQ Analyst was used to pre-process the data and perform both PC and PLS regression. Results are shown in the Table 4.8 and Table 4.9. NIR seems to give a smaller error (RMSEC) with both type of regression. The RMSEPs of PLSR and PCR for both probes are comparable but PLSR needs a smaller number of components. To deeply investigate the effect of non-homogeneity on the model the 5th measurement for the sample at 75% of form II was performed 7 times instead of three. The position of the probe was changed every time following a clockwise trajectory over the sample. For the same

sample, varying the position of the probe causes a variation of the calculated value of form II content using PCR of around ±5%. Using the NIR with the same sample the variation is only ±1.4%. This means that the precision of the Raman calibration model could be improved using an optical probe with a bigger spot area.

Table 4.8: Optimized parameter used for a multivariate calibration with NIR and Raman for dry solid mixtures of OABA form I and II

Probe	Region	Pre-processing techniques	PLS factors	PCR components
NIR	4300-10000 nm	2nd derivative, Norris filter (5,5), SNV	4	5
Raman	200-1700 cm-1	2nd derivative, Norris filter (5,5), SNV	2	5

Table 4.9: Results of a multivariate calibration with NIR and Raman for dry solid mixtures of OABA form I and II

Probe	R^2 PLS	R^2 PCR	RMSEC PLS	RMSEC PCR	RMSEP PLS	RMSEP PCR
NIR	0.9997	0.9998	0.584%	0.497%	0.634%	0.567%
Raman	0.9892	0.9894	3.74%	1.98%	3.24%	4.11%

However, considering that the Raman probe's spot area is 100 times smaller than for the NIR but the error is only 4 times higher it can be affirmed that the Raman calibration model works better in evaluating the composition of form I and II solid mixtures of OABA.

4.3.6 Calibration in solution

To build a good calibration model that can be used during a cooling crystallization a set of experiments must be carefully planned in order to include all the parameters that can affect the Raman spectra during the process itself. Therefore the following parameter should be considered during calibration: (i) temperature/solute concentration, (ii) suspension density, (iii) ratio of form II and I. As shown in the previous sections of this chapter solute concentration, solid density and polymorphic ratio are the parameters that can strongly

affect the Raman spectrum and also change during a cooling crystallization of a polymorphic compound. A set of calibration experiments that considered all these factors was developed using the Box-Behnken design of experiments. Second derivative (with a 2nd order polynomial and 25 points window smoothing) was applied to the calibration spectra together with autoscaling. Multivariate PLSR and PCR were both investigated considering all the samples. K-fold cross validation was performed to choose the correct number of components or factors, as the one that minimizes the root mean square error of cross validation (RMSECV). It was also noticed that using the concentration of form II instead of the polymorphic ratio gives better results. This is probably due to the strong dependence of Raman spectroscopy on solid concentration. Two spectra at the same polymorphic ratio but different solid concentration are usually very different and the model cannot predict the polymorphic ratio correctly. Figure 4.21 shows the PLSR and PCR multivariate calibration and prediction points and Table 4.10 shows the numerical results.

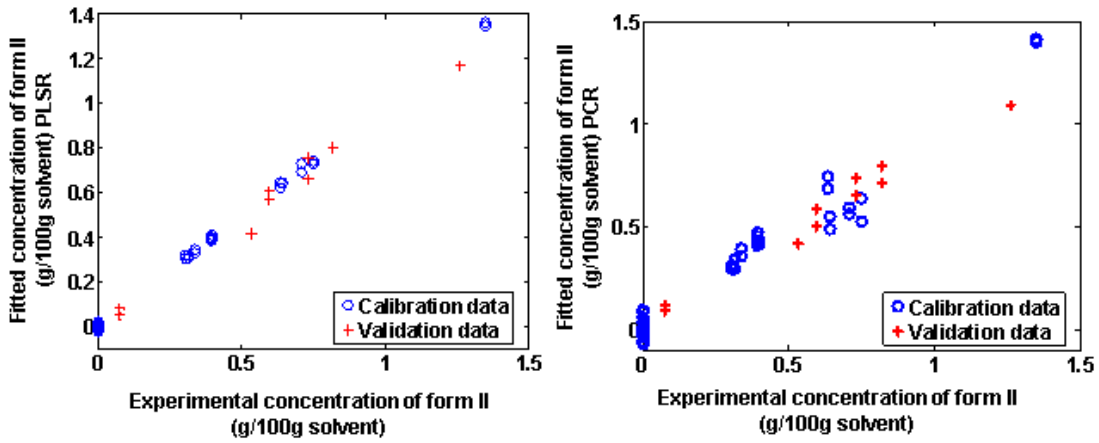

Figure 4.21: PLSR and PCR calibration and validation concentrations of form II with data obtained from the DoE.

PLS regression works better than PCR in predicting the concentration of form II although the number of factors used is 8 instead of 6. It must be noticed that because the design of experiments (DoE) was applied considering polymorphic ratio instead of concentration of form II, some calibration points are missing at high concentrations. Therefore two additional experiments (with the conditions shown in Table 4.11) were performed to improve the reliability of the calibration model.

Table 4.10: PCR and PLSR comparison for the DoE experiments only. The calculations were performed in Matlab

Technique	Region	Factors/components	R^2	RMSEC (g/100g solvent)	RMSEP (g/100g solvent)
PLS	500-3400 cm^{-1}	8	0.9990	0.0185	0.0436
PCR	500-3400 cm^{-1}	6	0.9589	0.1200	0.0611

The results with the new calibration points are shown in Table 4.12. Adding the two new points does not considerably affect the correlation coefficient. However, the root mean squared error of both calibration and validation are different. The error on calibration is higher but the one on prediction is lower. Compared to the first set of data the two errors of prediction and validation are very similar to each other, which is typical of good calibrations.

Table 4.11: Conditions of the additional two calibration experiments

Experiment	Temperature (°C)	Polymorphic ratio (%)	Total solid for 100g solvent (g)
16	25	50	1
17	40	100	1.2

Table 4.12: PCR and PLS comparison for the DoE experiments plus two additional calibration samples

Technique	Region	Factors/components	R^2	RMSEC (g/100g solvent)	RMSEP (g/100g solvent)
PLS	500-3400 cm^{-1}	8	0.9987	0.0253	0.0258
PCR	500-3400 cm^{-1}	6	0.9650	0.1333	0.059

Temperature and solid density were tentatively added to the input matrix together with the spectra but the prediction and calibration error did not improve significantly. This means

that the calibration experiments were performed in an optimized way that takes into account possible factors that affect the spectra.

4.4 Conclusions

The systematic investigation and results presented in this paper represent basis of the proposed "Good Calibration Practise Procedure" (GCPP) framework for quantitative analysis of polymorphic mixtures using Raman spectroscopy. The quantification of polymorphic purity during a cooling crystallization is very important to guarantee the required chemical-physical properties of the final product. In fact, for example, the presence of an unwanted polymorph in a drug tablet can have a dramatic effect on the solubility and dissolution rate of the API and, therefore, on the efficacy and safety on the patient. Since most APIs are produced by cooling crystallization a good calibration strategy for polymorphic form quantification was designed for this type of process. The parameters that can change during a cooling crystallization were identified and analysed systematically. In particular, the effect of crystal size, temperature, solute and solid concentration on Raman spectra were studied and used to design a set of calibration experiment for the quantification of polymorphic purity of OABA in slurry.

Solute and solid concentration were found to strongly affect Raman spectra while crystal size and temperature cause only minor changes. Additionally, it was found that, because of the strong effect of solid density on the Raman signal, the estimation of the solid concentration of the metastable form is more accurate than the estimation of the polymorphic ratio of the solid phase.

The GCPP proposed in this chapter is very general and can be applied to any other spectroscopic technique and process; its key points are:

1) Identification of the parameters that can vary during the process of interest;
2) Study of the effect of the identified parameters on the selected spectroscopic technique;
3) Determination of calibration experiments by design of experiment (DoE) using the most influencing parameters.

5 Quantitative application of Raman, UV, NIR and mid-IR spectroscopy with FBRM in monitoring polymorphic transformations: comparison and integration of signals

In this chapter several spectroscopic techniques are analysed, calibrated and compared for the quantitative estimation of solute concentration and polymorphic ratio of a slurry during a cooling crystallization process. A general experimental procedure is described as well as the chemometrics techniques used for the data manipulation.

5.1 Introduction

Raman, UV, NIR and IR spectroscopy are commonly used techniques to monitor solute concentration and solid composition during crystallization processes of polymorphic compounds. However, a comprehensive study and comparison of the ability of these techniques to detect polymorphic transformation in the same system has not been performed yet. The aim of this chapter is to provide a comprehensive comparison between the most common techniques used for in situ monitoring of polymorphic transformation and to explore the application of chemometrics to these different process analytical technology (PAT) tools in different stages of a cooling crystallization of a polymorphic system. The comparison between the different PAT tools was conducted using different physical and mathematical approaches. Chemometrics techniques were exploited to obtain quantitative information about the solute concentration and polymorphic ratio. The most suitable calibration approach was determined for each technique. Both multivariate and univariate approaches were tested as well as different regression techniques such as partial least square (PLSR) and principal component regression (PCR). Additionally a novel calibration approach that combined information from two PAT tools is proposed. Since the Raman signal depends on the solid concentration it is difficult to develop accurate calibration models that would predict accurately the polymorphic ratio during crystallization when the solid concentration changes significantly. Typically a large number of experiments are required to include the effect of this parameter in a calibration model. In the proposed approach, solid concentration is included as an additional input.

This parameter is obtained from other PAT tools that monitor solution concentration (and using a simple mass balance, knowing the initial solute concentration), such as ATR-UV/Vis. It is shown that the proposed integrated calibration model provides better accuracy in predicting the polymorphic ratio with a smaller number of calibration experiments than using the Raman signal alone. This approach can lead to faster calibration procedure with less material consumption.

5.2 Methodology, materials and Equipment

The compound used in this chapter is OABA. The transformation studied is the one from metastable form II to stable form I in a solution of 90% water and 10% IPA. The Raman probe, the ATR-UV/Vis and the two NIR probes (reflectance and transflectance) together with the mid-IR probe were used in the experiments.

5.2.1 Solute concentration calibration

To determine solute concentration calibration functions with the different probes, four solutions of OABA in water and IPA (90/10 w/w) at different concentrations were used: 10, 20, 30 and 40 °C saturation temperatures. Temperature profiles for each solution are shown in Figure 5.1. Temperature and solute concentration are the two main factors that can affect spectra in the case of clear solution; hence these two parameters were changed during the calibration experiments. Every solution was heated up to dissolve the material and then cooled in steps until nucleation. A smaller number of steps was performed for diluted solutions since very unlikely, during a crystallization experiment, a solution saturated at 10 °C will be kept at 30 or 40 °C. For this set of experiments the FBRM probe was also used to check when nucleation happened. It was important to perform the calibration experiments in absence of solids in order to know exactly the solute concentration. Raman, mid-IR and both the NIR probes were collecting samples every minute while UV was taking measurements every 10 seconds. Data were collected and processed with Matlab 2013a. The Matlab functions *plsregress* and *pca* were used to calculate partial least squares and principal components regressions. The best number of PLS factors and principal components (PCs) were chosen using k-fold cross validation in Matlab: the number of factors that minimize the root mean square error of cross validation (RMSECV) was chosen for the calibration models.

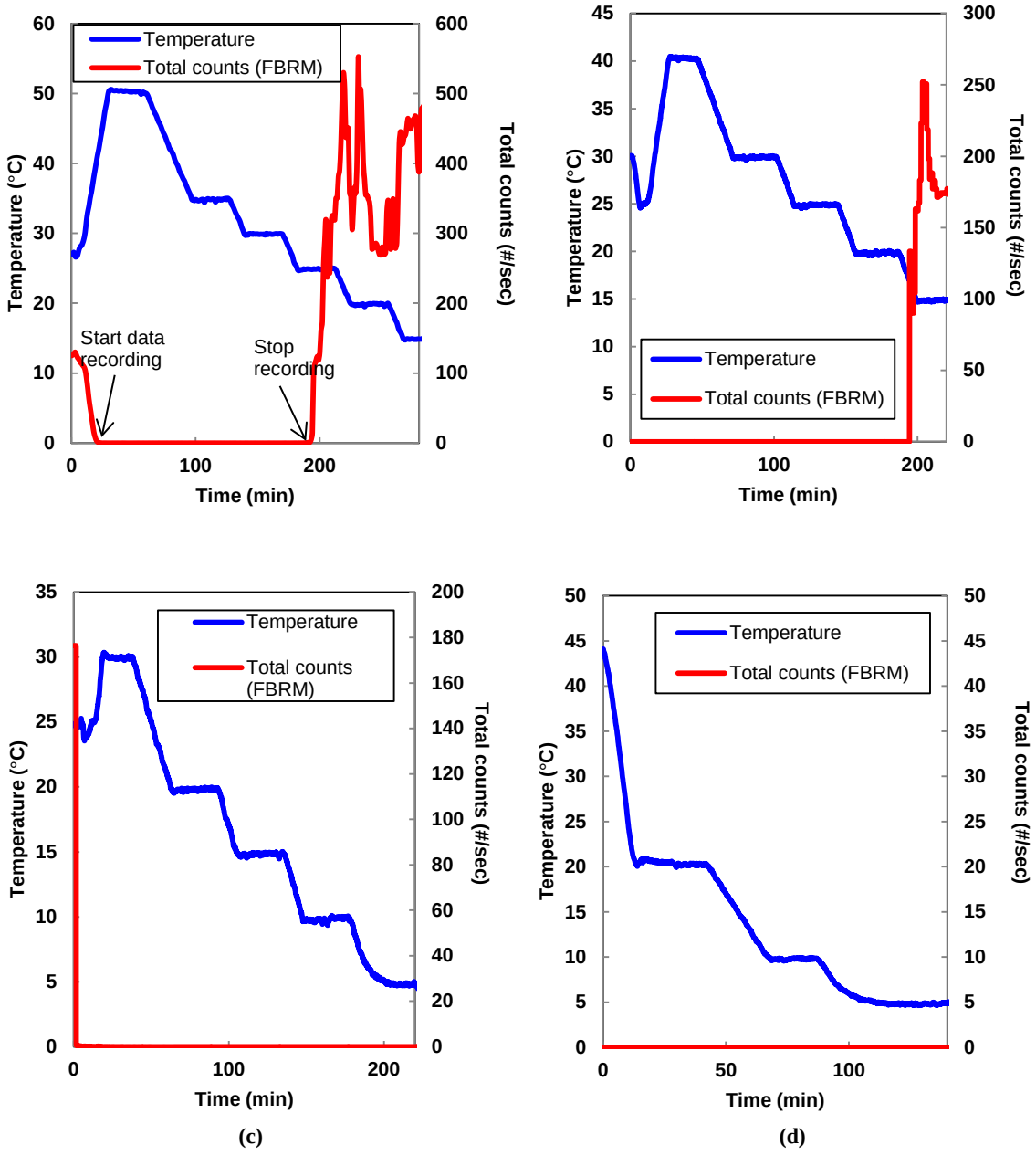

Figure 5.1: (a): Temperature profile for solute concentration calibration at 40°C saturation temperature. Data are taken from complete dissolution of the solids to the nucleation point (FBRM data). (b) Temperature profile for solute concentration calibration at 30°C saturation temperature. (c) Temperature profile for solute concentration calibration at 10°C saturation temperature. (d) Temperature profile for solute concentration calibration at 10°C saturation temperature

This procedure is commonly used to avoid overfitting of the calibration function. Increasing the amount of components generates a decrease of the cross validation error as a result of an increase in the function's precision but, if too many components are used, the cross validation error will start increasing because of model overfitting. For the UV signal

a non-linear calibration function was also determined and tested using the *fmincon* function in Matlab. An external validation was performed using a 40 °C saturation solution. The solids were completely dissolved (confirmed using FBRM) and then the temperature was decreased in steps until nucleation happened. Measurements were taken during both the dissolution and the cooling phase.

5.2.2 Polymorphic ratio calibration

Four saturation temperatures were used for these experiments: 10, 20, 30 and 40 °C in order to have different solute concentrations and slurry densities (both these factors can affect Raman and NIR spectra). The solvent was water and IPA 90/10 w/w. Every calibration was conducted at constant temperature changing only the concentration of solids in the solution. Four different 400 g solvents were prepared at each different temperature. After reaching the set-point temperature each solvent was first saturated with OABA form I and held for 20 minutes to ensure complete dissolution (the final concentration of each solution are indicated in the first column of Table 5.1). After reaching the saturation concentration, additional form I was added to the saturated solution in order to create a slurry (the amount of form I in the slurries is shown in the second column of Table 5.1 and the calibration measurements started. Form II was added in three steps during the measurement in order to have calibration samples at different polymorphic ratios for each temperature (25, 50 and 75% of form II). Four additional experiments at 10, 20, 30 and 40 °C were performed starting with pure form II: the solutions were similarly saturated at the decided temperatures and form II was added to create a slurry. The conditions used in the calibration experiments are shown in Table 5.1. For each calibration sample 10 measurements were taken. Temperature was controlled during all experiments and total slurry density was calculated using solubility data from a gravimetric analysis. Every experiment was performed in less than an hour to avoid transformation of the unstable form II into the stable form I and FBRM was used to monitor whether nucleation or growth were happening during the measurements. The probes used in these experiments are the ones that could potentially discriminate between the two solid forms of OABA: (1) Raman; (2) NIR reflectance; (3) NIR transflectance. Raman and NIR spectra of form I and II of OABA are shown and described in Chapter 3 of this thesis.

Table 5.1: Composition of the slurries of form I and form II used in the calibration experiments. The total mass of solvent was 400 g for each experiment.

Solubility (g/g solvent)	Temperature (°C)	Form I (g)	Form II (g)	% Form I	% Form II
0.0032	10	1.11	0	100%	0%
0.0032	10	1.11	0.42	73%	27%
0.0032	10	1.11	1.14	49%	51%
0.0032	10	1.11	3.39	25%	75%
0.0037	10	0	5.44	0%	100%
0.005	20	1.21	0	100%	0%
0.005	20	1.21	0.45	73%	27%
0.005	20	1.21	1.21	50%	50%
0.005	20	1.21	3.70	25%	75%
0.006	20	0	4.59	0%	100%
0.0082	30	1.31	0	100%	0%
0.0082	30	1.31	0.53	71%	29%
0.0082	30	1.31	1.41	48%	52%
0.0082	30	1.31	4.03	24%	76%
0.0084	30	0	3.54	0%	100%
0.0126	40	1.13	0	100%	0%
0.0126	40	1.13	0.49	70%	30%
0.0126	40	1.13	1.16	49%	51%
0.0126	40	1.13	3.32	25%	75%
0.0137	40	0	3.80	0%	100%

In this chapter Matlab 2013a was used to perform PLS and PC regressions in order to determine a calibration function that can measure the polymorphic ratio between OABA form I and II; the functions *plsregress* and *pca* were used for the calculations. K-fold crossed validation was chosen to determine the best number of factors and principal components as described in the previous section. Derivative, smoothing and autoscaling were performed using simple codes developed in Matlab 2013a.

5.3 Results and Discussion

Different chemometrics techniques and different inputs were investigated in order to obtain the best calibration results. The investigation indicates that using additional inputs in a multivariate approach other than the spectra (such as temperature or solid density) does not change the calibration results under two conditions: (i) the effect of the input on spectra is linear and (ii) experiments were conducted correctly including suitable variation of the inputs. For the solute concentration, calibrations experiments were designed to capture the effect of temperature on the absorbance and the calibration results indicated that the addition of temperature in the inputs does not generate any improvement. For the calibration for polymorphic content, experiments were not designed to completely cover all the factors that can affect Raman and NIR spectra (a good calibration practice procedure for Raman spectroscopy is presented in Chapter 4 of this thesis); nevertheless, it was still possible to obtain a more accurate calibration model including as input in the calculations solid concentration and temperature. If a good experimental plan is used, it is not necessary to include additional inputs other than the spectra to obtain an accurate calibration function, however this calibration procedure requires a larger number of experiments to cover properly the effects of all input parameters. In this work a shorter experimental procedure was used that required a smaller number of experiments by using an integrated calibration model approach (Wong et al. 2008). For this approach for polymorphic form quantification PLS and PC regressions were performed using the following integrated calibration model:

$$C_{F_{II}} = f_{calibration}^{Raman}\left(\left[S_i|_{i=1,\dots,N}, T, C_s\right]\right) \quad (5.1)$$

where $C_{F_{II}}$ is the concentration (g/g solvent) of form II, S_i with i = 1,…, N is the Raman intensity values at N different Raman shifts, T is the temperature and C_s is the solid concentration, which is calculated from the ATR-UV/Vis calibration model using the following equation:

$$C_s = C_0 - f_{calibration}^{UV/Vis}\left(\left[D_i|_{i=1,\dots,M}, T\right]\right) \quad (5.2)$$

where C_0 is the initial solute concentration and D_i are the derivatives of the UV/Vis absorbance spectra at i = 1,…, M wavelength used in the UV/Vis calibration model. The combined use of equations (5.1) and (5.2) allows taking the solid concentration into account in the Raman calibration model and integrates signals from two different sensors. The calculation of C_s allows to determine the amount of form I in slurry by the formula:

$$C_{F_I} = C_s - C_{F_{II}} \quad (5.3)$$

5.3.1 Solute concentration measurements

Table 5.2 and Table 5.3 report the results for solute concentration calibration for each sensor and using different chemometrics techniques. A non-linear calibration function was also used for the UV data (choosing two specific derivative peaks), since this technique gives a relatively simple calibration equation with a small number of coefficients to determine. Root mean square errors of calibration (RMSEC) and of prediction (RMSEP) for the external validation are reported in the last two columns of the tables. For each probe the region of spectra that contains more information and less noise (narrow and well defined peaks) was chosen. Different pre-processing techniques were evaluated but only the best results are shown. Using first derivative spectra in the calibration was found to improve the results for all the probes. While this technique is commonly used for NIR and Raman we found that it can improve also the performance of the ATR-UV/Vis probe. In fact, derivative can eliminate baseline effects generated in the ATR-UV/Vis spectrum by the solid particles that can reflect part of the signal. Cross validation in Matlab was used to determine the best number of factors. Solute concentration is calculated as g of solid/g solvent.

Table 5.2: Results for PLS calibration of solute concentration with different probes.

Probe	Region (cm^{-1})	Preprocessing	PLS factors	R^2 PLS	RMSEC PLS (g/g solvent)	RMSEP PLS (g/g solvent)
ATR-UV/Vis	47200-17000	Instrument 1st derivative	6	0.99998	5.2×10^{-6}	3.4×10^{-4}
Raman	450-2700	Autoscaling, 1st derivative (7points, 3rd order smoothing)	16	0.9998	5.4×10^{-5}	3.6×10^{-4}
ATR-mid-IR	900-1600	Autoscaling, 1stderivative (7points, 3rd order smoothing)	10	0.9976	1.7×10^{-4}	3.6×10^{-4}
NIR transflectance	5400-6400	Autoscaling, 1st derivative (13points, 1st order smoothing)	10	0.9999	3.4×10^{-5}	2.3×10^{-4}

From the calibration results it can be inferred that the more suitable probes for measuring solute concentration are, in order: UV, Raman, NIR transflectance and then mid-IR. The best results were obtained with UV and NIR transflectance using only 10 factors for PLSR. Raman needed a larger number of components or factors but the calibration model is as accurate as the UV/Vis. Usually, a calibration function is considered good enough if it gives similar RMSEC and RMSEP and if the relative prediction error is below 10%. All the probes conform to this general standard for PLSR. It is important to emphasize that only the calibration models that are developed based on data obtained from instruments with ATR probes can be used in the presence of solids because the signal is not strongly affected by the particles. For Raman and NIR it is necessary to use another calibration model after nucleation happens (and consequently a different calibration approach is required). In this case FBRM can be used in combination with NIR and Raman to detect the moment in which a switch in the calibration model is needed. For UV a non-linear model was also checked but the results are less accurate than both PCR and PLSR

(R^2=0.9707, RMSEC=8.2×10^{-5} g of solid/g solvent, RMSEP=5.5×10^{-4} g of solid/g solvent). The best non-linear function checked was in the form:

$$C = p_1T + p_2D_1 + p_3TD_1 + p_4D_2 + p_5TD_2 + p_6 \quad (5.4)$$

where T is temperature D_1 is the first derivative absorbance at 358 nm and D_2 is the first derivative absorbance at 309 nm. The model parameter values p_i, i = 1,…,6 were estimated using a nonlinear optimization technique implemented using the *fmincon* function in Matlab.

Table 5.3: Results for PCR calibration of solute concentration with different probes

Probe	Region (cm^{-1})	Preprocessing	PCR components	R^2 PCR	RMSEC PCR (g/g solvent)	RMSEP PCR (g/g solvent)
ATR-UV/Vis	47200-17000	Instrument 1st derivative	9	0.99996	6.4×10^{-6}	2.6×10^{-4}
Raman	450-2700	Autoscaling, 1st derivative (7points, 3rd order smoothing)	9	0.9956	2.3×10^{-4}	3.1×10^{-3}
ATR-mid-IR	900-1600	Autoscaling, 1st derivative (7points, 3rd order smoothing)	10	0.9940	2.7×10^{-4}	1.8×10^{-3}
NIR transflectance	5400-6400	Autoscaling, 1st derivative (13points, 1st order smoothing)	10	0.9998	4.7×10^{-5}	7.4×10^{-4}

5.3.2 Polymorphic ratio measurement

Matlab 2013a was used to perform the calibration for the polymorphic ratio. K-fold cross validation was used to determine the best number of factors for PLS and PC regression. It was found that the best correlation can be obtained not for the calculation of the polymorphic ratio but for the concentration of form II (in g of solid/100 g of solvent) similarly to what was observed in chapter 4 of this thesis. This can be explained by the fact

that both Raman and NIR signals are strongly influenced by the amount of solid in the slurry; therefore, similar polymorphic ratios will give different signal in variable solid concentrations. This variation can be captured by a calibration model that actually predicts the absolute concentration of a certain polymorph in the solid suspension. The concentration of the other polymorph can then be computed from a simple mass balance knowing the total solid and the solute concentration (which can be measured using another probe). Pre-processing and spectral regions of interest were chosen to optimize the results. In general NIR reflectance requires more smoothing than transflectance and second order derivative is preferable. Raman spectroscopy works better with a first derivative and slight smoothing. It was found that Raman gives better results than NIR spectroscopy in measuring concentration of OABA form II. The transflectance probe performed better than the reflectance but it can be easily affected by fouling. It is worth noting that both the transflectance and reflectance probes give good results in aqueous solutions despite the strong signal for water in the NIR region. Table 5.4 and Table 5.5 show the different results using as inputs only the spectra, spectra and temperature or spectra, temperature and slurry density. The pre-processing applied in all cases is exactly the same as well as the region chosen for the analysis. Table 5.4 shows the results in case of application of partial least square regression while Table 5.5 shows the results with principal components regression.

Table 5.4: Comparison of different regression inputs in PLSR for polymorphic calibration, S=Spectra, T=Temperature, ρ=slurry density. Round mean square errors of cross validation (RMSECV) are expressed in g/g solvent.

Probe	R^2 (S)	R^2 (S + T)	R^2 (S+T+ρ)	RMSECV (S)	RMSECV (S+T)	RMSECV (S+T+ρ)
Raman	0.9659	0.9645	0.9988	0.165	0.160	0.028
NIR transflectance	0.8376	0.9354	0.9965	0.263	0.206	0.041
NIR reflectance	0.7906	0.9017	0.9761	0.267	0.238	0.128

Table 5.5: Comparison of different regression inputs in PCR for polymorphic calibration, S=Spectra, T=Temperature, ρ=slurry density. Round mean square errors of cross validation (RMSECV) are expressed in g/g solvent.

Probe	R^2 (S)	R^2 (S + T)	R^2 (S+T+ρ)	RMSECV (S)	RMSECV (S+T)	RMSECV (S+T+ρ)
Raman	0.3922	0.3910	0.9748	0.346	0.350	0.074
NIR transflectance	0.3415	0.3729	0.9204	0.350	0.331	0.075
NIR reflectance	0.6267	0.6345	0.7796	0.267	0.265	0.206

It can be seen that solid concentration is an important factor for both Raman and NIR, while temperature affects more NIR than Raman (including or not the temperature in Raman calibration does not change the cross validation error significantly). The results also show that PLSR gives better calibration model compared to PCR in all the combinations of inputs, but the improvement in the R^2 with the addition of the slurry density in the input matrix is larger for PCR than PLSR.This is evident in particular for the Raman and NIR transflectance probe where the addition of the slurry density in the inputs, generates and increase of 149 % in the R^2 of the Raman calibration and 147 % in the one of NIR. In the case of PLSR, the improvement is only 3.7 % for Raman and 6.5 % for NIR. In general, PLSR seems to give good results even with a smaller number of inputs, while for PCR, to get an R^2 higher than 0.9 it is necessary to include all the available inputs. However, the addition of both slurry density and temperature to the input matrix improved the quality of the calibration model compared to the use of only spectroscopic data.

Table 5.6 shows more in detail the pre-processing, region used and number of factors/components needed in the best polymorphic calibration performed (considering S+T+ρ). With a specific design of experiment for Raman and NIR spectroscopy it is possible to determine polymorphic concentration using only spectroscopic data as input (as shown in Chapter 4). This kind of calibration approach is more time consuming, it requires more material because the more factors are considered in the calibration the more experiments are needed. The integrated approach proposed in this chapter, which includes

solid concentration in the calibration model obtained from other PAT tools, can save time and material required for the calibration model development.

Table 5.6: Results for the best polymorphic calibration model with different probes and techniques (considering S+T+ρ). Number of factors or components used is in parentheses. Round mean square errors of calibration and cross validation (RMSEC andRMSECV) are expressed in g/g solvent.

Probe	Region (cm^{-1})	Pre processing	R^2 PLS	R^2 PCR	RMSEC PLS	RMSEC PCR	RMSECV PLS	RMSECV PCR
Raman	450-1700	Autoscaling, 1st derivative (11 points, 2nd order smoothing)	1.00 (14)	0.98 (10)	0.016	0.069	0.028	0.074
NIR transflectance	5400-6400	Autoscaling, 2nd derivative (11 points, 2nd order smoothing)	0.97 (10)	0.92 (10)	0.042	0.126	0.041	0.075
NIR reflectance	4500-12000	Autoscaling, 2nd derivative (21 points, 2nd order smoothing)	0.98 (13)	0.78 (9)	0.066	0.202	0.128	0.206

5.4 Conclusions

This chapter provides a comprehensive comparison of spectroscopic techniques used for crystallization monitoring. Raman, NIR transflectance, UV and mid-IR were found to give reliable results for solute concentration measuring. ATR-UV/Vis and ATR-mid-IR are the least sensitive to the presence of solids while the signals of the other probes are considerably influenced by solid concentration in the slurry, hence would require different

calibration models to be used in clear solution or in the presence of solids. An automated approach to switch between the models (e.g. using FBRM signal) could be used in these cases. Raman and NIR could both measure polymorphic ratios with the more accurate prediction achieved using Raman spectroscopy. Different chemometrics techniques were evaluated, but PCR was found not to be suitable for polymorphic ratio measurement (low value of R^2). With the calibration experimental approach used in this chapter it was necessary to include other information to the regression inputs to have accurate results. While using a specific design of experiment that includes all factors that affect the calibration model, it is possible to determine polymorphic concentration using only spectroscopic data as input, this general approach is more time consuming because the more factors are considered in the calibration procedure the more experiments are required. The integrated approach proposed here, that combines signals from two PAT tools to include solid concentration in the calibration model of polymorphic composition, can provide accurate calibration faster and with less material required.

6 Active polymorphic feedback control of crystallization processes using a combined Raman and ATR-UV/Vis spectroscopy approach

The concept of active polymorphic feedback control (APFC) is introduced in this chapter. This strategy allows the control of polymorphic during batch cooling crystallization processes and involves a combination of Raman and UV/Vis spectroscopy to select and then grow the desired polymorph.

6.1 Introduction

In this chapter a control strategy to quickly obtain crystals of pure stable form of OABA was developed. An active polymorphic feedback control (APFC) strategy is proposed, based on the use of a combination of Raman and ATR-UV/Vis spectroscopy using a hierarchical control implementation. The approach detects the formation of the polymorphic mixture and eliminates the metastable form by triggering a controlled dissolution cycle, and then allows the growth of the stable form using supersaturation control. A calibration-based approach is used to measure the solute concentration for the supersaturation control; while for the Raman measurement a calibration-free technique is applied based on the identification of a specific peak in the spectrum associated with the presence of the metastable form. It is shown that the proposed APFC technique can lead to pure polymorphic forms in the case of unseeded crystallization processes where nucleation of polymorphic mixtures occurs, or for seeded crystallizations with contaminated seed with unwanted polymorph impurity. A simple schematic of the control strategy developed is shown in Figure 6.1. The Raman signal is used in the feedback control strategy to detect the presence of the polymorph contaminant and the APFC approach automatically triggers the dissolution cycle needed for its elimination both in the case of seeded and unseeded systems. After the polymorph purity correction step based on Raman signal, supersaturation control (with ATR-UV/Vis spectroscopy) is applied to maintain the operating curve in the phase diagram between the solubility curves of the stable and metastable polymorphs hence avoiding any further contamination with metastable form. For the first time, a combination of two PAT tools was used to control polymorphism. In

previous works, either only the Raman system was used to detect the formation of the unwanted polymorph and restart the crystallization process with a different cooling rate, or only ATR-FTIR was used to perform supersaturation control over the metastable polymorph. The APFC approach is experimentally evaluated in this chapter using ortho-aminobenzoic acid (OABA) as the model system.

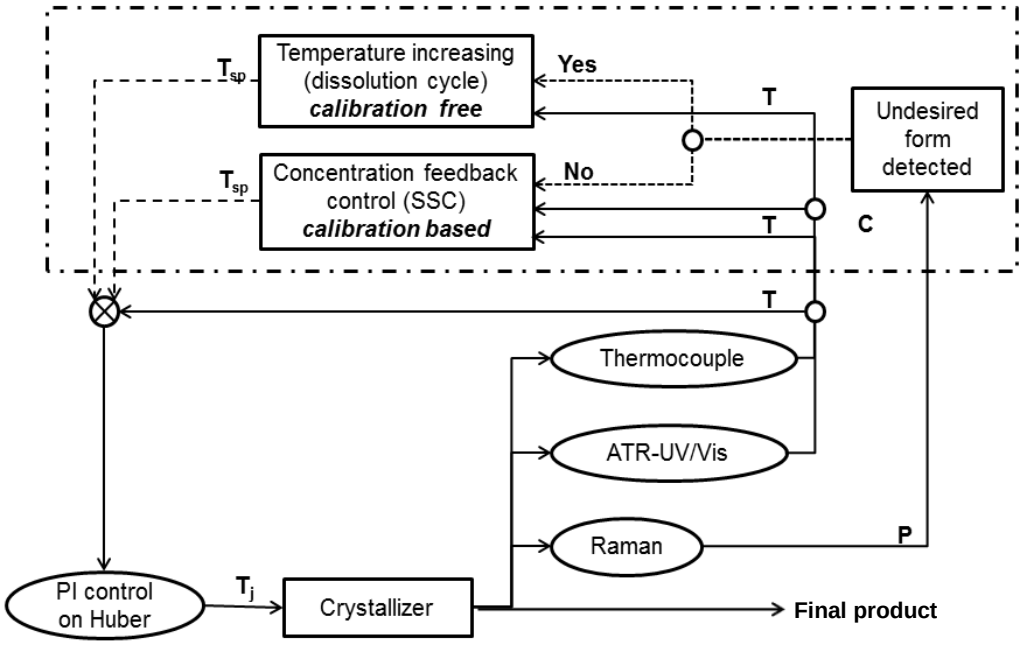

Figure 6.1: Schematic of the Active Polymorphic Feedback Control (APFC) approach. Raman spectroscopy is used to detect the presence of the undesired form (P) using a calibration-free approach; ATR-UV/Vis is used to measure the solute concentration (C) and perform SSC using a calibration-based approach to determine the setpoint for the temperature controller, T_{sp}).

In the first part of the experimental work the influence of solvent ratios and cooling rates on the formation of polymorphic forms of OABA has been investigated. Changing the solvent means changing the interfacial tension between crystals and the liquid phase and this may alter which polymorph is formed (Threlfall 2000); rapid cooling rate usually favours the formation of the metastable form (which can be the kinetically preferred). The results of the preliminary analysis have been used to perform APFC over OABA using ATR-UV/Vis data. Raman, FBRM, and PVM were also used to monitor the growth of the crystals and the polymorphic forms.

6.2 Methodology, materials and Equipment

6.2.1 Materials and Equipment

Ortho-aminobenzoic acid, isopropyl alcohol and ultrapure water were used for the experiments of this chapter. Form II of OABA was obtained in laboratory with the procedure described in Chapter 4 of this thesis. For the batch experiments the probes used were: (1) Raman, (2) FBRM, (3) ATR-UV/Vis and (4) PVM. The APFC was implemented using CryPRINS as the operating interface. The solubility curves of the two polymorphs in the chosen solvent (10% IPA w/w and water) are shown in equation 6.1 and 6.2. Measurements were taken using the spectroscopic method described in Chapter 3 and the equations were implemented in CryPRINS to perform supersaturation control:

$$S_{II} = 1.299 \cdot 10^{-5}T^2 - 2.082 \cdot 10^{-4}T + 4.808 \cdot 10^{-3}, \quad (6.1)$$

$$S_I = 1.267 \cdot 10^{-5}T^2 - 2.283 \cdot 10^{-4}T + 4.105 \cdot 10^{-3}, \quad (6.2)$$

where S_I is the solubility of form I, S_{II} the solubility of form II in g/g of solvent and T is the temperature in Celsius degrees. Experiments were performed using the composite PAT array shown in Chapter 3 in a 400 mL vessel: FBRM and PVM were used for monitoring and the Raman and ATR-UV/Vis in the APFC approach.

6.2.2 Effect of solvent ratio

The effect of solvent ratio on the formation of polymorphs for OABA was studied using several solutions of IPA and water. The percentages of IPA analysed are 0, 3, 4, 5, 6, 7, 10, 15, 20, 40, 60 and 80 w/w % IPA. The solutions were held at a constant temperature of 40 °C and form I was added in small quantities until saturation point. They were then heated to 50 °C and maintained at that temperature for at least 20 minutes to ensure complete dissolution of all particles. Finally they were cooled down to 10 °C using a cooling rate of -0.5 °C min^{-1}. FBRM was used to detect nucleation. Immediately after nucleation the solutions were filtered and the crystals left to dry overnight. The nucleated crystals were analysed by microscope and DSC to characterise the presence of a particular polymorph.

6.2.3 Effect of cooling rate and initial concentration

The effect of cooling rate was studied for two different solutions, one at 10% IPA and 40 °C saturation temperature and another at 10% IPA and 30 °C saturation temperature.

The first solution was prepared and heated up to 20 °C, then OABA form I was added. After that, the solution was heated up to 50 °C with a rate of 1 °C/min to dissolve all the solids and kept for 30 minutes at that temperature. Then it was cooled down to 10 °C at a cooling rate of -1 °C/min. Raman spectroscopy was used to check the polymorphic form nucleated and the solution was kept at 10 °C for about 30 minutes. After that time the temperature was increased to 50 °C again to re-dissolve the solid. The same solution was then cooled down at a cooling rate of -0.5 °C/min and the same procedure was repeated for other two different cooling rates (-0.25 and -0.12 °C/min). A different solution at the same initial concentration was prepared and OABA added. A similar procedure was repeated with that solution but using only one cooling rate (-1 °C/min) as a verification of the repeatability of the previous experiments. This second solution was heated up twice at different temperatures to make sure that the entire solid was dissolved and then cooled down twice to investigate if there is any memory effect in the solution. The third solution was prepared at a saturation temperature of 30 °C: the solid were added at the solution at ambient temperature and then heated up to 40 °C. When the solids were dissolved the temperature was decreased to 10 °C at a cooling rate of -1 °C. After holding the solution at 10 °C for 30 minutes it was heated up and then successively cooled down to 10 °C at -0.5 °C/min. Raman, FBRM and ATR-UV/Vis were used simultaneously to check the polymorphic form present in solution and to monitor changes in the particle chord length distribution and solute concentration. To better identify the polymorphic form nucleated second derivative was performed on Raman spectra and two specific peaks, one for the stable and the other for the metastable form of OABA were tracked. In particular the peak at 770 cm^{-1} was associated with Form II and the peak at 1038 cm^{-1} with Form I (Jiang et al. 2008; Jiang et al. 2010a; Jiang et al. 2010b).

6.2.4 Supersaturation control experiments

In this set of experiments mixtures of Form I and II were either seeded or nucleated and the APFC based on the combined used of Raman and ATR-UV/Vis was used to eliminate the metastable form and then grow the stable one. FBRM and PVM were also used to monitor the growth and the shape of the crystals. A simple non-linear function using two different wavelengths ($Abs1$ at 310 nm and $Abs2$ at 356.4 nm) was applied to the first derivative of the ATR-UV/Vis spectra to calculate and control the solute concentration. Equation 6.3 shows the exact formula used:

$$C = 3.365 \cdot 10^{-6}T + 11.20 \quad Abs1 - 9.051 \cdot 10^{-2}Abs1 \cdot T - 6.055 \quad Abs2 - 7.700 \cdot 10^{-2}Abs2 \cdot T - 8.347 \cdot 10^{-4} \quad (6.3)$$

where T is the temperature in °C and $Abs1$ and $Abs2$ the intensities of the first derivative spectra for the chosen wavelengths. The equation was implemented in CryPRINS to monitor the solute concentration of OABA and to perform supersaturation control with respect to form I. The absolute supersaturation setpoint was chosen to be at 0.0008 g/g solvent with respect to the solubility curve of form I. For the Raman signal second derivative was performed to eliminate the baseline effect and decrease the effect of fluorescence. Two peaks were associated to form I and II of OABA: the peak at 770 cm^{-1} was associated to form II and the peak at 1038 cm^{-1} to form I. Saturated solutions of OABA form I at T_{sat} = 40-45 °C were prepared at ambient temperature and heated up to 50-55 °C for complete dissolution of the solid. FBRM was used to check that no crystals remained in the solution. A cooling profile was then started (-1 °C/min for the seeded experiments and -0.5 °C/min for the unseeded) and seeds were added when the operating curve reached the solubility curve of form II. A seed mass of 10% of the total solid amount was used at two different percentages of form II (about 37% and 60% w/w). Two heating rates were also applied +1 °C/min and +0.5 °C/min, to investigate the differences in the in situ determined solubility curves with the heating rate and in comparison with the thermodynamic solubility.

6.3 Results and discussion

6.3.1 Effect of solvent ratio

From this set of experiments it was noticed that water tends to kinetically favour the nucleation of the stable form I while in IPA in most of the cases form II nucleated first. A more detail study of this phenomenon was performed and is presented in chapter 9 of this thesis. Using a percentage between 7-15 % IPA/water the nucleation of mixtures of the two forms were observed as shown in Table 6.1. The concomitant nucleation of form I and II was also reported in the case of nucleation in ethanol and water solutions (Jiang et al. 2008). A solution at 10% of IPA in water was used to investigate the effect of cooling rate on the nucleation of the polymorphic form. This solvent was chosen since it allows

nucleation of both polymorphs and it is, therefore, ideal to prove the concept of the APFC strategy.

Table 6.1: Polymorphic forms obtained at different solvent ratios, based on a joint use of DSC and microscopy

IPA in water (w/w %)	Polymorphic Form Nucleated
0	Form I
3	Form I
4	Form I
5	Form I (small amount of needles)
6	Form I (small amount of needles)
7	Form I (needles observed)
10	Mixture
15	Form II (trace amounts of prisms under microscope)
20	Form II
40	Form II
60	Form II
80	Form II

6.3.2 Effect of cooling rate

The solute concentration was monitored using ATR-UV/Vis during the experiments. Furthermore, PVM and Raman were used to check the polymorphic form nucleated and FBRM to monitor nucleation events. Two different solutions at the same concentration were used but the results are very different as shown in Table 6.2.

Table 6.2: Polymorphic forms obtained from the solutions used in the experiments during the cooling crystallization at different cooling rates (n.p. = not performed)

Cooling rate (°C/min)	Polymorphic form nucleated from solution 1 (T_{sat}=40°C)	Polymorphic form nucleated from solution 2 (T_{sat}=40°C)	Polymorphic form nucleated from solution 3 (T_{sat}=30°C)
-0.12	Form II	n.p.	n.p.
-0.25	Form II	n.p.	n.p.
-0.5	Form II	n.p.	Form I
-1	Form II	Mixture	Form I

Solution 1 was heated up and then cooled down four times at different cooling rates but Raman spectra report only the presence of form II in the nucleated crystals. For solution 2 instead, using the highest cooling rate a mixture of the two polymorphs was nucleated. The experiment was repeated and the dissolution temperature was increased during the second cycle to make sure that the entire solid was dissolved in the solution. A mixture was nucleated the second time, too. This indicates that under certain crystallization conditions (e.g. solvent composition and initial concentration) it is possible to have considerable variation in the polymorphic composition of the nucleated crystals (from pure form of one or the other or mixtures of different compositions), hence a direct feedback control in these cases is necessary to achieve consistency in product quality. A more detail study of the effect of solvent in the polymorphism of OABA is shown in Chapter 9 and 10 of this thesis. Figure 6.2a shows the Raman, ATR-UV/Vis and FBRM signals for solution 1 together with the temperature profile. The nucleation of form II only is clear from the Raman signal. During the nucleation of form II, only the signal for the peak at 770 cm^{-1} increased quickly while the signal for the peak at 1038 cm^{-1} tends to slightly decrease. PVM confirmed the presence of needle like crystals of form II. Interestingly the signal at 1038 cm^{-1} (corresponding to form I) shows a little increase just before nucleation and then a decrease, when the actual nucleation of form II occurs (which is also indicated by the FBRM at a similar time). This behaviour is not present if both form I and II nucleate at the same time as in the case of solution 2 (see Figure 6.2b) or if only form I nucleates as shown in Figure 6.2c for solution 3. This observation seems to indicate that the Raman signal may potentially be able to provide pre-nucleation information that might be correlated with the nucleation mechanism of a particular polymorph or provide an early indication if one or another polymorph is likely to nucleate. The analysis of this pre-nucleation signal variation however requires further investigations. In the case of the nucleation of a mixture the two signals both quickly increase as solids appear in solution (Figure 6.2b), while if only form I nucleates the peak at 1038 cm^{-1} is the only one which increase in intensity (Figure 6.2c). When both forms nucleate together (Figure 6.2b) it can be observed that after nucleation the metastable form II transforms entirely into the more stable form I (the form II peak decreases while the form I peak continues to increase). The same transformation can also be observed in the case of solution 1 for the slowest cooling rate. In the other experiments when only form II nucleated using faster cooling rates (Figure 6.2a) no transformation was

observed within the time period before heating started to dissolve the formed form II crystals.

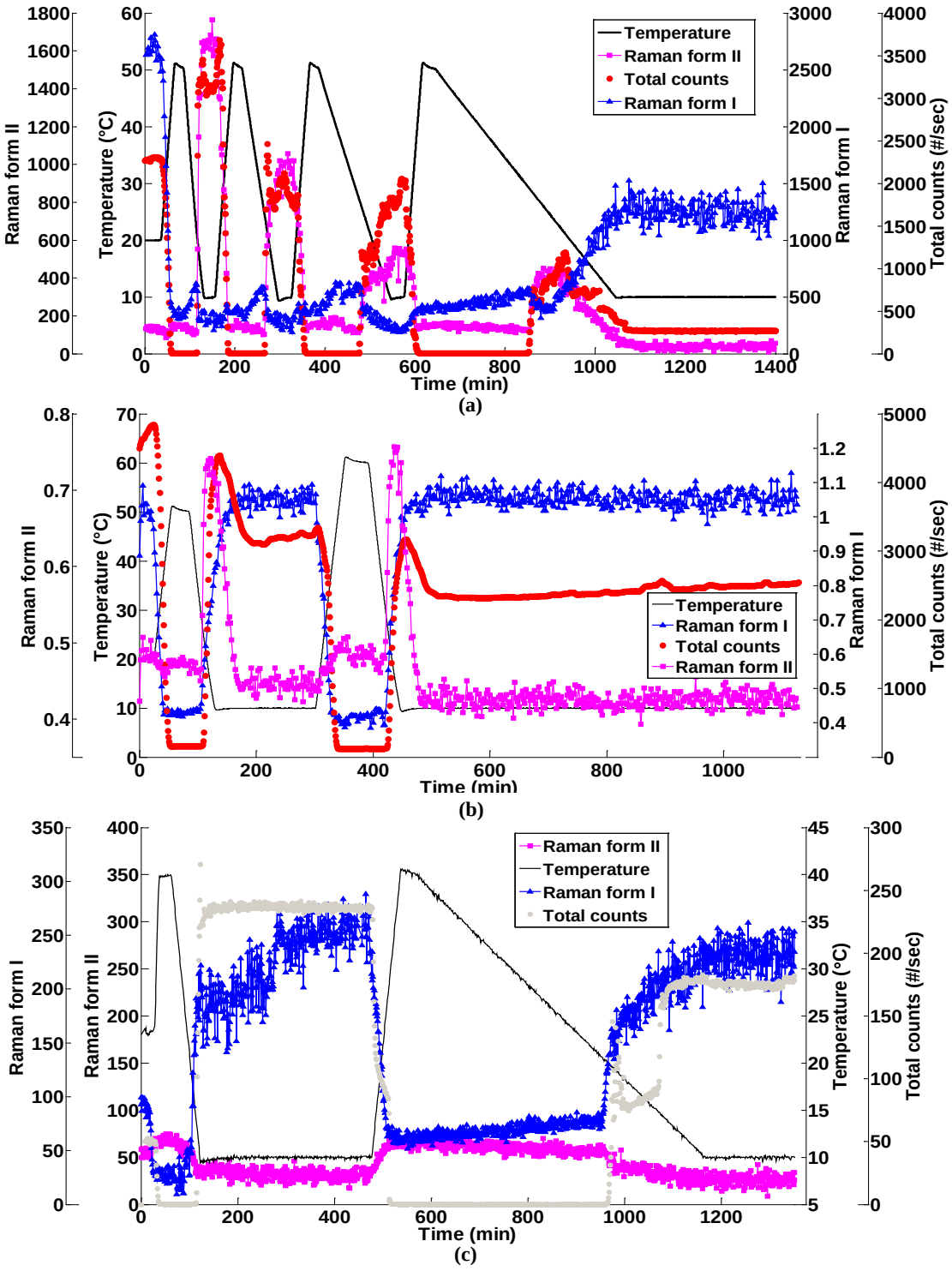

Figure 6.2: Results for the cooling rate effect on (a) solution 1; (b) solution 2 and (c) solution 3. The graphs show the Raman intensities of the specific peaks of form I and II, the total counts from FBRM and the temperature profile. Second derivative was applied for all the Raman spectra in the three experiments. In experiment 2 autoscaling was also performed on Raman spectra in order to eliminate the effect of fluorescence and have a better signal.

As expected these results appear to indicate that the transformation of form II into form I is faster when form I crystals are present in the solution, as it is the case when a mixture nucleates (Figure 6.2b). As expected no transformation is observed when only the more stable form I nucleates (Figure 6.2c). A further proof of the nucleation of form II only in solution 1 is given by the solute concentration trends during the heating phases, which generally follow the solubility curve of form II in all the intermediate heating steps as shown in Figure 6.3a, b and c. The heating profile for the third heating step (Figure 6.3c) is somewhat different from the other two, as the first part of the solute concentration profile does not exactly follow the solubility of form II but seems to be in the middle between the solubility curves of form I and II.

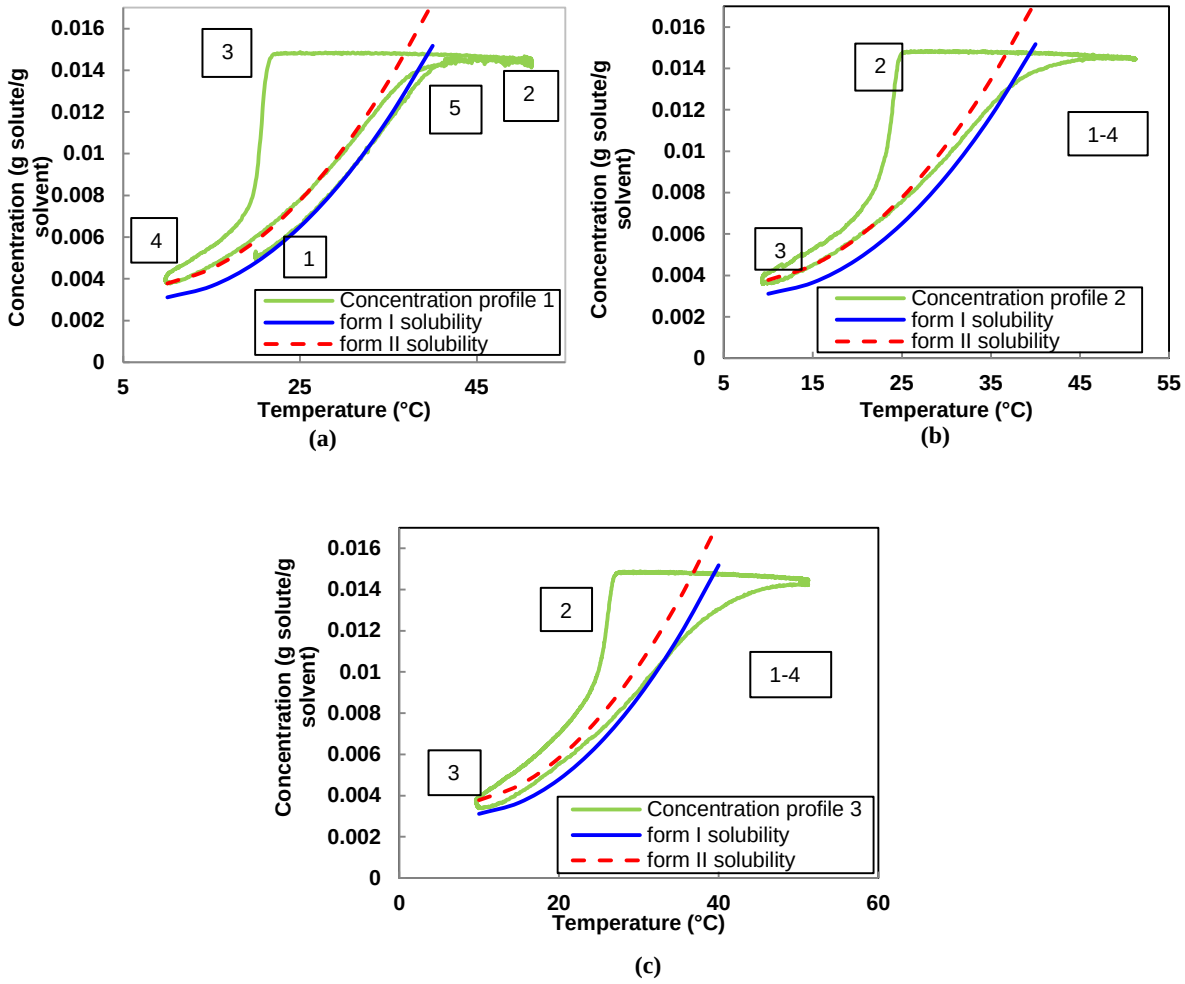

Figure 6.3: Operating curves in the phase diagram during the experiment with solution 1. (a) segment 1-2 heating of a slurry of form 1, segment 2-3 cooling down at -1 °C/min, 3-4 nucleation and growth of form II, 4-5 heating of the resulted slurry of form II; (b) segment 1-2 second cooling down at -0.5 °C/min, 3-4 nucleation and growth of form II, 3-4 heating up of form II (c) segment 1-2 cooling down at -0.25 °C/min, 2-3 nucleation and growth, 3-4 heating up.

After a while the concentration increases and starts to follow the solubility of form II in accordance with the Raman data that shows nucleation of form II only. The behaviour in the first part of the heating step can be an artefact of the UV system, as it does not match completely with the information given by the Raman system, which is the most sensitive to polymorphic changes. This concentration difference indicated by the UV may be caused by a drift in the UV signal as this was the last of a series of long experiments. It can also be noticed that in the second and third heating steps (Figure 6.3b and c) the concentration diverged from the solubility curve of form II at higher temperatures compared to the first heating step (Figure 6.3a). This is due to the fact that the nucleated crystals are larger in size than those used in the first run. Larger crystals dissolve slower compared to fines; as a result, the solution does not perfectly follow the solubility curve during the heating phase with a relatively fast heating rate and after the smaller particles had dissolved. This divergence is even larger for the third heating stage, since the crystallization before that step was conducted at an even slower cooling rate. Generally the slower the cooling rate used, the larger the crystals will be at the end of the batch, hence they will dissolve slower during a subsequent continuous heating phase of the slurry. The larger and fewer crystals are present in the slurry the more the operating curve diverges from the equilibrium solubility curve. If a mixture nucleates, as in the case of solution 2 (see Figure 6.3b) both Raman signals, peaks values at 770 cm^{-1} and 1038 cm^{-1}, increase due to the presence of both polymorphic forms.

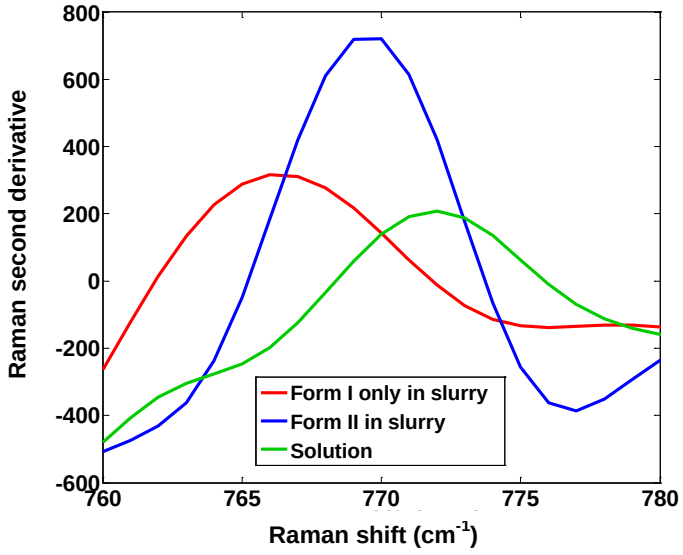

Figure 6.4: Peak at 770 cm^{-1} for clear solution, form I only, a mixture of form II and form I and the clear solution. Second derivative spectra.

The signal of form II increased together with the one of form I and then decreased as transformation happened. The specific behaviour of the two analysed peaks can be used as a calibration-free measurement in a polymorphic control strategy that detects and eliminates impurities of form II and facilitates the growth of form I. This is achieved by initiating controlled dissolution cycles, when and for as long as necessary to complete dissolution of form II, based on the selective monitoring of the corresponding Raman peak; thus without having to wait for the complete polymorphic transformation to occur (which may be longer than the typical batch times). The different spectra (2^{nd} derivative) obtained during a transformation experiment (slurry of pure form I, slurry of form II and I and solution) in the region between 765 cm^{-1} and 745 cm^{-1} are shown in Figure 6.4. The peak at 770 cm^{-1} has a very high intensity when form II is present in the slurry. However, it is still present in clear solution and in slurries of form I, but at lower intensity and slightly shifted. It is possible to distinguish nucleation of pure form I from pure form II looking at the intensity and relative position of this peak after nucleation. If only form I nucleates, the peak slightly shifts but does not change in intensity. In the case of nucleation of form II, even in small amount, the peak shifts and increases in intensity. The change in intensity of the peak at 770 cm^{-1} can be used to detect form II in the slurry and to control its dissolution. This free-calibration method requires a good understanding of the characteristic Raman shifts of the particular system but it is very easy to implement in a control strategy.

6.3.3 Active polymorphic feedback control (APFC) experiment based on combined Raman measurement and supersaturation control

As shown in the previous sections the nucleation of the undesired OABA metastable form or of a mixture of the two forms can often happen in 10% IPA and water. In this section a control strategy is proposed that is able to eliminate the metastable form (which may be present due to co-nucleation or in contaminated seeds) and promote the growth of the stable form. Both seeded and unseeded crystallization experiments were conducted. The active polymorphic feedback control (APFC) uses the Raman signal to detect the presence of form II after seeding or nucleation. As soon as the Raman detects the undesired form, the APFC triggers a heating cycle to dissolve it. A controlled dissolution is applied based on the Raman signal since, because form II is more soluble than form I, there is no reason to dissolve all the solids nucleated or seeded as the metastable form will finish dissolving before the stable one. Two different predetermined heating rates were evaluated, as shown in Table 6.3.

Table 6.3: Experimental conditions of the APFC experiments. The method of crystallization is reported (seeded or unseeded), together with the polymorphic ratio and the heating rate used

Experiment	Initial OABA concentration (g/g solvent)	Seeds amount (% of initial solute in g)	Form II in the seeds (%)	Heating rate (°C/min)	Final product and techniques used to detect the polymorphic form
Mixture seeding 1	0.015	10	37	1	Form I (*Raman spectroscopy, optical microscopy, XRD, DSC*)
Mixture seeding 2	0.016	6	58	1	Form I (*Raman spectroscopy, optical microscopy, XRD, DSC*)
Mixture seeding 3	0.015	10	60	0.5	Form I (*Raman spectroscopy, optical microscopy, XRD, DSC*)
Unseeded	0.017	n.a.	n.a.	0.5	Form I (*Raman spectroscopy, optical microscopy, XRD, DSC*)

After the complete dissolution of form II, which can be detected by the Raman, the APFC switches to a supersaturation control approach that will maintain the operating curve between the solubility curves hence making further contamination of the crystals with the metastable form impossible, allowing the remain stable crystals only to grow. The approach is implemented by the control systems in CryPRINS using ATR-UV/Vis for concentration measurement. The conditions of the different experiments are reported in Table 6.3. The final form of the product was checked on the dried samples using DSC, XRD, optical microscopy and Raman microscopy for all the final samples of each experiment. Results were compared with the data reported in the literature confirming the presence of form I only in the samples (Jiang et al. 2008; Jiang et al. 2010a; Jiang et al. 2010b). In the presentation of the results (Figure 6.5, Figure 6.6, Figure 6.7 and Figure 6.8), for each experiment, only the result from one technique was shown in the figures for more clarity. However, all the techniques were in agreement with each other for all the samples.

Figure 6.5 shows the results for the experiment when a seed consisting of a mixture of form I and II (simulating a contaminated seed). The initial raw material introduced in the system was form I. After complete dissolution the solution is cooled to just above the solubility of form II, so that the system was supersaturated with respect to both polymorphs. At the moment of seeding with the seed mixture, the total counts/s as well as both Raman signals (for form I and II) increases.

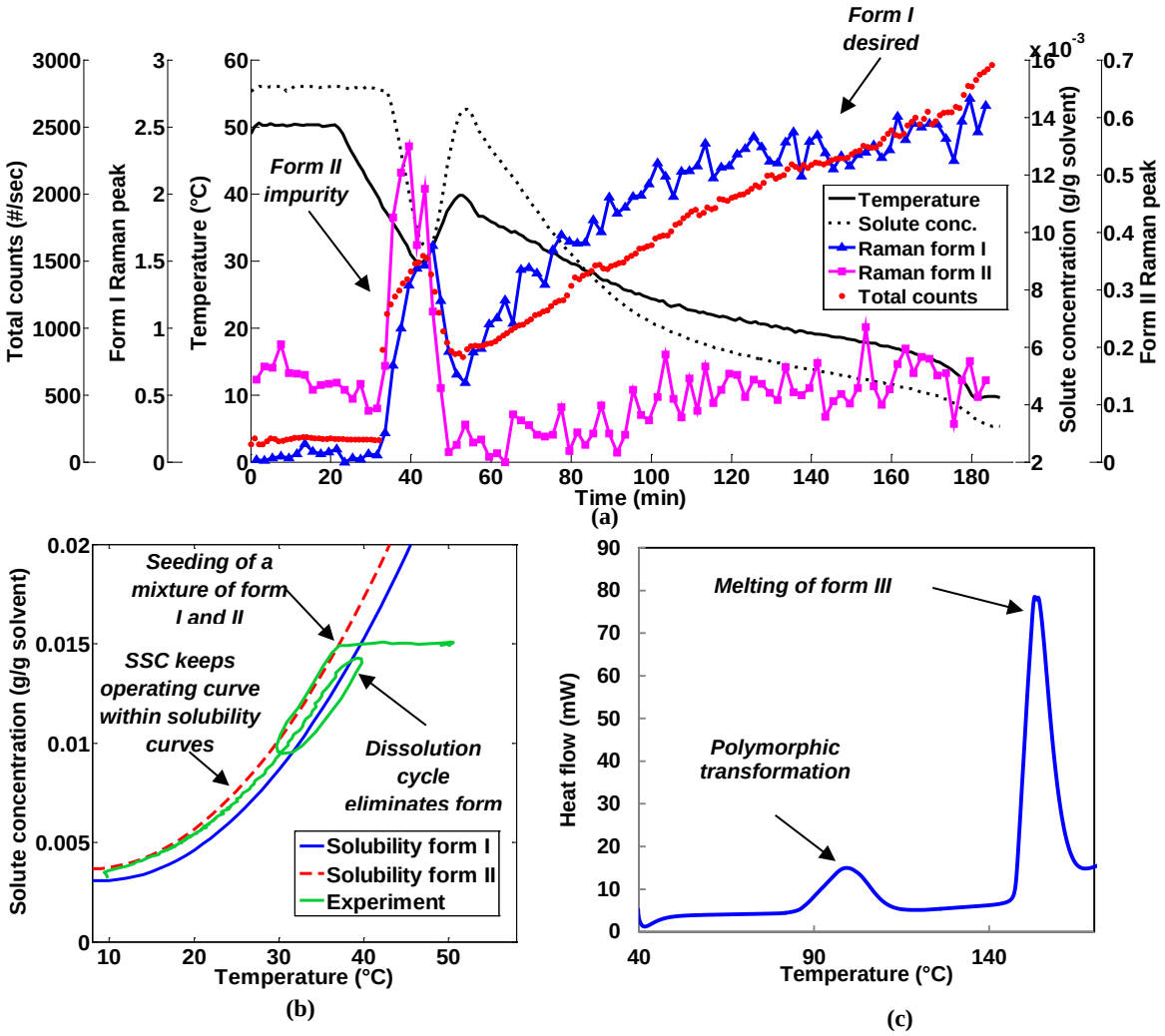

Figure 6.5: Results of the APFC experiment 1 in the case of seeded crystallization, using as seed a mixture of form I and II crystals (~37 % form II) and heating rate of 1°C/min: (a) time evolution of temperature, concentration, Raman signals for form I and II and total counts/s from FBRM; (b) operating curve in the phase diagram; and (c) DSC results for the final dried solid product heated from 40 °C to 180 °C at a rate of 5 °C/min.

Crystals also immediately start growing/ nucleating, as indicated by the rapid decrease in concentration, since the solution is supersaturated with respect to both forms (with higher

supersaturation for form I). As soon as Raman detected form II the APFC switched from cooling to heating. The heating continued until the Raman signal of form II stabilized at the same level as in the solution (which means complete dissolution of form II as shown in the previous sections) and then the control strategy switched to automatic supersaturation control with a setpoint between the solubility curves of the two forms. The supersaturation control approach in CryPRINS automatically calculates the temperature profile needed in order to maintain a constant level of supersaturation. With the amount of seed used (with ~37% of form II) and a rapid heating rate of +1 °C/min the temperature increased from 31 °C to 39 °C to completely dissolve form II. The small change in intensity for the Raman signal of form II after the dissolution cycle is due to changes in solute concentration during the supersaturation control step. The DSC analysis reported in Figure 6.5c shows the transition peak from the stable form to the metastable, which is typical of OABA form I. Form I continued nucleating after the supersaturation control was started as shown by both the total counts/s and the Raman signal for form I (Figure 6.5a). Since the solution was maintained undersaturated with respect to form II, this form did not nucleate again after the dissolution, thus a single cycle was enough to yield final product of pure form I.

Figure 6.6 shows the results obtained from a second seeded experiment with a higher amount of metastable form II in the seed (~58 %) than in the previous case. Using the same heating rate of +1 °C/min as before, the temperature increased from 32 °C to 44 °C to dissolve completely form II. Since more dissolution time was needed to dissolve the larger amount of form II in the seed, and the heating rate was relatively fast, the system reached a higher temperature at the end of the dissolution cycle causing also the concomitant dissolution of more form I during the heating phase. Because a higher amount of the seed introduced was dissolved in this case, at the end of the heating phase the amount of form I crystals was lower, and the concentration of the solution actually increased above the initial solution concentration (Figure 6.6b). After the dissolution cycle the supersaturation control started and the trends of the total counts/s and Raman signals are similar as in the previous run and pure form I was obtained at the end (as shown in the microscopic images shown in Figure 6.6c). The duration of the supersaturation controlled phase of the experiment is much shorter in this case (70 min versus about 2 hours in the other two experiments conducted), since the initial concentration and initial temperature were considerably higher for this run favouring higher growth rate.

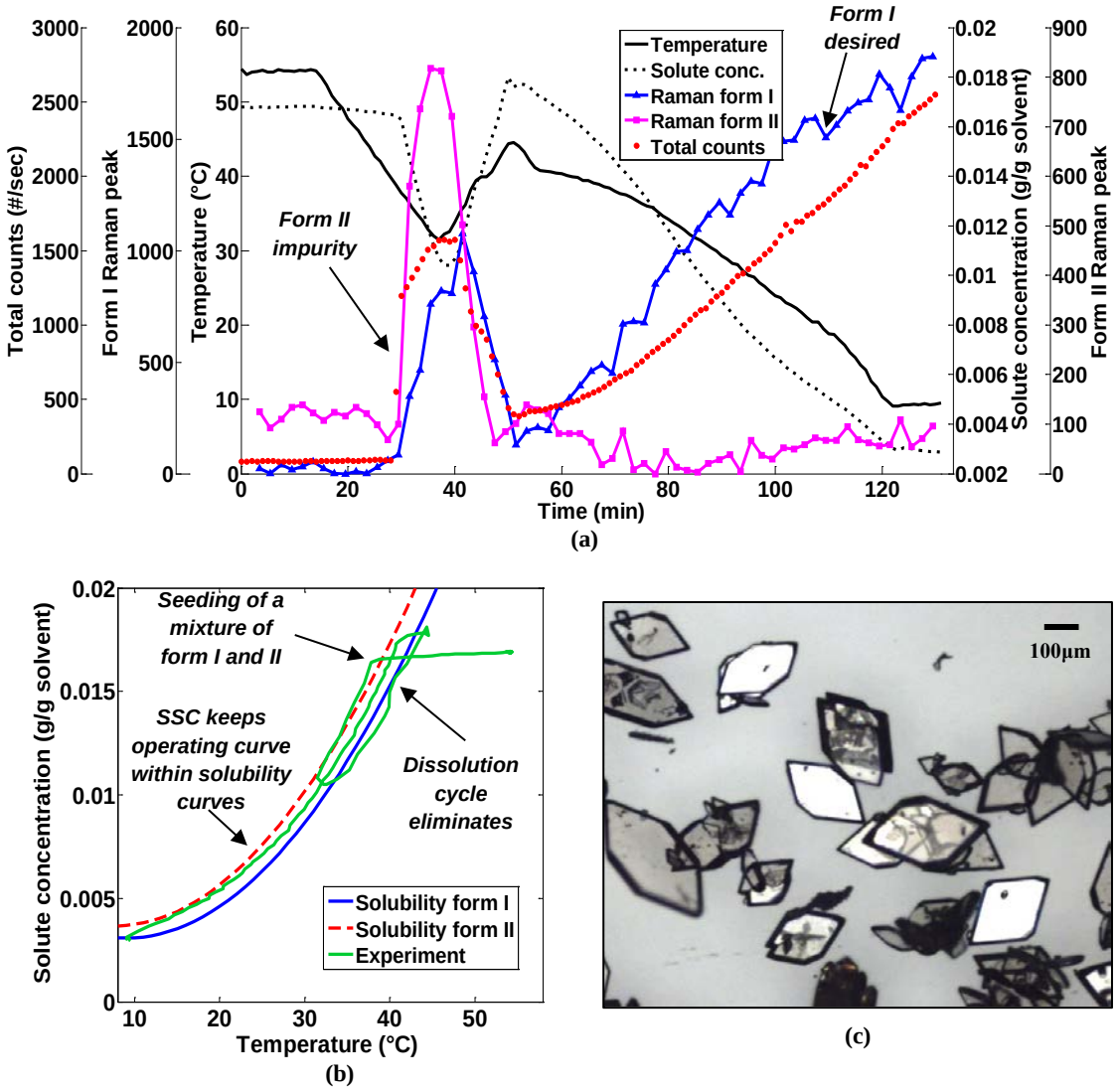

Figure 6.6: Results of the APFC experiment 2, in the case of seeded crystallization, using as seed a mixture of form I and II crystals with higher amount of form II (~58 % form II) and heating rate of 1 °C/min: (a) time evolution of temperature, concentration, Raman signals for form I and II and total counts/s from FBRM; (b) operating curve in the phase diagram; and (c) microscope image of the resulted dried crystals indicating only the presence of form I with no trace of needle-shaped form II crystals in the product.

Figure 6.7 shows the APFC results for Experiment 3 using again seed with higher amount of metastable form II (~60 %) but with a slower heating rate of 0.5 °C/min during the dissolution phase. In this case the temperature increased from 32 to only 39 °C (Figure 6.7b) as opposed to 44 °C as in the previous run; hence less form I dissolved during the heating phase, resulting in a smaller concentration increase than experiment 2. Similarly as in the other two experiments the Raman signal indicates complete dissolution of form II

and the continuous increase in the amount of form I during the supersaturation control phase (Figure 6.7a). The XRD analysis of the dry sample of the product confirmed pure form I (Figure 6.7c). When the contamination level is lower the approach is expected to work even better, with less amount of concomitant dissolution of the desired form.

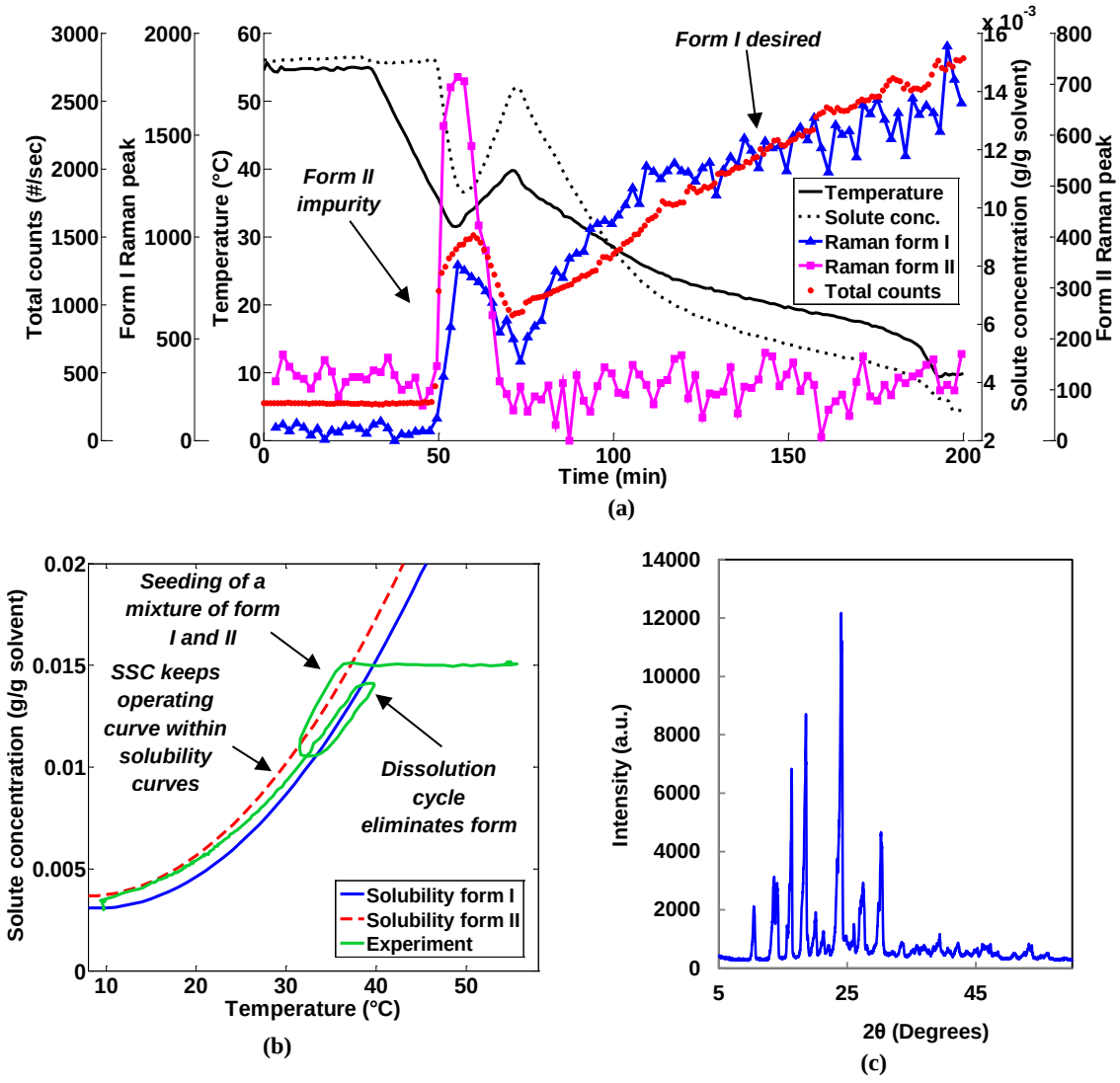

Figure 6.7: Results of the APFC in experiment 3, in the case of seeded crystallization, using as seed a mixture of form I and II crystals with higher amount of form II (~60 % form II) and lower heating rate (0.5°C/min): (a) time evolution of temperature, concentration, Raman signals for form I and II and total counts/s from FBRM; (b) operating curve in the phase diagram; and (c) XRD results for the final dried solid material confirming that the product is pure form I.

These three experiments evaluated the performance of the APFC approach for seeded crystallization in the case of contaminated seed with different but significant levels of polymorphic impurity. The results show that even in the case when the majority of the

seed is the unwanted polymorph this can be selectively dissolved without entirely dissolving the stable form too, since the metastable form has higher solubility. An unseeded experiment was also performed in which a mixture of polymorphs nucleated from a solution with a saturation temperature of 45 °C. A cooling rate of -0.5 °C/min was used for which the onset of nucleation occurred 45 min after the experiment started, at a temperature around 35 °C (Figure 6.8).

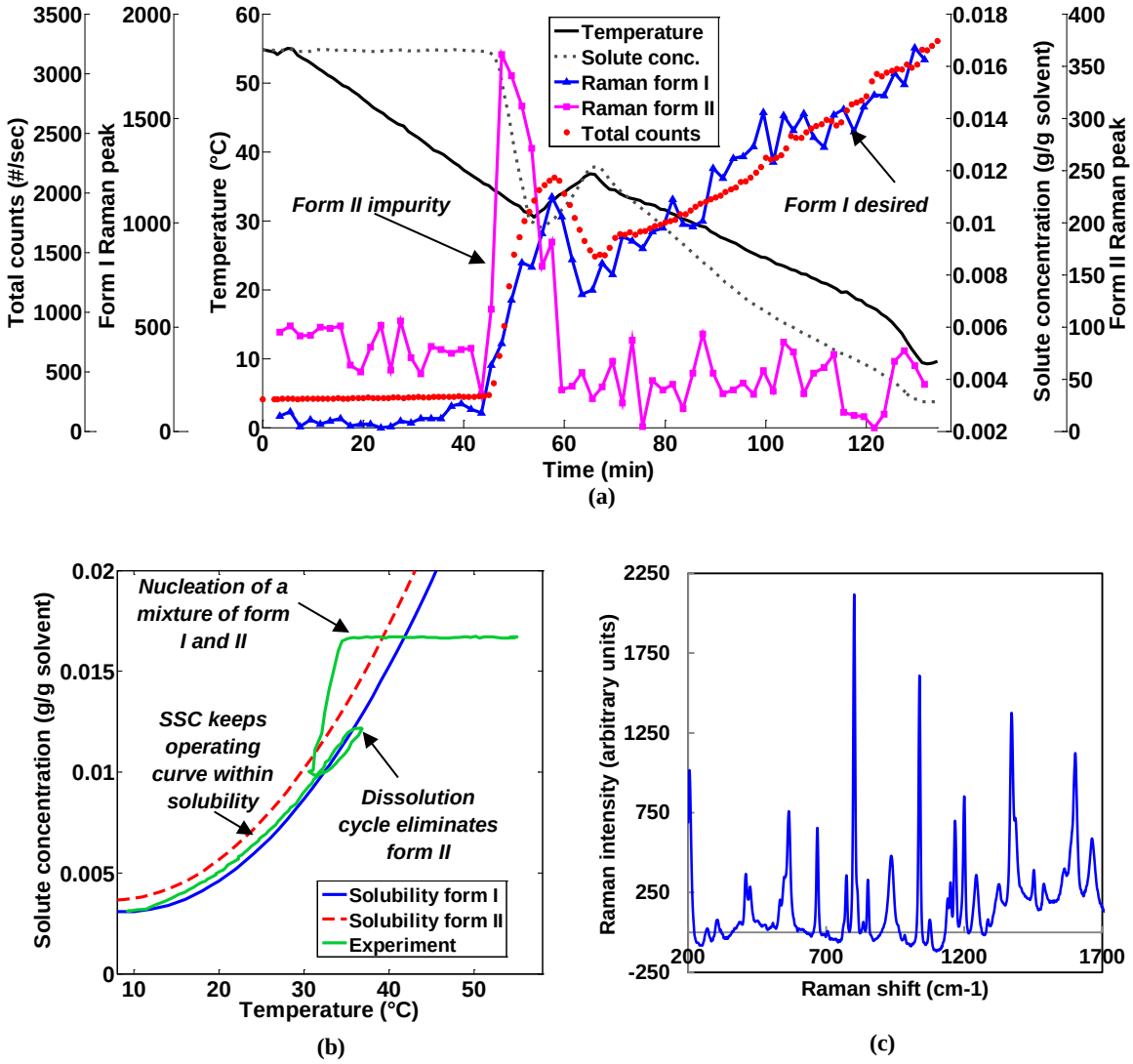

Figure 6.8: Results of the APFC approach applied in the case of an unseeded experiment: (a) time evolution of temperature, concentration, Raman signals for form I and II and total counts/s from FBRM; (b) operating curve in the phase diagram; and (c) Raman spectrum for the final dried solid material confirming pure form I.

Cooling continued and the heating phase was started as soon as the Raman signal of the tracked peak for form II (770 cm^{-1}) increased above the reference level which is the intensity of the peak in clear solution. The dissolution cycle started when the solution temperature was about 31 °C. The heating rate was +0.5 °C/min and the final temperature to complete the dissolution of form II (as indicated by the Raman) was 36 °C. In this case the counts/s remained above 1000 #/sec during the entire heating phase and increased further during the supersaturation control (Figure 6.8a). Although the supersaturation setpoint was reduced from 0.0008 g/g solvent to 0.0004 g/g solvent, the experiment lasted only about one hour since, due to the larger solid concentration in the system, the supersaturation was depleted faster than in the case of the seeded experiments with lower solid concentration (typically well below 1000 counts/s as indicated in all those cases during the initial phase). Similarly, to all the other experiments the use of the supersaturation control enabled to maintain the operating trajectory between the solubility curves of the two forms hence no subsequent nucleation/formation of form II was possible (Figure 6.8b). Therefore, again, only a single controlled dissolution cycle (Figure 6.8b), triggered and designed adaptively by the APFC approach was sufficient to eliminate the metastable polymorph, confirmed by Raman microscopy analysis of the dry product sample (Figure 6.8c). Note that the APFC approach is able to determine automatically when dissolution has to start and stop to eliminate the metastable contaminant adapting the dissolution cycle to the composition of the polymorphic mixture resulting from the nucleation or contaminated seed. Furthermore, although the APFC approach here was presented for experiments where the aim was the formation of pure stable polymorph, the approach can be applied also when the aim is to achieve a polymorph mixture with desired polymorph composition.

6.4 Conclusions

An active polymorphic feedback control (APFC) strategy is proposed to control the polymorphic purity during batch crystallizations using a combination of feedback control techniques based on Raman and ATR-UV/Vis signals. The strategy consists in using a combination of calibration-free Raman technique and calibration-based supersaturation control using ATR-UV/Vis for concentration measurement. The Raman signal is used to identify the presence of the undesired polymorphic form and to trigger its controlled and complete dissolution. This is followed by a supersaturation control phase, based on a

calibrated ATR-UV/Vis signal that maintains the operating curve in the phase diagram where the formation of the undesired polymorph is not possible. The approach can be applied in the case of seeded or unseeded crystallizations when the polymorphic mixture may result from concomitant nucleation of the polymorphs or from contaminated seed. The APFC approach based on the combined Raman and ATR-UV/Vis control strategy was successfully used to produce pure form I of OABA in batch crystallization experiments. For the detailed investigation of the robustness of the APFC approach different experiments were performed using both seeded or unseeded crystallizations, and varying the amount of form I and II at the moment of seeding/nucleation as well as the heating rate used for the controlled dissolution cycle. The APFC adaptively determines the dissolution cycle required for the elimination of the unwanted polymorph. It was found that the more form II is present at the moment of nucleation the higher is the temperature that will be reached in order to dissolve it all. A slow cooling rate reduces the final heating temperature and the dissolution of the stable form. The duration of the superstation controlled phase also strongly depends on the final temperature after that phase. The proposed APFC approach is a highly robust adaptive control strategy that can eliminate batch-to-batch variations in the polymorphic purity of crystalline products that may be caused due to variations in the nucleation composition or from varying polymorphic impurity in the seed (e.g. resulting from previous batch or downstream processing such as milling or drying). While the approach was demonstrated for the production and control of pure polymorphic form, it can also be used when a product with a desired polymorph mixture composition is desired.

7 Systematic model identification for the active polymorphic feedback control of crystallization processes

A model-based active polymorphic feedback control (APFC) is presented in this chapter. The kinetics parameters of ortho-aminobenzoic acid (OABA) are estimated with a series of systematic experiments and then applied to model and optimize the APFC using the population balance equations solved with the method of moments.

7.1 Introduction

The active polymorphic feedback control (APFC) strategy is based on the use of a combination of Raman and ATR-UV/Vis spectroscopy: the approach detects the formation of a polymorphic mixture and eliminates the metastable form by triggering a controlled dissolution cycle, and allowing the growth of the stable form using supersaturation control (see chapter 6 of this thesis). The APFC was found to be effective in obtaining the desired form of the studied compound (ortho-aminobenzoic acid) but little or no control was performed on the final size of the crystals. In fact, during the experiments performed, a partial dissolution of the desired form together with the elimination of the undesired form was observed: it is not clear if this partial dissolution of the stable form leads to its larger final crystal size distribution or not. A model based approach can help to understand if the initial dissolution cycle improves or worsens the final size of the crystals of the stable form and how the temperature profile could be optimized in order to maximize it.

The aim of this work is to determine the kinetic parameters of the growth and polymorphic transformation of ortho-aminobenzoic acid through properly designed experiments and then simulate and optimize the process. Parameter estimation and modelling of polymorphic transformation has rarely been performed because of the complexity of the phenomenon (see Literature Review chapter of this thesis). The parameters necessary to define and model the APFC of ortho-aminobenzoic acid are:

- Dissolution kinetics for both form I and II,
- Growth kinetics for both forms,

- Secondary nucleation of the stable form I (during transformation and after seeding far from the solubility curve)

The estimated parameters will be then validated and applied to an optimization problem in order to better understand the effect of the dissolution cycle generated by the APFC on the final crystal size distribution of form I.

7.2 Methodology, materials and Equipment

The model compound used for the experiments is OABA and the transformation studied is the one from metastable form II to stable form I in a solution of 90% water and 10% IPA. Experiments were performed in the jacketed vessel described in the methodology chapter using the Raman immersion probe for the polymorphic composition determination and the ATR-UV/Vis probe to measure the solute concentration. A Malvern Mastersizer 2000 was used to determine the crystal size distribution at the beginning and during the experiments for most of the samples. The mean and the standard deviation of the crystal size distribution obtained from the Mastersizer, were used to calculate a Gaussian curve that approximate the experimental data. The moments were calculated based on that curve. A previously developed (Chapter 5 and 6) calibration model was used to determine solute concentration from ATR-UV/Vis while specific Raman peaks for form I and II were tracked during the experiments to estimate the rate of transformation. The initial seeds were analysed with a Raman microscope (DXR Raman, Thermofisher) in order to check their purity.

7.2.1 Population balance model and solution

Population balance equations can be used to predict and simulate polymorphic transformations considering one system of equations for each polymorph. Three main mechanisms must be considered during the transformation: nucleation and growth of the more stable form and the dissolution of the less stable polymorph. In the APFC also dissolution of form I must also be considered and estimated. Indicating with the index *II* the parameters of the metastable form of OABA, and with *I* the ones of the stable one the PBEs for the studied system, considering only one dimension, are:

$$\frac{\partial f_{II}}{\partial t} = \frac{\partial (D_{II} f_{II})}{\partial L} \; if \; c_{II} < c_{sat,II} \tag{7.1}$$

for dissolution of form II,

$$\frac{\partial f_{II}}{\partial t} + \frac{\partial (G_{II} f_{II})}{\partial L} = 0 \; if \; c_{II} > c_{sat,II} \tag{7.2}$$

for growth of form II,

$$\frac{\partial f_I}{\partial t} = \frac{\partial (D_I f_I)}{\partial L} \; if \; c_I < c_{sat,I} \tag{7.3}$$

for dissolution of form I,

$$\frac{\partial f_I}{\partial t} + \frac{\partial (G_I f_I)}{\partial L} = B_I \delta (L - L_0) \; if \; c_I > c_{sat,I} \tag{7.4}$$

for growth of form I: where f_{II} and f_I are the average number density functions of the metastable and stable form of OABA and $\delta(L - L_0)$ is the Dirac delta function ($\delta = \infty$ if $L = L_0 = 0$ and $\delta = 0$ if $L \neq L_0$ with $\int_{-\infty}^{+\infty} \delta(x) dx = 1$). $D_{I,II}$ is the dissolution rate of the two forms and $G_{I,II}$ the growth rate defined as:

$$D_{I.II} = \; A_{dI,II} exp\left(\frac{-B_{dI,II}}{T}\right)(1 - S_{I,II}) \tag{7.5}$$

$$G_{I,II} = \; A_{gI,II} exp\left(\frac{-B_{gI,II}}{T}\right)(S_{I,II} - 1)^{a_{I,II}} \tag{7.6}$$

with the supersaturation defined as $S_{I,II} = \frac{C}{C_{satI,II}}$.

Two types of secondary nucleation of the stable form were estimated: (i) secondary nucleation induced by seeding of a mixture of polymorphs when $C > C_{sat,II}$ (ii) secondary nucleation during polymorphic transformation when $C \geq C_{sat,I}$. The different types of nucleation can be described by the equations:

$$B_I = \; A_b S_I^{a_b} + K_{b1} S_I exp(\frac{-K_{b2}}{(\ln S_I)^2}) \tag{7.7}$$

The method of moment was used to solve the equations (Randolph 1988). The j^{th} moment of the distribution of the two polymorphs $f_{I,II}$ is defined by:

$$\mu_{jI,II}(t) = \int_0^\infty L^j f_{I,II}(L,t) dL \tag{7.8}$$

Using this definition of moments the system of equations to solve becomes:

$$\frac{d\mu_{0,I}}{dt} = B_I \tag{7.9}$$

$$\frac{d\mu_{i,I}}{dt} = i(G_I - D_I)\mu_{i-1,I} \; with \; i = 1,2,3 \tag{7.10}$$

$$\frac{d\mu_{0,II}}{dt} = 0 \tag{7.11}$$

$$\frac{d\mu_{i,II}}{dt} = i(G_{II} - D_{II})\mu_{i-1,II} \; with \; i = 1,2,3 \tag{7.12}$$

$$\frac{dC_{liq}}{dt} = 3k_v\rho_c(-G_{II}\mu_{2,II} - G_I\mu_{2,I} + D_{II}\mu_{2,II}) \tag{7.13}$$

An additional condition was added in order to avoid the presence of negative moments: the dissolution terms were considered zero if the first moment became equal or less than zero. In this way the dissolution of each form can stop when all the material is consumed but the solution is not saturated in respect of that form. Matlab was used to solve the equations. The function *ode15s* was used to solve the system and a combination of *fminsearch* and *fmincom* was used to estimate the parameters. The solubility curves for both form I and II between 10 and 40°C were the same used in chapter 6 of this thesis. Despite the system being enantiontropic (Jiang et al. 2010b; Jiang et al. 2010a; Jiang et al. 2008), in the used interval the two OABA polymorphs can be considered monotropically related.

7.2.2 Systematic experimental design for the model identification

Experiments were planned carefully in order to simplify the estimation of the kinetic parameters: the different phenomena were isolated as shown in Figure 7.1 and Table 7.1. Growth and dissolution for both forms were estimated through seeded saturation or desupersaturation experiments. The secondary nucleation of the stable form was estimated through isothermal transformation experiments and using the dissolution and growth kinetics already estimated. Finally secondary nucleation of form I after seeding was evaluated through desupersaturation experiments with low seeds loading at high supersaturation. This approach has two main advantages: (i) Because only one phenomenon is estimated in each set of experiments a correlation between the estimated parameters is avoided (ii) Only concentration data and the initial crystal size distribution are needed for the estimation and no sampling is needed.

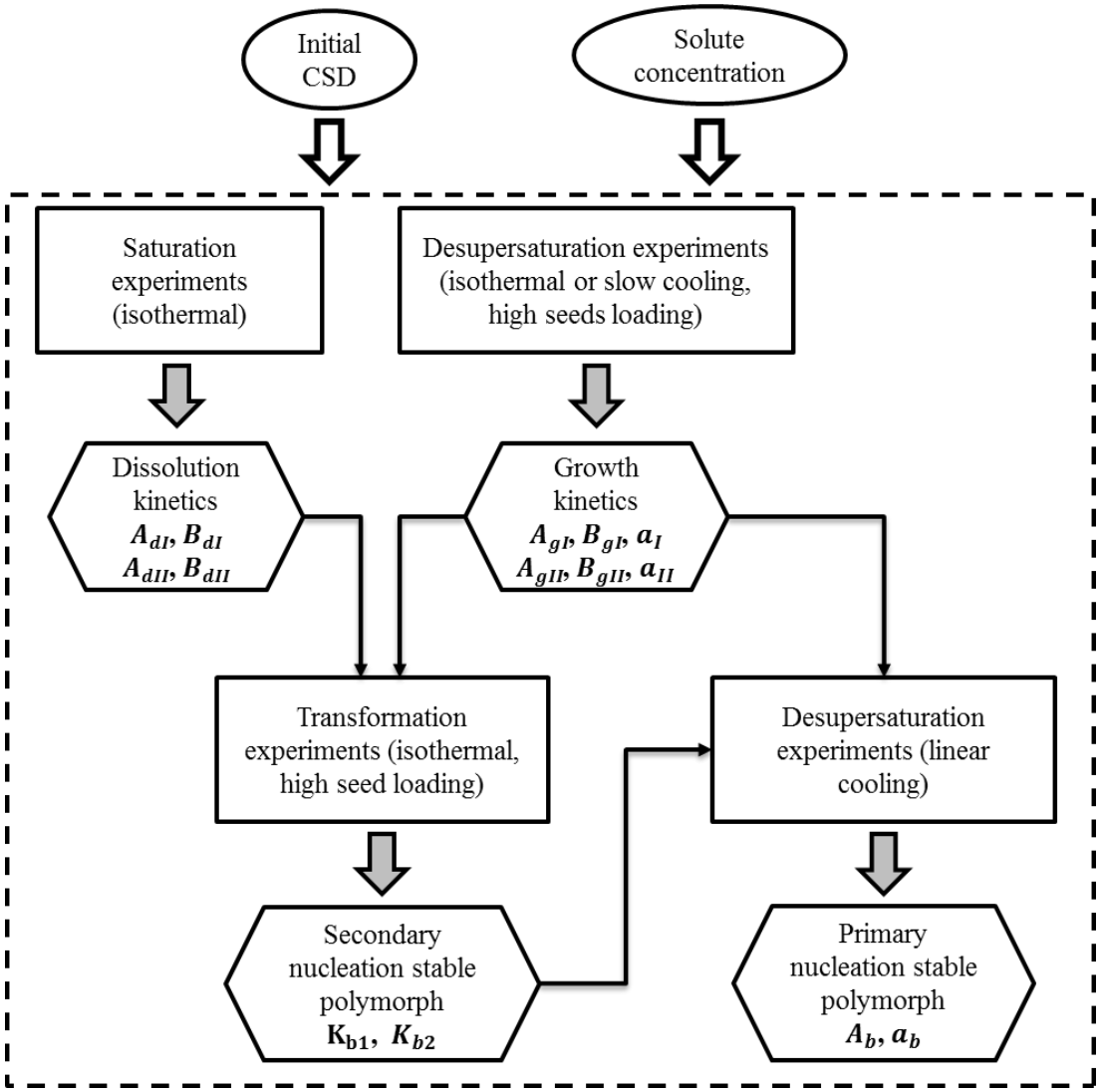

Figure 7.1: Schematic of the experimental design used for the parameters estimation. Growth and dissolution for both forms were estimated through seeded saturation or desupersaturation experiments. The secondary nucleation of the stable form was estimated through isothermal transformation experiments and using the dissolution and growth kinetics already estimated. Finally secondary nucleation of form I after seeding was evaluated through desupersaturation experiments with low seeds loading at high supersaturation.

A detailed list of the experiment performed and their conditions is shown in Table 7.1.

Table 7.1: Description of the conditions used in the different experiments to determine the kinetics parameters of OABA

Parameter estimated	Conditions
A_{dI} and B_{dI}	Four isothermal experiments (10, 15, 25 and 35°C). Seeds were added to the solvent in the amount necessary to have a saturated solution after the complete dissolution.
A_{dII} and B_{dII}	Four isothermal experiments (10, 15, 25 and 35°C). Seeds were added to the solvent in the amount necessary to have a saturated solution. Raman spectroscopy was used to check the absence of polymorphic transformation during dissolution.
A_{gI}, $G_{g,I}$ and a_I	Seeds (10% of the total solute) were added to a saturated solution at 40°C. A slow linear cooling was then applied to avoid nucleation. Two experiments at different cooling rates were performed (-0.1 and -0.05°C/min).
A_{gII}, $G_{g,II}$ and a_{II}	Four isothermal experiments (10, 15, 25 and 35°C). Seeds of the metastable form (10% of the total solute) were added to supersaturated solutions (5°C of supersaturation). Data were considered until the nucleation of the stable form started.
K_{b1} and K_{b2}	Isothermal seeded polymorphic transformation experiments at four different temperatures (10, 15, 25 and 35°C).
A_b and a_b	Seeding of a mixture of polymorph at saturated condition for form II (about 40°C) and cooling at -1°C/min (three experiments, amount of seeds of 10% of the total solute).

7.2.3 Optimization

After estimating the parameters the optimal temperature profile that maximizes the size of form I at the end of the batch and allows complete dissolution of form II was found. The initial temperature of seeding was fixed at around 37°C. The problem is formulated as follow:

$$\min_{T(k)}\left(-\bar{L}_{I,end}\right) \; with \; \bar{L}_{I,end} = \frac{\mu_{1,end}}{\mu_{0,end}} \tag{7.14}$$

Subject to the conditions:

$$-0.5 \leq \frac{dT}{dt} \leq 0.5 \quad (7.15)$$

$$11\ °C \leq T \leq 45\ °C \quad (7.16)$$

$$c_{end} \leq c_{max,end} = 0.005\text{g/g solvent} \quad (7.17)$$

$$\mu_{II1,end} = 0 \quad (7.18)$$

where T is the temperature and c_{end} the solute concentration at the end of the batch. The optimization initial conditions used are shown in Table 7.2.

Table 7.2: Initial conditions for optimization

Seeding Temperature	37.26 °C
Initial concentration of the clear solution	0.015 g/g solvent
Mass of seeds	0.6 g
Form II (% of the seeds)	40%
Mass of solvent	400 g
Seeds size distribution form I	μ = 50 μm; σ = 10 μm
Seeds size distribution form II	μ = 50 μm; σ = 10 μm
Batch time	3hrs

Both the *genetic algorithm* application in Matlab 2013 and the function *fmincon* were used to find the optimal temperature profile that satisfies the constraints imposed.

7.3 Results and Discussion

7.3.1 Parameters estimation and validation

Some of the experiments reported in Table 7.1 could be conducted consecutively in the same solution: growth of the metastable form can be estimated by a seeded experiment that

can then be used to estimate secondary nucleation of the stable form by just letting the metastable form transform. In these cases, sampling at the beginning of the transformation is necessary to estimate the crystal size distribution to use in the parameter estimation. The results of one of the combined experiments are shown in Figure 7.2: growth of metastable form and secondary nucleation of the stable form at 10°C are measured. The first 4000 s of the experiment were used, together with the other three isothermal growth experiments, to estimate growth of form II while the remaining time was used to estimate secondary nucleation of form I. Another important piece of information shown in Figure 7.2: Results for growth of form II and transformation experiment at 10°C. is that the system can be considered neither growth nor dissolution controlled as previously studied compounds.

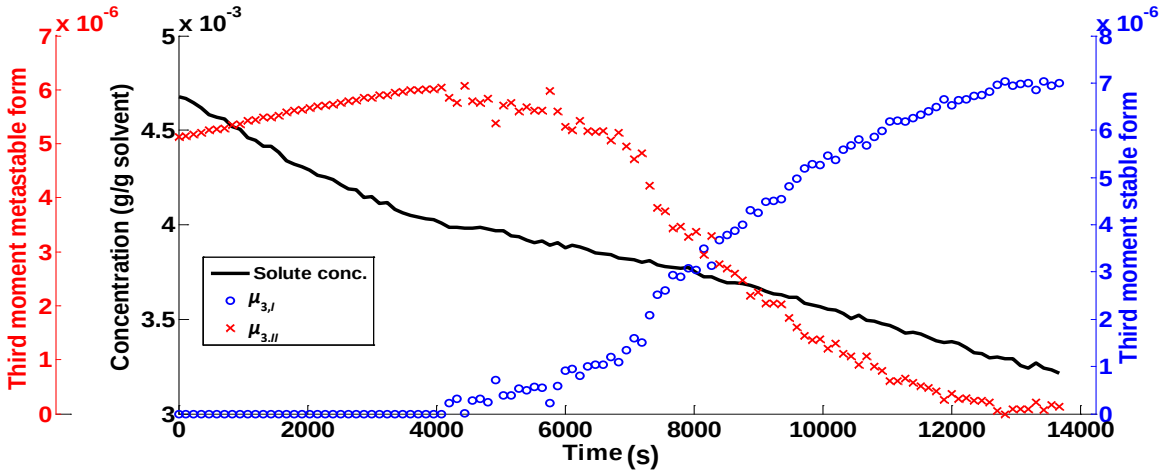

Figure 7.2: Results for growth of form II and transformation experiment at 10°C.

The kinetic parameters estimated from all the experiments are shown in Table 7.3 while Figure 7.3, Figure 7.4 and Figure 7.5 show the simulated and experimental data for dissolution and growth of form I and II at different conditions, as well as the two types of nucleation. The simulated curves follow reasonably well the experimental values.

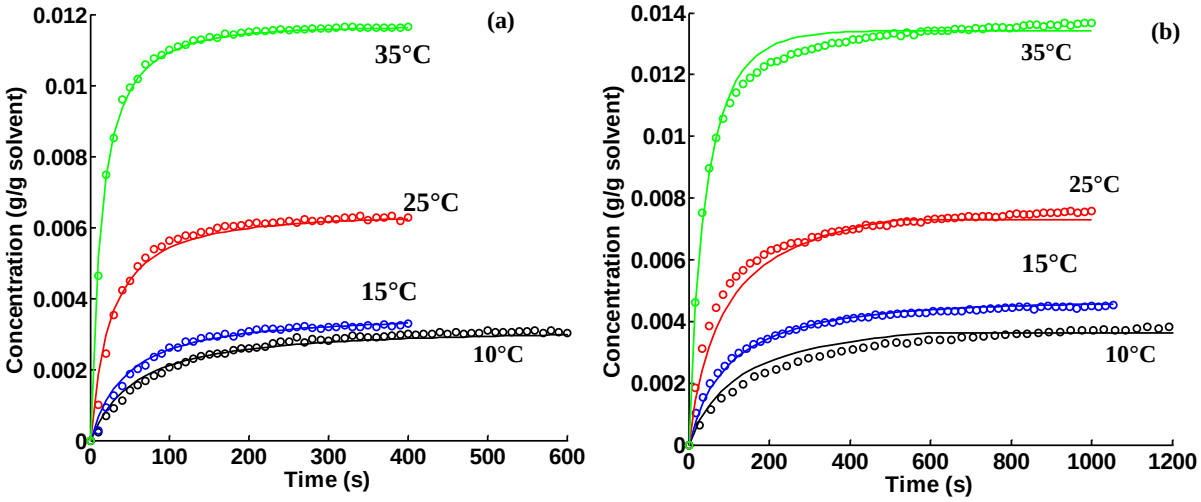

Figure 7.3: (a) Dissolution of form I: continuous line is simulated and dots are experimental data (b) Dissolution of form II: continuous line is simulated and dots are experimental data. Four isothermal experiments were performed to estimate the parameters.

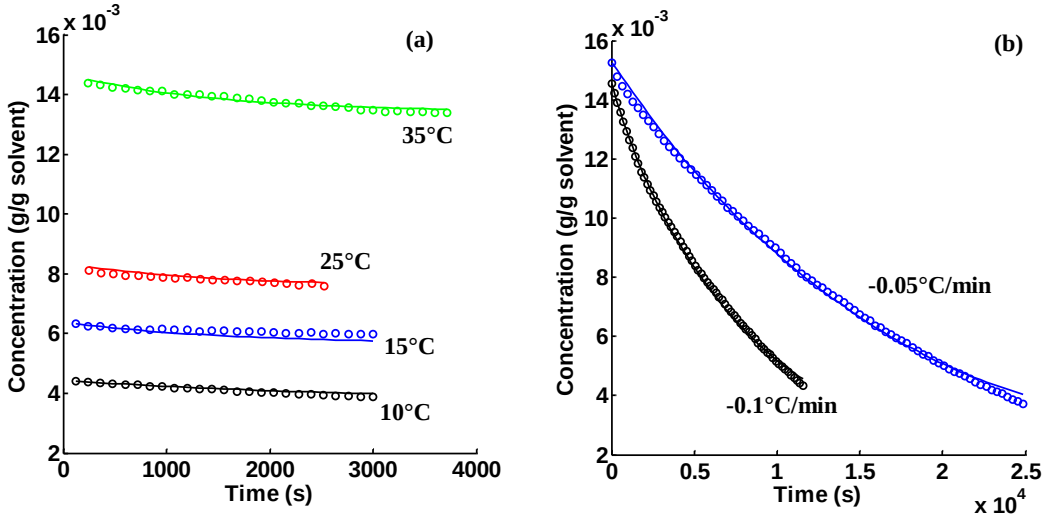

Figure 7.4: (a) Growth of form II at four different temperatures (isothermal experiments): continuous line is simulated and dots are experimental data (b) Growth of form I: continuous line is simulated and dots are experimental data at two different cooling rates.

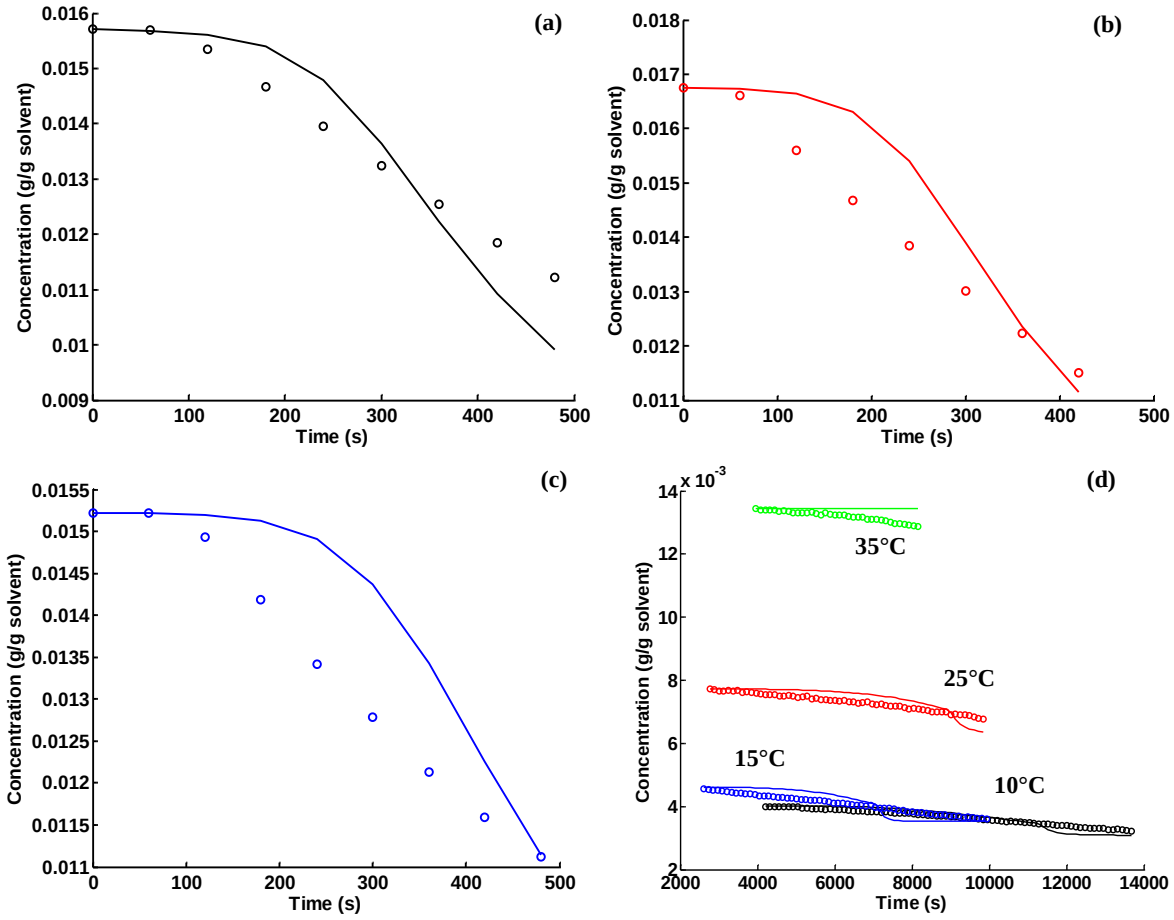

Figure 7.5: (a,b,c) Secondary nucleation of form I after seeding (three experiments, similar conditions): continuous line is simulated and dots are experimental data (d) Secondary nucleation of form I during transformation (four isothermal experiments): continuous line is simulated and dots are experimental data.

Table 7.3 also shows the limits of the 95% confidence interval for all the estimated values. All the parameters present a narrow interval of confidence apart from both the secondary nucleation rates estimated for form I. That is due both to the difficulty in estimating the kinetics parameters for a stochastic process like nucleation and the small amount of experiments performed.

Table 7.3: Kinetic parameters estimated from the performed experiments

Parameter	Value	Sum of square error of prediction (g/g solvent)	Upper limit of the interval of confidence	Lower limit of the interval of confidence
A_{dI} ($m\ s^{-1}$)	4.4	3.33e-6	2.1	9.2
B_{dI} (K)	434e3	3.33e-6	4.2e3	4.6e3
A_{dII} ($m\ s^{-1}$)	1.1e-3	1.25e-5	7.5e-4	1.8e-3
B_{dII} (K)	1.8e3	1.25e-5	1.7e3	2.0e3
A_{gI} ($m\ s^{-1}$)	2.4e8	2.67e-6	1.1e8	5.0e8
B_{gI} (K)	1.10e4	2.67e-6	1.08e4	1.12e4
a_I (-)	1.1	2.67e-6	1.0	1.2
A_{gII} ($m\ s^{-1}$)	1.3e-4	4.96e-7	6.2e-6	2.6e-3
B_{gII} (K)	2.0e3	4.96e-7	1.4e3	3.0e3
a_{gII} (-)	1.0	4.96e-7	0.77	1.2
K_{t1} ($\#\ m^{-3}s^{-1}$)	1.6e10	1.086e-5	1.2e10	2.1e10
K_{t2} (-)	3.94e-1	1.086e-5	3.8e-1	4.1e-1
A_b ($\#\ m^{-3}s^{-1}$)	1.7e8	1.753e-5	7.4e6	3.7e9
a_b (-)	2.4	1.753e-5	-13.8	18.5

One of the APFC experiments performed was used to validate the set of parameters estimated. Seeding and dissolution cycle were simulated with the intial conditions shown in Table 7.4.

Table 7.4: Initial conditions for optimization

Seeding Temperature	37.26 °C
Initial concentration of the clear solution	0.0151 g/g solvent
Mass of seeds	0.61 g
Form II (% of the seeds)	60%
Mass of solvent	400 g
Seeds size distribution form I	μ = 69 μm; σ = 6 μm
Seeds size distribution form II	μ = 225 μm; σ = 75 μm

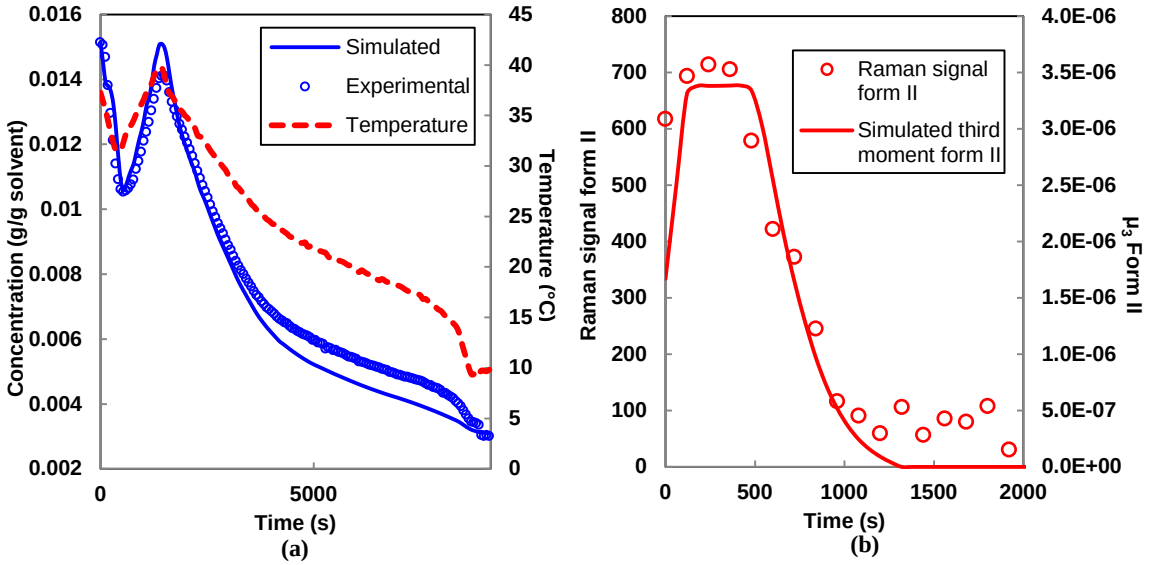

Figure 7.6: Model validation, experimental and simulated data for an APFC experiments (a) Temperature plotted with experimental and simulated concentration (b) Raman signal during the experiment and simulated first moment of form II.

The mean μ and the sigma σ of the initial crystal size distribution for form I and II for the validation experiment were estimated as:

$$\mu = \frac{L_{max}+L_{min}}{2} \tag{7.19}$$

$$\sigma = \frac{L_{max} - L_{min}}{2} \tag{7.20}$$

where L_{max} and L_{min} are the maximum and minimum size of the sieves used to prepare the seeds. Similarly to the procedure for the kinetic parameter estimation, the mean and sigma calculated from the size of the sieves were used to calculate a Gaussian distribution which was used as initial condition for the validation. The results of the validation experiment are shown in Figure 7.6 and Figure 7.7. The curve of the simulated concentration correctly follows the experimental data (Figure 7.6a) and the trend of the first moment of form II is similar to the corresponding Raman signal (as shown in Figure 7.6b where the two trends are plot together for comparison). Since Raman intensity is directly proportional to the amount of solid in suspension in the vessel (as shown in chapter 4 of this thesis), its trend can be directly compared to one of the third moment of form II. A discrepancy between experimental and simulated data is present in the cooling section and it is probably due to the uncertainty in the estimation of secondary nucleation (the form I first moment simulated is higher than the actual one and, therefore, the growth is overestimated). However, the maximum percentage error on the concentration measurement is 16.47% and it is localized in the cooling section, and the time of complete dissolution of the undesired form is picked up correctly. This means that the model is able to simulate and predict well the APFC dissolution cycle so it is suitable for optimization.

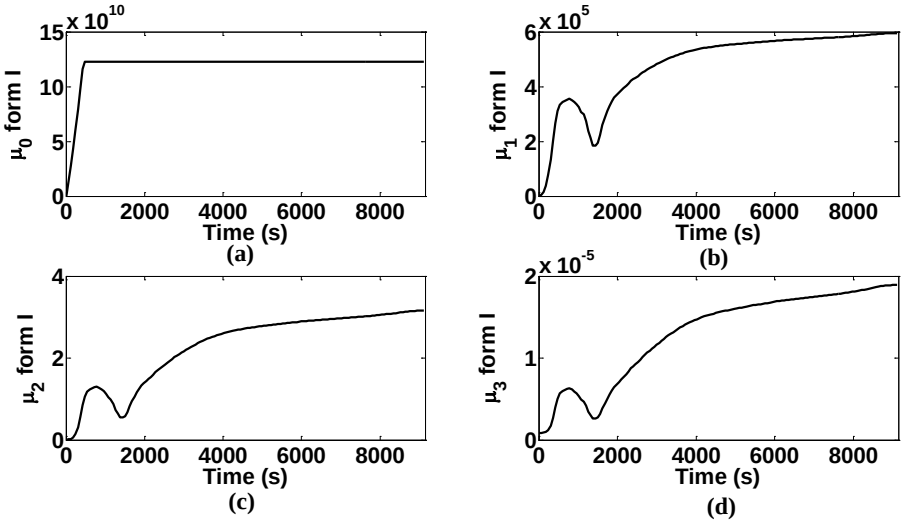

Figure 7.7: Model validation, experimental and simulated data for an APFC experiments (a) Simulated zeroth moment of form I (b) Simulated first moment of form I(c) Simulated second moment of form I (d) Simulated third moment of form I.

The simulated first, second and third moment of form I are shown in Figure 7.7. The third moment can be directly compared to the intensity of the Raman peak for form I (shown in Figure 7.8): the two trends are again very similar. The amount of form I increases because of seeding and nucleation, then decreases during the dissolution cycle because of partial dissolution of form I with form II and then increases again for the growth.

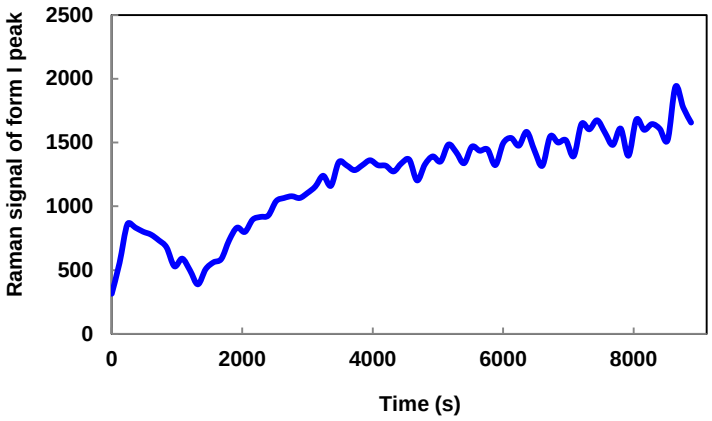

Figure 7.8: Trend of the Raman peak typical of form I during the all experiment. The signal is proportional to the amount of solid form I in the slurry and the trend resembles the simulated first, second and third moment of form I shown in Figure 7.7.

7.3.2 Optimization

Optimization was performed using the kinetics parameters to find the optimal temperature profile that eliminates form II and maximize the size of the crystals of form I at the end of the batch. Fifteen different points were estimated using the genetic algorithm application and then the *fmincon* function in Matlab 2013. The results of the optimization (shown in Figure 7.9a to d) demonstrated that a heating step is not only required to eliminate form II but also allow a larger crystal size of form I at the end of the batch. Imposing only cooling in the optimization code ($-0.5°\frac{C}{min} \leq \frac{dT}{dt} \leq -0.001°C/\text{min}$) resulted in lower crystal size, although all the metastable form naturally converted to the stable one by the end of the batch. The value of the objective function calculated was quite low compare to the experimental results ($\frac{\mu_{1,Iopt}}{\mu_{0,Iopt}} = 20.6\ \mu m$ against a normal end of batch value of around 100-150 µm) but this is most probably due to the uncertainty of the parameters for nucleation of form I. The presence of heating steps in optimized batch crystallization was already found by other authors (Majumder and Nagy 2013; Qamar et al. 2010; Yeom et al. 2013)

as a results of the inclusion of the dissolution kinetics in the PBEs. In those cases heating can correct a non-optimal seeding and allow a better final CSD. After the heating step the temperature is kept high in order to allow growth of the form I crystal and then drops in the end to reach the desired yield.

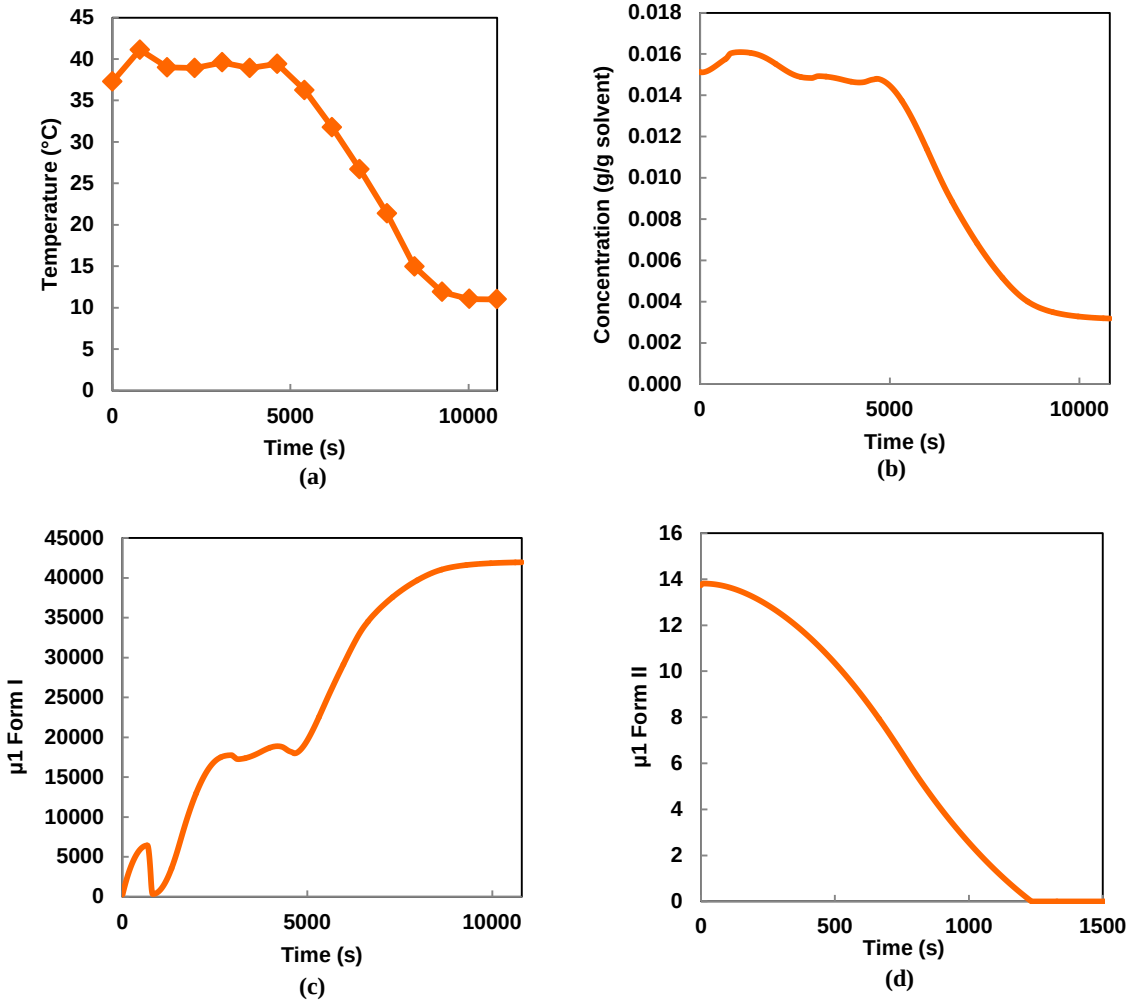

Figure 7.9: (a) Optimal temperature calculated (b) Concentration profile associated with the optimal temperatures estimated (c) First moment of form I profile associated with the optimal temperatures estimated (d) First moment of form II profile associated with the optimal temperatures estimated.

Figure 7.9a shows the evolution of the optimal temperature over the batch time: a first heating step allows dissolution of form II while the following two smaller ones (at around 3000s) are used to obtain larger crystal of form I. Figure 7.9b shows the calculated solute concentration over the optimal temperature profile while Figure 7.9c and d shows the calculated first moment of form I and II. Form II is completely dissolved after the first dissolution cycle that dissolve also part of form I. The remaining crystals of form I keep

growing until the end of the batch. Figure 7.10 shows the optimized temperature profile and supersaturation in the equilibrium graph. After the dissolution cycles the supersaturation is kept above the solubility of form I in order to grow its crystals but below the solubility of form II to avoid its further nucleation during the batch.

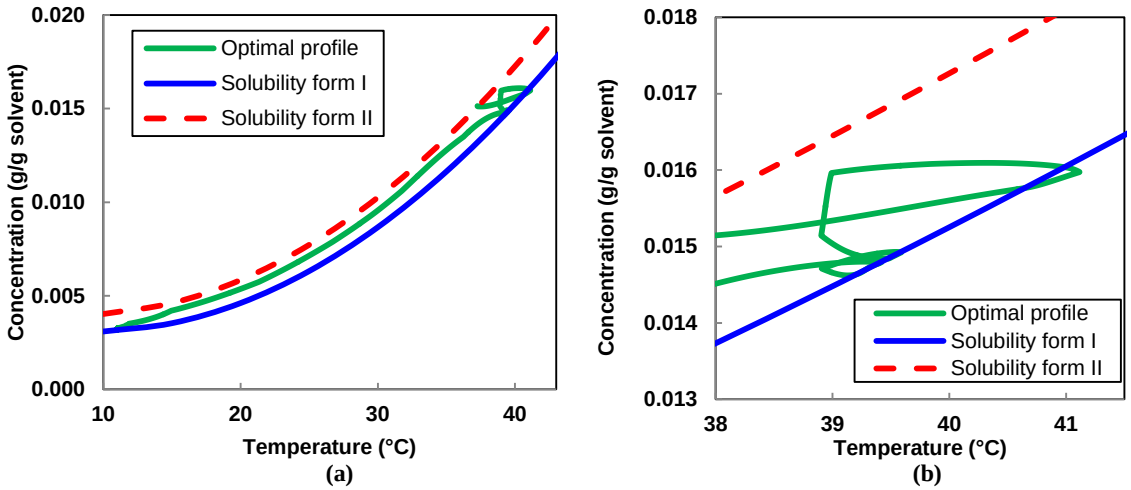

Figure 7.10: (a) Optimal temperature profile in the phase equilibrium graph. The solute concentration is always below the solubility of form II that, therefore, cannot nucleated again after its dissolution. (b) Detail view of the smaller dissolution cycles.

7.4 Conclusions

The active polymorphic feedback control (APFC, described in chapter 6) is a strategy that detects and eliminates the metastable polymorph after nucleation of a mixture or erroneous seeding. The approach uses a combination of Raman spectroscopy to detect the metastable polymorph and trigger a dissolution cycle to eliminate it, and then ATR-UV/Vis spectroscopy to grow the remaining crystals of the stable form through supersaturation control. Despite being very efficient in obtaining the pure stable polymorph, this model-free control does not lead to its optimal crystal size distribution at the end of the batch. In fact, the size distribution of the crystals of the stable form after the dissolution cycle is not controlled and it might not be the optimal to allow a good quality CSD at the end of the supersaturation control. For this reason a model-based APFC, that allows both the elimination of the metastable form and larger crystals of the stable form at the end of the batch, was developed in this chapter. The kinetic parameters that are needed to describe the APFC for ortho-aminobenzoic acid (dissolution and growth of form I and II, secondary

nucleation of form I) were estimated and validated using the data from one of the seeded experiment shown in chapter 6. A specific design of experiments was performed to estimate each parameter separately and therefore, to avoid correlations between them as well as to simplify the calculation. All the parameters estimated presented a narrow interval of 95 % confidence apart from the nucleation of the stable form, probably because of the stochastic nature of this phenomenon.

After the parameter estimation, optimization was performed. It was found that the dissolution cycle normally induced by the APFC not only allows the elimination of the metastable form II but it is also beneficial to obtain larger crystals of form I at the end of the batch. This is in accordance with experiments as well as with the results of other optimization studies where dissolution was included in the model. The final number mean diameter for the optimal profile obtained differs from what was normally obtained in the experiments but that is due to the uncertainty in the estimation of the secondary nucleation parameters.

8 In situ monitoring of polymorphic transformations using a composite sensor array of Raman, NIR, ATR-UV/Vis spectroscopy, FBRM and PVM, for an intelligent decision support system

This chapter introduces the concept of composite sensor array (CSA). Signals from multiple probes are merged and analysed using chemometrics during the polymorphic transformation of ortho-aminobenzoic acid. The CSA allows a quicker and easier interpretation of data from multiple instruments.

8.1. Introduction

Raman, Particle vision measurement (PVM) and infrared spectroscopy have already been used singularly to detect nucleation and polymorphic transformations during crystallization processes as well as to analyse powder mixtures of multiple polymorphic forms. However, a comprehensive study and comparison between these techniques used simultaneously with the integration of the signals, during polymorphic transformation has not been performed yet.

The aims of this chapter are to evaluate the capability of different PAT tools for monitoring polymorphic transformation during crystallization, to provide a systematic analysis of the signals and to investigate which combinations of tools is the best for the detection of various mechanisms in a particular system. Additionally, the framework of composite sensor array (CSA) is introduced, which is based on the integration of signals from multiple sensors using principal component analysis. The idea of combining multiple sensors in one measurement hardware cluster has been developed by Zeton B.V. (the Netherlands). The company manufactured a sensor skid that contains a microcamera, an ATR-FTIR spectrophotometer, an ultrasound devices as well as a refractometer (Kadam et al. 2012). A device composed of multiple probes was also used by Helmdach et al. (2013). Nevertheless, while these systems combined physically multiple pieces of hardware, they represent decentralized PAT arrays since none of the them provided any mechanism for the integration of signals and data fusion. An example of data processing with the

commercial softwares PEAXACT (S-PACT GmbH) and OPUS was performed on MID-IR data by Helmdach et al.(2013) but the concept of centralized CSA was first proposed by Nagy and Braatz (2012), and is based on the integration of information from multiple PAT tools for automated detection of various events that may occur during crystallization. More than one PAT tool is often used for development and scale up of crystallization processes, and while crystallization experts typically analyse and interpret the complementary information to understand the process, there is no framework available for automated signal integration and interpretation using model-based approach or chemometrics techniques (such as principal components analysis). According to the concept of CSA, combining the signals from all the techniques is the same as having a single global sensor that can monitor all the different phenomena detectable by different individual tools. The signals can be analysed simultaneously using chemometrics techniques and combined in principal components that can more easily interpreted and eventually used in control of the process (Nagy 2012; Nagy et al. 2013). The Crystallization Process Informatics Systems (CryPRINS) is a software platform, that consists of the communication interface required to integrate various PAT hardware from the CSA, the automated data fusion mechanism (e.g. based on chemometrics or model-based approaches) and intelligent algorithms that can be used to coordinate the various components of the CSA and exploit all signals from all measurement devices for automated decision support and feedback control (Nagy 2012). The present chapter provides a systematic comparative investigation of the potential of different PAT tools in monitoring polymorphic transformation and presents the first proof of concept of the CSA framework using chemometrics based data fusion as well as introduces a methodology for the determination of optimal sensor configuration for the automated detection of various crystallization events.

8.1 Methodology, materials and equipment

8.1.1 Materials and experimental setup

OABA in solutions of water and IPA (90/10 w/w) was used in the experiments described in this chapter. The system of PAT probes used included:

- Raman;
- NIR transflection;

- NIR reflection;
- ATR-UV/Vis;
- FBRM;
- PVM.

The data from the FBRM, ATR-UV/Vis and the Huber was transmitted in real-time to the Crystallization process Informatics System (CryPRINS) software. Raman and NIR data were collected with the software packages of the respective instruments. Experiments were performed using all the probes at the same time in order to compare the information under identical experimental conditions and integrate the signals. The probes were put close to the stirrer and all at the same height in order to have the best quality of measurement. This work is mainly focused on polymorphic transformation which happens in the solid state and that is why most of the tools used are related to solid state analysis (NIR and Raman). ATR-UV/Vis was also used because of its capacity to detect the different solubility of the two polymorphs.

8.1.2 Experimental methodology

Four experiments were conducted with the arrangement of probes shown in Table 8.1.

Table 8.1: probes used during the performed experiments

Experiment	Probes used
1	NIR reflectance (NIR ref.), Raman, FBRM
2	NIR transflectance (NIR trans.), Raman, FBRM
3	ATR-UV/Vis, Raman, FBRM
4	ATR-UV/Vis, Raman, FBRM

Solutions of OABA pure form I containing 0.017g/g solvent (saturation temperature of about 40°C) were used for the experiments. The solutions were heated up to 50°C, kept for 30 min in order to dissolve all the solids and then cooled down at a rate of -1°C/min. Data recording was started at 50°C after the complete dissolution of the starting material. Because of the high concentration of water in solution, which favours sticking of the crystals on the probes, FBRM signal was disturbed (total counts and chord length

distribution present spikes and peaks). However, it was still possible to distinguish nucleation and polymorphic change from the FBRM in both the experiments. NIR and Raman signal are apparently less influenced by sticking and also PVM could still give very good and useful information.

8.1.3 Signal integration using principal components analysis (PCA)

PCA (using the *svd* function in Matlab) was performed on the CSA matrix formed by the signals taken from all the probes at the same time interval. This technique can be effectively used to isolate the effect of different crystallization phenomena (such as nucleation, polymorphic transformation, agglomeration, etc.) on the Raman spectra and have useful real-time information about the process. This work represents the first step towards the realization of the CSA concept. PCA has been performed on a matrix formed by multiple signals from different probes and results have been analysed in order to understand the potential of this approach in automatically detecting polymorphic transformations and differentiating it from other potential mechanisms which may lead to changes in the signals. Raman signal, total counts, and NIR or ATR-UV/Vis were arranged in a single matrix. Data were pre-processed separately as shown in Table 8.2.

Table 8.2: Summary of the pre-processing for each probe measurement before performing principal component analysis. In the right column the indexes of the total merged matrix of signal are associated to each probe

Data	Pre-processing	Merged matrix index
Raman spectra	2^{nd} derivative, smoothing in region from 400 to 1700cm^{-1}	1-1286
ATR-UV/Vis	1^{st} derivative in region from 220 to 725 nm	1287-1526
NIR spectra	Smoothing in region from 5000 to 6500 cm^{-1} (higher smoothing for reflectance probe)	1287-1525 (NIR refl.) 1287-1575 (NIR trans.)
Data from FBRM	Time averaging (10 seconds)	1527 (ATR-UV/Vis) 1526 (NIR refl.) 1576 (NIR trans.)

Before merging the data in a unique matrix, autoscaling was performed individually for every type of signal. In this way the same weight is given to the signals from each probe. The crystallization process can be analysed and interesting information may be inferred

from the scores plotted versus time, the corresponding loadings plotted in scatter plots, as well as plotting the first and second principle component scores (PC1 versus PC2) and identifying clusters. The scores plots are generally used to detect similarities, differences or other interesting relationships among samples. Loadings are also often presented in two-dimensional scatter plots, but they can be plotted against the wavelength, too. The loadings are used to understand the relationship between the scores and the original variables and to select the optimal sensor configuration given the set of available PAT tools. In order to interpret in an easier way the loadings, Varimax rotation was performed on the CSA loadings using Matlab (function *rotatefactors*). This operation maximizes the sum of the variances of the square loadings: in this way every component is associated to a smaller amount of variables and the determination of the most influent probes in the set that compose the CSA is greatly simplified.

8.2 Results and discussion

8.2.1 Qualitative analysis of the single signals (decentralised CSA)

Raman and NIR spectra of the solid forms of OABA were already described in chapter three of this thesis. The Raman peaks tracked for this set of experiments are: 770 cm^{-1} for form II and 784 for form I. Second derivative and smoothing were used in order to partially eliminate the effect of fluorescence that was observed in the system even with clear solutions and peak values were multiplied by -1 in order to have the same sign of the raw spectrum. In the case of the NIR spectrum in slurry, the absorption of water overlaps the region that presents more differences between the two polymorphic forms in the solid state (6500-7500 cm-1). However, it is still possible to identify a peak for form I around 5950 cm^{-1} and also to distinguish the two forms from a baseline effect in both reflectance and transflectance mode. In fact, the amount of diffuse radiation going to the detector is affected by the total amount of solids, their shape and size. A change in one of these parameters, due to dissolution, nucleation or polymorphic transition, will generate a shift of the all spectrum to lower or higher absorbance intensity. In particular, form I of OABA is characterized by prismatic crystals instead of the needle-like form II, which results in a shift to higher absorbance values in the case of the reflectance probe and to lower values for the transflectance probe during the polymorphic transformation.

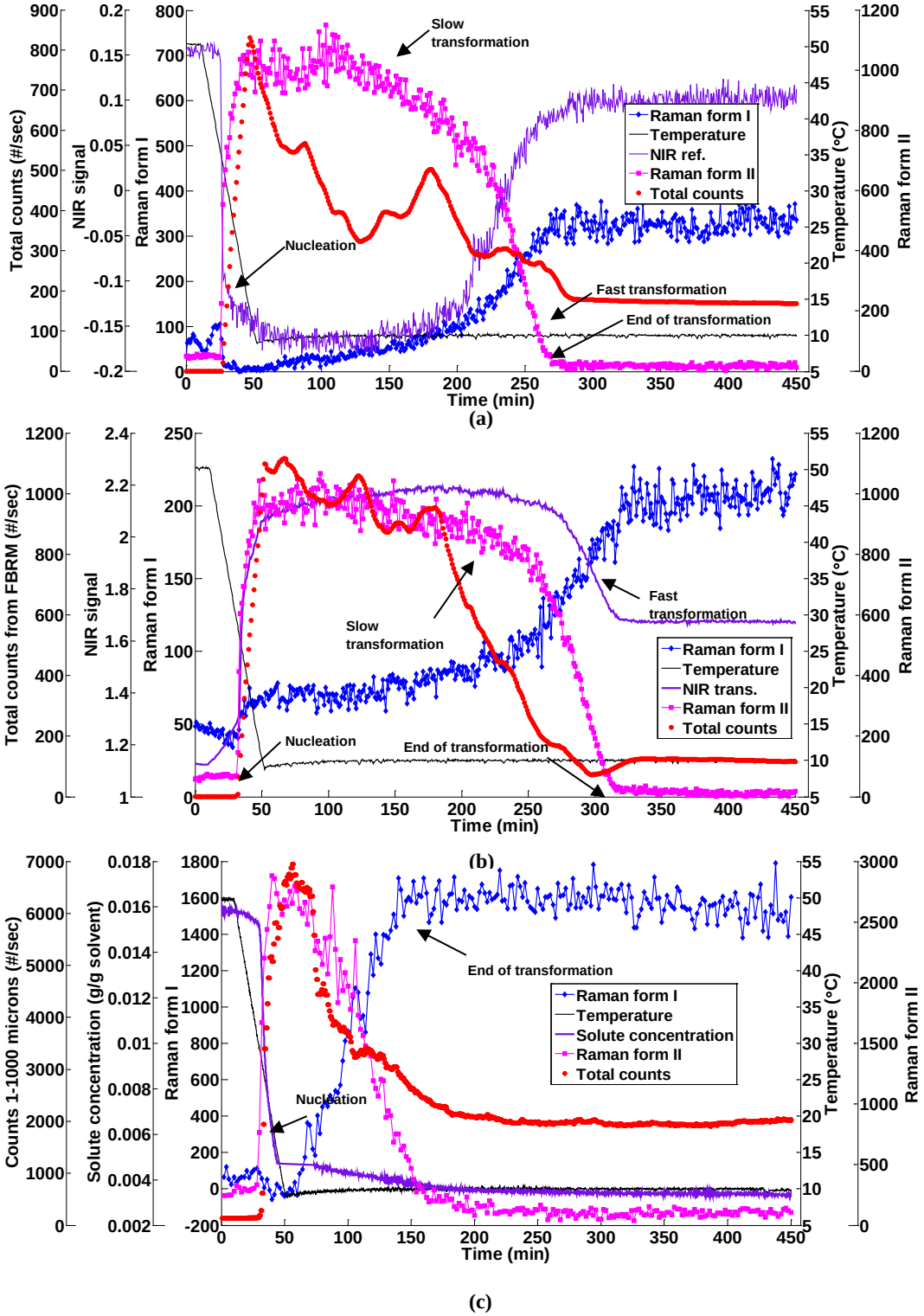

Figure 8.1: (a) Evolution of temperature, NIR signal and Raman intensities for specific peaks of form I and II in Experiment 1 (b) Evolution of temperature, NIR signal and Raman intensities for specific peaks of form I and II in experiment 2 (c) Evolution of temperature, ATR-UV/Vis signal and Raman intensities for specific peaks of form I and II in Experiment 3.

For this reason, every significant peak in the NIR spectrum (apart from the extreme zone at 4000−4500 cm^{-1}, where there is absorption by the optical fibre) could be followed.

Differences in the spectra of the two polymorphic forms were visible even in slurries of 2 mg of solid/g of solvent (the peak at 5950 cm^{-1} was still present and was tracked during the experiments), but it was found that the baseline effect was stronger than the changes in the specific regions of the spectrum. The ATR-UV/vis probe can monitor the liquid phase and detect changes in solute concentration during the experiment. In experiment 3, the calibration function developed in Chapter 5 of this thesis was used to calculate the solute concentration from the UV data, as shown in Figure 8.1c. FBRM can give important information about the amount of solid in solution (counts or counts per second) and also about the crystal size distribution and, indirectly, about the shape of the crystals. Raman, FBRM, and NIR data obtained during experiments 1 and 2 are shown in Figure 8.1 a and b respectively. Experiment 1 was conducted using an NIR reflectance probe. The absorbance signal from the reflectance probe in solution is noisy and shows high intensities because there are no solids that can reflect the radiation back to the detector. The NIR transflectance probe can also work with transmission, so the signal is specular: it is higher in slurries and lower in solution. The FBRM probe is the one with the largest measuring area and therefore the one most affected by fouling. The presence of particles on the probe made it difficult to interpret the results, since the repeated measurements of the sticking crystals generated meaningless peaks in the total counts and the chord length distribution (CLD). In experiment 1 in particular, the total counts trend has two peaks around 170 min; those peaks are just an artefact of the FBRM since none of the other probes detect any changes in the process (see Figure 8.1 a). Nevertheless, the principal component analysis applied on the composite sensor array showed good results for in detecting the real kinetic events in the process for all the performed experiments, demonstrating the robustness of this approach.

Table 8.3 and Table 8.4 show the detection times for nucleation, polymorphic transformation start and end for all the probes used in the first two experiments, while Table 8.5 reports the characteristic times for experiment 3. To extract information from the PVM images, the start of transformation was considered when the first recorded image presented prismatic crystals (typical of form I) as shown in Figure 8.2.

Table 8.3: Detection time of nucleation and polymorphic transformation from the different PAT tools in Experiment 1

Technique	Nucleation (min)	Polymorphic trans. start (min)	Polymorphic trans. end (min)
NIR reflectance	26	200	281
Raman	26	120	281
FBRM	26	268	283
PVM	27	105	261

Table 8.4: Detection time of nucleation and polymorphic transformation from the different PAT tools in Experiment 2

Technique	Nucleation (min)	Polymorphic trans. start (min)	Polymorphic trans. end (min)
NIR transflectance	31	280	330
Raman	31	150	320
FBRM	31	289	328
PVM	31	220	307

Table 8.5: Detection time of nucleation and polymorphic transformation from the different PAT tools in Experiment 3

Technique	Nucleation (min)	Polymorphic trans. start (min)	Polymorphic trans. end (min)
ATR-UV/Vis	30	72	190
Raman	30	70	190
FBRM	30	70	192
PVM	30	65	190

The end of transformation was considered when long needle crystals completely disappeared from the recorded images: this empirical way is not very accurate and justifies the different detection time between PVM and the other probes.

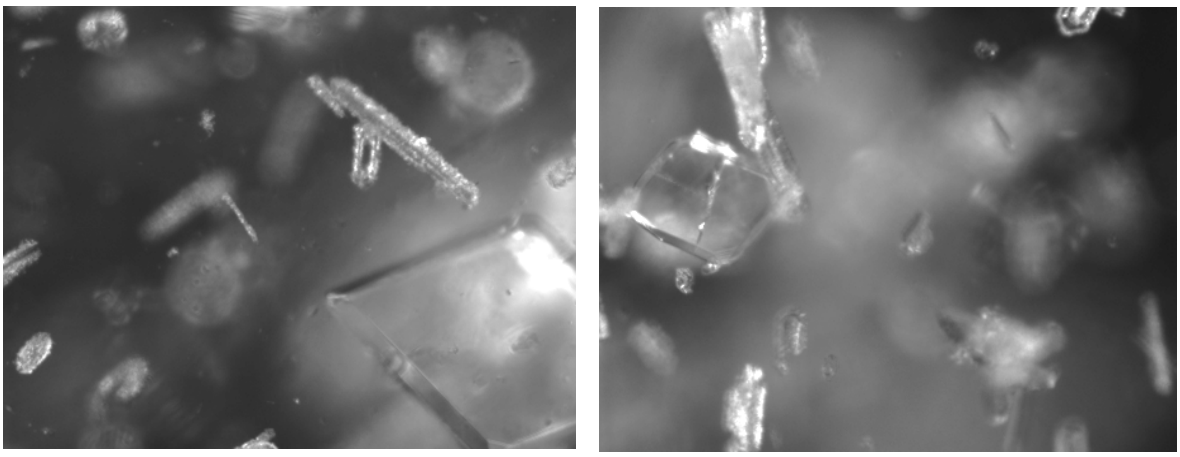

(a) **(b)**

Figure 8.2: PVM images at (a) Experiment 2 at 220 min, (b) Experiment 2 at 280 min.

PVM, Raman and NIR are practically equally efficient in detecting nucleation and polymorphic transformation. FBRM signal is less easy to interpret, but a significant variation in the total counts is present at the end of the polymorphic change. The increase in intensity in NIR transflectance before nucleation is related to the temperature change but nucleation is still distinguishable since it generated a more sudden increase in the signal. The end of polymorphic transformation is detected at the same time by Raman, FBRM and NIR for experiment 1. In experiment 2 Raman recorded the end of polymorphic transformation few minutes before the FBRM and NIR. The beginning of the transformation is detected first by Raman and PVM. The transformation from form II to I is known to be solvent mediated (Davey and Garside 2000) and, from the trend of the Raman signal; it is possible to infer that this transformation also proceeds in two steps: a slower and a faster one. The Raman signal is directly proportional to the ratio of the two polymorphic forms, therefore is the only tool that can distinguish between the two steps of the transformation. NIR changed in signal only at the beginning of the second step of transformation and this is related to the way the two probes can detect polymorphic transformation. Besides, Raman can detect new peaks from the stable form just nucleated but those crystals might be too small to be picked up and differentiated by FBRM or NIR which are mainly looking at the different shape and size of the two polymorphic forms.

The signal for the reflectance probe increases at the end of the transformation while for the transflectance probe it decreases: this behaviour can be explained considering that NIR is strongly influenced by crystal size and shape. For FBRM the decrease in the total counts is associated with the change in shape of the crystals. A similar behaviour in the total counts per second was observed for the same substance (but a different solvent) by Saleemi and Nagy (2012) who also compared the total counts trend during polymorphic transformation with the aspect ratio of the crystals. It is interesting to notice that in experiment 3, where the signal was less disturbed the two stages of the polymorphic transformation are both visible. Furthermore, between 100 and 130 min the total counts remain almost constant indicating a type of equilibrium between the rates of particles of form II dissolving and form I nucleating. Although the conditions of the three experiments were the same, the third experiments present a different transformation time. Many parameters that can't easily be controlled influence the time of transformation (mixing conditions, presence of dust or small amount of impurities): and this might explain the different behaviour of the system in experiment 3.

8.2.2 Centralized composite PAT array with PCA-based information fusion

The data from the CSA was combined in a single data matrix and PCA was applied to it. The first four principal components of the global CSA matrix resulting from combining information from three PAT tools (Raman, FBRM, and NIR) were analysed. The chosen components can detect nucleation and polymorphic transformation, which are the phenomena of interest in this study but the entire matrix contains additional information (for example agglomeration, secondary nucleation but also fluorescence, particles sticking on probes and simple noise). The scores and loadings were analysed together with the amount of variance covered by the first four principal components and the results are shown in Table 8.6. Also, all the principal components (among the first four) that can detect nucleation and/or polymorphic transformation are listed in the same tables. It can be observed that nucleation is always detected by the first three principal components in every combination of PAT tool while polymorphic transformation (in particular the beginning) can be observed in fewer components and in most cases it is not distinguishable in the first principal component. In experiment 3 in particular, PC1 and PC2 start changing after nucleation and stabilize to a constant value after the completion of the transformation.

Table 8.6: Results for the PCA performed on data from combinations of three probes and on the total data matrix in experiments 1, 2 and 3. The second column reports the variance covered by the first three principal components; the following columns report which phenomena are detected by each PC score. N=Nucleation; FST=first step of transformation, SST=second step of transformation, ET=end of transformation

Experiment	Variance (first 3 PCs)	PC1	PC2	PC3	PC4
1- FBRM + Raman + NIR reflectance	59.64%	N, FST, SST, ET	N, FST, SST, ET	N, SST, ET	Noise
2- FBRM + Raman + NIR transflectance	77.52%	N, SST, ET	N, FST, SST, ET	N	Noise
3- FBRM + Raman + ATR/UV/VIS	82.87%	N, ET	N, ET	N, FST, SST, ET	Noise

This trend is similar to the UV signal during the experiment demonstrating how different techniques can affect the PCA in different ways. In PCA the components are ordered according to the variance covered; because nucleation generates a more significant change in signal compared to transformation, it appears in more components and in particular in the first one. For all the experiments the forth principal component only shows noise while the other three can detect the phenomena of interest: nucleation of form II, start of the polymorphic transformation and end of the transformation. The variance covered by the first three principal components (the ones that do not contain noise) change significantly from one experiment to the other: this is due to the fact that reflectance spectroscopy is considerably noisier than transflectance; therefore, a large amount of variance in that technique is related to noise. If a signal is intrinsically noisy (such as NIR reflection and FBRM in the first experiment) most of the variance, which represents the change in the signal itself, will be associated to noise. In the case of NIR reflectance the 55% of the changes in the signal is due to changes during the process while the rest is considered noise. PCA is able to include the entire significant signal in the first components and separate this from the noise. Furthermore, the presence of a disturbed signal does not

compromise the PCA analysis. Figure 8.3a shows the scores of the first three principal components in experiment 1, using NIR refl. + Raman + FBRM. Nucleation is detected by all of them as well as the beginning and the end of polymorphic transformation. The clearest principal component is PC2: the signal is not too noisy and there is a considerable change corresponding to both nucleation and the end of polymorphic transformation. Furthermore, it is possible to distinguish the two steps of transformation due to the contribution given by the Raman probe. Figure 8.3b shows the scores of the first three principal components using NIR trans. + Raman + FBRM (experiment 2). Nucleation is indicated in all the scores but transformation is clear only in PC2. A significant change in the score of PC1 is present corresponding to the transformation but then the score keeps changing so the interpretation of this component becomes difficult. However, in PC2 the two steps of polymorphic transformation are recognizable. Figure 8.3c shows the scores versus time in experiment 3 where FBRM + Raman + ATR-UV/Vis were used. In the first two principal components a sudden change is present corresponding to nucleation and then the signal keeps increasing for PC2 and decreasing for PC1 until they both reach a stable value at the end of the polymorphic transformation. PC3 is sensitive to both nucleation and polymorphic transformation; this score has a trend very similar to the one of the total counts. The interpretation of the scores of the composite sensor array is easier by plotting two or more scores on the same graph and finding clusters and patterns that can be correlated with the various events in the process. It is worth noticing that the noisy features present in the FRBM signals in all the experiments are not present in any of the scores shown in Figure 8.3 demonstrating the advantage of performing PCA on the composite sensor array matrix. Figure 8.4 shows PC1 plotted versus PC2 in the three experiments: only points for pure form I, pure form II and the clear solution are represented in order to simplify the identification of main clusters. The three species are clearly distinguishable in all the three plots. In particular in Figure 8.4a (NIR refl. + Raman + FBRM) it can be notice that form I has a negative PC2 while form II has a positive one. The nucleation and transformation of one form could be easily identified in this system looking at the sign of PC2. For the CSA formed by NIR trans. + Raman + FBRM a similar behaviour of the components can be noticed, as shown in Figure 8.4b. In this case PC1 for form I is negative while is positive for form II. In experiment 3 (ATR-UV/Vis + Raman + FBRM) PC2 for form I is positive and for form II negative (see Figure 8.4c). Plotting PC1 and PC2 together allows the immediate identification of the form nucleated or transformed.

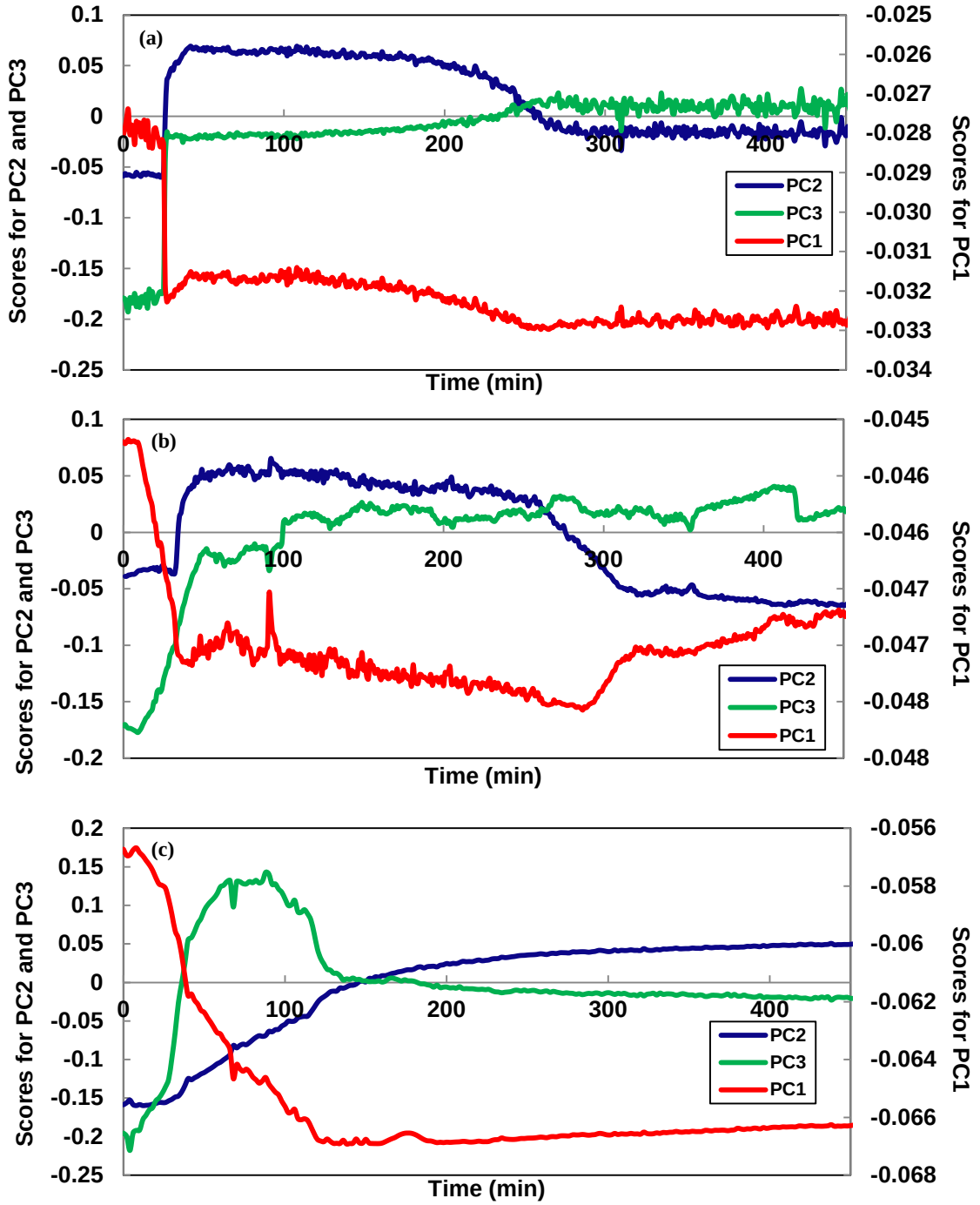

Figure 8.3: (a) Scores of the first three principal components in experiment 1, (b) in experiment 2, and (c) experiment 3.

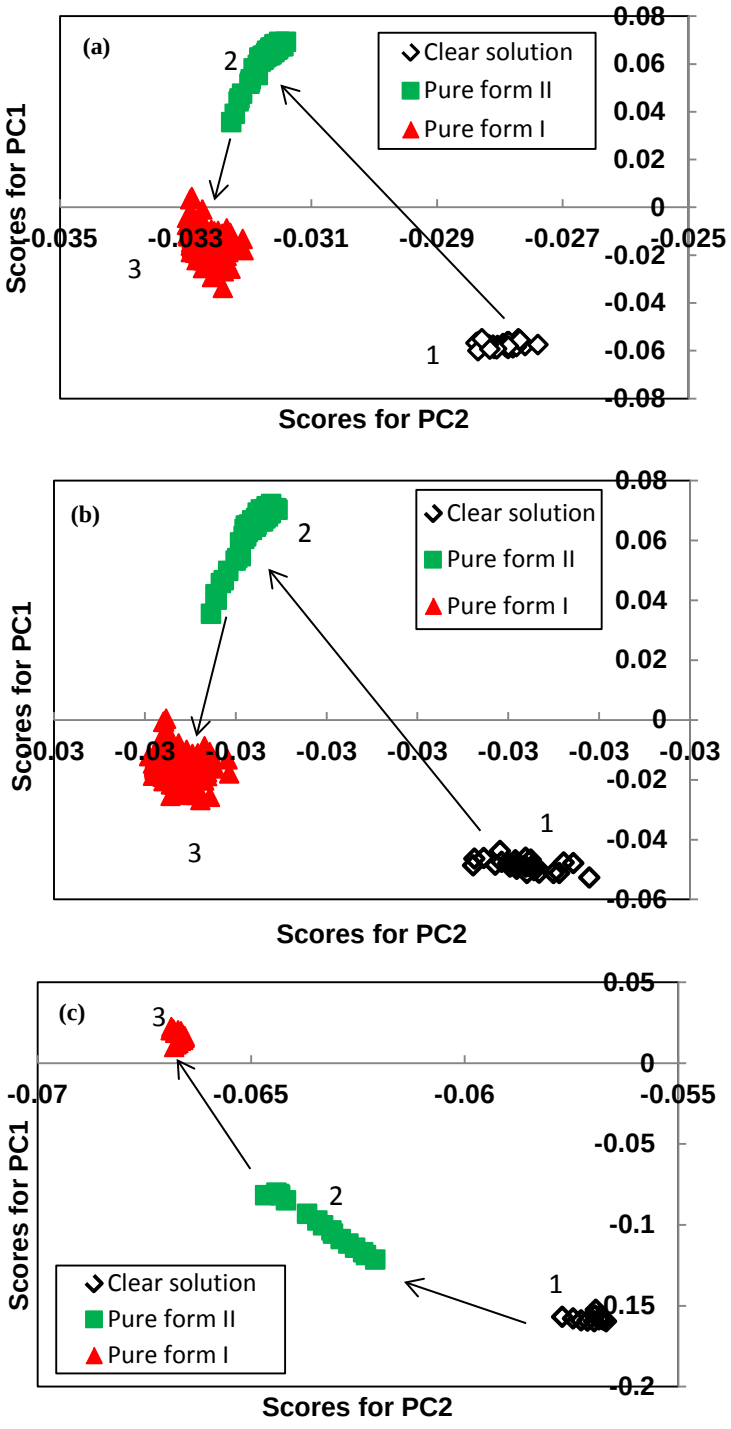

Figure 8.4: (a) Plot of PC1 vs PC2 for clear solution, pure form I and pure form II in experiment 1, (b) in experiment 2, and (c) in experiment 3.

PCA on the same CSA as in experiment 3 (ATR-UV/Vis, Raman and FBRM) was performed in the case of nucleation only of the stable form I (experiment 4).

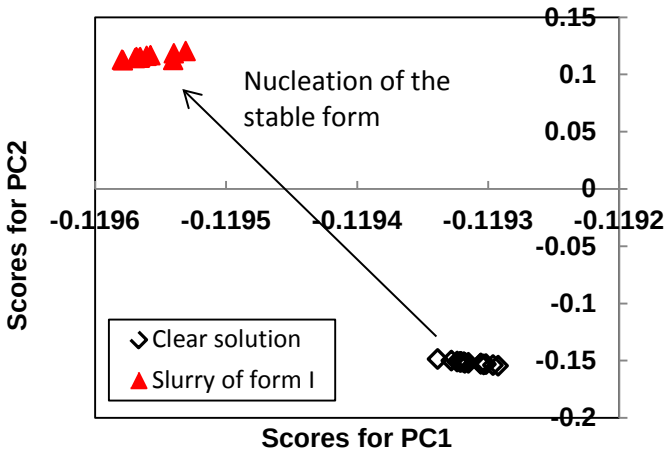

Figure 8.5: Plot of PC1 vs PC2 for clear solution and pure form I during a cooling crystallization experiment with no polymorphic transformation.

Plotting the first two principal components allow identifying only two clusters: one for solution and one for the solid (see Figure 8.5), which is in correlation with the lack of polymorphic transformation in this experiment. Discrimination between clear solution and slurry is also possible since the cluster for clear solution is in a different position compared to slurries of form I, II or a mixture. Using more tools is useful to avoid misinterpretation of signals due to operating problems with a single probe (e.g. fouling and particle sticking in the case of FBRM and NIR of fluorescence for Raman). In this way the use of the CSA enables not only a better understanding of the process, but also the identification of sensor failures or measurement problems. However, instead of always using a full CSA, identifying the best subset of PAT tools that should be included in the CSA to be able to monitor and identify particular combinations of crystallization mechanisms can save significant costs. The interpretation of the rotated loadings for the first three principal components (the fourth was not included as it shows noise for all performed experiments) can help to identify the sensors that affect most the PCs and help in the choice of an appropriate subset. Table 8.7 shows the most influent probes (the ones which have higher loading values) for the three performed experiments, while Figure 8.6 shows the plot of the rotated loadings.

Table 8.7: Most influent probes in the rotated loadings of the first two principal components (used for the clustering) for experiments 1, 2 and 3

Experiment	Rotated loading 1	Rotated loading 2
1 - FBRM + Raman + NIR reflectance	Raman	NIR
2 - FBRM + Raman + NIR transflectance	Raman	FBRM
3 - FBRM + Raman + ATR/UV/VIS	UV	FBRM

Only the loadings of the PCs used in the clustering analysis (see Figure 8.4) were analysed to identify the best subset of tool for each experiment. The clustering analysis and representation was found to be more effective than the scores plotted versus time, and therefore, was used as basis for the loading study. It is immediately clear that, for experiment 1, the information from FBRM is less influent than Raman and NIR. In Figure 8.6 (1) and (2) the loading for FBRM is always lower than for the other probes (although still significant). This tool does not strongly affect any of the rotated loadings for the most important PCs; therefore, it could be excluded by the optimal subset of PAT tools for the combination FBRM + NIR ref. + Raman. In the case of experiment 2, PC1 is strongly affected by the Raman signal (see Figure 8.6 (3)) while PC2 is affected mainly by FBRM as shown in Figure 8.6 (4); therefore, those two probes are the most important for the understanding of the process. Finally, for experiment 3 only the UV/Vis and FBRM strongly influence the first two PCs. The methodology presented here can provide a generic framework for the automated selection of optimal sensor combinations for the detections of particular crystallization events.

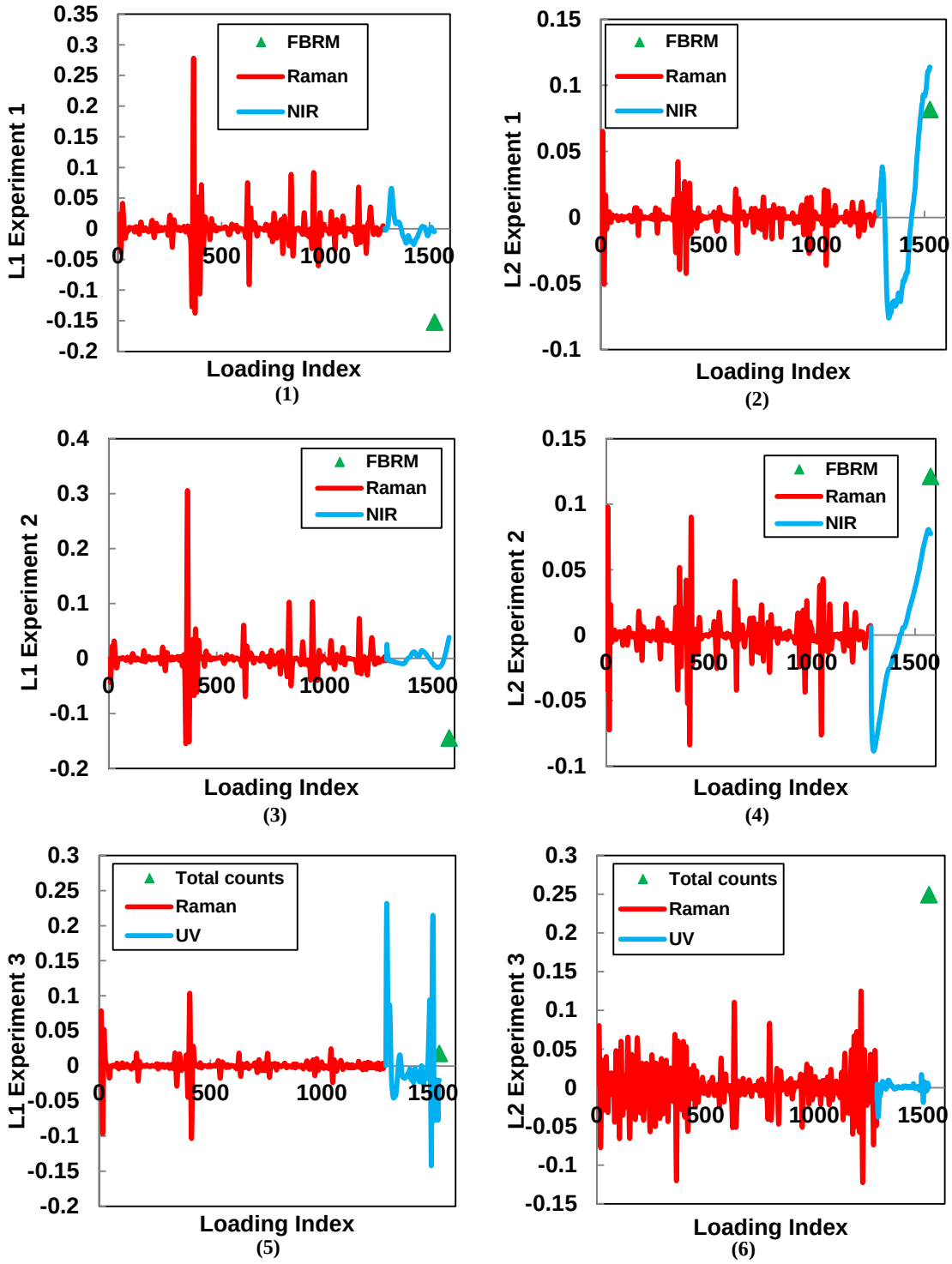

Figure 8.6: (1) Rotated loading of PC1 (L1) in experiment 1; (2) Rotated loading of PC2 (L2) in experiment 1; (3) Rotated loading of PC1 (L1) in experiment 2; (4) Rotated loading of PC2 (L2) in experiment 2; (5) Rotated loading of PC1 (L1) in experiment 3; (6) Rotated loading of PC2 (L2) in experiment 3.

While for a particular crystallization system and phenomenon of interest, one can often recommend the suitable tool, in the context of an automated decisions support system, the

proposed approach can automate this selection. Such a system could also automatically change the signals collected from multiple sensors and use different sensor configurations present in the crystallization vessels during different phases of the crystallization depending on the phenomenon of interest (e.g. certain signal combination may provide highest sensitivity during nucleation, whereas a different set of signals during polymorphic transformation).

8.3 Conclusions

Nucleation and polymorphic transformation of OABA from metastable form II to stable form I was studied using different PAT tools, including FBRM, ATR-UV/Vis, Raman as well as reflectance and transflectance NIR spectroscopy. PVM images were also used to analyse and explain the results found from the other probes. It was found that Raman spectra can give the most information about nucleation, crystal growth and polymorphic transformation. NIR could also be a powerful tool but the presence of water in the system limits its usage; although from its baseline effect it was possible to detect nucleation, crystal growth and polymorphic transformation. FBRM also provides very useful information about polymorphic transformation even if it shows lower sensitivity compared the other tools. The advantages of using more than one PAT tool in a composite sensor array (CSA) configuration to monitor complex processes and capture different phenomena was demonstrated. The application of the proposed PCA-based data fusion and information extraction approach represents the first centralized CSA structure reported. A real benefit of this approach can be visualized in a processing plant environment where more signals are monitored at the same time. Once a robust process has been established during the development stage and the output of the PCA is well understood, the monitoring of the signals can be shifted from a decentralized to a centralized composite array. The major advantage of this method is the reduced amount of signal to monitor which will greatly assist the plant operators in process monitoring. The signals can be analysed all together in the CSA, or in various subsets of configurations (e.g. two or more probes can be combined) in order to capture the crystallization phenomena of interest. The loadings and the principal components scores can be used to determine the best PAT subset. The approach proposed in this chapter can be used for optimal sensor configuration as well as a more efficient and automated information extraction that are key elements for

the implementation of automated intelligent decision support and control systems for crystallization processes. The CSA concept proposed in the chapter is very general and can include all types of PAT signals: the choice of the best component is, instead, system dependent and varies as a function of the phenomena of interest and the available set of tools.

9 A link between the ATR-UV/Vis and Raman spectra of zwitterionic solutions and the polymorphic outcome in cooling crystallization

In this chapter ATR-UV/Vis and Raman spectroscopy are used to study the effect of solvent on the polymorphic outcome of the zwitterionic OABA. A relation between spectra and polymorph nucleated is shown.

9.1 Introduction

The type of molecular interactions in solutions is very important in the determination of the polymorphic form of the early nucleated crystals (Bernstein 2011; Blagden and Davey 2003; Vekilov 2010; Davey et al. 2013). For this reason, significant research effort is currently directed towards trying to understand how the nature of the chemical bonding between solute-solute and solvent-solute molecules in solution affects the polymorphic form nucleated (Chiarella et al. 2007; Davey et al. 2001; Davey et al. 2006; Kulkarni et al. 2012; Parveen et al. 2005; Mattei et al. 2013; Khamar et al. 2014; Sullivan et al. 2014). The most used technique to detect changes in the liquid state is attenuated total reflectance-Fourier transform infrared spectroscopy (ATR-FTIR) although Kulkarni et al. (2012) have successfully used Raman spectroscopy to understand the type of bonding between molecules of isonicotinamide in different solvents and their relationship to the polymorphic outcome of crystallization. Nuclear magnetic resonance (NMR) was used to detect dimers of carbamazepine (Hunter et al. 2012) and tolfenamic acid (Mattei and Li 2012) in different solvents and neutron scattering for the study of supersaturated solutions of benzoic acid in methanol (Burton et al. 2010). Few studies also reported detection of pre-nucleation clusters of calcium carbonate, whose structure is related to the polymorphic form nucleated, using transmission electron microscopy (TEM) coupled with solid state NMR and IR spectroscopy (Gebauer and Cölfen 2011; Gebauer et al. 2008). Pre-nucleation clusters and molecular self-assemblies are not always possible to detect, nevertheless understanding the effect of solvent on the chemistry of the compound studied can help in predicting the polymorphic outcome. For example, a simple change in solubility of one polymorph due to the use of a different solvent can have a drastic effect on the nucleation outcome since the metastable zones of the

possible forms are altered (Trifkovic and Rohani 2007; Khoshkhoo and Anwar 1993). Additionally, the chemical interactions between solvent and solute can favour specific arrangements of the molecules in the crystal lattice or affect the growth kinetic determining the development of specific polymorphs (Weissbuch et al. 2005; Kitamura et al. 2006). Furthermore, the level of supersaturation in organic solvents can change the monomer-dimer equilibrium and affect the polymorphic form nucleated (Mattei et al. 2012). It has to be noted that kinetic conditions (for example the cooling rate during a cooling crystallization) also affect polymorphism and have to be taken into account during every thermodynamic study of clear solutions. Anthranilic acid and its polymorphism were described in chapter 3 of this thesis. This compound can exist in three different polymorphic forms: I, II and III. Form I is stable in air at low temperature while form III is the most stable form at higher temperature. Form II is enantiotropically related with form I and monotropically related to form III and it is metastable at every temperature below the melting point. The initial composition of the solvent together with the supersaturation can affect the form of OABA nucleated: under suitable conditions of solvent type and supersaturation it is possible to nucleate a mixture of form I and II as shown in chapter 6 of this thesis. Form III is usually more difficult to nucleate or obtain through polymorphic conversion in solutions below the transition temperature (around 50 °C). A peculiar difference between form I and II of OABA is the presence of zwitterions in the crystal structure of form I, which are not present in form II; therefore, solvents that favour the formation of zwitterions will likely favour the nucleation of form I. A Raman spectroscopic characterization of different solutions of OABA was performed by Towler and Taylor (2006) but a clear relation between spectra and the polymorphic outcome was not found. A recent study was performed to accurately determine the equilibrium of the charged and neutral species of OABA in water and several organic solvent solutions (Zapala et al. 2009). In the study classical titrations were coupled with Ultraviolet/Visible (UV/Vis) spectroscopy in order to determine the percentage of zwitterions on the total neutral molecules. UV/Vis, in fact, is sensitive to changes in the amount of zwitterions in solution: a shift towards higher wavelength of the peak at 328 nm is observed when the zwitterion amount decreases. The maximum amount of zwitterions for OABA is around 82 % of the total molecules and can be found in pure water (see Figure 9.1 for the equilibrium of OABA species in water). The addition of an organic solvent usually generates a decrease in the percentage of zwitterions (Zapala et al. 2009; Murugan et al. 2011); in general organic solvents at low dielectric constant favour the unionized form of OABA which

tend to arrange itself in dimers (Zapala et al. 2009; Abou-Zied et al. 2013). Isopropyl alcohol in particular, if added to water, reduces considerably the dissociation constant of the carboxylic groups of OABA (Bosch et al. 1995) generating, consequently, a decrease in the zwitterions and a possible increase in dimers.

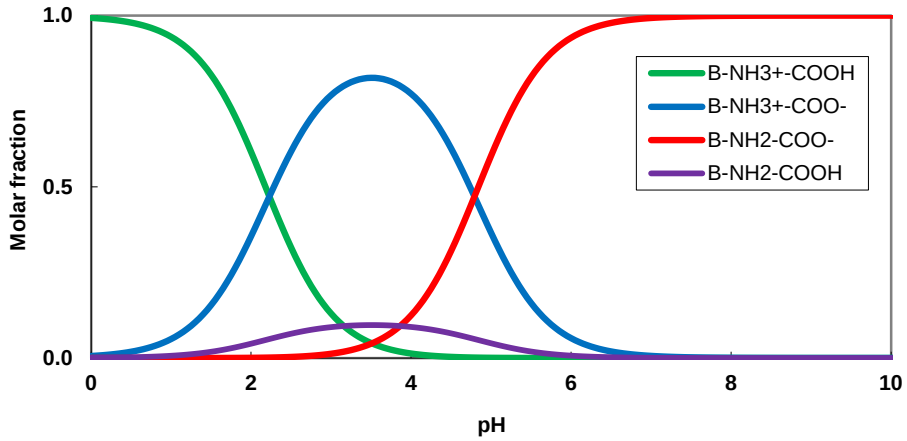

Figure 9.1: Solution speciation of OABA in water (Zapala et al., 2006).

Because dimers are typically present in form II and zwitterions in form I, solutions at high content of an organic solvent should favour the metastable form II, while water rich solutions will nucleate preferentially form I. This behaviour was already experimentally confirmed (see Chapter 6 of this thesis), but in this work a specific correlation between spectroscopic data of solutions of OABA (in particular the position of Raman and UV/Vis peaks in undersaturated solutions) and the polymorphic outcome of cooling crystallizations will be studied. Attenuated total reflectance ultraviolet/Visible (ATR-UV/Vis) spectroscopy is used together with Raman spectroscopy, which is also potentially able to distinguish between zwitterions and neutral molecules as shifts or appearance/disappearance of peaks (Bosch et al. 1995; Ding and Krogh-Jespersen 1996; Stalin and Rajendiran 2006; Sebek et al. 2009; Susindran, et al. 2012; Deplazes et al. 2008; Zhang et al. 2008).

9.2 Methodology, materials and Equipment

Ortho-aminobenzoic acid, isopropyl alcohol (IPA) and ultrapure water were used as compounds for the experiments. The ATR-UV/Vis and Raman immersion probes were used for the analysis of clear solutions. The Raman probe also helped in the determination of the polymorph nucleated in each experiment. The FBRM probe was also used to check the

presence of undissolved particles in solution. All experiments were conducted in the 400 mL jacketed vessel described in Chapter 3 of this thesis. The data from FBRM, ATR-UV/Vis and Huber is transmitted in real-time to the CryPRINS software. Additionally a pH meter (Jenway, model 3540) was used to measure the pH in aqueous solutions. The Avantium Crystal16 system was used to estimate solubility data of OABA form I and II in different mixtures of IPA and water.

9.2.1 ATR-UV/Vis spectroscopy

Different preliminary experiments were conducted in order to explore the behaviour of UV/Vis in different solutions of OABA in IPA/water mixtures at different compositions. The effects of concentration, organic solvent addition and temperature were analysed. Cooling crystallization experiments were then conducted using the same cooling rate, starting temperature and saturation temperatures but different percentages of IPA in water. ATR-UV/Vis spectra were then analysed with Matlab 2013a. Additionally**,** FBRM was used during the experiments to ensure the absence of particles during the study of clear solution while a Raman probe allowed to determine the polymorphic form nucleated.

Aqueous solutions experiments (pH, temperature and concentration effect of ATR-UV/Vis spectra)

A set of preliminary experiments was performed on two solutions of OABA in water. The solutions were prepared (C=0.0035 g/g solvent) and NaOH or HCl were added with a pipette in order to change pH. The pH was recorded together with the ATR-UV/Vis spectra of the solutions. The temperature was kept constant at 30 °C in order to have sufficient material dissolved in the solution, since OABA is not very soluble in water. FBRM was used during the experiment to ensure that nucleation of salts or any other solid didn't occur. In order to study the effect of temperature, a third water solution at high concentration of OABA was prepared: pure form I was added and then dissolved. The temperature was then changed from 70 °C to 40 °C and UV spectra recorded. FRBM was again used to check eventual nucleation. The effect of dilution was then determined in a fourth experiment where an aqueous solution of OABA was diluted with water (flow rate of 1 mL/min). Temperature was kept constant at 30 °C with the Huber and complete dissolution of the starting material was determined using FBRM.

IPA and water mixtures experiments (organic solvent effect on ATR-UV/Vis spectra)

For the first experiment, solutions at different ratios of IPA and water were prepared using the same amount of OABA (1 g of form I in 100 g of solution). The solutions were stirred and kept closed in a dry place for two days in order to ensure complete dissolution of the solids. The second and last experiment of this section consisted in alternatively pumping water and IPA at a flowrate of 2 mL/min to an aqueous solution of initial concentration of 0.011 g OABA/g water. IPA was first pumped for 30 min, then water for other 30 min, IPA and water again. Both solvent and dilution effect on the UV spectra were checked with this experiment.

Cooling crystallizations experiments (link between solution characteristics and polymorphic outcome)

Several cooling crystallization experiments were performed using similar conditions: starting temperature at 45-50 °C, cooling rate of -1 °C/min and -0.5 °C/min, initial saturation temperature of 30 °C and 40 °C (with respect to form II of OABA).

Table 9.1: Experiments performed for the ATR-UV/Vis spectroscopy analysis

Exp. number	Solvent composition (IPA % in water)	Saturation temperature (°C)	Cooling rate (°C/min)
1-10	0%,5%,10%,20%,30%	30	-1
11-16	0%,5%,10%,20%,30%	30	-0.5
17-27	0%,5%,10%,20%,30%	40	-1
28-33	0%,5%,10%,20%,30%	40	-0.5

ATR-UV/Vis spectra were recorded during all crystallization experiments. A Raman immersion probe was used to check the polymorphic outcome of the nucleation validated using off-line differential scanning calorimetry (DSC) and Raman microscopy of the filtered and dried crystals. Table 9.1 shows in detail the conditions of the experiments conducted for the analysis of the ATR-UV/Vis spectra in solution.

9.2.2 Raman spectroscopy

In the case of Raman spectroscopy only a part of the experiments performed with the ATR-UV/Vis could be conducted with satisfactory results. In particular, experiments in pure water resulted in a very disturbed signal due to the small concentration of OABA and the high tendency of OABA to develop fluorescence. The Raman probe was used for the second experiment of section 9.2.2. Cooling experiments were then performed with the same methodology reported in the section 9.2.3. Table 9.2 shows the experiments and their conditions performed for the analysis of Raman spectra of zwitterionic solutions.

Table 9.2: Experiments performed for the Raman spectroscopy analysis

Exp. number	Solvent composition (IPA % in water)	Saturation temperature (°C)	Cooling rate (°C/min)
1-7	0%,5%,10%,20%,30%	30	-1
8-13	0%,5%,10%,20%,30%	30	-0.5
14-19	0%,5%,10%,20%,30%	40	-1
20-24	0%,5%,10%,20%,30%	40	-0.5

The choice of Raman spectroscopy instead of the more traditional FTIR spectroscopy is mainly due to the characteristics of the system studied. The solvents used in this work were pure water or mixtures of water/IPA with relatively low content of OABA (because of its poor solubility). Water has very broad and intense peaks in the FTIR spectrum, which tend to overlap with the OABA signal and make the interpretation of the data very difficult especially for diluted solutions. Raman spectroscopy is still a vibrational technique, which can give similar information to FTIR, but it has a very weak signal from water and, therefore, was found to be more suitable for the studied system.

9.3 Results and discussions for using ATR-UV/Vis spectroscopy for linking solution spectra to polymorphic outcome

9.3.1 Aqueous solutions experiments

The first step of the experimental work was to determine the capability of the available ATR-UV/Vis probe to detect changes in the amounts of the different ionic species in water. Experiments were conducted at 30 °C since OABA is poorly soluble in water at ambient temperature. Data from Zapala et al. (2009) were used to calculate the percentage of zwitterions over the total neutral species (Table 9.3). Those equilibrium data are measured at 25 °C, therefore the absolute values calculated may slightly differ from the actual ones. NaOH was added to the first solution of water and OABA to increase the pH, while HCl was added to the second identical solution in order to decrease its pH. Spectra of the solutions at different pH values are shown in Figure 9.2 while calculated equilibrium percentages of the ionic species in solution are reported in Table 9.3 (equilibrium data were taken from Zapala et al. 2009).

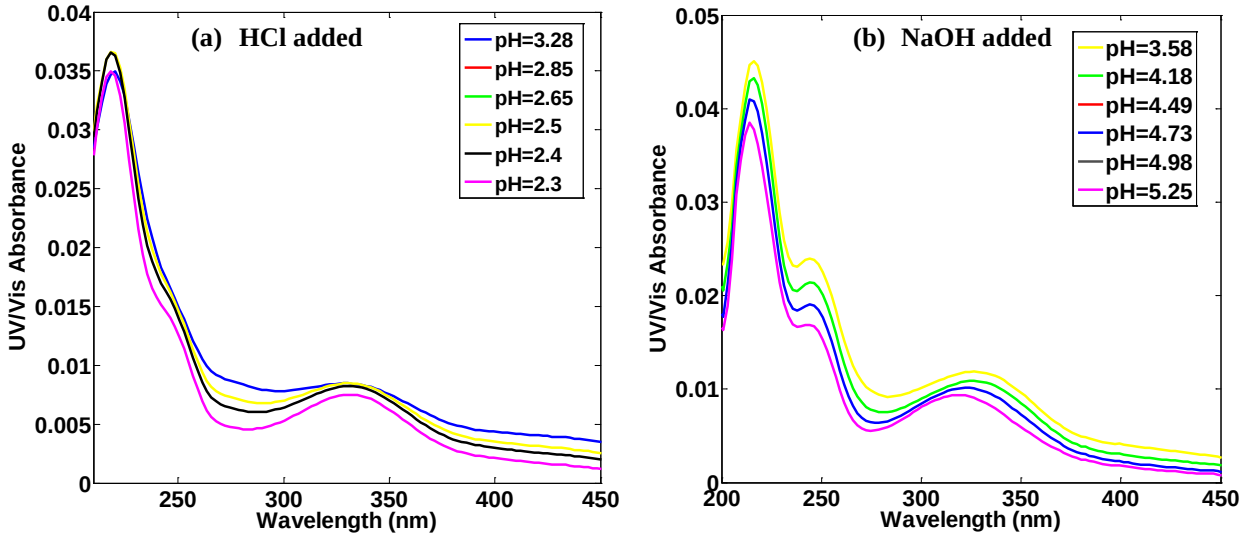

Figure 9.2: UV/Vis spectra of OABA in water at different pH values during the two experiments.

In Figure 9.2a and b, a shift towards lower or higher wavelengths in the main peak of OABA (at around 330 nm) and a baseline shift of the whole spectrum can be noticed as pH changes. This behaviour is consistent with the literature (Zapala et al. 2009; Abou-Zied et al. 2013). The positions of the UV peak reported in Table 9.3 are calculated from the first derivative of

the spectrum using the Matlab function *polyxpoly* that finds the intersection between the UV signal and the x-axis.

Table 9.3: Equilibrium at different pH for aqueous solutions of OABA (combined data from experiments with two identical solution and addition of either NaOH or HCl from the equilibrium point)

pH	Specific peak of OABA	Positive (%)	Neutral (%)	Negative (%)	Zwitterion (%)	Non-Ionic (%)
-	*Peak position (nm)*	*B-NH3+-COOH*	*Z+N*	*B-NH2-COO-*	*B-NH3+-COO-*	*B-NH2-COOH*
Addition of HCl						
3.28	331.2	0.072	0.903	0.025	0.808	0.095
2.85	330.8	0.175	0.817	0.008	0.731	0.086
2.65	330.4	0.252	0.743	0.005	0.665	0.078
2.5	329.8	0.323	0.674	0.003	0.603	0.071
2.4	329.3	0.375	0.623	0.002	0.557	0.065
2.3	328.7	0.431	0.568	0.002	0.508	0.060
Addition of NaOH						
3.58	326.1	0.036	0.913	0.050	0.817	0.096
4.18	325.7	0.008	0.814	0.178	0.728	0.086
4.49	324.1	0.003	0.689	0.308	0.616	0.072
4.73	322.3	0.002	0.562	0.436	0.503	0.059
4.98	320.4	0.001	0.420	0.580	0.376	0.044
5.25	318.3	0.000	0.280	0.720	0.251	0.029

Temperature and concentration of OABA can also generate a shift of the analysed peak as shown in Figure 9.3a and b. Temperature does not seem to have a significant effect on the studied region. In fact, there is a shift of less than 1 nm related to a change in temperature of over 25 °C. A variation in the concentration from 0.0082 to 0.0118 g/g solvent also generates

a similar amount of peak shift. However, in order to compensate those effects on the UV peak position all measurements in the cooling crystallization section will be taken at the same temperature and similar supersaturations.

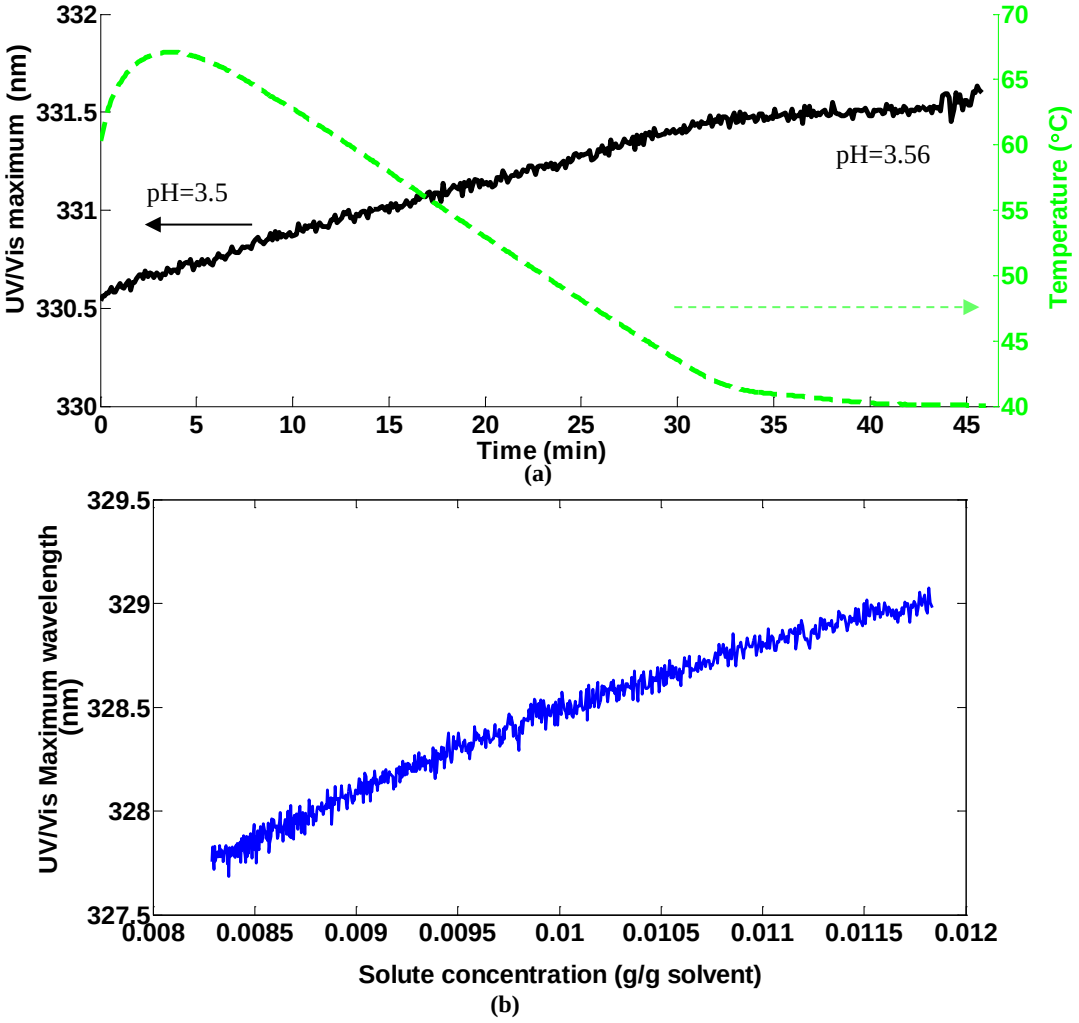

Figure 9.3: (a) Effect of temperature at C=0.019 (b) Effect of dilution in water and IPA.

The sensitivity of the instrument available is about 1 nm, which is in similar range with the peak shifts observed; therefore, it is difficult to find a specific quantitative correlation between concentration, temperature, pH and the peak position. Nevertheless, the presence of a trend in the shown data is clearly visible, not only in the peak positions calculated from the first derivative (shown in Table 9.3) but even in the raw spectra shown in Figure 9.2, and can give useful qualitative information.

The calculation of the first derivative allows the determination of the UV peak maximum with higher precision compared to the analysis of the raw spectrum and compensates in certain extent the low sensitivity of the instrument. If the change in the data was too close to the sensitivity of the instrument it would not be possible to see a clear trend between the peak position and the pH, temperature and concentration, since in this case only noise would be present. Nevertheless, a quantitative analysis cannot be performed and data has to be interpreted qualitatively only.

9.3.2 IPA and water mixtures experiments

Once the analysis of the system water-OABA was concluded the organic solvent IPA was introduced in the system and its effect was studied. Anthranilic acid mainly exists in the non-ionized form in organic solvent with low dielectric constant (such as methanol, IPA, ethanol or dioxane), whereas the molecules are ionized in water as shown in the previous studies. The spectroscopy of OABA in water-organic mixtures is quite complicated as spectral changes are due not only to the solvent effect but also to structural changes in the molecule. Usually buffer and organic solution mixtures are studied in order to have specific information on the chemical species in solution (Zapala et al. 2009; Abou-Zied, et al. 2013; Takacs-Novak and Tam 2000; Takacs-Novak et al. 1994). The addition of an organic solvent to the buffer containing OABA generates an increase in the absorbance and a shift of the specific peak around 328 nm to higher wavelengths (Abou-Zied et al. 2013). In this study water was used since it is the common solvent for batch crystallization. Because of the complexity of the system (the pH of de-ionized water is more difficult to control compared to a buffer solution), the results shown might not be as accurate as in other studies but it was still possible to find a good correlation between the ATR-UV/Vis peak position and the amount of organic solvent in solution (which is related to the zwitterions content). First of all, different solutions at the same concentration of OABA in g/g solvent but different IPA/water ratio were prepared. ATR-UV/Vis spectra were collected and the peak position was determined using Matlab.

Table 9.4 shows the peak position in the different mixtures. A clear trend can be noticed between percentage of IPA in solution and position of the UV peak as shown in Figure 9.4b. This trend is similar to the one found by Abou-Zied et al. (2014) with dioxane and buffer mixtures.

Table 9.4: OABA peak position as a function of the % of IPA in solution

% IPA in solution (w/w)	Peak maximum (nm)
10	332.8
30	334.5
50	336.1
70	336.9
100	337

Figure 9.4a shows the raw spectra for different mixtures of IPA and water while Figure 9.4b shows the position of the peak as a function of the amount of IPA in solution. The UV/Vis peak of OABA shifts to higher wavelengths as the amount of neutral molecules over zwitterions increases. The peak position does not change much from 75 % to 100 % of IPA indicating that probably all the molecules are already all non-ionized in solutions of 75 % IPA.

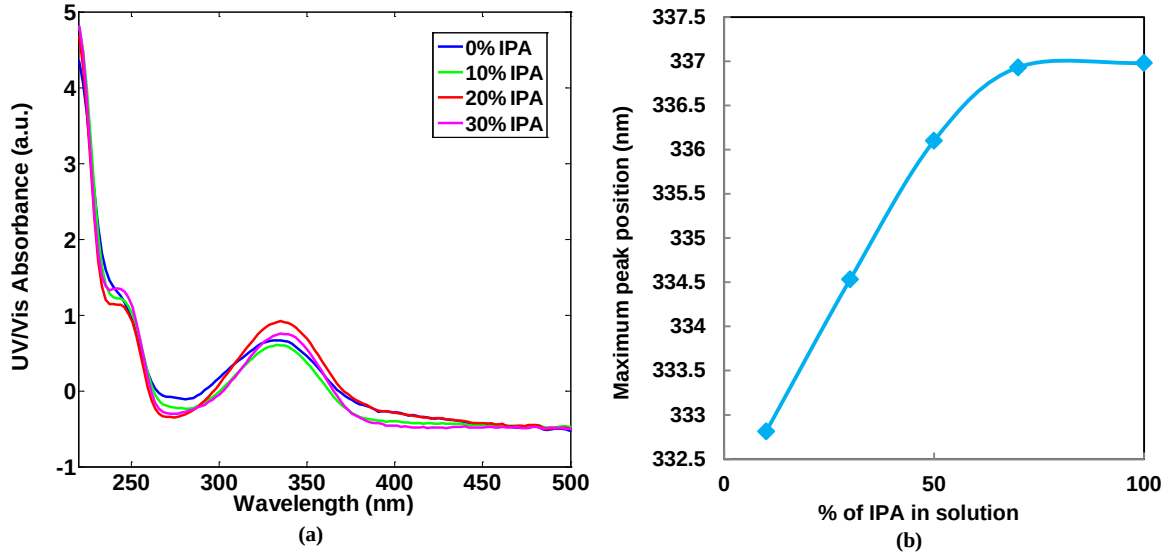

Figure 9.4: (a) UV/Vis spectra of OABA solutions of different IPA/water composition and (b) OABA peak position as a function of the % of IPA in solution. The solid line is a guide for the eye.

The second experiment of this section was conducted using a peristaltic pump and mixing an aqueous solution of OABA with a combination of water and IPA at controlled constant temperature. The purpose of this experiment was to qualitatively show how the analysed peak shifts with the addition of IPA or water and to check the presence of an eventual dilution effect. The results can be observed in Figure 9.5. The flowrate was of 2 mL/min and water and IPA were pumped alternatively for about 30 min, twice. The peak shifts to higher wavelengths during the addition of IPA, and then goes back when water is added. A slight dilution effect can be noticed; in fact, after the addition of the water for the first time the peak position is not the same as at the beginning of the experiment. However these trends clearly indicate that the shift in the peak position is due to the zwitterion equilibrium governed by the water/IPA composition in the system. The experiment was repeated several times using slightly different conditions (flow rate of IPA, initial concentration and even organic solvent pumped) and a clear shift was always observed indicating that a genuine trend in the UV/Vis spectrum is present when modifying the solvent composition. In conclusion, in this section, the capability of the available UV instrument in detecting changes in the ionic content of the solution was demonstrated. The simple Matlab code described in the previous section allowed the calculation of the exact position of the OABA peak.

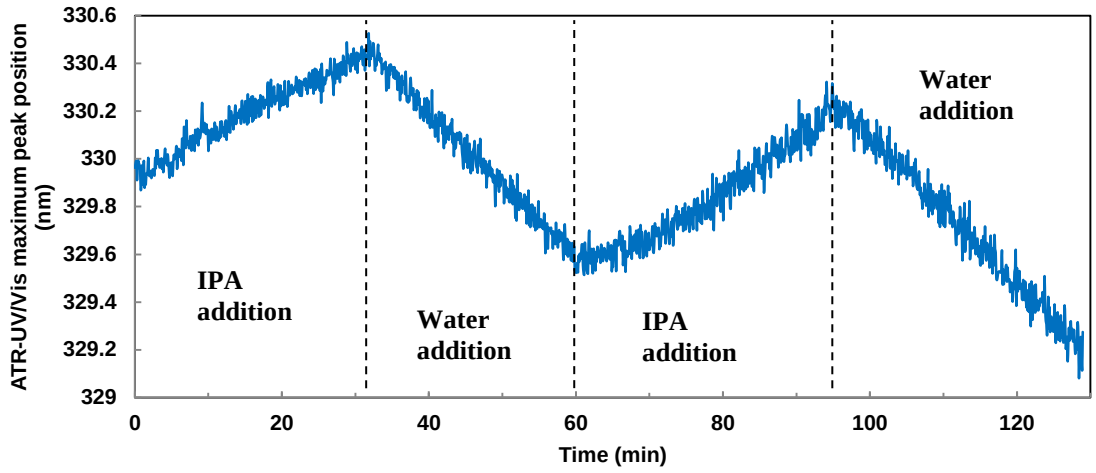

Figure 9.5: Effect of IPA and water addition to an aqueous solution of OABA.

9.3.3 Cooling crystallizations experiments

After the preliminary study, a set of cooling crystallizations was performed using the same kinetic conditions on different IPA/water solutions of OABA in order to find a correlation

between polymorphic outcome and position of the UV peak maximum. Raman spectroscopy was used to check the polymorphic form nucleated while FBRM determined the moment of dissolution and nucleation. Solubility data for the different solvents were measured using the Avantium Crystal16 (see Figure 9.6a and b).

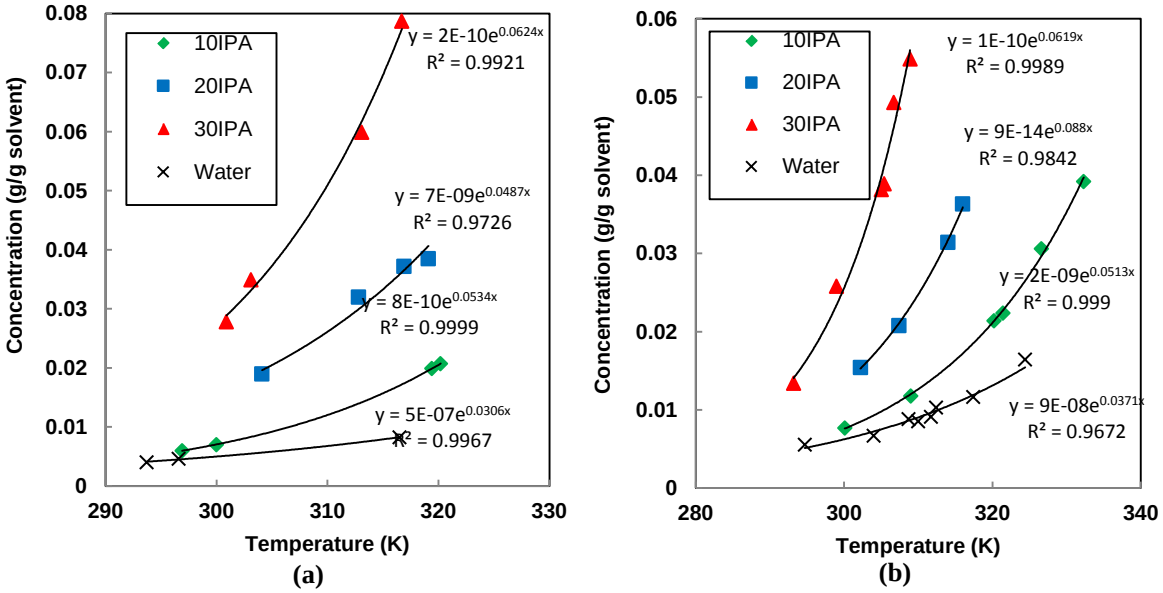

Figure 9.6: Solubility data of OABA (a) form I and (b) form II in different IPA/water mixtures and pure water. Data from Crystal16.

This system can give quickly and easily just an indication of the solubility for the design of a crystallization experiment, but for more accurate solubility data other methods (gravimetric of spectroscopic techniques for example) were proved to be more reliable.

Cooling crystallization experiments were carried out in order to establish, given the kinetic conditions, the positions of the UV/Vis maximum over which only form II nucleates, and below which only form I can appear during crystallization. All measurements were recorded in undersaturated conditions and at the same temperature (50 °C) in order to be able to compare the results. Figure 9.7 shows the results for solutions at different percentage of IPA in water, and same saturation temperature of around 30 °C. The maximum peak positions in the solution are shown with the polymorphic outcome of the crystallization. Two cooling rates were used: -1 °C/min and -0.5 °C/min. At low cooling rate only pure form I or II was obtained while at high cooling rate also a mixture was nucleated. The turning point for polymorphic outcome at -1 °C/min and T_{sat}= 30 °C is at 10 % IPA and corresponds to a maximum position of around 331 nm (when a mixture was nucleated). Even with the low

cooling rate, over 331 nm only form II was nucleated, while form I resulted from solutions at peak positions below that value.

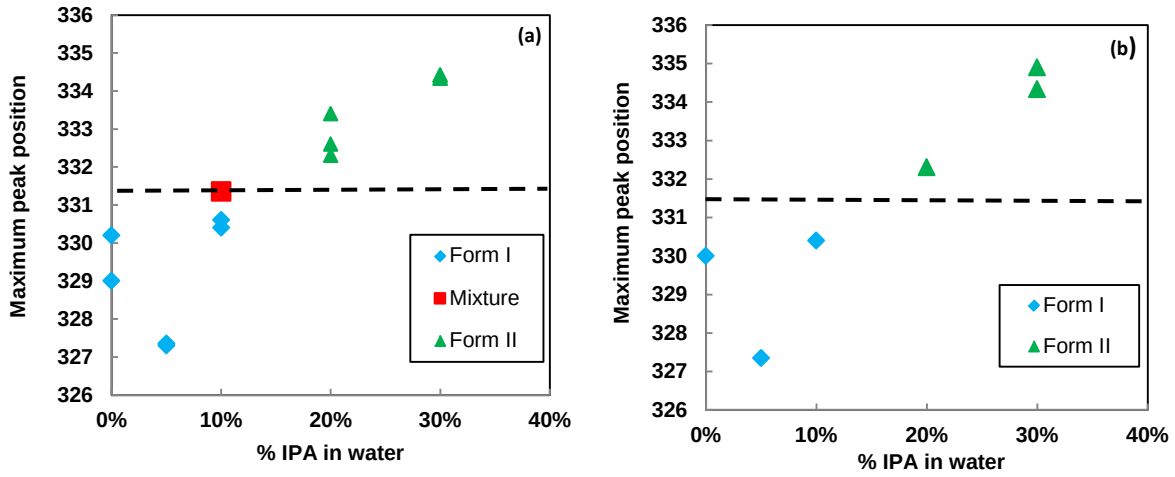

Figure 9.7: (a) Polymorphic outcomes for solutions at T_{sat}=30 °C and a cooling rate of -1 °C/min. (b) Polymorphic outcomes for solutions at T_{sat}=30 °C and a cooling rate of -0.5 °C/min.

Figure 9.8 shows results for the cooling crystallizations of higher concentration solutions (around 40 °C saturation temperature). In the case of low cooling rate (-0.5 °C/min), again, 331 nm seems to be the limit peak position to nucleate pure form I or II. For the high cooling rate, pure form II was obtained from a solution with the peak at around 329.5 nm and pure form I nucleated at 330 nm of maximum peak position.

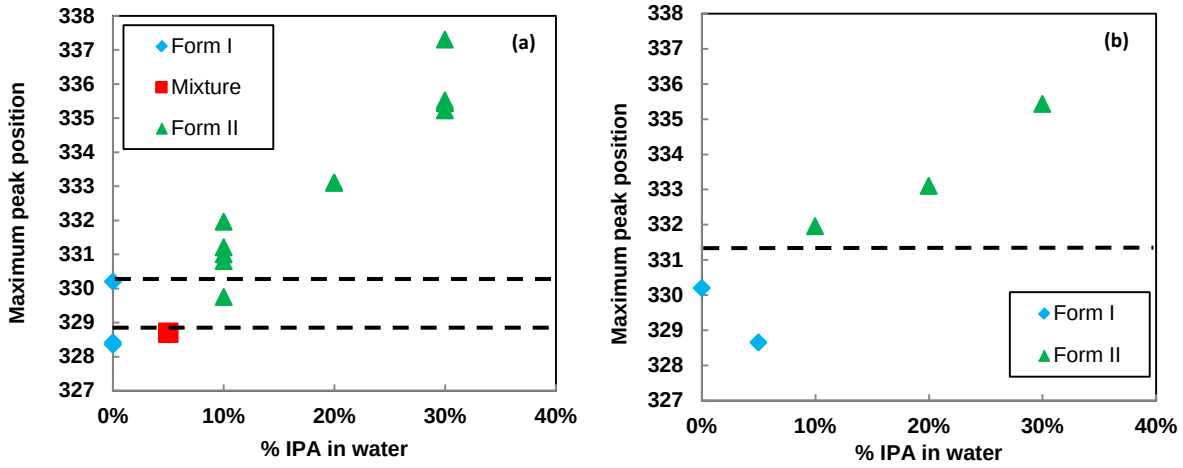

Figure 9.8: (a) Polymorphic outcomes for solutions at T_{sat}=40 °C and a cooling rate of -1 °C/min. (b) Polymorphic outcomes for solutions at T_{sat}=40 °C and a cooling rate of -0.5 °C/min.

Nevertheless, over 331 nm only form II was obtained in accordance with the other cooling crystallizations, while form I can be exclusively obtained if the peak maximum is below 328.5 nm. In both Figure 9.7 and Figure 9.8 a clear trend for the position of the peak maximum as a function of the IPA percentage in solution can be noticed, similarly to the one shown in Figure 9.5. However, some of the solutions of OABA in pure water present a higher maximum peak wavelength compared to the trend of the other mixtures. This is probably due to the fact that equilibrium in pure water is more complex compared to organic solvent mixtures as mentioned by both Zapala et al. (2009) and Abou-Zied et al. (2014).

9.4 Results and discussion for using Raman spectroscopy for linking solution spectra to polymorphic outcome

The Raman spectra of solid forms I and II were analysed and, using tables and information from the literature, typical vibrations were tentatively assigned to the strongest peaks (Susindran et al. 2012; Samsonowicz et al. 2005; Colthup et al. 1975). The most significant peaks and their assignment are shown in Table 9.5.

Using the immersion Raman probe, additional peaks from the sapphire window appear in the Raman spectra, together with the peaks of the solvent (IPA only in this case since water does not have strong Raman peaks). Furthermore, because of the interaction between solute and solvent some of the OABA peaks can be shifted from their position in the solid spectrum. Also, the intensities of the peaks in solution and slurries depend on the concentration of OABA; therefore, in diluted systems some of the peaks shown in Table 9.5 are not clearly visible. The form I peak at around 1037 cm^{-1} (which is at 1031 cm^{-1} for form II) is associated to the ring vibration and it is easily detectable in solutions with the immersion probe even at low concentration; hence it was chosen as the reference peak in the cooling crystallization experiments. The position of the peak during these experiments was calculated using the function polyxpoly in Matlab applied to the first derivative Raman spectra similarly to the previous section. The position was then compared to the polymorphic outcome of the cooling crystallizations.

Table 9.5: Selected peaks of Raman spectra of solid form I and form II of OABA. Aromatic ring vibration types assigned using the nomenclature from Versanyi (1973)

Solid form I	Solid form II	Frequency assigned
563		NH_2 symmetric out of plane bending (Samsonowicz et al. 2005)
667		Ring vibration 4 (Samsonowicz et al. 2005)
770	769	Ring vibration 11 (Samsonowicz et al. 2005)
800		Ring vibration 17a (Samsonowicz et al. 2005)
933		OH out of plane bending (Samsonowicz et al. 2005)
1037	1031	Ring vibration 12 (Samsonowicz et al. 2005)
1166	1165	Ring vibration 13 (Samsonowicz et al. 2005)
1199		Ring vibration (Colthup et al. 1975)
1238	1240	C-OH stretching (Samsonowicz et al. 2005)
1370	1348	C-N stretching (Samsonowicz et al. 2005)
	1434	Ring stretching (Colthup et al. 1975)
	1565	Ring stretching, doublet (Colthup et al. 1975)
1601		Ring vibration 8b (Samsonowicz et al. 2005)
	1624	C=O cyclic dimer symmetric stretching (Colthup et al. 1975)
1660		C=O stretching (Samsonowicz et al. 2005)

Results are shown in Figure 9.9a and b (saturation temperature of 30 °C) and Figure 9.10a and b for saturation temperature of 40 °C.

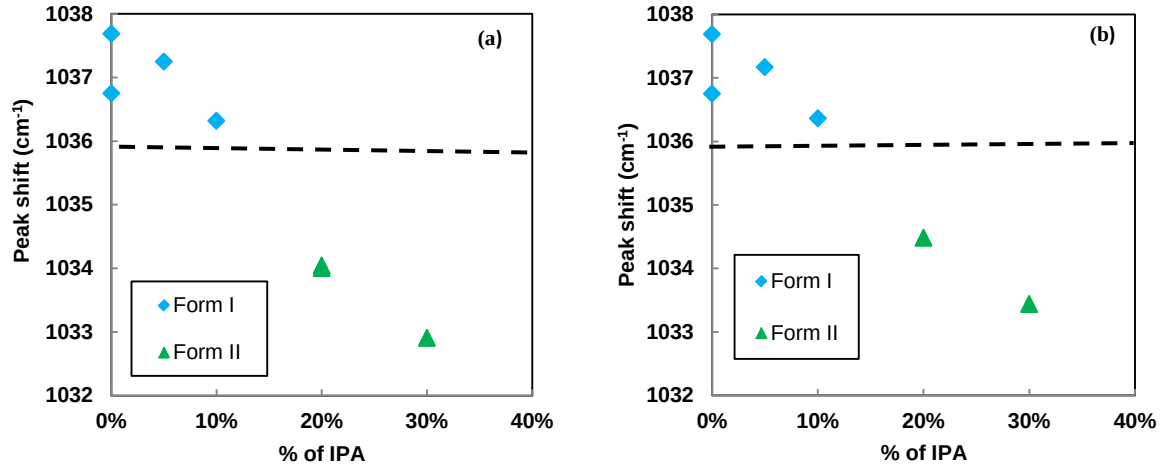

Figure 9.9: (a) Polymorphic outcomes for solutions at T_{sat}=30 °C and a cooling rate of -1 °C/min. (b) Polymorphic outcomes for solutions at T_{sat}=30 °C and a cooling rate of -0.5 °C/min.

It can be noticed that the position of the ring vibration peak in clear solution is shifted to higher Raman shifts compared to the solid samples. The maximum Raman shift is around 1038 cm^{-1} for pure water solution which presents the maximum amount of zwitterions and leads to nucleation of mainly form I. Increasing the amount of IPA (and decreasing the total zwitterions in solution) moves the peak to lower Raman shift and generates nucleation of form II only. A decreasing trend is clearly visible and a comparison between solid samples and solutions can be made. In solid form I the analysed peak is at a higher Raman shift compared to form II. Similarly, solutions that nucleated form I presented the peak at higher Raman shift compared to solutions nucleating form II. Even for Raman spectroscopy, a maximum wavelength above which only form I is nucleated can be distinguished: in none of the experiments at saturation temperature of 30 °C form II was nucleated if the peak position was at a Raman shift higher than 1036 cm^{-1}. At higher saturation levels, similarly to the case of ATR-UV/Vis, a mixture of polymorphs was obtained at a Raman shift of 1037 cm^{-1} but only form II could be nucleated if the peak position was lower than around 1036 cm^{-1}.

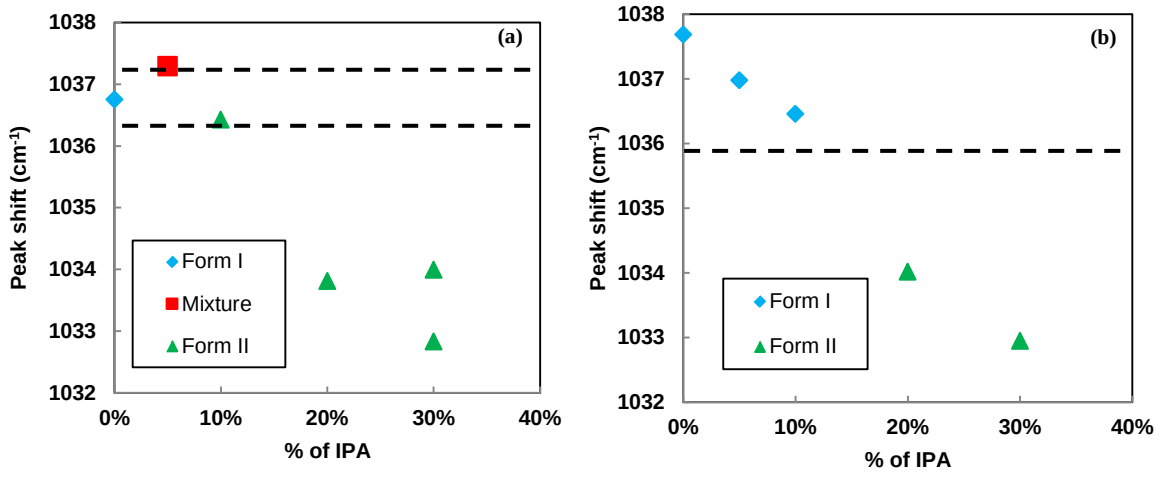

.

Figure 9.10: (a) Polymorphic outcomes for solutions at T_{sat}=40 °C and a cooling rate of -1 °C/min. (b) Polymorphic outcomes for solutions at T_{sat}=40 °C and a cooling rate of -0.5 °C/min.

To confirm that the shift of this peak is really associated to the amount of zwitterions, Raman data were analysed for the experiment show in Figure 9.5 (addition of IPA and water at a solution of OABA).

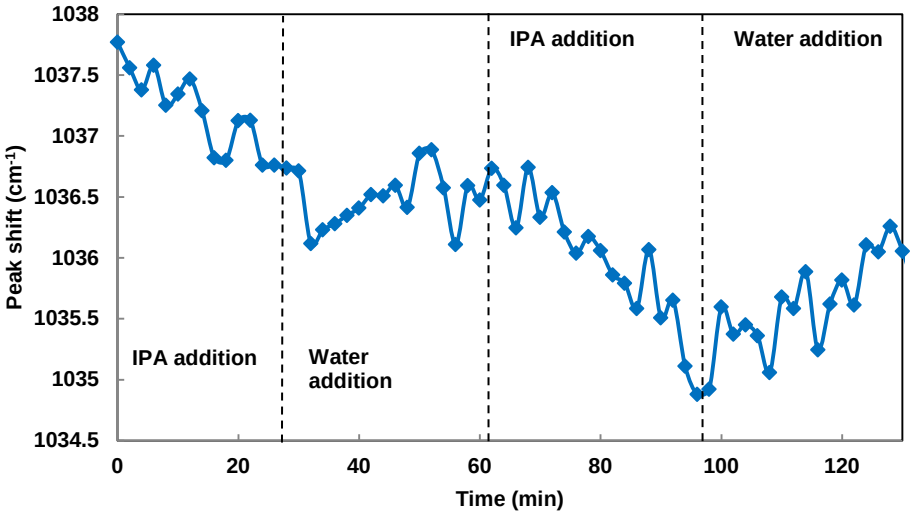

Figure 9.11: Effect of IPA and water addition of Raman spectrum of an OABA aqueous solution.

Although the Raman signal is noisier than the UV/Vis, the studied peak is shifting from around 1038 cm^{-1} to 1036 cm^{-1} during the first addition of IPA. Adding water slightly moves it back to 1037 cm^{-1} and then, the second IPA addition generates a shift to 1035 cm^{-1} (see Figure 9.11). The last water addition moves back the peak to 1036 cm^{-1}.These results clearly

indicate that the shift in the position of the Raman peak is due to the amount of zwitterions in the solution governed by the IPA/water composition and provide evidence that peak position of Raman and UV/Vis spectra of the clear solutions can be correlated with the polymorphic outcome of the crystallization of zwitterionic compounds. The approach presented here could be potentially used for the design of suitable solvent system for the consistent production of the desired polymorphs of OABA.

9.5 Conclusions

In this work a link between polymorphic outcome of a cooling crystallization and UV/Vis and Raman spectra of the clear solutions was found for anthranilic acid. Limit positions for a typical UV/Vis and Raman peak of OABA, over which only form II was nucleated and below which only form I resulted, were determined. The limit value for the UV peak position was found to be 331 nm at cooling rates of 0.5 °C/min and saturation temperatures of 30 °C and 40 °C. For a cooling rate of -1 °C/min and saturation temperature of 30 °C, 331 nm is still the limit peak position to obtain pure form I, whereas for higher OABA concentration it was found that pure form II is always obtained above 331 nm and pure form I always nucleates below 328 nm. For Raman spectroscopy the limiting value of the studied peak was found to be 1036 cm^{-1} for all the experiments. These results can be used to predict nucleation of zwitterions polymorph for UV and Raman sensitive substances and to design suitable solvent systems that favour the consistent production of the desired polymorphic form.

10 Tailoring crystal shape and polymorphism using combinations of solvents and a structurally related additive

In this chapter the effects of combinations of solvents and a structurally related additive on the cooling crystallization of ortho-aminobenzoic acid (OABA) are studied. Variations in nucleation kinetics, growth, agglomeration and polymorphism of the studied compound are presented and explained.

10.1 Introduction

The choice of solvent has a very strong effect on the polymorphic outcome of cooling crystallization, as well as pH, kinetics conditions and presence of impurities. It is well known that certain impurities or additives present during crystallization can have a profound effect on the properties of the crystals produced in term of their size distribution, shape/aspect ratio, polymorphic form and crystalline purity. In this chapter the crystallization of ortho-aminobenzoic acid (OABA) in the presence of a structurally related additive (benzoic acid, BA) will be analysed using both in situ PAT tools and offline techniques. OABA is a quite complex system to study and the morphology and polymorphic form of its crystals are strongly related to the solvent used and the kinetic conditions of crystallization as shown in the previous chapters of this thesis. The stable form of BA has a monoclinic structure (Sim et al. 1955) and its ability to form dimers with its derivatives has been frequently used to form co-crystals and solid solutions (Dubey and Desiraju 2014; Brittain 2009b; Brittain 2009a; Seaton and Parkin 2011) or simply to alter the morphology of growing crystals (Mullin 2001).

Cooling crystallization experiments from different solvents and with different ratios of BA and OABA were performed with the final aim of demonstrating how BA, in combination with a specific solvent, can be efficiently used to control morphology and polymorphism of an organic zwitterionic compound.

10.2 Materials and equipment

Benzoic acid and ortho-aminobenzoic acid were used as solid compounds for the experiments in water and mixtures of water and IPA (10 and 20% IPA). The Raman probe was used together with the ATR-UV/Vis and the FBRM probes during all the experiments. The crystals after filtration and drying were analysed using both off-line Raman and ATR-FTIR spectroscopy. Additionally, X-ray powder diffraction (XRPD) and differential scanning calorimetry (DSC) analyses were performed. The level of BA incorporated in the OABA crystals was measured using high pressure liquid chromatography (HPLC).

10.2.1 HPLC analysis

The type of column used was an Analytical Column Waters Spherisorb® 5 μm C8 4.6x250 mm. The mobile phase for the HPLC analysis was constituted by water at pH=2 (deionized water from a Millipore Elix 5 and pH adjusted with H_3PO_4 from Fisons Analytical Agents) and methanol (Fisher Scientific). The composition of the mobile phase changed gradually during the measurement from 50/50 (w/w) to 40% w/w water and 60% w/w methanol. The flow rate used was 1 mL/min and measurements lasted 10 minutes. The injection volume was 5μL and the wavelength used was 230 nm. Calibration samples were prepared at different ratios of benzoic acid and water and a univariate model was developed using the ratio between the BA and OABA peaks' areas. The relation between BA and OABA ratio and the ratio of the two peaks' areas was found to be well described by a second order polynomial.

10.3 Methodology

Three different solvents were used for the experiments: pure water, water with 10% IPA (w/w) and water with 20% IPA (w/w). Two levels of OABA saturation temperature were used (about 35 and 45 °C with respect to form I) for each solvent; each experiment was repeated at least three times to check consistency. Table 10.1 shows the conditions used in the experiments performed. Solid OABA was added to the solvent and the temperature was raised to 50 °C in order to dissolve all the particles. The solution was kept at high temperature (50 °C) for 20-30 minutes and then cooled down at a rate of -1 °C/min; the final temperature was determined from the solubility data of benzoic acid in order to be always in undersaturated conditions for this compound (between 10 and 25 °C). Then a small amount of solid benzoic acid was added to the slurry and the solution was heated up

again and then cooled down with the same previous cooling rate. More consecutive additions of benzoic acid in the same solution were performed maintaining the same kinetic conditions (initial temperature and cooling rate) but increasing the ratio of BA to OABA in solution. In situ probes, including PVM, FBRM and UV were used to detect nucleation and monitor OABA concentration and crystals during the experiment, while in situ Raman was used to determine the polymorphic form nucleated. A 5 mL sample was taken at the end of the temperature profile in order to observe closely the morphology (using an optical microscope) and the polymorphic form (using ATR-FTIR, XRD and a Raman microscope) of the crystals. Raman was also found very useful in detecting the presence of benzoic acid in solid solution in the crystals of OABA nucleated.

Table 10.1: Experimental conditions used

Experiment number	Solvent	OABA concentration (g/g solvent)	Maximum BA/OABA (w/w)
1	Water	0.0097	0.25
2	Water	0.0096	0.18
3	Water	0.0098	0.16
4	Water	0.0099	0.14
5	Water	0.0067	0.25
6	Water	0.0069	0.34
7	Water	0.0069	0.41
8	10% IPA	0.0089	0.29
9	10% IPA	0.0087	0.39
10	10% IPA	0.0088	0.40
11	10% IPA	0.0148	0.19
12	10% IPA	0.0148	0.21
13	10% IPA	0.0148	0.26
14	10% IPA	0.0148	0.34
15	20%IPA	0.0298	0.27
16	20%IPA	0.0299	0.27
17	20%IPA	0.0298	0.10
18	20%IPA	0.0163	0.35
19	20%IPA	0.0162	0.53
20	20%IPA	0.0162	0.64

Additionally, DSCs were also conducted for some samples in order to double check the crystal structure and the benzoic acid incorporation. The choice of the solvents was based on the results shown in chapter 9 where it was found that deionized water (which contains the highest amount of OABA zwitterions in solution, about 82% of the total molecules) favours the crystallization of the zwitterionic polymorph Form I, while mixtures of IPA and water (where non-ionized molecules prevail on zwitterions in solution) favour nucleation of the metastable form II. Form III was never observed during the cooling crystallization experiments of chapter 9. According to the current literature this polymorph is extremely difficult to nucleate from solution and it is usually obtained by sublimation, or trough solvent mediated or melt transformation at high temperature.

10.3.1 Transformation experiments

In order to study the incorporation of BA in the three OABA polymorphs and its effect on the kinetics of polymorphic conversion, few transformation experiments in water and 10% IPA w/w were performed. Mixtures of form II and III were nucleated in the presence of different amounts of benzoic acid and the polymorphic transformation at 20 °C from II to III and then to I was monitored. The cooling rate and starting temperature were the same as the experiments described in the previous section. Samples were taken and analysed with both ATR-FTIR and HPLC.

10.4 Results and discussion

10.4.1 Polymorphic outcome in the three solvents

In pure water about 82% of the molecules of OABA are in the form of zwitterions while the rest are neutral (Zapala et al. 2009). This condition favours nucleation of form I during cooling crystallizations as shown in Figure 10.1. The addition of benzoic acid to the OABA solutions in water does not change significantly the chemical equilibrium: the change in pH associated to the addition of about 2600 ppm of benzoic acid is only from 3.53 to 3.29 (corresponding to a decrease in the zwitterions of less than 1%). For small BA/OABA ratios in water form I was always nucleated while, at higher ratios, mixtures of form I and III or pure form III were obtained. Form II was rarely nucleated, practically it was observed only once, and in mixture with form III from highly concentrated solution. Unfortunately it is not possible to clearly distinguish forms II and III with the in situ

Raman probe since the spectra of these two polymorphs are very similar. Analysing the filtrated and dried crystals with a Raman microscope also did not help since differences are minimal so ATR-FTIR was used to unequivocally determine the form nucleated. From III was consistently observed nucleating in water together with form I when the weight ratio between benzoic acid and ortho-aminobenzoic acid in solution was between 0.1-0.3. At ratios higher than about 0.35 all the crystals nucleated were form III. The transformation kinetics observed for form III was very slow. Slurries of form III in water were kept and stirred at 10 °C for 12-18 hours and transformation did not even start. In case of nucleation of both form III and form I a polymorphic transformation from form III to I was observed but still, was found to be very slow.

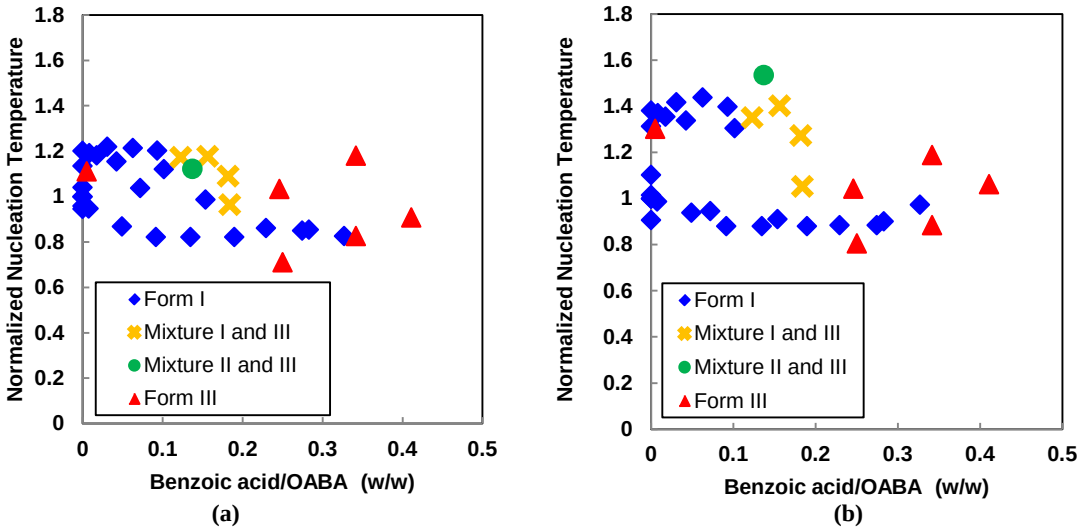

Figure 10.1: (a) Normalized nucleation temperatures recorded with FBRM for the experiments in water at about 45 °C and 35 °C saturation (b) Normalized nucleation temperatures recorded with PVM or UV for the experiments in water at about 45 °C and 35 °C saturation. Normalization is done dividing every nucleation temperature, for each saturation value, by the nucleation temperature with no benzoic acid. The ratio BA/OABA is calculated considering the density of the slurry at the sampling temperature 1 kg/L.

The normalized nucleation temperature (calculated by dividing the nucleation temperature of each crystallization experiment by the one recorded for the solution of OABA with no BA) varies between 0.7 and 1.2 but there is not a clear trend with the increase of the BA/OABA ratio. The solubility of OABA in the presence of BA in water was measured using a gravimetric method and a moderate difference in solubility was found for temperatures lower than 20 °C (at 15 °C and BA concentration of 0.0027 g/g solvent the solubility of OABA was 0.0024 g/g solvent against 0.0032 g/g solvent measured in water

only). This change of about 25% in solubility concentration can explain the variability in the normalized nucleation temperature especially at low concentration of benzoic acid. Form III of OABA was obtained at high BA/OABA ratio also in the other two solvents tested, 10% w/w IPA/water and 20% w/w IPA/water (see Figure 10.2 and Figure 10.4). In 10% w/w IPA/water form II or mixtures of form I and II were nucleated in the absence of BA. This specific solvent composition is characteristic because it can generate nucleation of a mixture of form I and II depending on the kinetic conditions (as shown in chapter 6). However, the addition of a certain amount of benzoic acid favoured, instead, the nucleation of form III without a significant change in the nucleation temperature as shown in Figure 10.2. Form III started nucleating together with form II at ratios BA/OABA in solution of 0.08-0.1 similarly to the experiments in water only. Only form III was obtained for BA/OABA ratios above 0.25-0.3.

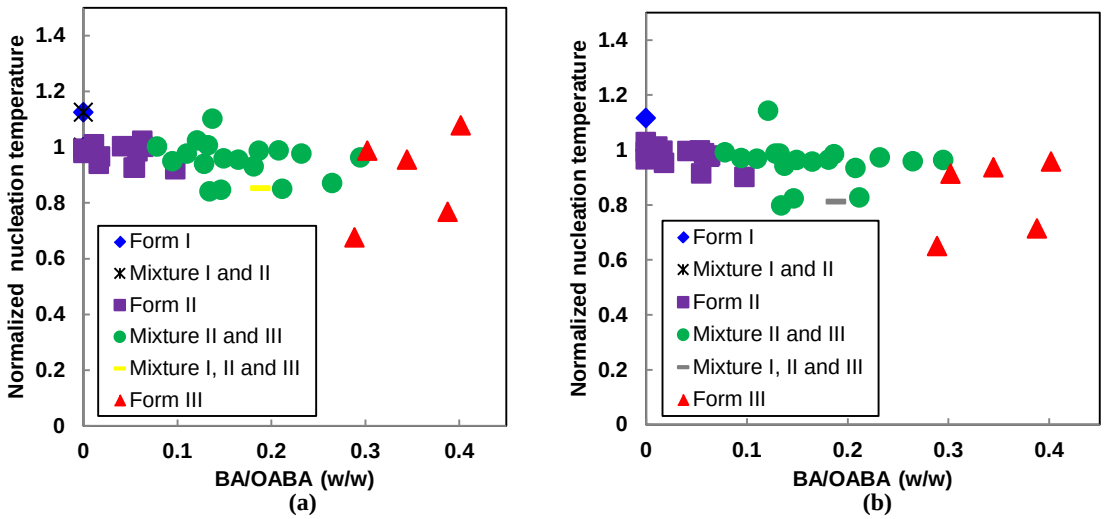

Figure 10.2: (a) Normalized nucleation temperatures recorded with FBRM or Raman for the experiments in 10% IPA/water at about 45 °C and 35 °C saturation (b) Normalized nucleation temperatures recorded with PVM or UV for the experiments in 10% IPA/water at about 45 °C and 35 °C saturation. Normalization is done dividing every nucleation temperature, for each saturation value, by the nucleation temperature with no benzoic acid. The ratio BA/OABA is calculated considering the density of the slurry at the sampling temperature 1 kg/L.

Figure 10.3 shows the ATR-FTIR spectra of the solid samples (washed, filtered and dried) obtained during one of the experiments in 10% w/w IPA/water solvent. The first sample nucleated is a mixture of form I and II, then only form II is obtained and finally mixtures of II and III with an increasing amount of form III as the ratio BA/OABA increases. The

region between 3200 and 3600 cm^{-1} contains enough information to distinguish the three polymorphs and it also does not contain peaks from the benzoic acid (Carter, Ward 1994). Form I is characterized by two broad peaks at 3315 and 3228 cm^{-1}, Form II presents one peak at 3470 cm^{-1} and one at 3370 cm^{-1} while Form III has two sharp peaks at 3490 and 3380 cm^{-1}. Mixtures of polymorphs present three or four peaks in positions and intensities that depend on the type of polymorph and its amount in the mixture.

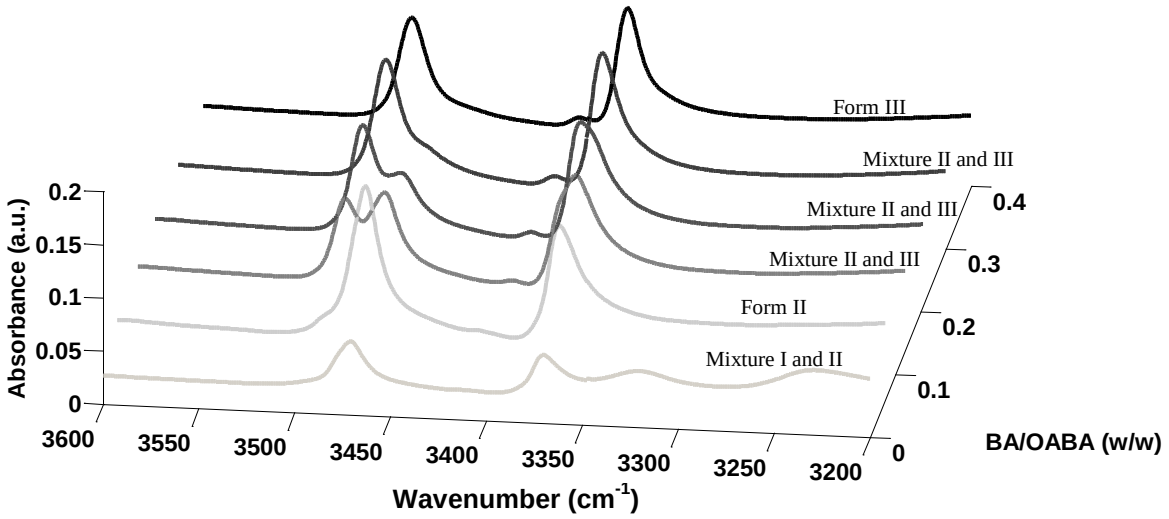

Figure 10.3: ATR-FTIR spectra of solid samples after filtration. The graph has IR wavenumbers on the x-axis, ratio between benzoic acid and OABA on the y-axis and absorbance intensity on the z-axis.

In 20% IPA and water form I was never nucleated but only form II, mixtures of form II and III (with increasing concentration of form III with the increase in BA/OABA ratio) and finally form III only were obtained. Similarly to the other solvents, form III started nucleating in mixtures with form II for BA/OABA ratio higher than 0.1. For ratios above 0.4 only form III nucleated. In the two IPA/water mixtures tested the variation in normalized nucleation temperature is even smaller than in water: nucleation happened at roughly the same temperature for all experiments at a given saturation (as shown in Figure 10.2 and Figure 10.4). The solubility of OABA in the presence of BA was measured with a gravimetric method even for these two solvents. It was found that BA does not significantly affect solubility of OABA in 10% and 20% IPA/water mixtures. However, the solubility of the solid solution BA/Form III in the three solvents tested might be lower than the solubility of pure form III and, therefore, the nucleation of the solid solution could be more kinetically favourable than in the case of the pure polymorphs. Another possibility is that benzoic acid in solution could lower the surface energy for nucleation of the crystals

of form III favouring the formation of that polymorph similarly to what is described and calculated by Sun et al. for the aragonite/calcite system (Sun et al. 2015). The results of this study shows that the presence of atoms of Magnesium in water (in a ratio with the ions Mg:Ca>2) favours the nucleation of the metastable form of calcium carbonate, aragonite, instead of the stable calcite. Surface energies were obtained by density functional theory (DFT) calculations of hydrated calcium carbonate surface slabs with partial Mg^{2+} substitution and showed that the incorporation of Magnesium on the calcite can drastically inhibit its nucleation (Sun et al. 2015).

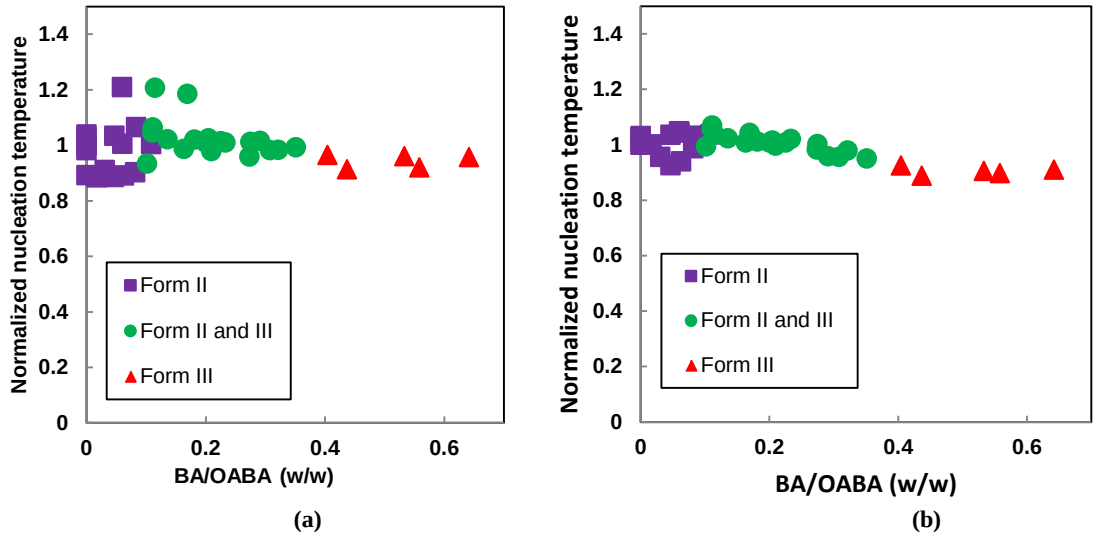

Figure 10.4: (a) Normalized nucleation temperatures recorded with FBRM for the experiments in 20% IPA/water at about 45 °C and 35 °C saturation (b) Normalized nucleation temperatures recorded with PVM or UV for the experiments in 20% IPA/water at about 45 °C and 35 °C saturation. Normalization is done dividing every nucleation temperature, for each saturation value, by the nucleation temperature with no benzoic acid. The ratio BA/OABA is calculated considering the density of the slurry at the sampling temperature 1 kg/L.

The system BA/OABA presents many similarities to what was calculated by Sun et al. In fact, OABA form III is always nucleated above certain ratios of BA/OABA in solution. However, surface energy measurements as well as molecular dynamics calculations would be necessary to strongly confirm the validity of the hypothesis suggested also for the BA/OABA system.

10.4.2 Incorporation of benzoic acid in the three polymorphs

The crystals obtained at the end of the crystallizations were analysed with HPLC in order to quantify the amount of BA incorporated. Figure 10.6 shows the results of the analysis for samples crystallized in the three solvents as well as the polymorphic form of each sample. There seems to be a linear correlation between the amount of benzoic acid incorporated in the ortho-aminobenzoic crystals and the BA/OABA ratio in solution which is typical of solid solutions. Further solid state analyses were conducted in order to confirm that BA was actually incorporated in the crystal structure of OABA and the samples were not physical mixtures of BA and OABA. DSC was performed on the samples and showed a single melting peak whose temperature decreased linearly with increasing the amount of BA in the sample (from 148.8 °C at 0% w/w BA to 127.5 °C at 34% w/w BA as shown in Figure 10.5).

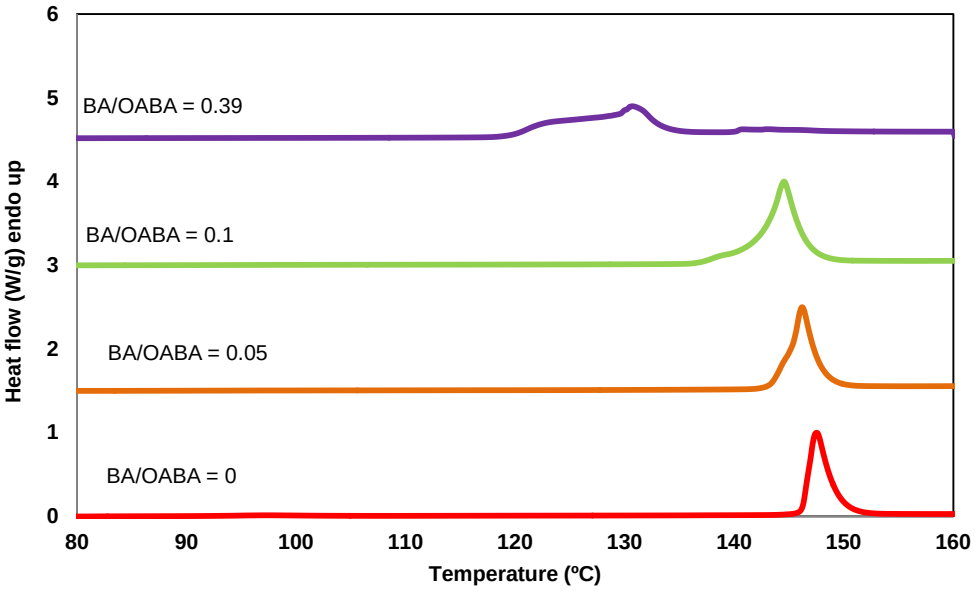

Figure 10.5: DSC results for several solid solutions of BA and OABA (form II and III).

Furthermore, XRPD of the samples at high amount of BA showed the same peaks of the pure polymorphs (although broader or slightly shifted because of the presence of BA molecules in the crystal structure) confirming the presence of a single phase. Raman and ATR-FTIR were also performed and while the FTIR spectra did not show any BA peaks, it was possible to notice a specific peak of BA in the Raman spectra at 1005 cm^{-1} whose

intensity increased with increasing amount of BA incorporated. In Figure 10.6a it is possible to notice that the incorporation of BA in form I is linear but considerably lower than in form II or III with equal ratio BA/OABA in solution.

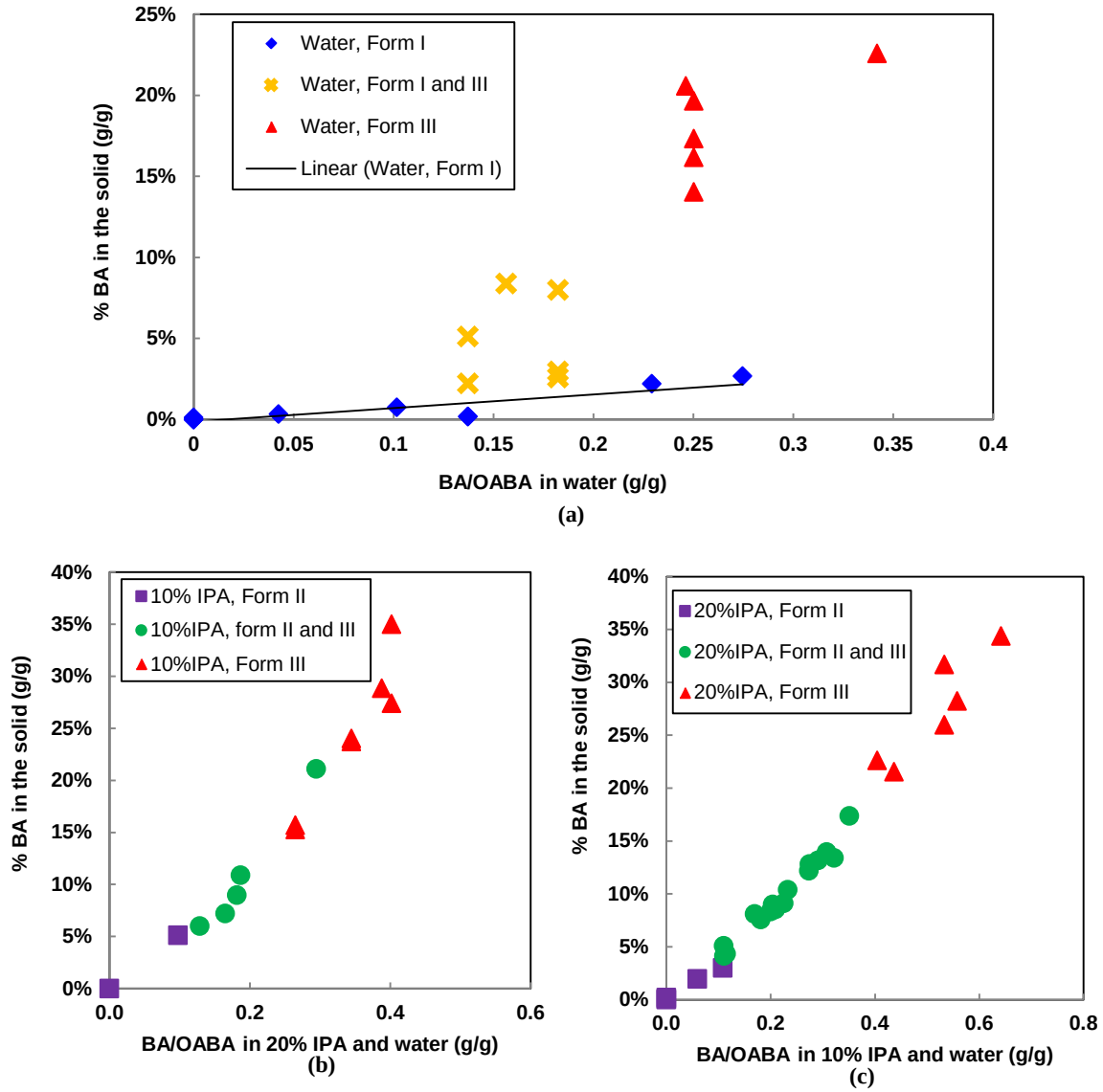

Figure 10.6: Percentage of BA incorporated in the crystals versus the ratio BA/OABA in water (b) 10% IPA in water and (c) 20% IPA in water.

This phenomenon can be explained comparing the crystal structure of the three polymorphs. Form II and III are characterized by carboxylic acid dimers arranged in the crystal lattice without any intermolecular hydrogen bonds involving the amino groups of OABA, while form I presents both intermolecular and intramolecular hydrogen bonds

between the carboxylic acid and the amino group. Besides BA is a weak acid with pKa= 4.2: in aqueous solution saturated at 25 °C less than 5% of the BA molecules are in the ionic form. In its undissociated form BA can easily substitute a molecule of OABA in the dimers of form II and III and be incorporated in their crystal structure. BA can still form hydrogen bonds with the carboxylic groups of OABA of form I but then it will prevent the attachment of further OABA molecules because of the lack of the amino group and, therefore, it will inhibit growth of this polymorph. A further analysis of the incorporation of BA in the three polymorphs and its effect on the kinetics of polymorphic transformation was conducted. Mixtures of form II and III were nucleated in 10% IPA and water and the time of transformation II→III and then III→I was measured as well as the amount of BA incorporated in the crystals at the different stages of the transformation itself. Figure 10.7a shows the amount of BA in the solid crystals during the polymorphic transformation for an initial BA/OABA ratio of 0.12.

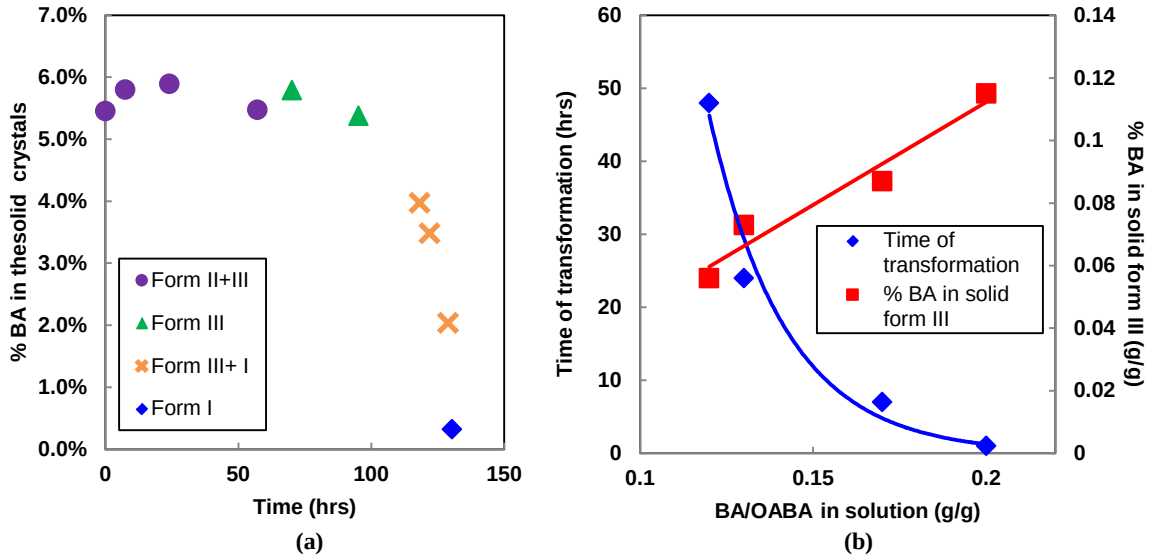

Figure 10.7: (a) Incorporation of BA during the different stages of polymorphic transformation II→III and then III→I for the experiment at BA/OABA = 0.12 (b) Time of transformation II→III as a function of the ratio BA/OABA in solution and % BA incorporated in form III after complete transformation for four experiments performed. A fifth experiment was performed using a BA/OABA ratio of 0.1 but form I started appearing before the completion of the II→III transformation.

The amount of BA incorporated in the crystals does not change with the conversion from II to III but drops down when form I appears. The same transformation experiment was repeated at different ratios of BA/OABA and the time of conversion from form II to form

III is shown in Figure 10.7b. The transformation is very slow and the time increases exponentially with decreasing the BA/OABA ratio. That is probably also related to the fact that, at high amount of BA in solution, the amount of form III nucleated is higher than at low BA. Therefore, the time to complete the transformation is higher since there is more form II to convert into form III. The same experiment was performed with BA/OABA = 0.1 but form I appeared before the complete conversion II→III could take place. This set of experiments confirmed the tendency of BA to be incorporated equally in both form II and III but not in form I.

10.4.3 Morphology of the three polymorphs

PVM, SEM and an optical microscope were used to analyse the effect of benzoic acid on the morphology of OABA in the three solvents used. In the previous section it was shown how BA cannot be incorporated in OABA form I and, therefore, should act as a growth modifier. Figure 10.8 shows some PVM images of crystals of form I nucleated and grown in the presence of BA in different concentrations.

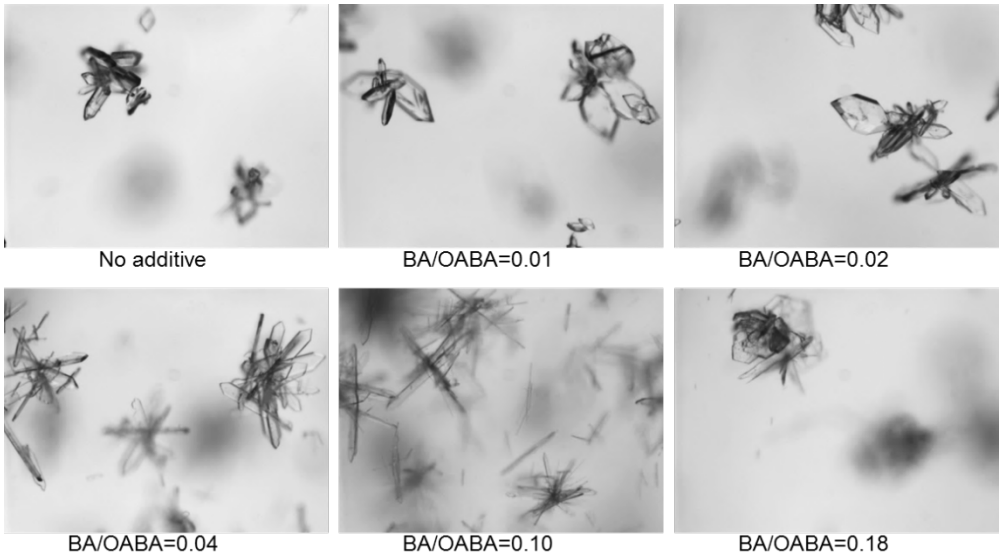

Figure 10.8: PVM images of OABA crystals (form I) in water in presence of benzoic acid. The additive, in small amounts, modifies the morphology of form I crystals from prismatic to needle-like and favours agglomeration. The presence of plate-like crystals at high BA/OABA (0.18 corresponding to the last image) is due to nucleation of another polymorph (form III).

It can be seen that the shape of the crystals is prismatic at very low concentrations of BA and then becomes needle-like as the ratio BA/OABA increases: this is a clear proof of growth inhibition. The growth along the b-axes is inhibited by the presence of molecules

of BA which prevents the attachment of new OABA molecules as well as the incorporation of large quantities of BA in the crystal structure. As shown in Figure 10.8 crystals became more needle-like as the amount of BA increases. The presence of BA seems also to favour agglomeration of the crystals as shown in the PVM images of Figure 10.8. At high ratios of BA/OABA plate-like crystals of form III start to appear. The morphology of form III is not very clear because of the presence of high amount of BA incorporated which distort the crystalline structure, as well as causing agglomeration of the crystals. A schematic of the evolution of the shape of OABA form I with the increase of BA/OABA is shown in Figure 10.9.

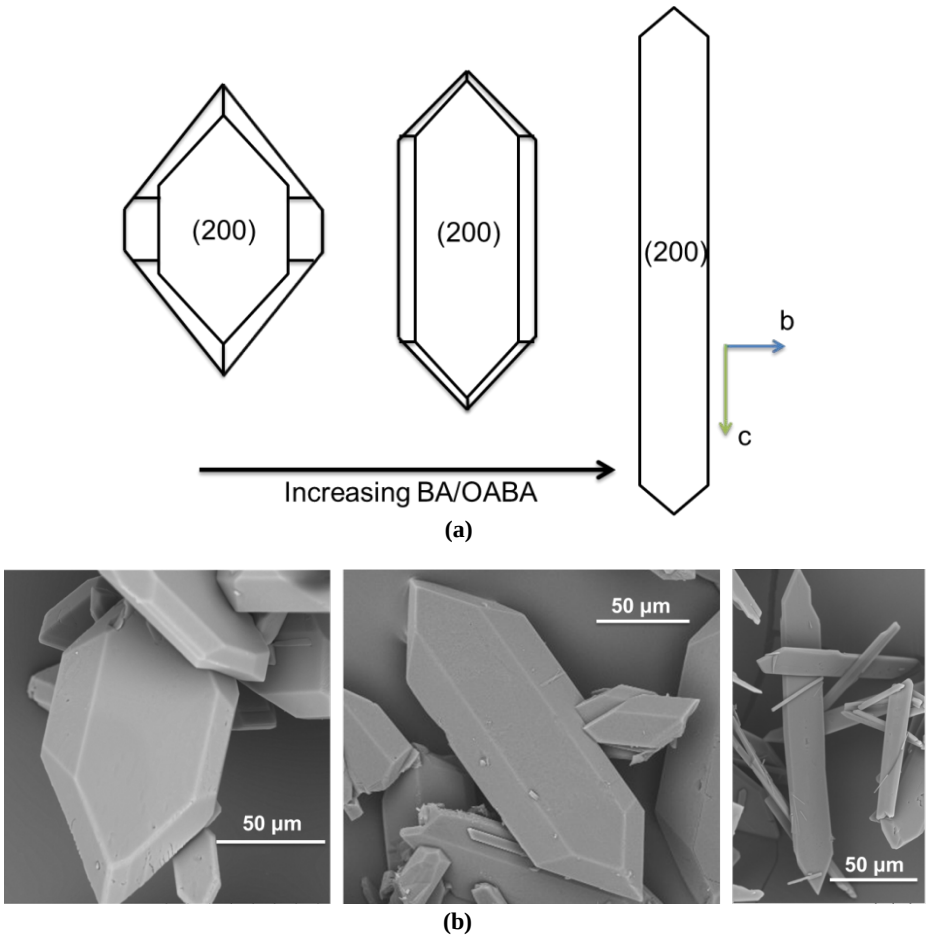

Figure 10.9: Evolution of the shape of OABA in the presence of BA (a) Schematic (b) SEM images at BA/OABA ratios of 0, 0.017 and 0.102 (w/w ratio increasing from left to right).

The difference in morphology between form III and I is also noticeable in the FBRM data. The number of counts after nucleation gradually increases with the addition of benzoic acid as a result of the change in shape of the crystals of form I (needles usually have higher counts because the short side is counted many times) and then suddenly decrease with the

nucleation of a mixture of form I and III, which is characterized by a lower total counts as well as a change in the Raman spectrum.

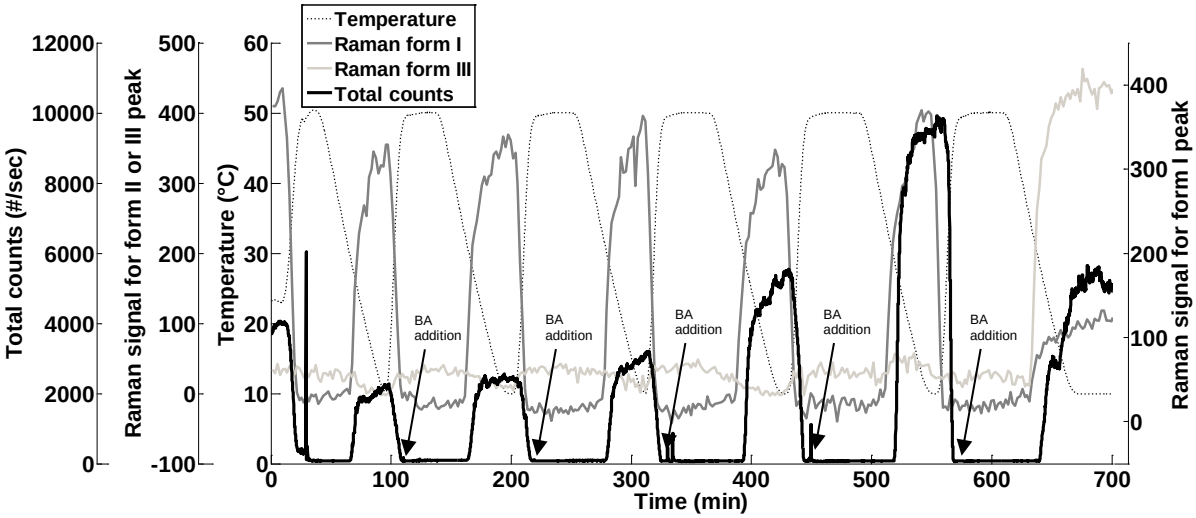

Figure 10.10: FBRM and Raman signal for experiment 2 of Table 10.1. The same temperature profile was repeated 6 times with addition of BA before the cooling step. Form I was nucleated for the first five profiles and during the sixth a mixture of form I and III was obtained.

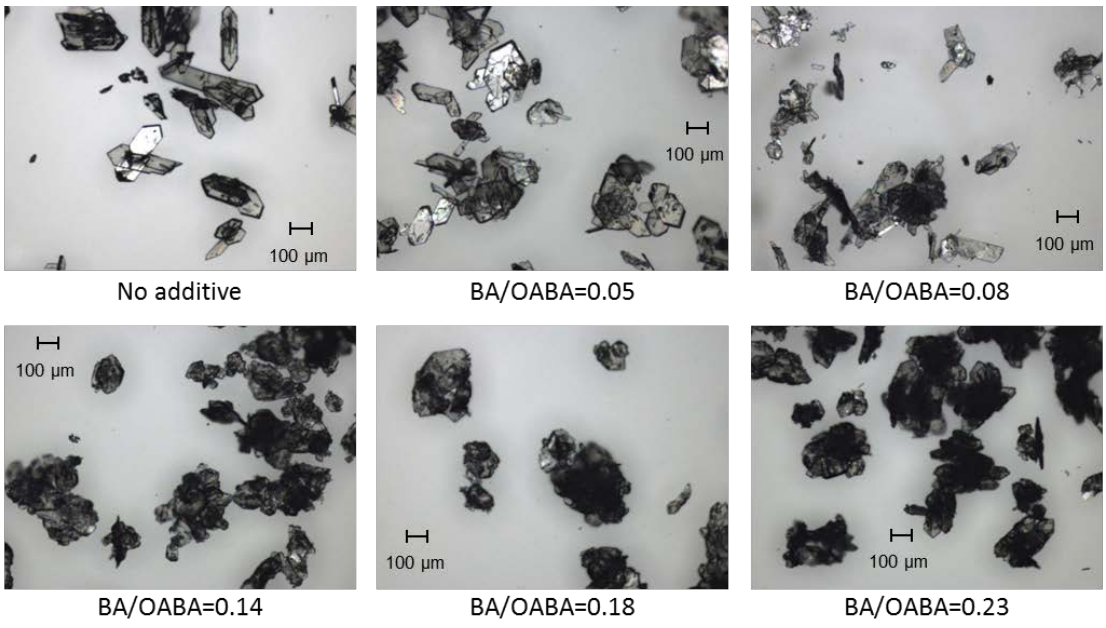

Figure 10.11: Microscopic images of the filtered samples taken during one of the experiment conducted in 20% IPA (experiment 15 from Table 1). The first three samples (first row) are form II only, while the last three (second row) are mixtures of II and III.

The FBRM and Raman signals from experiment 2 of Table 10.1 are shown in Figure 10.10. Small amounts of BA in 10% w/w IPA/water do not significantly change the morphology

of Form II which remains needle-like (as shown in Figure 10.11). However, there is an increasing tendency to agglomeration and needle become more irregular as the benzoic acid content in solution increases as shown in Figure 10.11. A similar behaviour could be observed also in 20% w/w IPA/water (see Figure 10.11). Additionally, high amounts of BA strongly distort the crystalline lattice of form II and III making very difficult to understand the exact morphology of the crystals nucleated. SEM images of form III crystals obtained in water at BA/OABA = 0.24 and in 10 % w/w IPA/water at BA/OABA = 0.36 are shown in Figure 10.12. The agglomerates of form III obtained from water are bigger than the ones obtained in 10% IPA and they have a more spherical and compact shape. In 10% IPA the crystals of form III are plate-like and they form agglomerates of a more irregular and loose shape. These results indicate that using a structurally related additive and suitable solvent system it is possible to tailor the polymorphic purity of OABA crystals, and even more, form III crystals can be consistently and reproducibly obtained, which are otherwise very difficult to produce. Further tailoring the amount of additives, within the ranges that correspond to a desired polymorphic form, crystal morphology and degree of agglomeration can be tailored. These experimental result provide and exemplary case how tailoring solvent composition and structurally related additive concentration can be used to achieve complex particle engineering targets.

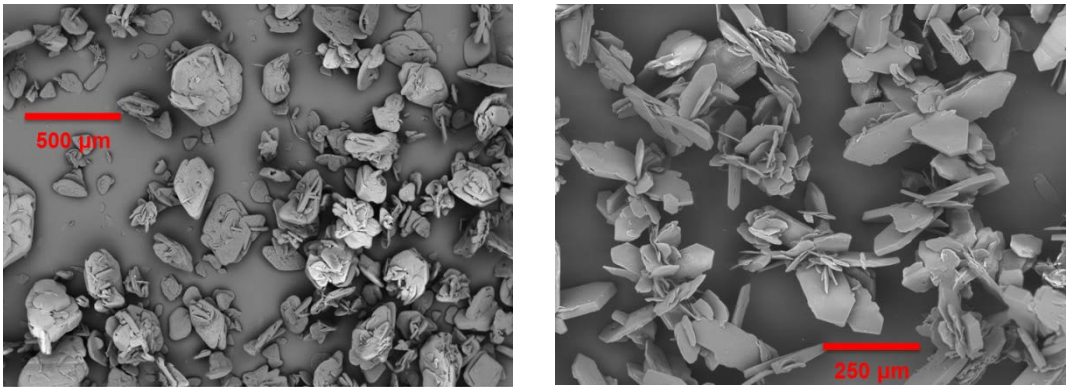

(a) **(b)**

Figure 10.12: SEM images (a) Agglomerates of form III nucleated from water (BA/OABA = 0.24) (b) Agglomerates of form III nucleated from 10%IPA (BA/OABA w/w= 0.36).

10.5 Conclusions

The effect of benzoic acid (BA) on the crystallization of OABA in different solvents was studied in this work. It was possible to nucleate all the three known polymorphs of OABA using specific combinations of solvent and BA/OABA ratios. The presence of benzoic acid seems to favour nucleation of OABA form III: at ratios BA/OABA higher than 0.3-0.4 it was possible to nucleate form III in all the three different solvents. It is well known from the literature that this polymorph is very difficult to nucleate in solution, but the addition of a benzoic acid in solution favoured its formation although in an impure form (benzoic acid was always incorporated in the crystal lattice of form III).

The incorporation of BA in the OABA polymorphs was quantified using HPLC and it was found that form II and III can equally incorporate BA as solid solutions while the specific system of hydrogen bonding in the crystal structure of form I prevents the inclusion of molecules of BA. It was also found that in small amount in water, benzoic acid can inhibit the growth along the b-axis of form I and change its morphology. BA also promotes agglomeration of all the polymorphs and speeds up the polymorphic transformation II→III. The agglomerates are easy to filtrate and for the case of water used as solvent they tend to have a spherical shape which is highly desired by pharmaceutical industry.

11 Analysis of the crystallization process of a biopharmaceutical compound in the presence of impurities using process analytical technology (PAT) tools

In this chapter PAT tools are used to study the crystallization of a biopharmaceutical compound (vitamin B12). In particular the effect of impurities on the growth kinetic of vitamin B12 is analysed using focused beam reflectance measurement (FBRM) and ATR-UV/Vis spectroscopy.

11.1 Introduction

Over the last decade the investment in research and development of biopharmaceutical companies has more than doubled: there is a great interest in formulating and optimizing the manufacturing of bio-molecules and biopharmaceuticals such as proteins, lipids, vitamins, hormones and DNA. Those compounds can be used in the treatment of serious diseases or just as nutritional supplement. The crystallization of biopharmaceuticals can be problematic since, because the biosynthesis of these compounds is very difficult to control, they can present a significant amount of impurities that has to be eliminated. In fact, impurities can lead to changes in the properties of the drug that can significantly reduce its effectiveness or even put in danger the user. In this chapter the crystallization of a relatively small biological molecule, vitamin B12, will be studied with PAT tools (ATR-UV/Vis, FBRM and CryPRINS) and the effect of impurities on the growth and nucleation rate will be analyzed. The produced crystals are analyzed with optical microscopy, HPLC and Raman. Most of the impurities in cyanocobalamin have high levels of fluorescence and, therefore, Raman can give an indication of the purity of the crystals since it is highly sensitive to this phenomenon (Mayer et al. 1973; Zhang et al. 2009). However, for a precise quantification of the type and level of impurity in vitamin B12 samples HPLC is necessary. This chapter provides one of the first comprehensive case studies that illustrate how an array of PAT tools can be used for the systematic understanding and design of a biopharmaceutical crystallization process.

11.2 Methodology, materials and equipment

11.2.1 Materials and Equipment

Crude Vitamin B12 produced by fermentation was donated by Hebei Welcome Pharmaceutical Co., LTD (China). Ultrapure water was obtained via a Millipore ultra-pure water system while ethanol was purchased by Fisher Scientific (purity >95% v/v). Pure water or solutions of water and ethanol were used as solvents for the experiments. Experiments were conducted at both Loughborough University, UK and Purdue University, USA with similar, but not exactly identical instruments. Two 500 mL glass jacketed vessels and the same Raman system (an RXN1 Raman analyzer with immersion probe and 785 nm laser, Kaiser with iC Raman 4.1 software) were used. The experiments at Loughborough University were performed using an ATR-UV/Vis probe; an FBRM probe and a Huber thermoregulator (see Chapter 3 for details on instrumentation). CryPRINS was used to set the temperature profiles and control the experiments. The instrumentation at Purdue University consisted in a Zeiss MCS621 UV/Vis spectrophotometer with UV-VIS 190-720 nm Zeiss probe (Zeiss Process Xplorer software version 1,3-Build 1.3.1.30), an FBRM G400 0.5-2000microns (Mettler Toledo with ic.FBRM software version 4.3) and a JULABO F25-ME thermoregulator. The samples of vitamin produced were analyzed using a Raman RXN1 microprobe (Kaiser) and an HPLC Agilent 1100 series (Hewlett Packard) with ChemStation software rev. A.09.03[1417].

11.2.2 Procedure for linear cooling experiments

Mixtures of water and ethanol and pure water were used as solvents for the linear cooling experiments. The concentrations used were about 0.118-0.13 g/g solvent in water and ethanol (saturation temperature of about 50 °C) and between 0.09 and 0.11 g/g solvent for water (saturation temperature of about 60 °C). The material was dissolved and the hot solution was filtered (using a filter paper) before starting the cooling profile because of the presence of insoluble particles in the raw material. The solubility of vitamin B12 in water at different temperatures was provided by the supplying company and is shown in Table 11.1, while data for ethanol/water mixtures at different temperatures was not available from the literature and the amount of material donated was too small to accurately measure it. However, two inferential curves of the solubility expressed as UV signal (absorbance value at 361 nm) were obtained in order to compare the two solvents. Those curves can

also be directly compared with the UV data in the Results and Discussion section (which is actually an absorbance and not a concentration value).

Table 11.1: Solubility of vitamin B12 in water at different temperature (data provided by Hebei Welcome Pharmaceutical Co., LTD)

Temperature (°C)	Solubility (g/l water)
10	9.25
20	10
25	11.5
30	13.5
45	24

The curves were acquired by slow heating (0.075 °C/min) of two slurries of vitamin B12 in water and ethanol/water. The amount of vitamin dissolved at any time and temperature is proportional to the absorbance value recorded.

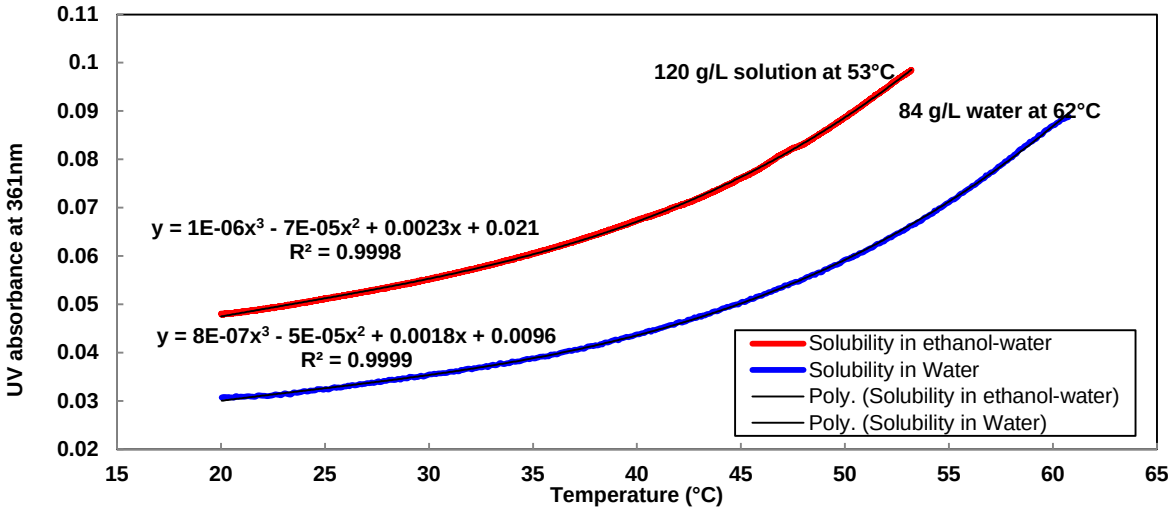

Figure 11.1: inferential solubility curve expressed as UV signal versus temperature in the two solvents used. The addition of ethanol increased the solubility of vitamin B12 especially at high temperature. This type of curve can replace the classical concentration versus temperature relationship in cases in which only a small amount of material is available and literature data are not available.

Figure 11.1 shows the inferential curves as well as the exact solubility in the two solvents at high temperatures (120 g/L ethanol/water solution at 53 °C, and 84 g/L water at 62 °C). Table 11.2 shows the conditions of the experiments performed in this chapter. The material was added to the solvent at ambient temperature and then dissolved by heating the solution and keeping it at high temperature for 15-20 min. In ethanol and water the higher temperature was around 75 °C while in pure water it was around 70 °C. Four cooling rates were used: -0.075, -0.1, -0.5 and -1 °C/min (slower, slow, fast and faster cooling), both seeded and unseeded experiments were performed. The cooling rates were chosen based on experience with similar types of crystals, equipment and scale (Saleemi et al. 2012b; Saleemi et al. 2012a; Saleemi et al. 2012). The final temperature after cooling was 5-6 °C. In the case of the seeded experiments the mass of seeds was of about 2.5 % of the total solid dissolved in the vessel. Seeds were obtained after three successive crystallizations of the raw material. The same seeds were used for all the seeded experiments: crystals were in the form of short needles with fairly homogenous width (around 40-60 μm) and variable length (up to around 200 μm). At the end of the profile, the temperature was kept constant for few hours (until both FBRM and ATR-UV/Vis signals stabilized); after that, crystals were filtered and washed with acetone. CryPRINS was used to select the desired heating/cooling rate and to monitor the UV and FBRM signals during the experiments. In addition to the linear cooling experiments, three consecutive crystallizations of the same material were conducted using ethanol and water or pure water as solvents. Recrystallizing the same material more than once allows obtaining very pure crystals but the overall yield of the process is penalized. These three experiments were conducted to check the purity that could be obtained by using multiple steps of crystallization compared to a single linear cooling profile.

Table 11.2: Experiment conditions, slow and fast cooling of raw and crystallized material

Experiment	Solvent	Concentration (g/g solvent)	Type of material	Cooling rate (°C/min)	Seeding
1	Ethanol/water	0.118	Raw	-0.5 (fast cooling)	No
2	Ethanol/water	0.118	Raw	-0.1 (slow cooling)	No

3	Water	0.097	Crystallized (more than once)	-0.5 (fast cooling)	No
4	Water	0.097	Crystallized (more than once)	-0.1 (slow cooling)	No
5	Water	0.089	Raw material	-0.1 (slow cooling)	No
6	Water	0.106	Crystallized	-0.075(slower cooling)	No
7	Water	0.089	Raw material	-0.1 (slow cooling)	Yes
8	Water	0.097	Crystallized	-0.1 (slow cooling)	Yes
9	Ethanol/water	0.119	Raw	-1 (faster cooling)	No
10	Ethanol/water	0.119	Raw	-1 (faster cooling)	Yes
11	Ethanol/water	0.119	Raw	-0.5 (fast cooling)	No
12	Ethanol/water	0.119	Raw	-0.5 (fast cooling)	Yes
13	Ethanol/water	0.119	Raw	-0.1 (slow cooling)	No
14	Ethanol/water	0.119	Raw	-0.1 (slow cooling)	Yes
15	Ethanol/water	0.13	Crystallized	-1 (faster cooling)	No
16	Ethanol/water	0.13	Crystallized	-0.5 (fast cooling)	No(150 rpm)
17	Ethanol/water	0.13	Crystallized	-0.5(fast cooling)	No(240rpm)
18	Ethanol/water	0.13	Crystallized	-0.5 (fast cooling)	Yes
19	Ethanol/water	0.13	Crystallized	-0.1 (slow cooling)	No
20	Ethanol/water	0.115	Raw	-0.5	No
21	Ethanol/water	0.137	From exp. 20	-0.5	No
22	Water	0.082	From exp. 21	-0.5	No

11.2.3 HPLC analysis

The mobile phase for the HPLC analyses was prepared dissolving 7.4 g of $Na_2HPO_4 \cdot 2H_2O$ (HPLC purity grade, Fisher Scientific) in 740 mL of deionized water (from a Millipore Elix 5) and then adding 260 mL of methanol (Fisher Scientific). The solution pH was adjusted to 3.5 using H_3PO_4 (Fisons analytical reagents). The solid samples were dissolved in purified water (concentration of about 1 mg/mL). For the detection of the sample constituents the UV wavelength at 351 nm was used. The flow rate applied was 0.8 mL/min for a total running time of 40 min for each sample. The temperature of the column was kept constant at 35 °C and the injection size was 20 μL. The type of column used was an Analytical Column Waters Spherisorb® 5 μm C8 4.6×250 mm. The main peak at about 14 min corresponds to cyanocobalamin while the other peaks are byproducts (50-carboxyl cyanocobalamin, 34-mehil cobalamin, 8-Epi- cyanocobalamin, 7β,8β-cyanocobalamin lactate) and other unspecified impurities. All samples were analyzed at least twice and purity was calculated as the average relative area of the cyanocobalamin peak.

11.2.4 Principal component analysis on Raman spectroscopic data

A principal components analysis (PCA) was performed over Raman spectroscopic data of vitamin B12 in order to determine a relation between the purity of the analyzed crystals and their Raman spectra. Matlab 2013a was used for the calculation of the principal component scores (*pca* function). Details of the PCA calculation can be found in Chapter 2 of this thesis.

11.3 Results and discussion

11.3.1 Linear cooling experiments

Simple linear cooling was applied to the raw and recrystallized vitamin B12 and the results were studied using FBRM and images from an optical microscope. The crystal size distribution (CSD) was found to be strongly affected by the purity of the material used and the cooling rate. Usually large crystals and a narrow crystal size distribution are preferred because they facilitate the downstream operations (such as filtration, washing and milling). For this reason a good quality CSD is characterized by large crystals of similar size. The solvent used did not have a significant effect on the CSD but it affected the final purity of the crystals. The effect of seeding was also analyzed and it was found that a slightly purer

material can be obtained at the end of the crystallization using purified seed. Figure 11.2 shows the results of experiment 1 and experiment 2 described in Table 11.2, in which raw vitamin B12 was crystallized from an ethanol/water mixture at two different cooling rates (-0.5 and -0.1 °C/min, fast and slow cooling). From the microscopic images of crystals at the end of the two experiments (see Figure 11.2a and Figure 11.2b) it can be noticed that in both cases the size distributions look very broad with both small and large crystals; but a considerably larger size is clearly generated by the slow cooling shown in Figure 11.2b. This behaviour is similar to what normally happens for common pharmaceuticals such as paracetamol (Saleemi et al. 2012a; Saleemi et al. 2012; Abu Bakar et al. 2009). In general, during a fast cooling experiment, nucleation happens at high superaturation generating a large amount of small nuclei while in a slow cooling experiment, few nuclei are nucleated at low supersation.

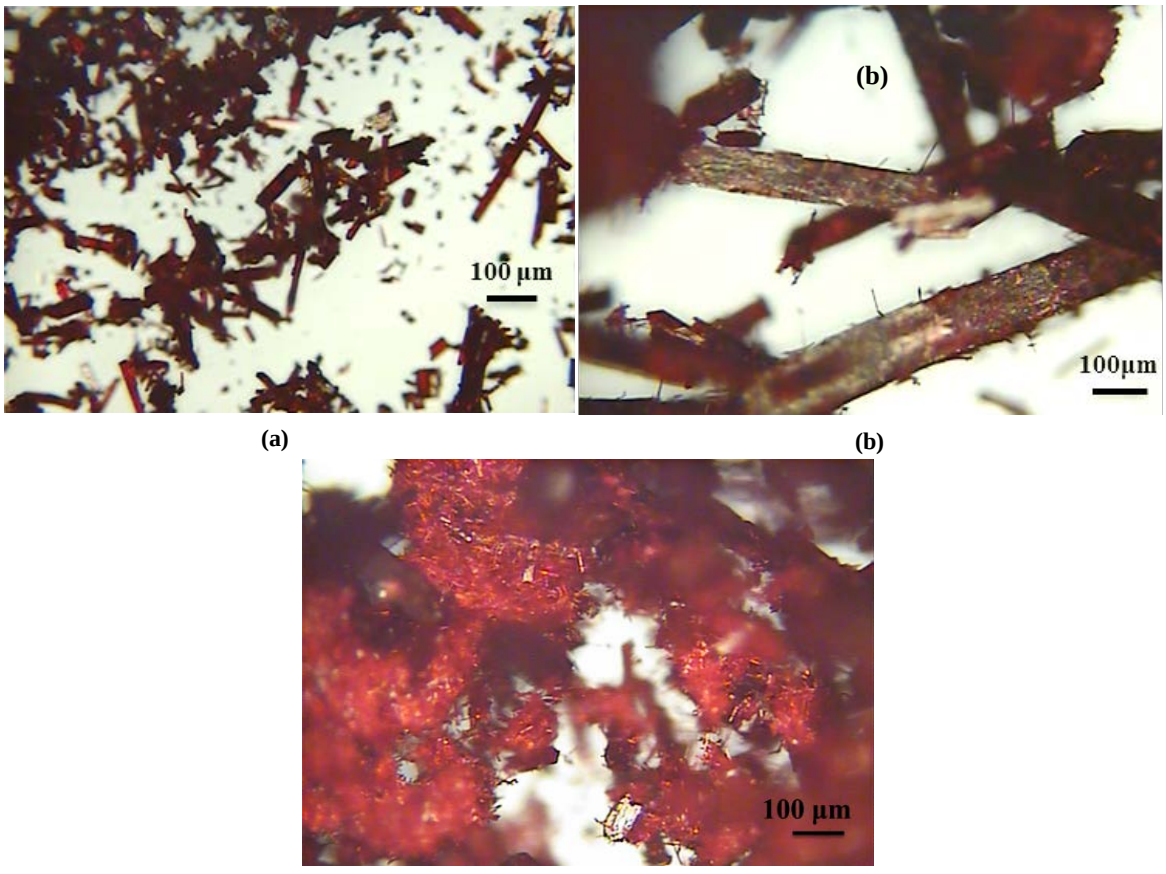

Figure 11.2: (a) Microscope image of the crystals at the end of experiment 1 (fast cooling) (b) Microscope image of the bigger crystals at the end of experiment 2 (slow cooling) (c) Microscope image of the smaller crystals at the end of the experiment 2.

However, for paracetamol, a fast cooling generates a high number of total counts from the FBRM due to the large number of nuclei generated at high supersaturation. In the case of Vitamin B12 the trend seems to be the opposite, as shown in Figure 11.3a and b.

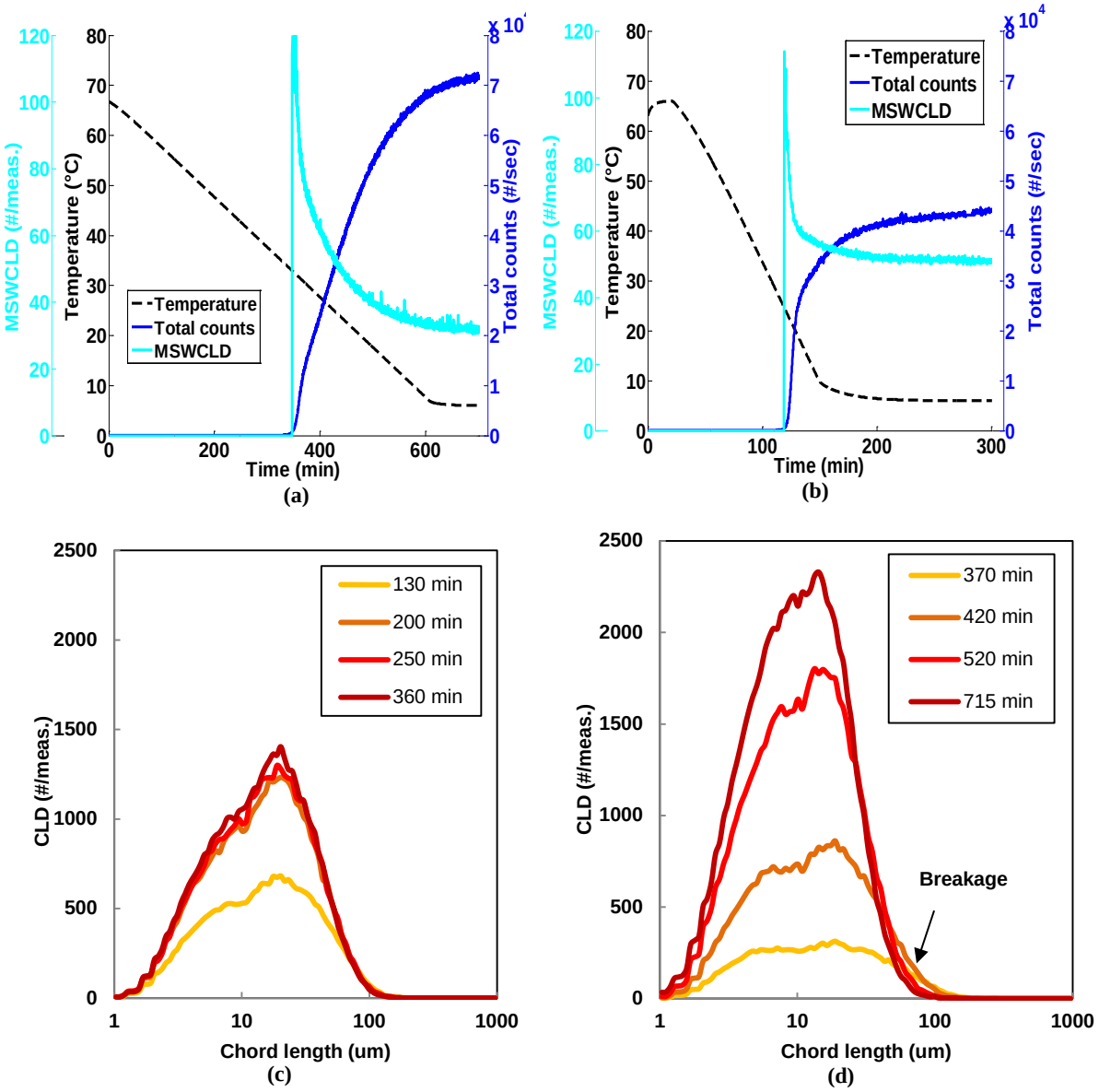

Figure 11.3: (a) Experiment 1: fast cooling of raw material in water and ethanol, -0.5°C/min. The graph shows the total counts per measurement and the mean of the square weighted chord length distribution (MSWCLD) from the FBRM (b) Experiment 2: slow cooling of raw material in water and ethanol, -0.1°C/min. The graph shows the total counts per measurement and the mean of the square weighted chord length distribution (MSWCLD) from the FBRM (c) Experiment 1: chord length distribution (CLD) for the fast cooling experiment (d) Experiment 2: chord length distribution (CLD) for the slow cooling experiment.

In experiment 1 (Figure 11.3a) when slow cooling was used, the number of counts was lower than in experiment 2 (Figure 11.3b) which was conduced at a fast cooling rate. Furthermore, the images from the microscope seem to contrast with the data from FBRM data since, clearly less and bigger particles were generated using slow cooling (Figure 11.2b) compared to fast cooling (Figure 11.2a). Additionally, the final mean of the square weighted chord length distribution is higher for the fast cooling rate (Figure 11.3a) than the slow one (Figure 11.3b). This discrepancy between images and FBRM data is related to the needle shape of the vitamin B12 crystals. As the particles grow in length, the shorter size of the crystals is counted by the FBRM more times than the longer giving the erroneous larger number of counts for small crystal size present in the vessel. A similar behavior for this probe was observed by Leyssens et al. for a small needle-like molecule prodrug antagonist called CDP323-2 (2011). The longer the crystals are, the higher is the value of the total counts recorded by FBRM; and that is the reason why slow cooling of raw vitamin B12 generated a higher value of the total counts than fast cooling (70,600 #/meas. in the slow cooling against 44,000 #/meas. as shown in Figure11.3 a and b). However, considering the large amount of small crystals present at the end of both experiments (in particular see Figure 11.2a for experiment 1 and Figure 11.2c for experiment 3), it is clear that secondary nucleation prevails on growth for raw vitamin B12. This can be explained by the fact that the presence of impurities inhibits growth, and supersaturation is used mainly to nucleate new small crystals. Some breakage is also present in the slow cooling after 400 min as shown in the CLD distribution of Figure 11.3d, where a reduction in the number of larger particles can be observed. Breakage of crystals also contributed to the higher number of counts in the case of slow cooling. Figure 11.4a and c show the FBRM and UV data for fast and slow cooling crystallization of a purified solution of vitamin B12 (experiment 3 and 4 of Table 11.2). The use of recrystallized material with fewer impurities reduced considerably both primary and secondary nucleation during the cooling phase and promoted growth of the existing crystals. Figure 11.5b and d show the microscopic images of the resulting crystals; the crystal size distribution is narrower compared to experiment 1 and 2 and crystals are considerably larger with the maximum total counts that reaches only 5,200 #/meas. in the fast cooling experiment and 26,900 #/meas. for the slow cooling. The effect of the shape of the crystals on the FBRM data is clearer in these two experiments because of the absence of breakage or secondary nucleation; crystals in Figure 11.5d are clearly longer than the ones shown in

Figure 11.5b and the CLD (Figure 11.6a and b) present a bimodal shape with a growing peak at low sizes due to the increasing counts of the shorter size of the crystals.

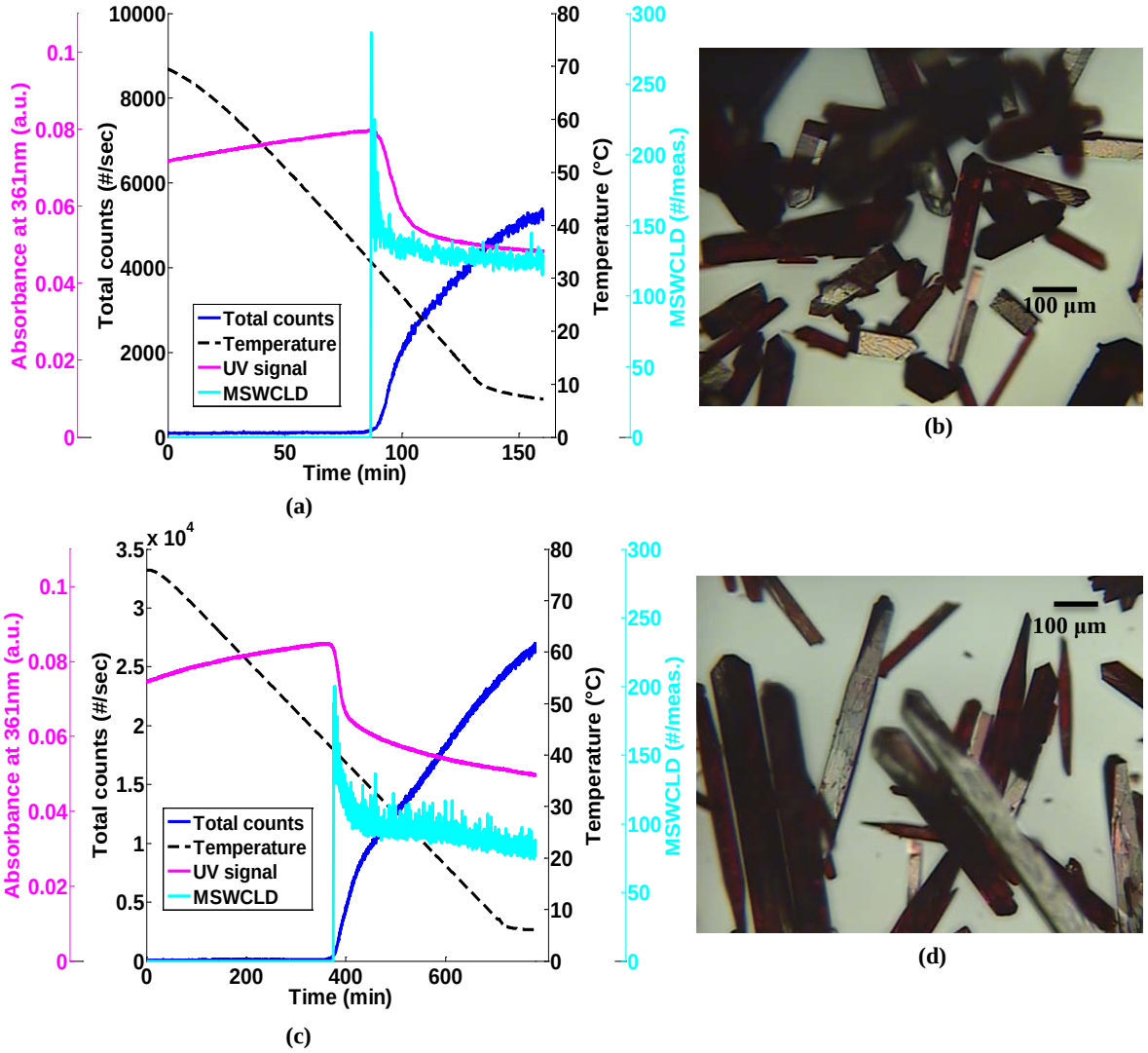

Figure 11.4: Absorbance value at 361nm, Total counts from FBRM and mean of the square weighted chord length distribution (MSWCLD) for (a) Experiment 3: fast cooling and crystallization of purified material dissolved in water (b) Experiment 3: microscopic image of the final crystals for the fast cooling experiment in water (c) Experiment 4: slow cooling and crystallization of purified material dissolved in water (d) Experiment 4: microscopic image of the final crystals for the slow cooling experiment in water.

It is clear that growth of vitamin B12 is strongly inhibited by impurities and very broad crystal size distributions are generated by secondary nucleation and breakage. Additionally, in some cases, multiple nucleation events can happen as shown in Figure 11.6b, c and d,

which is also a clear indication of growth inhibited crystallization processes in the presence of impurities.

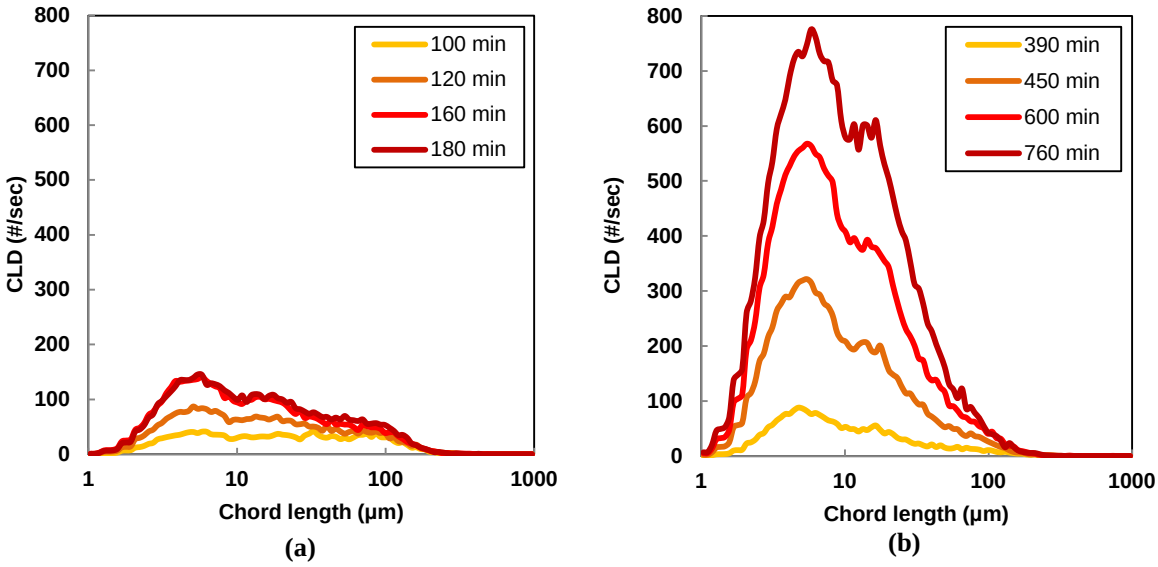

Figure 11.5: (a) Experiment 3: chord length distribution (CLD) during the fast cooling experiment in water with purified material (b) Experiment 4: chord length distribution (CLD) during the slow cooling experiment in water with purified material.

Figure 11.6a shows the results for experiment 5 (Table 11.2) where vitamin B12 nucleated and grew throughout the entire cooling period. Figure 11.6b, c and d instead, show cases in which a second major nucleation event happened during the cooling phase. The UV signal dropped suddenly during the second nucleation and the counts increased at the same time. This phenomenon appeared with both raw and recrystallized material, for seeded and unseeded experiments and for both the solvents used. During these experiments growth was so inhibited that supersaturation accumulated during the cooling until it reached a level at which a second major nucleation event could happen. In these cases the final CLD is very broad and many small particles are present as a result of this double nucleation as shown in Figure 11.7 (for experiment 7).

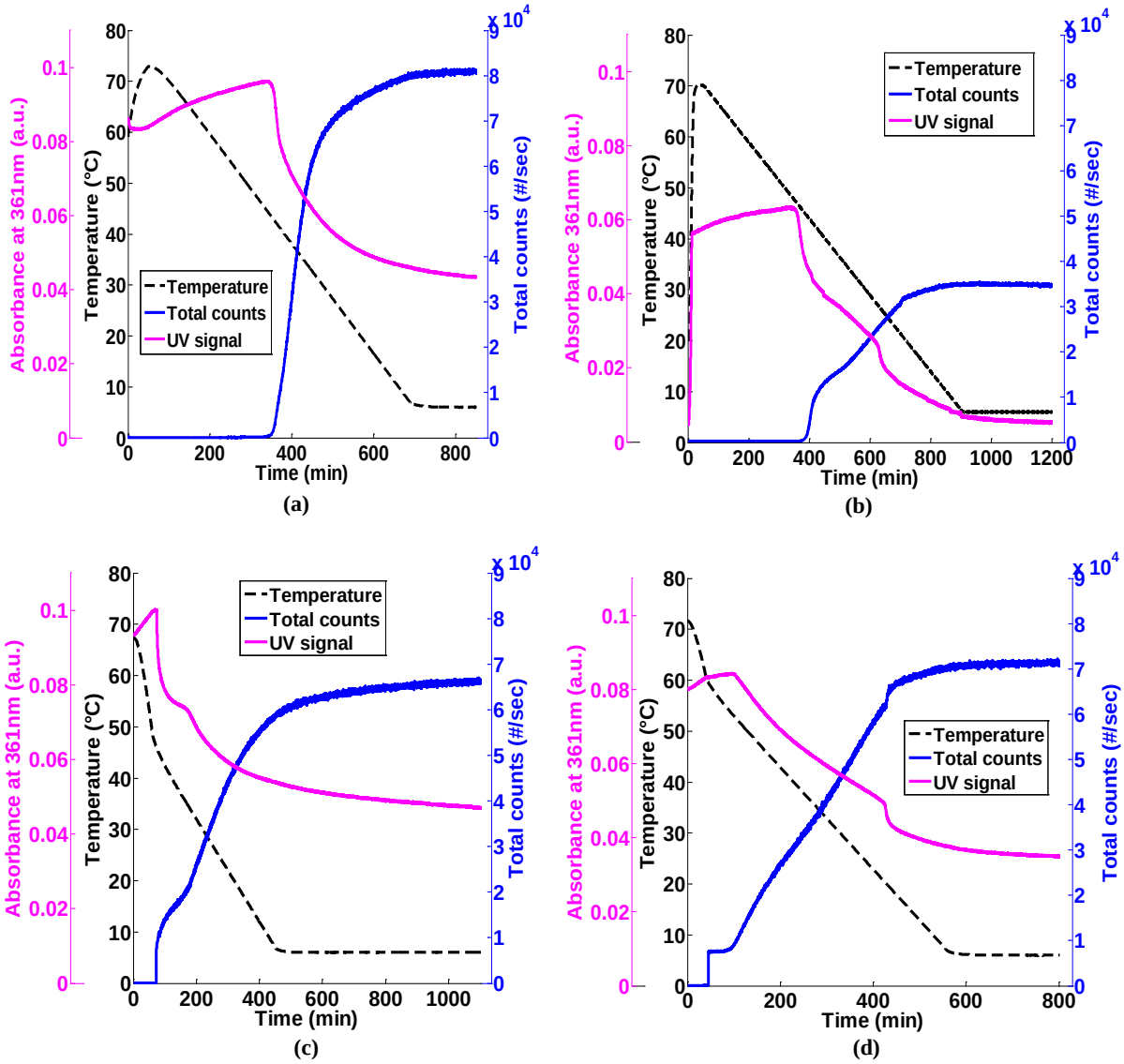

Figure 11.6: (a) Experiment 5: slow cooling -0.1°C/min of raw material. Total counts per measurement from FBRM and absorbance from ATR-UV/Vis. (b) Experiment 6: slow cooling -0.075°C/min of recrystallized material. Total counts per second from FBRM (Loughborough University) and UV absorbance. (c) Experiment 7: seeded and slow cooling of raw material in water (-0.1°C/min) (d) Experiment 8: seeded and slow cooling of recrystallized material in water (-0.1°C/min). Total counts per measurement from FBRM and absorbance from ATR-UV/Vis.

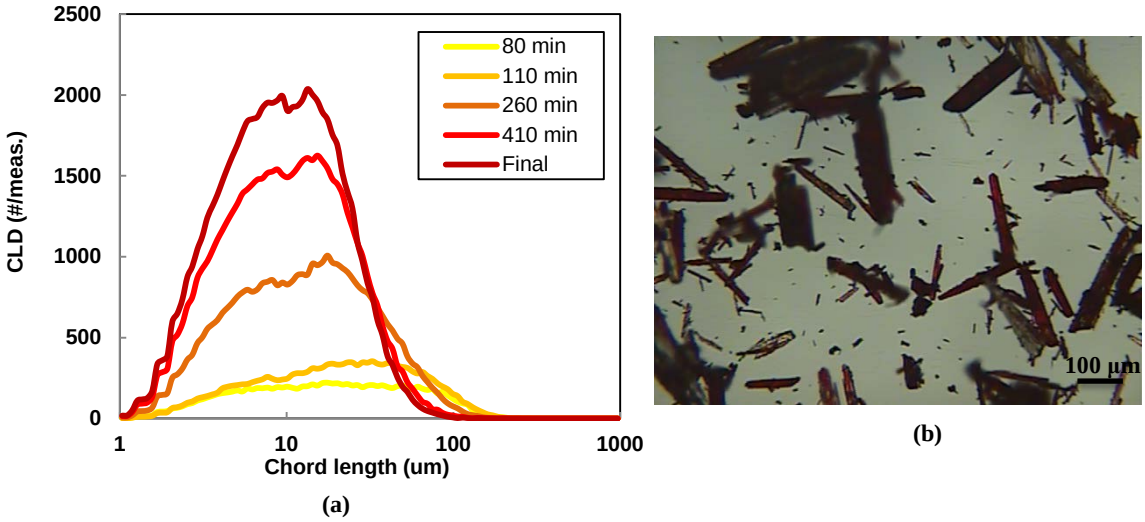

(a) (b)

Figure 11.7: (a) Chord length distribution (CLD) in the seeded and slow cooling of raw material in water (Experiment 7) (b) Microscopic image of the final crystals for the seeded and slow cooling of raw material in water (Experiment 7).

11.3.2 Purity analysis using HPLC and Raman spectroscopy

A first qualitative screening of both the raw material and the crystals obtained by consecutive crystallizations (with increasing purity as shown in Table 11.3) was performed using Raman microscopy. The inert material filtered during the crystallizations was also analysed. Figure 11.8a shows the Raman spectra of raw and filtered material; a strong fluorescence, due to impurities can be noticed (high intensity and no defined peaks). It is interesting to observe that just the filtration of the hot solution eliminates part of the fluorescent material. A loss of fluorescence due to less impurity can also be noticed in the samples of the consecutive crystallizations (Figure 11.8b).

Table 11.3: HPLC results for selected experiments performed

Sample	Purity (%)	Improvement in purity (%)	Solvent used	Material used	Cooling rate (°C/min)	Seeded
Raw material	93.11	0	n.a.	n.a.	n.a.	n.a.

First crystallization	96.14	3.03	n.a.	n.a.	n.a.	n.a.
Second crystallization	97.29	1.16	n.a.	n.a.	n.a.	n.a.
Third crystallization	98.03	0.74	n.a.	n.a.	n.a.	n.a.
LC experiment 8	97.54	1.24	Water	Crystallized	-0.1	Yes
LC experiment 9	96.35	3.24	Ethanol/water	Raw	-1	No
LC experiment 10	96.28	3.17	Ethanol/water	Raw	-1	Yes
LC experiment 11	96.28	3.17	Ethanol/water	Raw	-0.5	No
LC experiment 12	96.72	3.61	Ethanol/water	Raw	-0.5	Yes
LC experiment 13	96.51	3.40	Ethanol/water	Raw	-0.1	No
LC experiment 14	**96.76**	**3.65**	**Ethanol/water**	**Raw**	**-0.1**	**Yes**
LC experiment 15	97.66	0.94	Ethanol/water	Crystallized	-1	No
LC experiment 16	97.70	0.98	Ethanol/water	Crystallized	-0.5	No
LC experiment 17	97.72	1.00	Ethanol/water	Crystallized	-0.5	No
LC experiment 18	97.95	1.23	Ethanol/water	Crystallized	-0.5	Yes
LC experiment 19	97.77	1.05	Ethanol/water	Crystallized	-0.1	No
LC experiment 20	96.14	3.03	Ethanol/Water	Raw	-0.5	No
LC experiment 21	97.29	1.16	Ethanol/Water	Crystallized once	-0.5	No
LC experiment 22	98.03	0.74	Water	Crystallized twice	-0.5	No

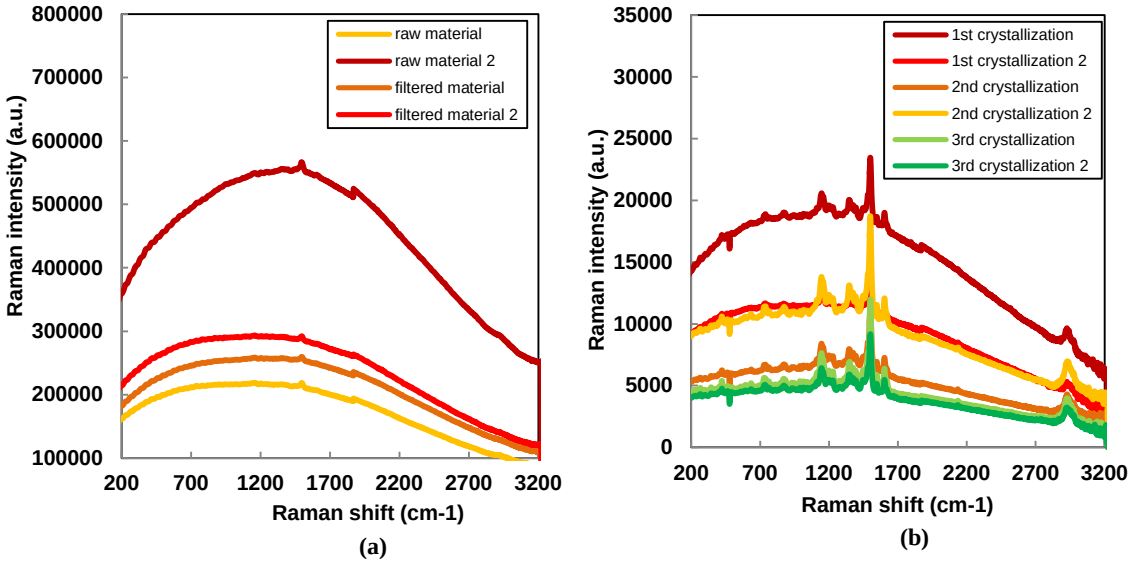

Figure 11.8: (a) Raman spectra of the raw material donated and the particles filtered at high temperature (b) Raman spectra of the crystals from the three consecutive crystallizations. A loss in fluorescence can be noticed.

The number and position of the peaks is the same for all the samples but they tend to become broader and less intense as fluorescence (and, therefore impurity) increases. In order to have some quantitative information from Raman spectroscopy a principal component analysis was performed over the Raman spectra of the recrystallized material, the raw material and the filtered one. Figure 11.9a shows the score of principal component PC2 plotted versus the score of principal component PC1. The raw and filtered material points are isolated and very far from the crystallized samples because of their high impurity content. Figure 11.9b shows only the crystallized samples: a clear trend of the scores as a function of purity is present. This example provides an illustration for the non-conventional use of Raman spectroscopy for monitoring low concentration of impurities based on fluoresce. While fluorescence is in general undesirable in Raman spectroscopy, since it makes the interpretation of the significant peaks difficult, monitoring the amount of fluorescence in the Raman spectra can serve as a method of detecting the existence and changes in impurity levels in the case of fluorescent impurities.

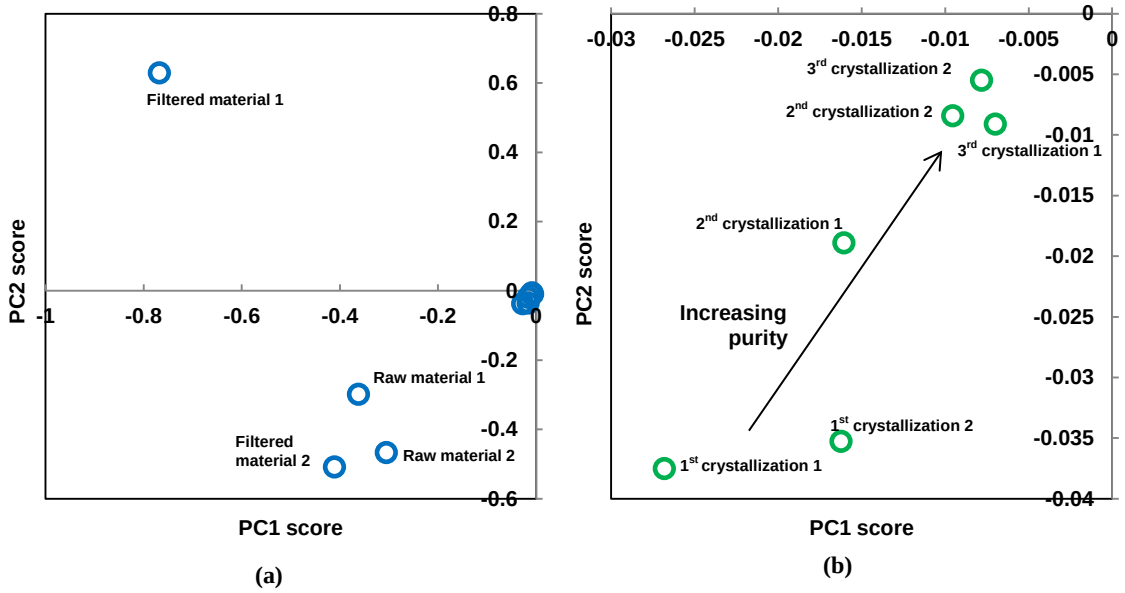

Figure 11.9: (a) Score of the second principal component (PC2) plotted against the first principal component (PC1) for all the samples analysed. (b) Score of the second principal component (PC2) plotted against the first principal component (PC1) for the crystallized samples.

The loss of impurity during the consecutive crystallizations also considerably improved the size of the crystals as shown in Figure 11.10. The raw material showed in Figure 11.10a is highly fluorescent and amorphous; particles are very small and hygroscopic and the colour is intense red. Crystalline vitamin B12 is darker as shown in Figure 11.10b to d. The mean size of the crystals increases during the consecutive crystallization as a result of less inhibited growth.

The results of HPLC analyses of the samples from selected experiments out of those performed are shown in Table 11.3. A higher purity can be reached if slow cooling rates are applied and seeding also helps in increasing the purification efficiency. The largest increase in purity was reached using raw material in an ethanol/water mixture with seeding and slow cooling (linear cooling experiment 14, increase in purity of 3.65 %). The second crystallizations (using purified material) as expected present a lower increase in purity; however, even for this set of experiments, slow cooling and seeding helped reaching a relatively higher purity. The effect of the solvent on the final crystal size distribution is negligible but choosing the suitable solvent seems to help increasing the purity of the

product. It also seems not to affect purification efficiency since the final purity of similar experiments in different solvents is very close.

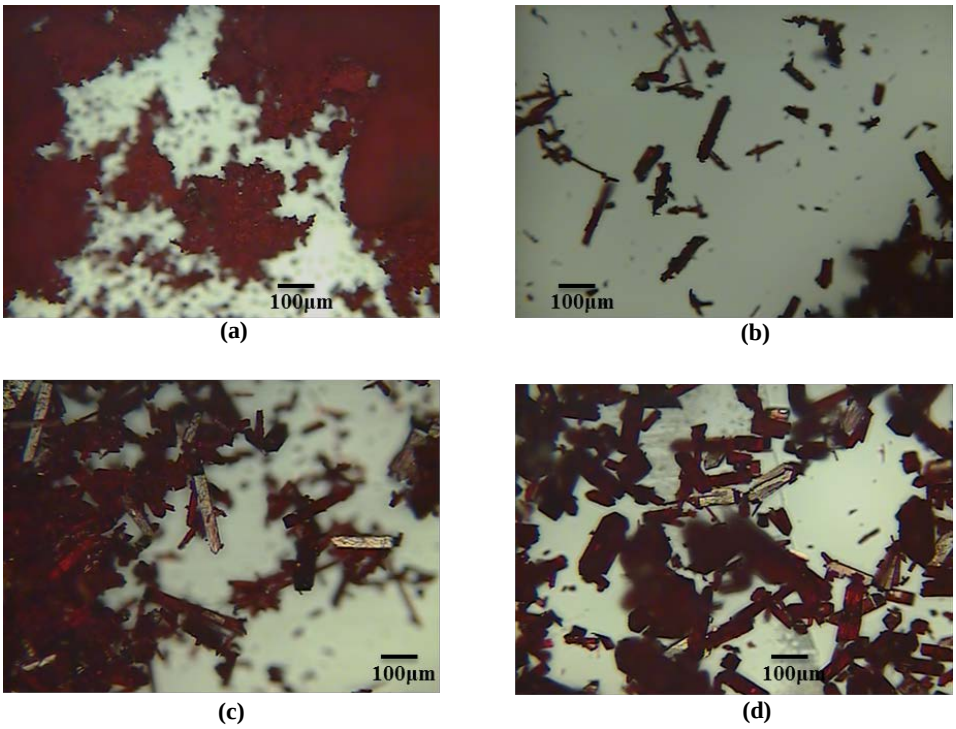

Figure 11.10: microscopic images of (a) Raw vitamin B12 from fermentation (b) Crystal obtained after the first crystallization (c) Crystal at the end of the second crystallization (d) Crystals after the third crystallization.

11.4 Conclusions

A set of PAT tools was used to study the crystallization in the presence of impurities of a small biomolecule produced by fermentation (vitamin B12). Materials produced by biosynthesis often contain a high amount of impurities that can significantly reduce the quality of the final crystals in term of size distribution. Multiple successive recrystallizations of the same material can help eliminating impurities and reaching a better crystal size distribution, but they also contribute to decrease the yield. Using PAT tools can help understanding the characteristics of the studied compound and developing a correct crystallization strategy to improve crystal size and purity of the final product.

It was found that impurities strongly affect the growth rate, promoting nucleation and, in some cases, generating multiple nucleation events during the cooling profile. The final crystal size distribution for these cases was found to be very broad, with very large crystals

together with significant amounts of fines. Slow cooling of very impure material increases the probability of multiple nucleation events and, therefore, leads to a broad crystal size distribution. However, slow cooling was found to generate more pure crystals compared to fast cooling. The best quality of the crystals, in terms of size, was reached using already crystallized material to prepare the solution and slow cooling rates. Seeding was also found to help in increasing the purity of the final crystal while a change in the solvent composition did not largely affect purity or final CSD. The needle shape of the vitamin B12 crystals also had to be considered before interpreting the FBRM results. The growth of the long size of the needles generates an increase in the FBRM total counts that can be confused with nucleation. An analysis of the crystals with the optical microscope was necessary to interpret the counts and chord length distribution recorded by the FBRM. Monitoring the level of fluorescence due to impurities in the Raman spectrum, can serve as a method of detecting changes in the impurity concentrations in the crystalized products.

12 Application of PAT-based feedback control strategies to improve purity and size distribution in biopharmaceutical crystallization

Several PAT-based feedback control strategies are tested in this chapter to improve purity and crystal size distribution of impure vitamin B12. Direct nucleation control, simple slow linear cooling, temperature cycling and supersaturation control were analyzed.

12.1 Introduction

Purity is a critical quality attribute for both pharmaceutical and biopharmaceutical products. The presence of impurities (solvents, salts or byproducts of the synthetic path) in drugs can cause a reduction of their effectiveness or can even be toxic for the patients. Biopharmaceuticals are produced by biological processes which are difficult to control. Therefore the amount of impurities that has to be removed can be significantly higher than in the case of synthetic pharmaceuticals. In this chapter process analytical technology (PAT) tools and different feedback control strategies (T-control, direct nucleation control and supersaturation control) were tested for the crystallization of a biopharmaceutical product. UV/Vis spectroscopy, focused beam reflectance measurement (FBRM) combined with CryPRINS were used to improve the crystal size distribution and purity of crystallized vitamin B12. The different feedback control strategies were compared to classical crystallization techniques in terms of purity of the final crystal and quality of the crystal size distribution and it is shown that using suitable crystallization feedback control strategies, the purity and quality of crystals can be improved.

The fragility of the vitamin B12 molecule and the presence of impurities, together with its needle-like morphology made the implementation of PAT based control strategies particularly challenging. A direct nucleation control based on FBRM data and a calibration-free supersaturation control using ATR-UV/Vis were implemented on the system and compared to specific T-control strategies (for example temperature cycling). In the direct nucleation feedback control strategy the number of counts obtained from the FBRM is kept constant by heating and cooling steps. If the counts are higher than the desired setpoint range, the controller reacts by increasing the temperature in the crystallizer and dissolving the smaller particles. If the number of counts is too low instead, the system

is cooled down promoting growth or maybe nucleation. This strategy does not require any calibration and was found to be effective in obtaining large crystals of paracetamol (Saleemi et al. 2012b; Saleemi et al. 2012a; Saleemi 2011), glycine (Abu Bakar et al. 2009) as well as in enhancing the crystalline properties of a cardiovascular API (Saleemi et al. 2012). Temperature cycling (with no feedback control) was also implemented in order to check its efficacy. This technique was successfully used to control both size and polymorphic form of sulfathiazole (Abu Bakar et al. 2010; Abu Bakar 2010; Abu Bakar et al. 2010) and to reduce liquid inclusion in the crystallization of cyclotrimethylene trinitramine (RDX) (Kim et al. 2011). Calibration based supersaturation control is now a common technique widely tested for different APIs; however, only few examples of calibration-free strategies are present in literature (Duffy et al. 2013; Barrett et al. 2010; Kee et al. 2009; Chew et al. 2007). A calibration-free supersaturation control approach is also implemented for the crystallization of vitamin B12 and the results are compared among all feedback control approaches. The results demonstrate the benefits of using PAT-based feedback control technologies in the crystallization of biopharmaceuticals to improve purity and crystal quality and achieve larger and more uniform size distribution.

12.2 Materials and equipment

Crude Vitamin B12 extracted from biofermentation was donated by Hebei Welcome Pharmaceutical Co., LTD (China). Ultrapure water was obtained via a Millipore ultra-pure water system while ethanol was purchased by Fisher Scientific. Pure water or solutions of water and ethanol (13.8% of ethanol v/v) were used as solvents for the experiments. Experiments were conducted at both Loughborough University and Purdue University with similar, but not exactly identical instruments. Two 500 mL glass jacketed vessels and the same Raman system were used (details of the instruments are reported in chapter 2 of this thesis). The supersaturation control and the temperature cycling experiments were performed at Loughborough University, UK, using the available ATR-UV/Vis, FBRM and thermoregulatory (described in Chapter 3 of this thesis). The data from the FBRM, ATR-UV/Vis and the Huber are transmitted in real-time to the CryPRINS software. The instrumentation at Purdue University consisted of a JULABO F25-ME thermoregulator, an FBRM G400 0.5-2000 μm (Mettler Toledo with iCFBRM software version 4.3) a Zeiss MCS621 UV/Vis spectrophotometer with UV-VIS 190-720nm Zeiss probe (Zeiss ProcessXplorer software version 1.3-Build 1.3.1.30). Direct nucleation control

experiments were all performed at Purdue University. The samples of vitamin B12 produced were analyzed using the Raman microscope and the HPLC available at Loughborough University.

12.3 Methodology

12.3.1 Slow linear cooling experiment

An unseeded slow cooling experiment was carried out over a solution of previously crystallized vitamin B12 (initial purity of the material was 96.3 %). The solution concentration was around 0.112 g/g solvent. Solids were introduced in the liquid at ambient temperature and then dissolved by heating up the solution to 70 °C. Because of the presence of some inert material, the hot solution was filtered and then kept at high temperature for 30 min in order to re-dissolve crystals that might have nucleated during the filtration. After that time the solution was cooled down at a rate of -0.075 °C/min.

12.3.2 Supersaturation control experiments

A calibration-free approach was used to perform the seeded supersaturation control experiments. The conditions of the performed experiments are shown in Table 12.1. In order to obtain quantitative information on its solubility, vitamin B12 was added to the solvent (pure water) at 5-6 °C and the temperature was slowly raised (+0.075 °C/min) to 70 °C. The saturation temperature of the solution was around 60 °C, so all the vitamin dissolved at the end of the temperature profile. Also, for this set of experiments the hot solution was filtered before starting the control profile, in order to remove the inert material present in the crude vitamin B12.

Table 12.1: Experimental conditions for the supersaturation control experiment

Experiment	Supersaturation set point (in UV signal)	Solvent	Type of material	Vitamin concentration (g/g solvent)
1	0.0025	Water	Raw	0.089
2	0.0025	Water	Raw	0.094
3	0.0024	Water	Raw	0.097
4	0.0022	Water	Crystallized	0.106
5	0.00195	Water	Crystallized	0.109
6	0.002	Water	Crystallized	0.112

ATR-UV/Vis spectra and their derivatives were recorded and a polynomial relation was found between the first derivative of the signal (*F*) at 350 nm (correlated with the vitamin concentration) and temperature (*T*). This correlation, $F = f(T)$, corresponds to an inferential solubility curve expressed as UV signal versus temperature, instead of the classical concentration versus temperature relationship, generally used in calibration-based supersaturation control. Both crude material and purified (vitamin B12 crystallized and washed with acetone once) were used for the experiments, and because of their difference in purity two solubility equations were measured:

$$F_{raw} = 2.48923 \cdot 10^{-8}T^3 - 5.01056 \cdot 10^{-8}T^2 - 2.70984 \cdot 10^{-5}T + 1.547812 \cdot 10^{-3} \quad (12.1)$$

$$F_{cryst} = 2.14232 \cdot 10^{-8}T^3 + 1.55857 \cdot 10^{-8}T^2 - 1.69056 \cdot 10^{-5}T + 1.44211 \cdot 10^{-3} \quad (12.2)$$

Equations (12.1) and (12.2) were implemented in the CryPRINS software and the experiments followed the procedure:

1) Crude vitamin B12 from fermentation or previously recrystallized was added to pure water (about 0.09 g/g water, corresponding to a saturation temperature of 60 °C);
2) The temperature was raised to 70 °C to allow complete dissolution of the solid and then the hot solution was filtered in order to eliminate insoluble material;
3) After filtration the temperature was kept constant at 70 °C for about half an hour and then the system was cooled down to about 58-57 °C;
4) Crystalline seeds were added in an amount of about 3% of the total solid mass and the supersaturation control option in CryPRINS was switched on;
5) The supersaturation setpoint was adjusted during the first minutes of control in order to guarantee the growth of the crystals.

The supersaturation setpoint is calculated as the difference between the desired UV signal at a given temperature and the value of the inferential solubility of vitamin B12 at that temperature. This value can be directly inserted in CryPRINS.

12.3.3 Direct nucleation control experiments

The direct nucleation control procedure was already described in detail by other authors (Saleemi et al. 2012a; Saleemi et al. 2012b; Abu Bakar et al. 2009). The technique is based

on the use of both FBRM and CryPRINS to keep the number of crystal counts/s in the vessel constant during the whole batch. One of the statistics (usually total counts/s) measured by the FBRM is sent to CryPRINS and temperature is decreased if the measured total counts/s is lower than the set point range, or increased if it is higher (crystals in excess are then redissolved). The parameters that have to be inserted in CryPRINS are the chosen statistics setpoint as well as the desired cooling and heating rate. Those parameters are usually system dependent and can be selected after few trials. In this work, for the DNC experiments, ethanol/water mixtures were used as solvents and the amount of solid used for each experiment is around 0.12 g/g solvent. The selected statistics was total counts and different setpoints were tried as shown in Table 12.2.

Table 12.2: Experimental conditions for the DNC experiments

Experiment	Set point (#/sec)	Solvent	Type of material	Heating/cooling rate (°C/min)
1	10000±1000	Ethanol/water	Raw	0.3/-0.3
2	30000±1000	Ethanol/water	Raw	0.2/-0.4

12.3.4 Temperature cycling experiments

Several experiments using different cooling/heating rates and number of cycles were performed. Both crude and recrystallized material were used to prepare the solution, while pure seeds were added (about 3 % of the total solute). The amplitude of every cycle was 7-9 °C and cycles converged towards a final temperature of 6 °C. Table 12.2 shows a list of the experiments performed and their most important parameters.

Table 12.3: Experimental conditions for the temperature cycling experiments

Experiment	Number of cycles	Solvent	Type of material	Vitamin concentration (g/g solvent)	Heating/cooling rate (°C/min)
1	13	Water	Raw	0.089	0.2/-0.2
2	17	Water	Raw	0.089	0.5/-0.5
3	13	Water	Raw	0.089	0.2/-0.5
4	12	Water	Crystallized	0.104	0.5/-0.5
5	13	Water	Crystallized	0.11	0.2/-0.2
6	18	Water	Crystallized	0.11	0.2/-0.5

12.3.5 HPLC analysis

The HPLC method was developed by the company who provided the material and then slightly changed for the available instrument. Details of the methods are discussed in Chapter 11.

12.4 Results and discussion

12.4.1 Slow cooling experiments

The results of the first slow cooling experiment are shown in Figure 12.1a, b and c. Despite the use of material that was already crystallized once (and therefore more pure than the raw) the presence of impurities determined a very broad crystal size distribution at the end of the profile, with few very big crystals together with many small ones (as shown in Figure 12.1c).

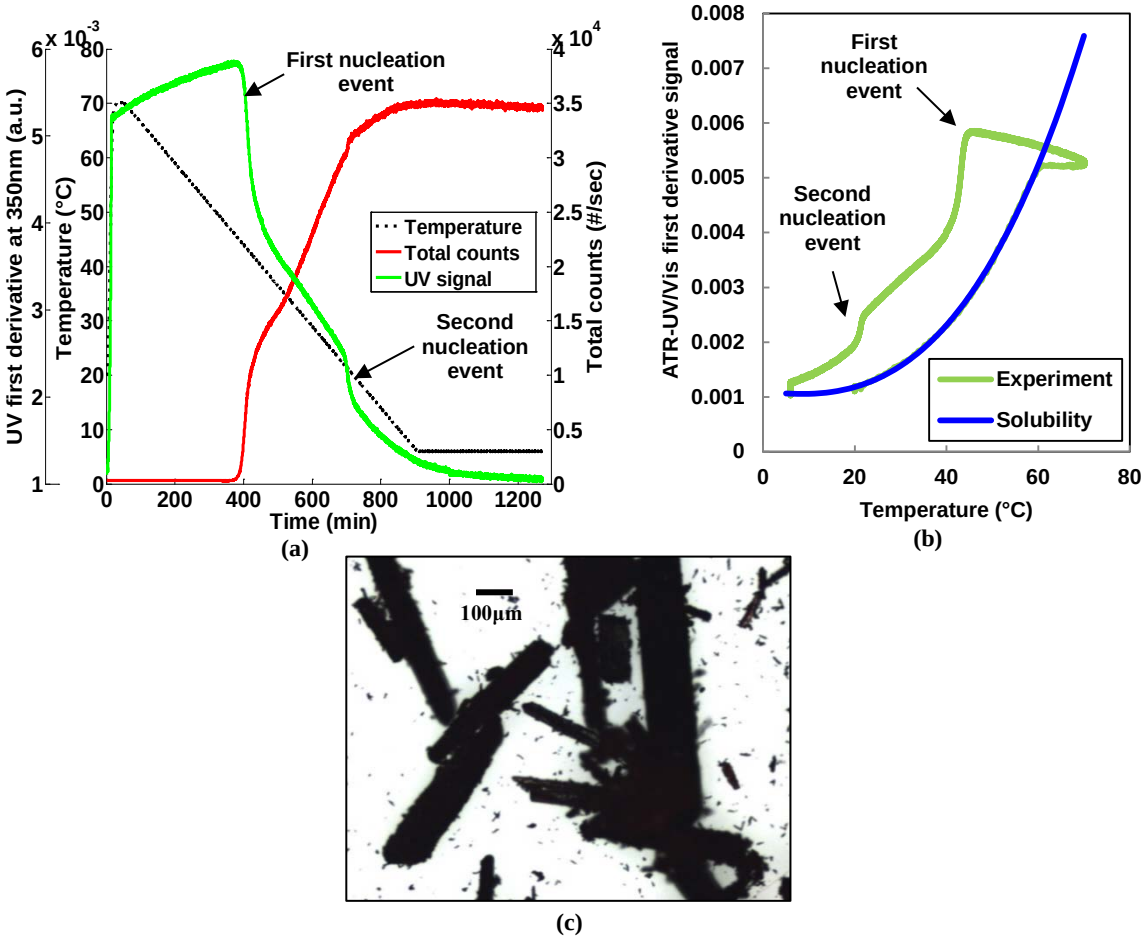

Figure 12.1: (a) UV/Vis first derivative at 350 nm, temperature and total counts/s plotted versus time in min for the slow cooling experiment; (b) Solubility of raw vitamin B12 expressed as UV derivative signal and values recorder during the SSC experiment; (c) Microscopic image of the crystals at the end of the profile.

The reason for the poor CSD is the presence of multiple nucleation events during the cooling as shown in Figure 12.1a and b. Because of the presence of impurities the growth of vitamin B12 crystals was so inhibited that supersaturation accumulated during the cooling until it reached a level at which a second nucleation event could occur. These multiple nucleation events are characteristic for systems in which growth is inhibited by nucleation (Fevotte and Fevotte 2010). In conclusion, although slow cooling is usually the simplest solution to get better CSD and improve purity it was proved to be unsuccessful for the studied compound. In order to avoid the development of high level of supersaturation that can cause multiple primary nucleation events feedback control strategies can be used. Supersaturation control could be a good solution since it can keep the level of supersaturation below the limit that triggers subsequent nucleation events. Also temperature cycling and direct nucleation control could potentially help in avoiding multiple primary nucleation events and/or eliminating the fines from the unwanted nucleation events.

12.4.2 Supersaturation control experiments

The first feedback strategy proposed to control the crystallization of vitamin B12 is supersaturation control (SSC). Because of the difficulty of getting solubility data and its variability due to impurities, a calibration-free supersaturation control (SSC) approach was used. Figure 12.2 shows the results for experiment 2 and 3 (see Table 12.1 for details of the experimental conditions). The solution was prepared from raw material and purified seed was used. Because of the impurities, the supersaturation setpoint (which is the difference between the measured UV signal and the solubility of vitamin B12 expressed as UV signal) needed to be quite high in order to enable growth of the seeds: the steps in the temperature profiles on Figure 12.2a and b are due to manual changes in the setpoint just after seeding (see Figure 12.2c and d). When small changes in the FBRM counts or in the UV signal were noticed the setpoint was not further modified. The desired supersaturation profile was followed for about 2.5 hours in experiment 2 and for about 3.5 hours in experiment 3 (Figure 12.2c and d). After that, supersaturation was depleted quickly probably because of the secondary nucleation of new crystals (also confirmed by the sudden increase in the FBRM total counts/s) and the control mechanism stopped working since the temperature decrease could not keep up with such fast supersaturation depletion. The apparent increase in the inferential solubility of the raw vitamin B12 (Figure 12.2e) is

due to the temperature effect on the UV signal: there is an inverse proportionality between the UV signal and temperature at constant concentration.

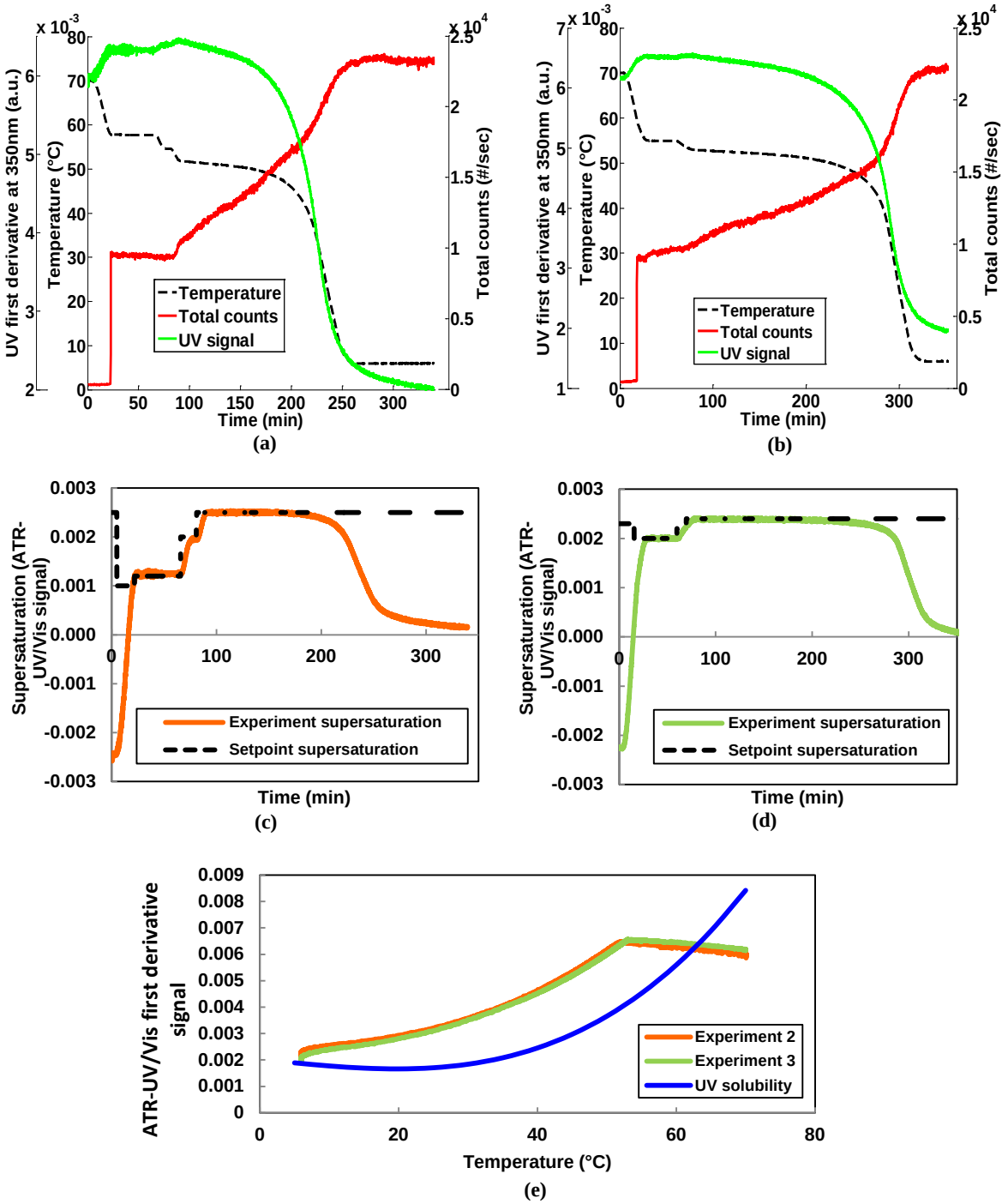

Figure 12.2: Experiment 2 and 3: supersaturation control of raw material in water. (a) UV/Vis first derivative at 350 nm, temperature and total counts/s plotted versus time for experiment 2; (b) UV/Vis first derivative at 350 nm, temperature and total counts/s plotted versus time for experiment 3; (c) Setpoint and experimental supersaturation during experiment expressed as ATR-UV/Vis signal for experiment 2; (d) Setpoint and experimental supersaturation during experiment expressed as ATR-UV/Vis signal for experiment 3; (e) Solubility of recrystallized vitamin B12 expressed as UV derivative signal and values recorder during the SSC experiment 2 and 3.

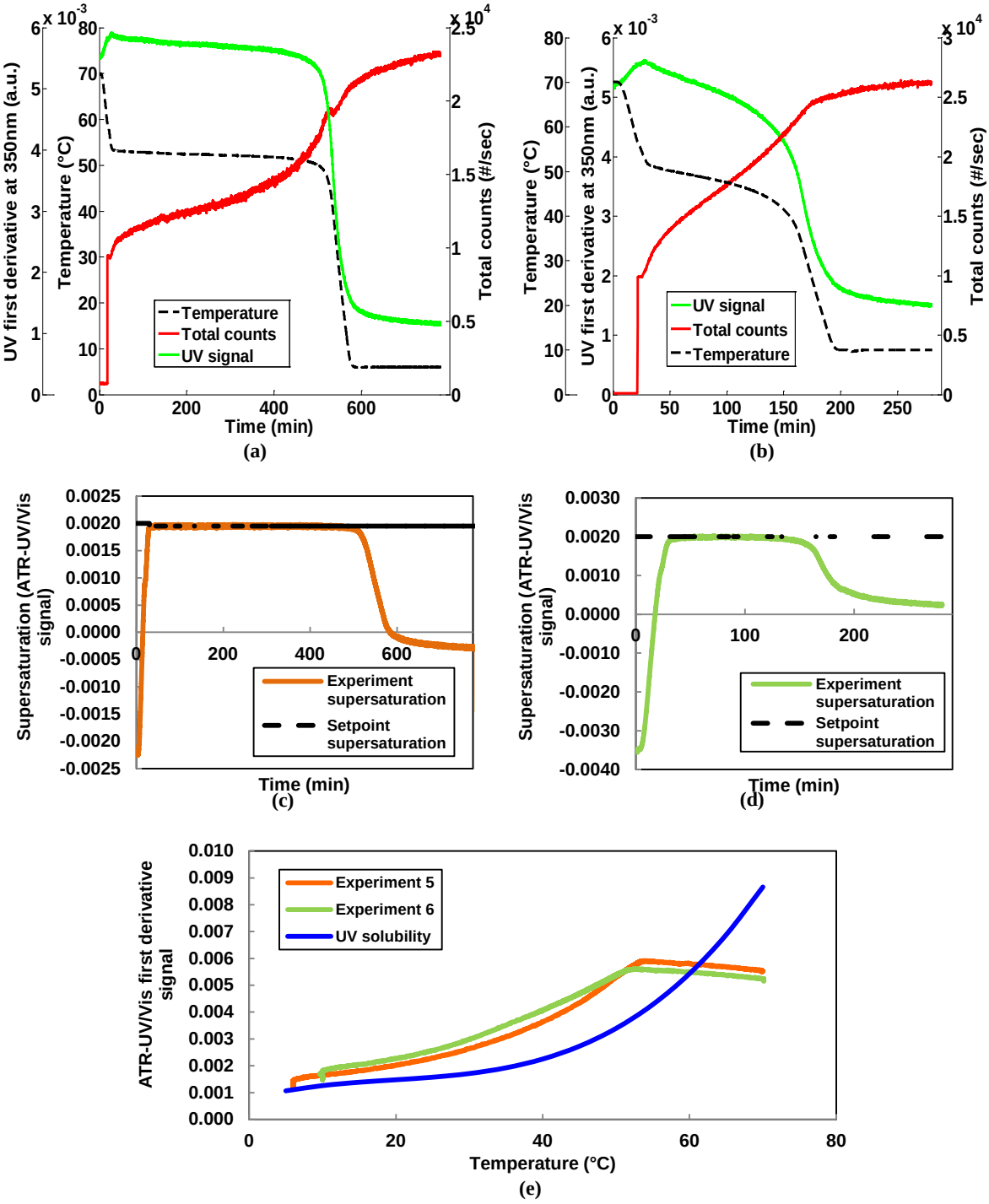

Figure 12.3: Experiment 5 and 6: supersaturation control of raw material in water. (a) UV/Vis first derivative at 350 nm, temperature and total counts/s plotted versus time for experiment 5; (b) UV/Vis first derivative at 350 nm, temperature and total counts/s plotted versus time for experiment 6; (c) Setpoint and experimental supersaturation during experiment expressed as ATR-UV/Vis signal for experiment 5; (d) Setpoint and experimental supersaturation during experiment expressed as ATR-UV/Vis signal for experiment 6; (e) Solubility of recrystallized vitamin B12 expressed as UV derivative signal and values recorder during the SSC experiment 5 and 6.

That effect is more significant at low concentration where the gradient of the solubility versus temperature is usually low and the decrease in signal due to the temperature prevails on its increase due to the increase in concentration due to dissolution. A very quick drop in concentration was also observed in experiment 5 (solution prepared with recrystallized material, results shown in Figure 12.3a) while a smoother temperature profile can be noticed for experiment 6 (shown in Figure 12.3). The supersaturation profile was followed for about 8 hrs in experiment 5 while experiment 6 was quite short and lasted only about 2 hrs (this is probably due to the slightly higher supersaturation setpoint chosen for experiment 6 and the fact that the experiment was stopped when the temperature reached 10 °C instead of 6 °C). Figure 12.4 shows microscopic images of the final crystals for the four experiments performed: the size distribution seems to be quite similar for all experiments with a slightly higher amount of small crystals for experiments 2 and 3 (performed with raw material).

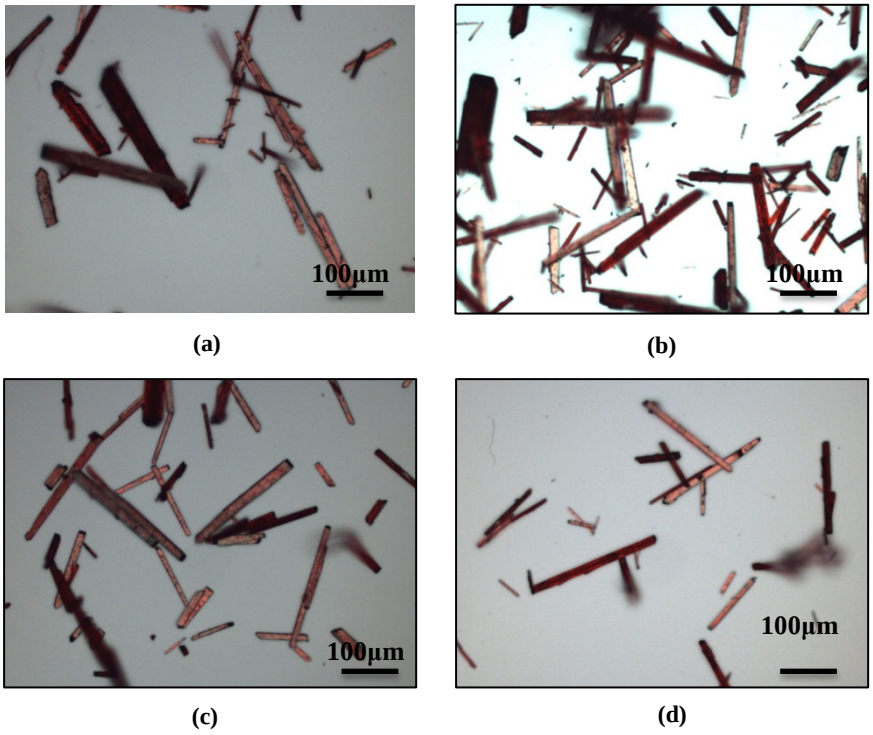

Figure 12.4: Microscopic images of final crystals for (a) Experiment 2 (b) Experiment 3 (c) Experiment 5 (d) Experiment 6.

FBRM data also confirmed the similarity between the CLD at the end of all the experiments (see Figure 12.5). It is also worth noticing the absence of breakage for all of the SSC experiments performed. In conclusion, supersaturation control gave a better CSD

compared to the slow cooling experiment even when raw material was used to prepare the solution. That suggests that SSC could be a feasible solution for the crystallization of vitamin B12, allowing a better size distribution of the final product. It is worth noticing that in all the experiments the temperature profile resulting from applying the supersaturation control could be easily approximated with two consecutive linear cooling profiles with different slopes.

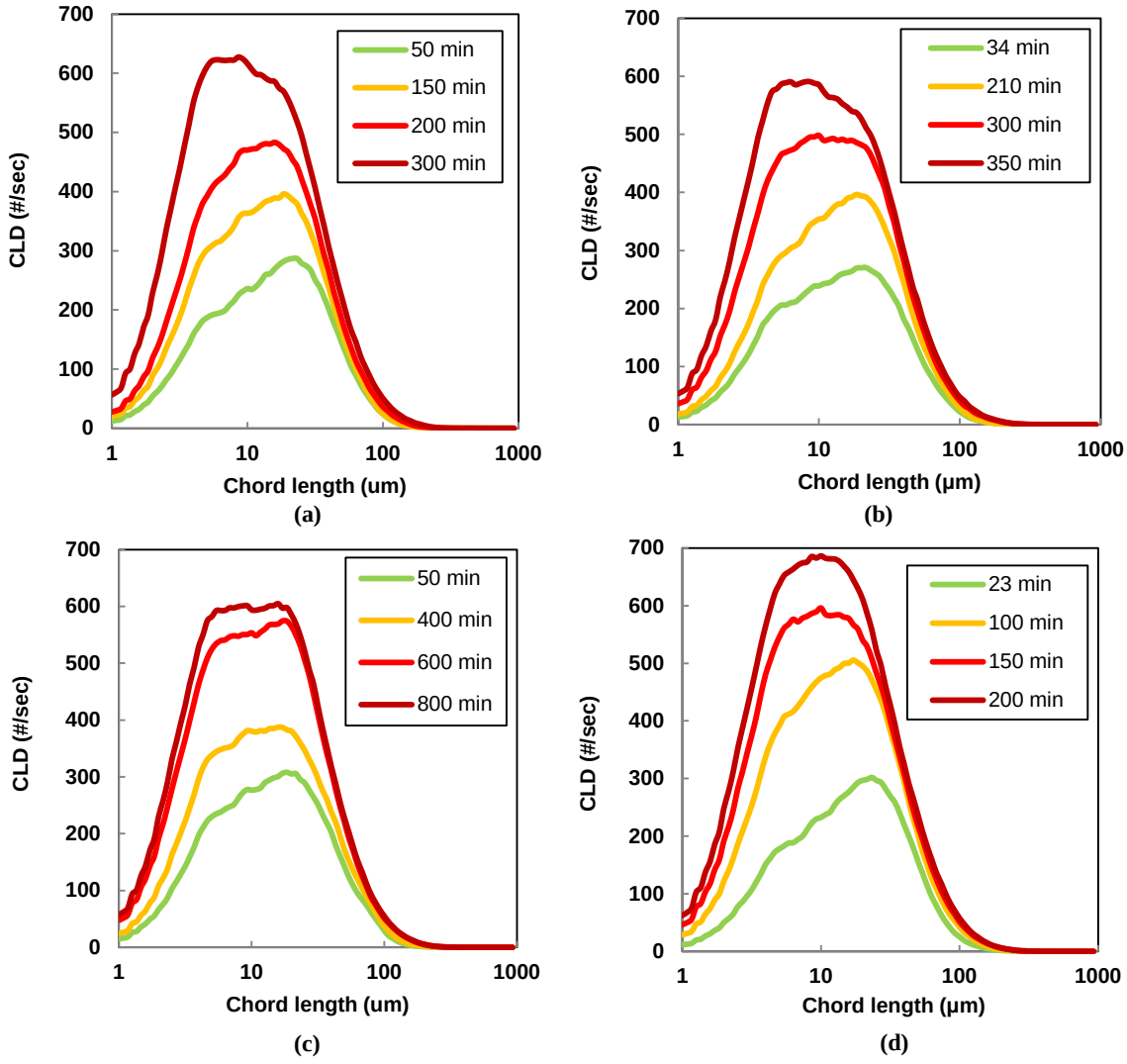

Figure 12.5: Chord length distribution for the SSC experiments a) Experiment 2 (b) Experiment 3 (c) Experiment 5 (d) Experiment 6.

Those could be easily implemented in a simple T-controlled batch crystallization experiment with no need of additional PAT tools and control algorithms, using a direct design concept. This is a good example of the "Quality-by-Control" (QbC) paradigm, whereby feedback control strategies can be easily and quickly used to develop optimal

crystallization processes that can be implemented for example at larger scale with minimum usage of instrumentation. The QbC approach could be used to replace the traditional design of experiment (DoE) based approaches that constitutes the standard procedure during process development for a particular drug. The QbC approach, designs suitable operating procedures by direct adaptation of the operating conditions during crystallization using a feedback control based approach, hence it provides a much faster methodology to find the optimal operating procedure, requiring less material as traditional quality-by-design (QbD) approaches based on standard DoE techniques.

12.4.3 Direct nucleation control experiments

A DNC approach was also used with vitamin B12. This approach is usually very easy to implement and was proved to improve the purity of several APIs (Saleemi et al. 2012a). For vitamin B12 this approach failed because of the needle shape of the crystal: the total counts/s recorded by FBRM increases during the growth of long needles, therefore, keeping that value constant using DNC does not actually allow the crystal to grow. The results for two DNC experiments at different setpoints are shown in Figure 12.6 and Figure 12.7, in both cases temperature keeps oscillating without converging to a lower value.

In fact, whenever crystals start to grow, the total counts/s rise and the controller responds by increases the temperature, which will dissolve again the particles counteracting the growth made in the cooling phase. Figure 12.6c shows an image of the crystals at the end of the first cycle (sample taken at about 300 min) while Figure 12.6d shows the crystal at the end of the run. The size distribution becomes worse during the cycles and breakage tends to prevail on growth. Furthermore, because of the oscillation of temperature it is impossible to get a sufficient yield. A second example of failed DNC is shown in Figure 12.7 using a setpoint of 30,000 #/measurement.

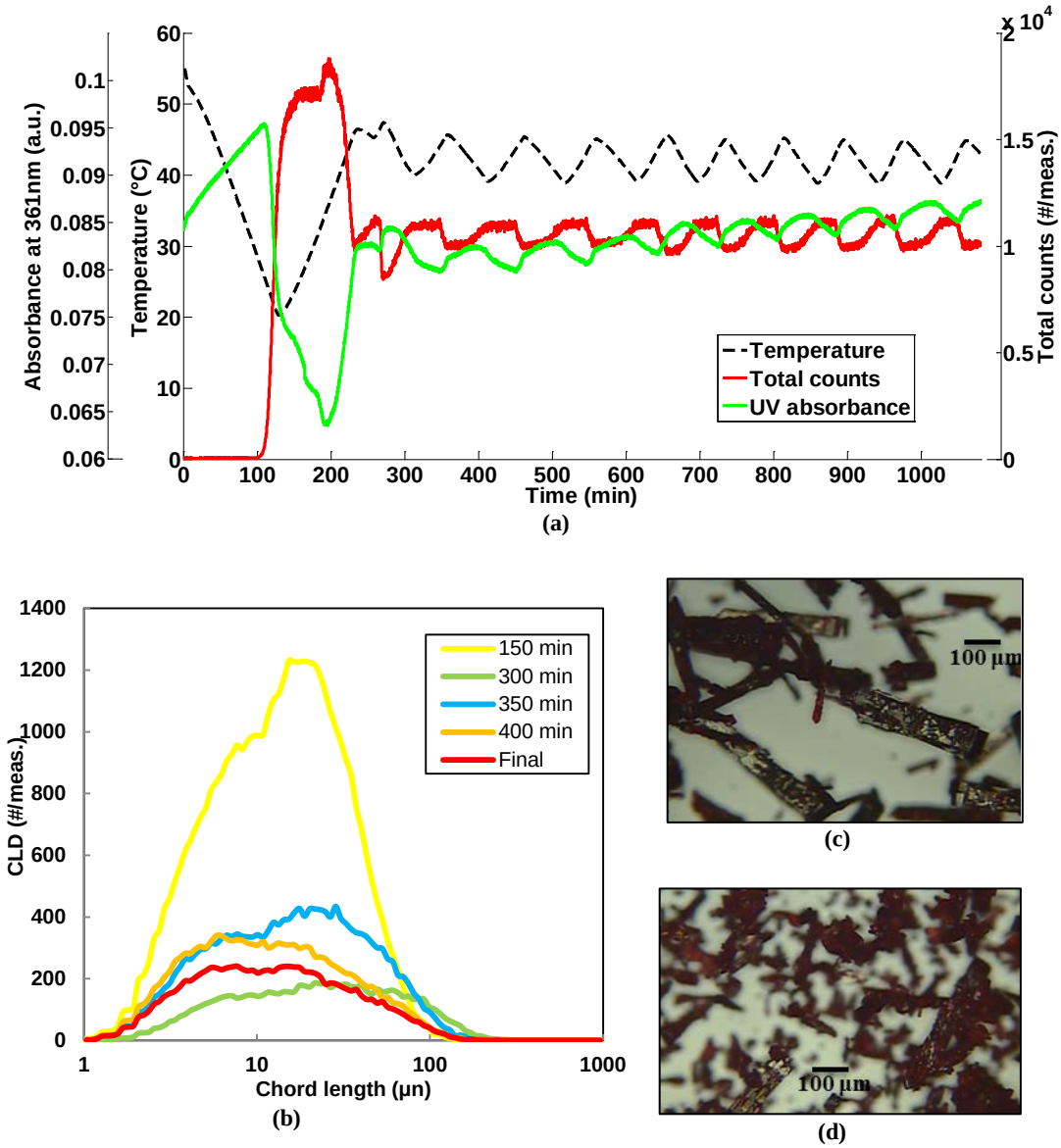

Figure 12.6: (a) Direct nucleation control of raw material in water and ethanol with a set point of 10000#/measurement for the value of the total counts. UV/Vis absorbance at 361 nm, temperature, total counts and mean square weighted chord length distribution (FBRM) plotted versus time in min. (b) Evolution of the CLD from FBRM during the experiment (c) Microscopic image of crystals taken after the first cycle (d) Microscopic image of the crystals taken at the end of the run.

In conclusion, DNC was found to be unsuitable for crystals with the morphology of vitamin B12, promoting breakage over growth and preventing the reach of a sufficient yield. While these experiments did not lead to an improved crystallization process, we believe they provide a very useful case study to illustrate the limitation of DNC in the case of high aspect ratio needle-shaped particles with growth inhibition.

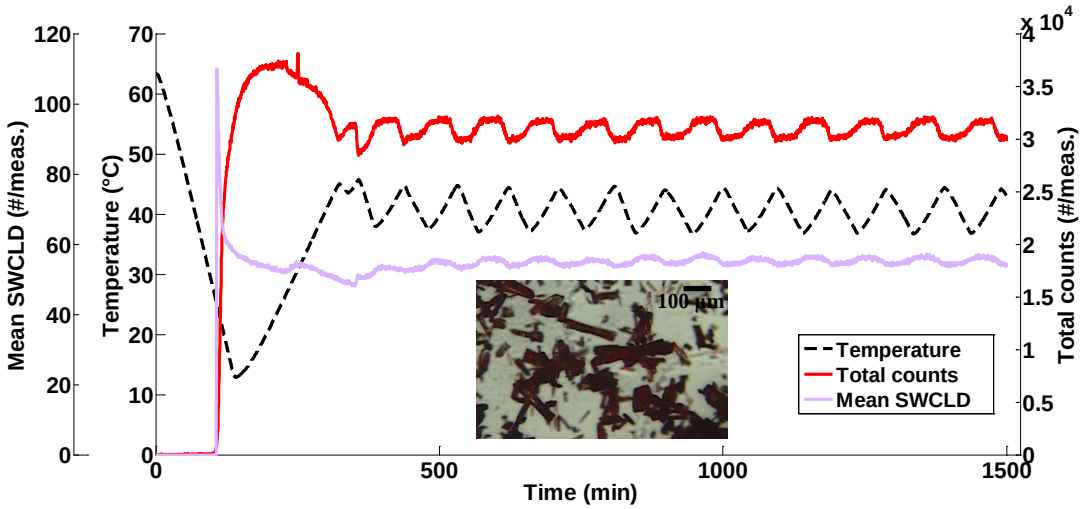

Figure 12.7: Direct nucleation control of raw material in water and ethanol with a set point of 30,000 #/measurement for the value of the total counts/s. UV/Vis absorbance at 361 nm, temperature, total counts/s and mean square weighted chord length (FBRM) plotted versus time. The image shows the crystals at the end of the run analyzed with an optical microscope.

12.4.4 Temperature cycling experiments

The last approach used with vitamin B12 was temperature cycling with a fixed temperature profile that was forced to converge by design: after the heating steps of every cycle the temperature was brought back to a slightly lower value compared to the initial one; therefore overall the temperature decreased from about 70 °C to 7-10 °C. Temperature, concentration and total counts/s profiles during some of the experiments performed are shown in Figure 12.8 and Figure 12.9. Experiments 1 and 2 were conducted using a solution made with raw material and seeding with purified crystals of the vitamin, whereas the solutions for experiments 4 and 5 were prepared using recrystallized material. The value of the total counts/s increases during all the experiments reaching more than 30,000 #/sec in experiments 1 and 2 (solution prepared with raw material) and almost the same amount in experiment 5. The final crystal size distribution in these experiments is very broad and the presence of large crystals can be noticed together with fines (as shown in Figure 12.10). Breakage can be observed at the end of the temperature profile for experiment 1 and 5 (see Figure 12.9a and b).

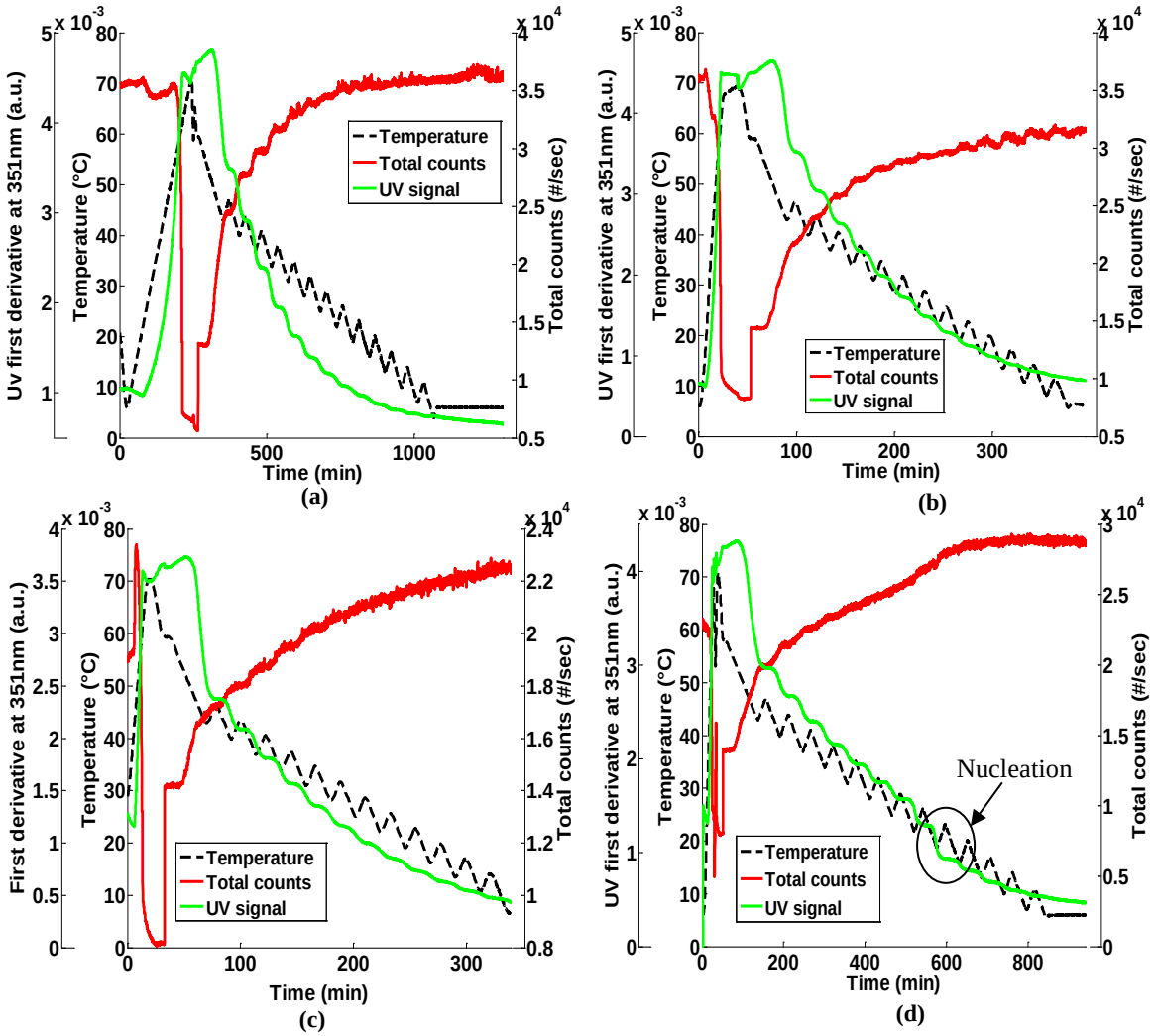

Figure 12.8: Temperature, UV signal and total counts/s for (a) experiment 1; (b) experiment 2; (c) experiment 4; and (d) experiment 5; all from Table 12.3.

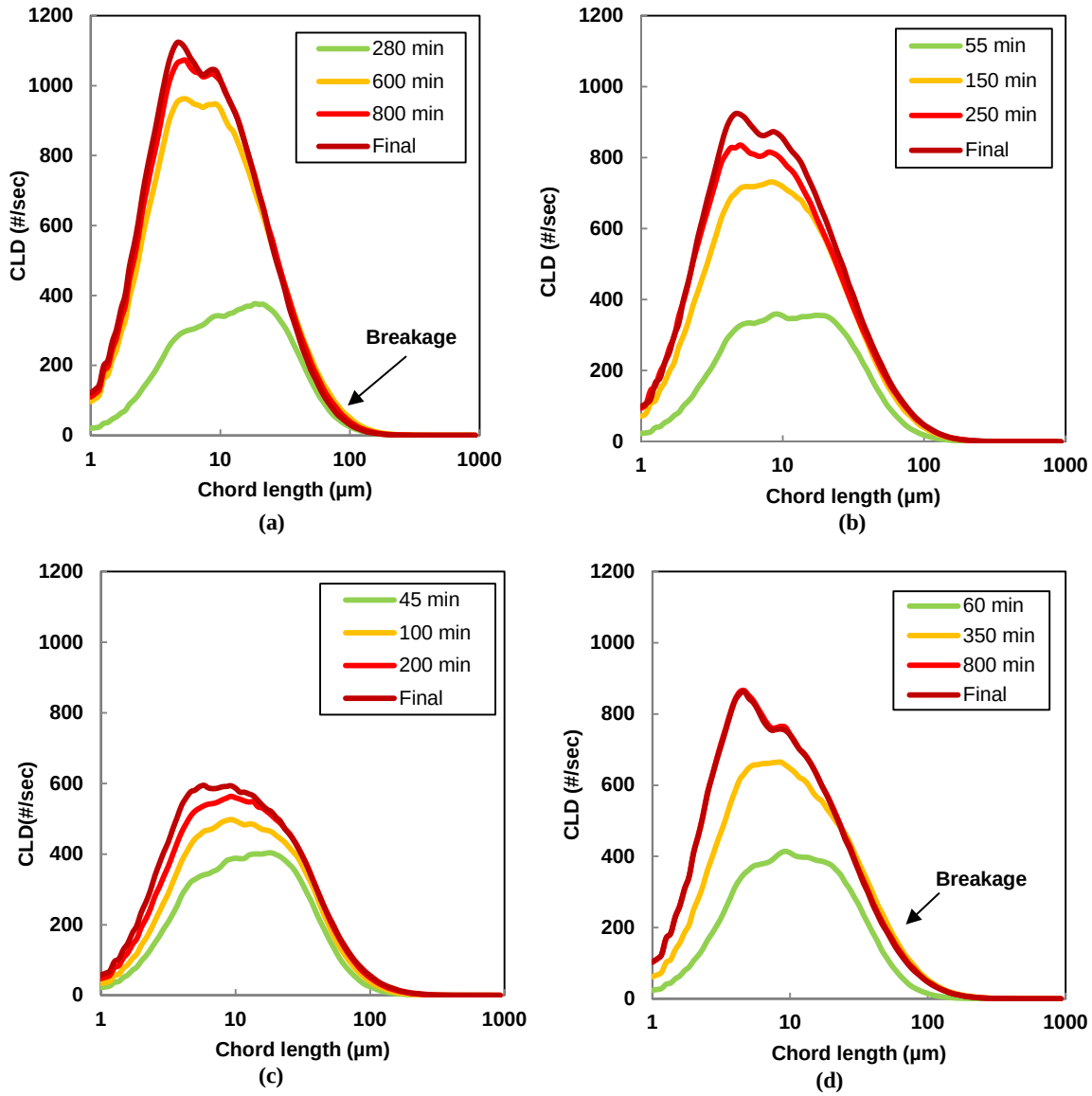

Figure 12.9: Chord length distribution evolution for (a) experiment 1; (b) experiment 2; (c) experiment 4; and (d) experiment 5; all from Table 12.3.

Figure 12.10 shows microscopic images of the crystals at the end of each of the temperature cycling experiments. Larger crystals were obtained with solutions made from crystallized material (experiment 4 and 5), although crystals from experiment 5 presents a broader distribution, probably because both breakage and nucleation occurred during the cooling profile. Temperature cycling seems to give better crystal size distribution compared to slow cooling but cooling/heating conditions has to be determined with several experiments using statistical design of experiments in order to optimize the process as the direct nucleation control based direct design approach may not work for this type of system (high aspect ratio needles).

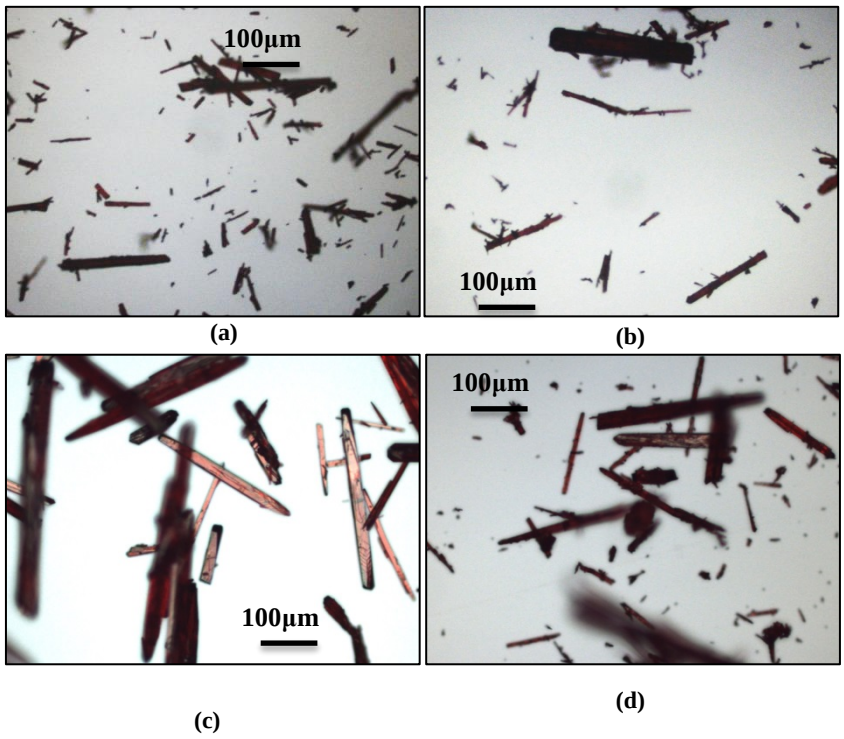

Figure 12.10: Microscopic image of final crystals from (a) experiment 1; (b) experiment 2; (c) experiment 4; and (d) experiment 5; all from Table 12.3.

12.4.5 Purity analysis using HPLC

The final crystals of all experiments were analyzed with HPLC: the results are shown in Table 12.4. Seeded SSC over a solution of raw material gave an average improvement of purity of 3.19 % against about 3.4 % obtained with temperature cycling. Even when using purified material to prepare the solution, temperature cycling gave the highest improvement in purity, even higher than seeded slow cooling in water. Using the same solvent and the same type of starting material, it is clear that temperature cycling have slightly higher purification efficiency than supersaturation control and simple seeded slow cooling. This is due to the fact that the multiple steps of partial surface dissolution and regrowth at low supersaturation that occur during the temperature cycles have an effect of rejecting impurities from the crystal lattice. The results illustrated the benefits of using PAT for the understanding and design of a biopharmaceutical crystallization and provide a proof-of-concept on how suitable feedback control strategies can be applied to improve crystal purity and CSD.

Table 12.4: HPLC purity results for unseeded experiments performed

Sample	Purity (%)	Improvement in purity (%)	Starting material
Raw material	93.11	0	n.a.
SSC Experiment 1	96.29	3.18	Raw material (93.11%)
SSC Experiment 2	96.31	3.20	Raw material (93.11%)
SSC Experiment 3	96.30	3.19	Raw material (93.11%)
SSC Experiment 4	97.47	1.17	Crystal from SSC experiment 3 (96.3%)
SSC Experiment 5	97.42	1.12	Crystal from SSC experiment 3 (96.3%)
SSC Experiment 6	97.5	1.20	Crystal from SSC experiment 3 (96.3%)
TC Experiment 1	96.51	3.40	Raw material (93.11%)
TC Experiment 2	96.60	3.49	Raw material (93.11%)
TC Experiment 3	96.40	3.29	Raw material (93.11%)
TC Experiment 4	97.68	1.28	Crystals from TC experiment 3 (96.40%)
TC Experiment 5	97.69	1.29	Crystals from TC experiment 3 (96.40%)
TC Experiment 6	97.67	1.27	Crystals from TC experiment 3 (96.40%)
Slow cooling of purified material in water	97.54	1.24	Crystal from SSC experiment 3 (96.30%)
Seeds used for supersaturation control experiments	97.57	4.46	n.a.
Seeds used for temperature cycling experiments	97.54	4.43	n.a.

12.5 Conclusions

Different crystallization strategies using PAT tools were tested on a relatively small biomolecule produced by fermentation. This method of production usually leads to the presence of a large amount of impurities in the material that makes the design of the crystallization process particularly difficult and reduces the quality of the final crystals in term of purity, size distribution and consistency of these critical quality attributes. Multiple

successive recrystallizations of the same material can help eliminating impurities but also contribute to decrease the total yield of the purification process. In this chapter supersaturation control, temperature cycling and DNC were tested and compared to simple slow cooling in order to improve the final crystal size distribution and purity of the produced crystals, avoiding multiple recrystallization processes. It was found that direct nucleation control is not suitable because of the specific morphology of the compound: the growth of needle crystals is accompanied by an increase in the total counts/measurement, therefore, trying to keep the counts constant prevent the particles from growing. In general, using material which was crystallized once to prepare the solution, helped in improving the final crystal size distribution regardless of the type of crystallization strategy used. Among the experiments with material recrystallized once, temperature cycling with fast heating/cooling rate gave the highest purification efficiency. Temperature cycling can also give good final size distribution but cooling/heating conditions has to be chosen properly, eventually using design of experiment. Supersaturation control is a simpler approach that also gave a narrow distribution with larger crystals compared to simple linear cooling of material crystallized the same number of times. In conclusion, three feedback control strategies were tested on a biopharmaceutical and two of them were proved to increase the quality of the CSD and purity of the final product compared to traditional slow cooling.

13 Conclusions and future work

13.1 Conclusions

The polymorphic outcome of a crystallization from solution (cooling, evaporation or anti-solvent) is strongly related to the conditions of the process: the choice of solvent, pH, kinetic conditions and presence of impurities in solution will determine the polymorph nucleated and, therefore, the properties of the final product (in particular solubility and bioavailability). For this reason understanding polymorphism, as well as being able to monitor and control it during industrial crystallization, is very important. In this thesis process analytical technology (PAT) tools were used to both monitor and control polymorphic purity of the solids in a batch crystallization process and to gain a better understanding of the effect of solvent and additives on polymorphism of an organic compound (OABA) commonly used for the production of dyes and as an intermediate for the production of pharmaceuticals.

The correct interpretation of signals from PAT tools during a crystallization experiment and the development of efficient calibration strategies is very important to control the process and obtain crystals with the desired characteristics. In this thesis, Raman spectroscopy was studied in details and a good calibration practice procedure was developed to optimize the measurement of the polymorphic composition of slurries during batch cooling crystallization processes. Other spectroscopic techniques (NIR transflectance, ATR-UV/Vis and mid-IR) were also tested and compared for the measurement of solute concentration using multivariate calibration. Furthermore, a concept of composite sensor array (CSA) which combines signals from different instruments using principal components analysis was experimentally tested for the first time. This approach could be very useful in a processing plant environment where more signals are monitored at the same time: the reduction of the amount of information to two or three principal components only would make the monitoring of the process much easier and quicker for the operators.

Both a model-free and a model-based feedback control strategy (APFC) that combines Raman and ATR-UV/Vis spectroscopy was developed for the selection and optimal growth of the stable polymorph in a batch crystallization, after erroneous seeding or

nucleation of a mixture of polymorphs. In the calibration-free strategy Raman spectroscopy is used to detect the presence of the undesired (metastable) polymorph and trigger a dissolution cycle until its complete elimination. The remained crystals of the desired (stable) polymorph are then grown using a calibration-based supersaturation control. The solute concentration is kept below the solubility curve of the undesired polymorph during the cooling profile in order to avoid its further nucleation. The proposed approach is a highly robust adaptive control strategy that can eliminate batch-to-batch variations in the polymorphic purity of crystalline products due to either nucleation of mixture of polymorphs or erroneous seeding. It also represents the first example of feedback control over polymorphic purity using a combination of two different spectroscopic techniques. A model-based optimization of the APFC was also performed, and the optimal temperature profile that maximises the size of the crystals of the stable form at the end of the batch allowing, at the same time, elimination of the metastable form was determined. The model-based approach is an improvement of the model-free since it can control and optimize both the size distribution and the polymorphic purity of the crystals.

For the model-free and model-based APFC PAT tools were used to control the polymorphic purity of the solid phase in a crystallization process. However, they are also a very useful resource to investigate the fundamentals of polymorphism and, in particular, the role of solvent and impurities on polymorphic outcome of crystallization from solution. In this thesis, Raman, ATR-FTIR and ATR-UV/vis spectroscopy were used to understand the effect of the solvent composition and a structurally related additive on the polymorphic outcome of a zwitterionic compound were analysed using PAT tools and off-line characterizations techniques. A strong relationship between the amount of zwitterions in solution and the polymorph of OABA nucleated in cooling crystallization was found using ATR-UV/Vis and Raman spectroscopy. Additionally, all the three known polymorphs of OABA were obtained using different combinations of solvents and additive/OABA ratios in solution. Furthermore, in specific conditions, the additive was used to tailor shape and size of the crystals of the stable polymorph of OABA. These results show how polymorphism and crystal size and shape of organic compounds can be tailored by an opportune design of the crystallization process and, in particular, by choosing the correct solvent and the amount of additive.

In the last decade the production of biopharmaceuticals has tremendously increased. Biomolecules are used as medicines to treat a wide range of diseases but also as nutritional supplements. The biological synthesis of these compounds often leads to a high amount of impurities in the product that have to be removed. Crystallization can be used as a purification technique for biopharmaceuticals but the processing conditions have to be chosen carefully in order to guarantee efficient removal of the impurities and also good quality crystals at the end of the batch. In this thesis the crystallization step of an impure biopharmaceutical compound (vitamin B12) was studied using FBRM and ATR-UV/Vis and different feedback control strategies were tested in order to improve the final crystal size distribution and purity of vitamin B12. The use of PAT tools allowed a better understanding of the system and, in particular, of the effect of impurities on nucleation and growth kinetics of vitamin B12 crystals. Furthermore, supersaturation control and temperature cycling were successfully used to improve final purity and crystal size distribution of the product.

The experimental and modelling work of this thesis shows how PAT tools can be used to efficiently monitor and control polymorphic system during a crystallization process. Additionally, the same tools can be used to gain a better understanding of the effect of solvent and impurities on polymorphic systems.

13.2 Future work

In this section some recommendations for future work are given:

- The good calibration practice procedure for Raman spectroscopy should be improved using different types of probes and optics (PhAT probe for example) to better suit the quantitative analysis of solid suspensions. The same analysis of the effect of different parameters (temperature, solid density, polymorphic purity, size and shape) can be performed on the desired probe and Design of Experiments can be applied to find the best set of calibration experiments.
- The concept of composite sensor array (CSA) could be easily developed and implemented in the existing CryPRINS software. Data from FBRM, ATR-UV/Vis and Raman sensors could be sent to the software and arranged in a single matrix after opportune pre-processing (autoscaling for all the signal and derivative of

baseline corrections for spectroscopic techniques). A principal component analysis would be then automatically performed and the main scores displayed on a user friendly interface. After a proper calibration the principal component scores could be easily used for monitoring of crystallization processes and, eventually, automatic control.

- The solute-solvent interactions and their effect on polymorphism should be further investigated using both simulations (with the Gaussian software and molecular dynamics) and analytical techniques (solid state nuclear magnetic resonance, ssNMR, X-ray photoelectron spectroscopy, XPS, and near edge X-ray absorption fine structure, NEXAFS).
- The effect of benzoic acid on the nucleation of OABA should also be analysed more in detail by surface free energy measurement of the crystals (using inverse gas chromatography for example) and simulation techniques such as Hirshfeld analysis.
- The analysis of impure systems could also be carried on and, in particular, the effect of impurities over shape and morphology of the crystals should be studied more in details using XRD and SEM spectroscopy. The dissolution and growth kinetics can be systematically determined using PAT tools (using the methodology shown in chapter 7 of this thesis) in order to estimate the best conditions to control and tailor shape and size of the crystals during a crystallization process.

References

Aaltonen, J., Rantanen, J., Siiria, S., Karjalainene, M., Jorgensen, A., Laitinen, N., Savolainen, M., Seitavuopio, P., Louhi-Kultanen, M. and Yliruusi, J. 2003, "Polymorph screening using Near-Infrared spectroscopy", *Analytical Chemistry*, vol. 75, pp. 5267-5273.

Aamir, E., Nagy, Z.K. and Rielly, C.D. 2010, "Optimal seed recipe design for crystal size distribution control for batch cooling crystallisation processes", *Chemical Engineering Science*, vol. 65, no. 11, pp. 3602-3614.

Abbas, A. and Romagnoli, J.A. 2007, "Multiscale modeling, simulation and validation of batch cooling crystallization", *Separation and purification technology*, vol. 53, pp. 153-163.

Abu Bakar, M.R., Nagy, Z.K. and Rielly, C.D. 2009, "Seeded Batch Cooling Crystallization with Temperature Cycling for the Control of Size Uniformity and Polymorphic Purity of Sulfathiazole Crystals", *Organic Process Research and Development*, vol. 13, pp. 1343-1356.

Abu Bakar, M.R., Nagy, Z.K., Saleemi, A.N., Rielly, C.D. 2009, "The impact of direct nucleation control on crystal size distribution in pharmaceutical crystallization processes", *Crystal Growth and Design*, vol. 9, no. 3, pp. 1378-1384.

Abu Bakar, M.R. 2010, *Process analytical technology based approaches for the monitoring and control of size and polymorphic form in pharmaceutical crystallization processes*, Doctoral thesis, Loughborough University.

Abu Bakar, M.R., Nagy, Z., Rielly, C.D. 2010, "Investigation of the effect of temperature cycling on surface features of sulfathiazole crystals during seeded batch cooling crystallization", *Crystal Growth and Design*, vol. 10, pp. 3892-3900.

Abu Bakar, M.R., Nagy, Z.K., Rielly, C.D. and Dann, S.E. 2011, "Investigation of the riddle of sulfathiazole polymorphism", *International journal of pharmaceutics*, vol. 414, no. 1–2, pp. 86-103.

Abou-Zied, O., Al-Busaidi, B.Y., Husband, J. 2014, "Solvent effect on anthranilic acid spectroscopy", *The journal of physical chemistry*, vol. 118, no. 1, pp 103–109.

Acevedo, D. and Nagy, Z.K. 2014, "Systematic classification of unseeded batch crystallization systems for achievable shape and size analysis", *Journal of Crystal Growth*, vol. 394, pp. 97-105.

Acevedo, D., Tandy, Y. and Nagy, Z.K. 2015, "Multiobjective optimization of an unseeded batch cooling crystallizer for shape and size manipulation", *Industrial and Engineering Chemistry Research*, vol. 54, no. 7, pp. 2156-2166.

Agarwal, P., Berglund, K.A. 2003, "In Situ Monitoring of Calcium Carbonate Polymorphs during Batch Crystallization in the Presence of Polymeric Additives Using Raman Spectroscopy", *Crystal Growth and Design* , vol. 3, no. 6, pp. 941-946.

Alatalo, H., Hatakka, H., Kohonen, J., Reinikainen, S.P., Louhi-Kultanen, M. 2010, "Process control and monitoring of reactive crystallization of L-glutamic acid", *AIChE Journal*, vol. 56, no. 8, pp. 1063-2076.

Alatalo, H., Kohonen, J., Qu, H., Hatakka, H., Reinikainen, S.P., Louhi-Kultanen, M., Kallas, J. 2008, "In-line monitoring of reactive crystallization process based on ATR-FTIR and Raman spectroscopy", *Journal of Chemometrics*, vol. 22, pp. 644-652.

Allan, P., Bellamy, L.J., Nordon, A., Littlejohn, D., Andrews, J., Dallin, P. 2013, "In situ monitoring of powder blending by non-invasive Raman spectrometry with wide area illumination", *Journal of Pharmaceutical, Biomedical Analysis*, vol. 76, pp. 28-35.

Alonzo, D.E., Raina, S., Zhou, D., Gao, Y., Zhang, G.G.Z. and Taylor, L.S. 2012, "Characterizing the impact of hydroxypropylmethyl cellulose on the growth and nucleation kinetics of felodipine from supersaturated solutions", *Crystal Growth and Design*, vol. 12, pp. 1538-1547.

Al-Zoubi, N., Koundourellis, J.E., Malamataris, S. 2002, "FT-IR and Raman spectroscopic methods for identification and quantitation of orthorhombic and monoclinic paracetamol in powder mixes", *Journal of Pharmaceutical and Biomedical analysis*, vol. 29, no. 3, pp. 459-467.

Anwar, J., Boateng, P.K., Tamaki, R. and Odedra, S. 2009, "Mode of action and design rules for additives that modulate crystal nucleation", *Angewandte Chemie International Edition*, vol. 48, pp. 1596-1600.

Barrett, M., Hao, H., Maher, A., Hodnett, K., Glennon, B., Croker, D. 2011, "In situ monitoring of supersaturation and polymorphic form of piracetam during batch cooling crystallization", *Organic Process Research and Development*, vol. 15, no. 3, pp. 681-687.

Barrett, M., McNamara, M., Hao, H., Barrett, P., Glennon, B. 2010, "Supersaturation tracking for the development, optimization and control of crystallization processes", *Chemical Engineering Research and Design*, vol. 88, no. 8, pp. 1108-1119.

Barthe, S.C., Grover, M.A., Rousseau, R.W. 2008, "Observation of polymorphic change through analysis of FBRM data: transformation of paracetamol from form II to form I", *Crystal Growth and Design*, vol. 8, no. 9, pp. 3316-3322.

Beckmann, W. 2000, "Seeding the desired polymorph: background, possibilities, limitations, and case studies", *Organic Process Research and Development*, vol. 4, pp. 372-383.

Bernstein, J. 2011, "Polymorphism - A perspective", *Crystal Growth and Design*, vol. 11, no. Perspective, pp. 632-650.

Berntsson, O., Danielsson, L.-., Johansson, M.O. and Folestad, S. 2000, "Quantitative determination of content in binary powder mixtures using diffuse reflectance near infrared spectrometry and multivariate analysis", *Analytica Chimica Acta,* vol. 419, no. 1, pp. 45-54.

Bhambure, R., Kumar, K. and Rathore, A.S. 2011, "High-throughput process development for biopharmaceutical drug substances", *Trends in biotechnology,* vol. 29, no. 3, pp. 127-135.

Bird, R., Stewart, W. and Lightfoot, E. (eds) 1960, *Transport phenomena*, Wiley, New York, London.

Blagden, N., Davey, R.J. 2003, "Polymorph selection: Challenges for the future?", *Crystal growth and design,* vol. 3, no. 6, pp. 879-885.

Bonafede, S.J. and Ward, M.D. 1995, "Selective nucleation and growth of an organic polymorph by ledge-directed epitaxy on a molecular crystal substrate", *Journal of American Chemical Society,* vol. 117, no. 30, pp. 7853-7861.

Borsos, Á., Majumder, A. and Nagy, Z.K. 2014, "Model Development and Experimental Validation for Crystal Shape Control by Using Tailored Mixtures of Crystal Growth Modifiers", *Computer Aided Chemical Engineering,* vol. 33, no. 0, pp. 781-786.

Bosch, E., Ràfols, C., Rosés, M. 1995, "Variation of acidity constants and pH values of some organic acids in water—2-propanol mixtures with solvent composition. Effect of preferential solvation", *Analytica Chimica Acta,* vol. 302, no. 1, pp. 109-119.

Boxall, J.A., Koh, C.A., Sloan, E.D., Sum, A.K., Wu, D.T. 2010, "Measurement and calibration of droplet size distributions in water-in-oil emulsions by particle video microscope and a focused beam reflectance method", *Industrial and Engineering Chemistry Research,* vol. 49, pp. 1412-1418.

Braatz, R., Fujiwara, M., Nagy, Z., Wubben, T., Rusli, E. 2012, "Crystallization: Particle size control" in *Encyclopedia of Pharmaceutical Technology,* ed. Informa Heathcare USA.

Braun, D.E., Maas, S.G., Zencirci, N., Langes, C., Urbanetz, N.A., Griesser, U.J. 2010, "Simultaneous quantitative analysis of ternary mixtures of d-mannitol polymorphs by FT-Raman spectroscopy and multivariate calibration models", *International Journal of Pharmaceutics,* vol. 385, no. 1–2, pp. 29-36.

Brereton, R.G., 2003, *Chemometrics: data analysis for the laboratory and chemical plant*. West Sussex, UK: John Wiley and Sons.

Brittain, H.G. 2009a, "Vibrational spectroscopic studies of cocrystals and salts. 2. The benzylamine-benzoic acid system", *Crystal Growth and Design,* vol. 9, no. 8, pp. 3497-3503.

Brittain, H.G. 2009b, "Vibrtational studies of cocrystals and salts. 1. The benzamide-Benzoic acid system", *Crystal Growth and Design,* vol. 9, no. 5, pp. 2492-2499.

Burton, R.C., Ferrari, S.E., Davey, R.J., Finney, J.L., Bowron, D.T. 2010, "The relationship between solution structure and crystal nucleation: a neutron scattering study of supersaturated methanolic solutions of benzoic acid", *Journal of Physical Chemistry B*, vol. 114, pp. 8807-8816.

Caillet, A., Fevotte, G., Sheibat-Othman, N. 2007, "Crystallization of monohydrate citric acid. 2. Modeling through population balance equations", *Crystal Growth and Design,* vol. 7, no. 10, pp. 2088-2095.

Caillet, A., Puel, F., Fevotte, G. 2006, "In-line monitoring of partial and overall solid concentration during solvent-mediated phase transition using Raman spectroscopy", *International Journal of Pharmaceutics*, vol. 307, no. 2, pp. 201-208.

Caillet, A., Rivoire, A., Galvan, J.M., Puel, F., Fevotte, G. 2007, "Crystallization of monohydrate citric acid. 1. In situ monitoring through the joint use of Raman spectroscopy and image analysis", *Crystal Growth and Design*, vol. 7, pp. 2080-2087.

Caillet, A., Puel, F., Fevotte, G. 2008, "Quantitative in situ monitoring of citric acid phase transition in water using Raman spectroscopy", *Chemical Engineering and Processing: Process Intensification,* vol. 47, no. 3, pp. 377-382.

Cajigal, S. 2008, "Recalled transdermal PD patch should be down-titrated", *Neurology today,* vol. 8, no. 8, pp. 1-8.

Campbell Roberts, S.N., Williams, A.C., Grimsey, I.M., Booth, S.W. 2002, "Quantitative analysis of mannitol polymorphs. FT-Raman spectroscopy", *Journal of Pharmaceutical and Biomedical Analysis,* vol. 28, pp. 1135-1147.

Cardew, P.T. and Davey, R.J. 1985, "The kinetics of solvent-mediated phase transformations", *Proceedings of the Royal Society of London,* vol. 398, no. 1815, pp. 415-428.

Carter, P.W. and Ward, M.D. 1994, "Directing polymorph selectivity during nucleation of anthranilic acid on molecular substrates", *Journal of American Chemical Society,* vol. 116, pp. 769-770.

Chadwick, K., Myerson, A.S. and Trout, B. 2011, "Polymorphic control by heterogeneous nucleation- A new method for selecting crystalline substrates", *Crystal engineering communications,* vol. 13, pp. 6625.

Chemburkar, S.R., Bauer, J., Deming, K., Spiwek, H., Patel, K., Morris, J., Henry, R., Spanton, S., Dziki, W., Porter, W., Quick, J., Bauer, P., Donaubauer, J., Narayanan, B.A., Soldani, M., Riley, D. and McFarland, K. 2000, "Dealing with the impact of Ritonavir polymorphs on the late stages of bulk drug process development", *Organic Process Research and Development,* vol. 4, pp. 413-417.

Chen, Z., Lovett, D., Morris, J. 2011, "Process analytical technologies and real time process control a review of some spectroscopic issues and challenges", *Journal of Process Control,* vol. 21, pp. 1467-1482.

Chen, Z.P., Fevotte, G., Caillet, A., Littlejohn, D., Morris, J. 2008, "Advanced calibration strategy for in situ quantitative monitoring of phase transition processes in suspensions using FT-Raman spectroscopy", *Analytical Chemistry*, vol. 80, pp. 6658-6665.

Chen, Z.P., Li, L.M., Jin, J.W., Nordon, A., Littlejohn, D., Yang, J., Zhang, J., Yu, R.Q. 2012, "Quantitative analysis of powder mixtures by Raman spectrometry: the influence of particle size and its correction", *Analytical Chemistry*, vol. 84, pp. 4088-4094.

Chew, J.W., Black, S., Chow, P.S., Tan, R.B.H., Carpenter, K.J. 2007, "Stable polymorphs: difficult to make and difficult to predict", *Crystal engineering communications*, vol. 9, pp. 128-130.

Chiarella, R.A., Gillon, A.L., Burton, R.C., Davey, R.J., Sadiq, G., Auffret, A., Cioffi, M. and Hunter, C. 2007, "The nucleation of inosine: the impact of solution chemistry on the appearence of polymorphic and hydrated crystal forms", *Faraday Discussions*, vol. 136, pp. 179-193.

Chieng, N., Rades, T. and Aaltonen, J. 2011, "An overview of recent studies on the analysis of pharmaceutical polymorphs", *Journal of pharmaceutical and biomedical analysis*, vol. 55, no. 4, pp. 618-644.

Choong, K.L. and Smith, R. 2004, "Optimization of batch cooling crystallization", *Chemical Engineering Science*, vol. 59, pp. 313-327.

Clydesdale, G., Roberts, K.J. and Docherty, R. 1994, "Modelling the morphology of molecular crystals in the presence of disruptive tailor-made additives", *Journal of Crystal Growth*, vol. 135, pp. 331-340.

Colthup, N.B., Daly, L.H., Wiberley, S.E. 1975, *Introduction to infrared and Raman spectroscopy*, Second edn.

Cornel, J., Lindenberg, C. and Mazzotti, M. 2009, "Experimental characterization and population balance modeling of the polymorph transformation of L-glutamic acid", *Crystal Growth and Design*, vol. 9, no. 1, pp. 243-252.

Cornel, J., Lindenberg, C. and Mazzotti, M. 2008, "Quantitative application of in situ ATR-FTIR and Raman spectroscopy in crystallization processes", *Industrial and Engineering Chemistry Research*, vol. 47, pp. 4870-4882.

Cornel, J. and Mazzotti, M. 2008, "Calibration-free quantitative application of in situ Raman spectroscopy to a crystallization process", *Analytical Chemistry*, vol. 80, pp. 9240-9249.

Cox, T.F. 2005, *An introduction to multivariate data analysis*, Hodder Arnold, Great Britain.

Davey, R.J. 2003, "Pizzas, polymorphs and pills", *Chemical Communications*, vol. 9, no. 13, pp. 1463-1467.

Davey, R.J., Allen, K., Blagden, N., Cross, W.I., Lieberman, H.F., Quayle, M.J., Righini, S., Seton, L. and Tiddy, G.J.T. 2002a, "Crystal engineering- nucleation, the key step", *The Royal Society of Chemistry,* vol. 4, no. 47, pp. 257-264.

Davey, R.J., Blagden, N., Righini, S., Alison, H. and Ferrari, S.E. 2002b, "Nucleation control in solution mediated polymorphic phase transformations: the case of 2,6-dihydroxybenzoic acid", *Journal of Physical Chemistry,* vol. 106, pp. 1954-1959.

Davey, R.J., Blagden, N., Righini, S., Alison, H., Quayle, M.J. and Fuller, S. 2001, "Crystal polymorphism as a probe for molecular self-assembly during nucleation from solutions: the case of 2,6-dihydroxybenzoic acid", *Crystal Growth and Design,* vol. 1, no. 1, pp. 59-65.

Davey, R.J. and Cardew, P.T. 1986, "Rate controlling processes in solvent-mediated phase transformations", *Journal of Crystal Growth,* vol. 79, pp. 648-653.

Davey, R.J., Dent, G., Mughal, R.K. and Parveen, S. 2006, "Concerning the relationship between structural and growth synthons in crystal nucleation: solution and crystal chemistry of carboxilic acids as revealed through IR spectroscopy", *Crystal Growth and Design,* vol. 6, no. 8, pp. 1788-1796.

Davey, R.J. and Garside, J. (eds) 2000, *From molecules to crystallizers: an introduction to crystallization,* First edn, Oxford university press.

Davey, R.J., Schroeder, S.L.M. and ter Horst, J.H. 2013, "Nucleation of organic crystals - A molecular perspective", *Angewandte Reviews,* vol. 52, pp. 2166-2179.

De Anda, J.C., Wang, X.Z., Lai, X., Roberts, K.J., Jennings, K.H., Wilkinson, M.J., Watson, D., Roberts, D. 2005, "Real-time product morphology monitoring in crystallization using imaging techniques", *AIChE Journal,* vol. 51, no. 5, pp. 1406-1414.

De Beer, T., Burggraeve, A., Fonteyne, M., Saerens, L., Remon, J., Varvaet, C. 2011, "Near infrared and Raman spectroscopy for the in-process monitoring of pharmaceutical production processes", *International Journal of Pharmaceutics,* vol. 417, pp. 32-47.

De Beer, T.R.M., Baeyens, W.R.G., Ouyang, J., Vervaetc, C., Remonc, J.P. 2006, " Raman spectroscopy as a process analytical technology tool for the understanding and the quantitative in-line monitoring of the homogenization process of a pharmaceutical suspension", *The Analyst,* vol. 131, pp. 1137-1144.

Deplazes, E., van Bronswijk, W., Zhu, F., Barron, L.D., Ma, S., Nafie, L.A., Jalkanen, K.J. 2008, "A combined theoretical and experimental study of the structure and vibrational circular dichroism, Raman and Raman optical activity spectra of the L-histidine zwitterion", *Theoretical Chemistry Account,* vol. 119, pp. 155-176.

De Spiegeleer, B., Seghers, D., Wieme, R., Schaubroeck, J., Verpoort, F., Slegers, G., Van Vooren, L. 2005, "Determination of the relative amounts of three crystal forms of

benzimidazole drug in complex finished formulations in FT-Raman spectroscopy", *Journal of Pharmaceutical and Biomedical analysis,* vol. 39, pp. 275-280.

Deeley, C.M., Spragg, R.A., Threlfall, T.L. 1991, "A comparison of Fourier transform infrared and near-infrared Fourier transform Raman spectroscopy for quantitative measurements: An application in polymorphism", *Spectrochimica Acta Part A: Molecular Spectroscopy,* vol. 47, no. 9–10, pp. 1217-1223.

Delaney, S.P., Witko, E.M., Smith, T.M. and Korter, T.M. 2012, "Investigating tautomeric polymorphism in crystalline anthranilic acid using terahertz spectroscopy and solid-state density functional theory", *The journal of physical chemistry,* vol. 116, pp. 8051-8057.

Di Profio, G., Fontanova, E., Curcio, E. and Drioli, E. 2012, "From tailored supports to controlled nucleation: exploring material chemistry, surface nanostructure, and wetting regime effects in heterogeneous nucleation of organic molecules", *Crystal Growth and Design,* vol. 12, pp. 3749-3757.

Ding, Y., Krogh-Jespersen, K. 1996, "The 1:1 glycine zwitterion-water complex: an ab initio electronic structure study", *Journal of Computational Chemistry,* vol. 17, no. 3, pp. 338-349.

Doki, N., Seki, H., Takano, K., Asatani, H., Yukota, M. and Kubota, N. 2004, "Process control of seeded batch cooling crystallization of the metastable α-form glycine using in-situ ATR-FTIR spectrophotometer and an in-situ FBRM particle counter", *Crystal Growth and Design,* vol. 4, no. 5, pp. 949-953.

Doki, N., Yukota, M., Kido, K., Sasaki, S. and Kubota, N. 2003, "Reliable and selective crystallization of the metastable α-form glycine by seeding", *Crystal Growth and Design,* vol. 4, no. 1, pp. 103-107.

Dubey, R. and Desiraju, G.R. 2014, "Structural landscape of the 1:1 benzoic acid:isonicotinamide cocrystal", *Chemical Communications,* vol. 50, pp. 1181-1184.

Duffy, D., Barrett, M., Glennon, B. 2013, "Novel, calibration-free strategies for supersaturation control in antisolvent crystallization processes", *Crystal Growth and Design,* vol. 13, pp. 3321-3332.

Erdemir, D., Lee, A.Y. and Myerson, A.S. 2009, "Nucleation of crystals from solution: classical and two-step models", *Accounts for chemical research,* vol. 42, no. 5, pp. 621-629.

European commission Enterprise and Industry 2009, *The financing of biopharmaceutical product develpment in Europe - Study on the competitiveness of the European biotechnology industry*.

Falcon, J.A., Berglund, K.A. 2004, "In situ monitoring of antisolvent addition crystallization with principal components analysis of Raman spectra", *Crystal Growth and Design,* vol. 4, no. 3, pp. 457-463.

Fevotte, F., Fevotte, G. 2010, "A method of characteristics for solving population balance equations (PBE) describing the adsorption of impurities during crystallization processes", *Chemical Engineering Science,* vol. 65, pp. 3191-3198.

Fevotte, G., Gherras, N. and Moutte, J. 2013, "Batch cooling solution crystallization of ammonium oxalate in the presence of impurities: study of solubility, supersaturation, and steady-state inhibition", *Crystal Growth and Design,* vol. 13, pp. 2737-2748.

Fevotte, G., Caillet, A. and Nida, S.O. 2007, "A population balance model of the solution-mediated phase transition of citric acid", *AIChE Journal,* vol. 53, no. 10, pp. 2578–2589.

Flood, A., and Wantha, L. 2012, "Population balance modeling of the solution mediated transformation of polymorphs: limitations and future trends", *Journal of Crystal Growth,* Vol. 373, pp. 7–12.

Freitas, M.P., Sabadin, A., Silva, L.M., Giannotti, F.M., do Couto, D.A., Tonhi, E., Medeiros, R.S., Coco, G.L., Russo, V.F.T. and Martins, J.A. 2005, "Prediction of drug dissolution profiles from tablets using NIR diffuse reflectance spectroscopy: A rapid and nondestructive method", *Journal of pharmaceutical and biomedical analysis,* vol. 39, no. 1–2, pp. 17-21.

Garnier, S., Petit, S. and Coquerel, G. 2002, "Influence of supersaturation and structurally related additives on the crystal growth of α-lactose monohydrate", *Journal of Crystal Growth,* vol. 234, pp. 207-219.

Gavira, J.A., Cera-Manjarres, A., Ortiz, K., Mendez, J., Jimenez-Torres, J.A., Patiño-Lopez, L.D. and Torres-Lugo, M. 2014, "Use of cross-linked poly(ethylene glycol)-based hydrogels for protein crystallization", *Crystal Growth and Design,* vol. 14, pp. 3239-3248.

Gebauer, D., Cölfen, H. 2011, "Prenucleation clusters and non-classical nucleation", *Nano Today,* vol. 6, pp. 564-584.

Gebauer, D., Völkel, A., Cölfen, 2008, "Steble prenucleation calcium carbonate clusters", *Science,* vol. 322, pp. 1819-1822.

Gemperline, P. (ed) 2006, *Practical guide to chemometrics,* CRC Press Taylor aand Francis Group.

Gimet, R. and Luong, A.T. 1987, "Quantitative determination of polymorphic forms in a formulation matrix using the near infra-red reflectance analysis technique", *Journal of Pharmaceutical and Biomedical Analysis,* vol. 5, no. 3, pp. 205-211.

Glassey, J., Gernaey, K.V., Clemens, C., Schulz, T.W., Oliveira, R., Striedner, G. and Mandenius, C.F. 2011, "Process analytical technology (PAT) for biopharmaceuticals", *Biotechnology Journal,* vol. 6, pp. 369-377.

Gu, C.H., Chatterjee, K., Young, V.J. and Grant, D.J.W. 2002, "Stabilization of a metastable polymorph of sulfamerazine by structurally related additives", *Journal of Crystal Growth*, vol. 235, pp. 471-481.

Hamilton, P., Littlejohn, D., Nordon, A., Sefcik, J., Slavin, P. 2012, "Validity of particle size analysis techniques for measurements of the attritions that occurs during vacuum agitated powder drying of needle shape particles", *Analyst*, vol. 137, pp. 118-125.

Hao, H., Su, W., Barrett, M., Caron, V., Healy, A.M. and Glennon, B. 2010, " A Calibration-Free Application of Raman Spectroscopy to the Monitoring of Mannitol Crystallization and Its Polymorphic Transformation", *Organic Process Research and Development*, vol. 14, pp. 1209-1214.

Hargreaves, M.D., Macleod, N.A., Smith, M.R., Andrews, D., Hammond, S.V., Matousek, P. 2011, "Characterisation of transmission Raman spectroscopy for rapid quantitative analysis of intact multi-component pharmaceutical capsules", *Journal of pharmaceutical and biomedical analysis*, vol. 54, pp. 463-468.

He, X., Stowell, J.G., Morris, K.R., Pfeiffer, R.R., Li, H., Stahly, G.P. and Byrn, S.R. 2001, "Stabilization of a metastable polymorph of 4-methyl-2-nitroacetanilide by isomorphic additives", *Crystal Growth and Design*, vol. 1, no. 4, pp. 305-312.

Helmdach, L., Feth, M.P., Minnich, C. and Ulrich, J. 2013, "Application of ATR-MIR spectroscopy in the pilot plant-Scope and limitations using the example of Paracetamol crystallizations", *Chemical Engineering and Processing: Process Intensification*, vol. 70, pp. 184-197.

Helmdach, L., Feth, M.P. and Ulrich, J. 2013, "Integration of process analytical technology tools in pilot-plant setups for the real-time monitoring of crystallizations and phase transitions", *Organic Process Research and Development*, vol. 17, no. Polymorphism and Crystallization 2013, pp. 585-598.

Hendriksen, B.A., Grant, D.J.W., Meenan, P. and Green, D.A. 1998, "Crystallization of paracetamol (acetaminophen) in the presence of structurally related substances", *Journal of Crystal Growth*, vol. 183, pp. 629-640.

Hennigan, M.C. and Ryder, A.G. 2013, "Quantitative polymorph contaminant analysis in tablets using Raman and near infra-red spectroscopies", *Journal of pharmaceutical and biomedical analysis*, vol. 72, pp. 163-171.

Herman, C., Haut, B., Douieb, S., Larcy, A., Vermylen, V. and Leyssens, T. 2012, "Use of in situ Raman, FBRM, and ATR-FTIR probes for the understanding of the solvent-mediated polymorphic transformation of II-I etiracetam in methanol", *Organic Process Research and Development*, vol. 16, no. 1, pp. 49-56.

Hermanto, M.W., Chiu, M.S. and Braatz, R.D. 2009, "Nonlinear model predictive control for the polymorphic transformation of L-glutamic acid crystals", *AIChE Journal*, vol. 55, no. 10, pp. 2631-2645.

Hermanto, M.W., Chiu, M.S., Woo, X.Y. and Braatz, R.D. 2007, " Robust Optimal Control of Polymorphic Transformation in Batch Crystallization", *AIChE Journal,* vol. 53, no. 10.

Hiremath, R., Basile, J.A., Varney, S.W. and Swift, J.A. 2005, "Controlling molecular crystal polymorphism with self assembled monolayer templates", *Journal of American Chemical Society,* vol. 127, pp. 18321-18327.

Hodgkin, D.C., Kamper, J., Mackay, M., Pickworth, J. 1956, "Structure of vitamin B12", *Nature,* vol. 178, pp. 64-66.

Hodgkin, D.C., Pickworth, J., Robertson, J.H., Trueblood, K.N., Prosen, R.J., White, J.G. 1955, "Structure of vitamin B12", *Nature,* vol. 4477, pp. 325-328.

Howard, K.S., Nagy, Z.K., Saha, B., Robertson, A.L. and Steele, G. 2009a, "Combined PAT-Solid State Analytical Approach for the Detection and Study of Sodium Benzoate Hydrate", *Organic Process Research and Development,* vol. 13, pp. 590-597.

Howard, K.S., Nagy, Z.K., Saha, B., Robertson, A.L., Steele, G. and Martin, D. 2009b, "A process analytical technology based investigation of the polymorphic transformations during the antisolvent crystallization of sodium benzoate from IPA/Water mixture", *Crystal Growth and Design*, vol. 9, no. 9, pp. 3964-3975.

Hu, Y., Wikström, H., Byrn,S.R., Taylor,L.S. 2006, "Effect of Particle Size on Polymorphic Quantitation by Raman Spectroscopy", *Applied Spectroscopy,* vol. 9, no. 60, pp. 977-984.

Hu, Y., Liang, J.K., Myerson, A.S., Taylor, L.S. 2005, " Crystallization Monitoring by Raman Spectroscopy: Simultaneous Measurement of Desupersaturation Profile and Polymorphic Form in Flufenamic Acid Systems", *Industrial and Engineering Chemistry Research,* vol. 44, pp. 1233-1240.

Huang, J., Romero-Torres, S., Moshgbar, M. 2010, "Practical considerations in data pre-treatment for NIR and Raman spectroscopy", *American pharmaceutical review,* http://www.americanpharmaceuticalreview.com/Featured-Articles/116330-Practical-Considerations-in-Data-Pre-treatment-for-NIR-and-Raman-Spectroscopy/.

Hunter, C., McCabe, J.F., Spitaleri, A. 2012, "Solvent effects of the structures of prenucleation aggregates of carbamazepine", *Crystal engineering communications,* vol. 14, pp. 7115-7117.

Ilevbare, G.A., Liu, H., Edgar, K.J. and Taylor, L.S. 2012a, "Effect of binary additive combinations on solution crystal growth of the poorly water-soluble drug, Ritonavir", *Crystal Growth and Design,* vol. 12, pp. 6050-6060.

Ilevbare, G.A., Liu, H., Edgar, K.J. and Taylor, L.S. 2012b, "Understanding polymer properties important for crystal growth inhibition- impact of chemically diverse polymers on solution crystal growth of ritonavir", *Crystal Growth and Design,* vol. 12, pp. 3133-3143.

Jiang, S. 2009, *Crystallization kinetics in polymorphic organic compounds*, Doctoral thesis, Technische Universiteit Delft.

Jiang, S., ter Horst, J.H., Jansens, P.J. 2010a, "Control over polymorph formation of o-aminobenzoic acid", *Crystal Growth and Design,* vol. 10, pp. 2541-2547.

Jiang, S., ter Horst, J.H., Jansens, P.J. 2010b, "Mechanism and kinetics of polymorphic transformation of o-aminobenzoic acid", *Crystal Growth and Design,* vol. 10, pp. 2123-2128.

Jiang, S., ter Horst, J.H., Jansens, P.J. 2008, "Concomitant polymorphism of o-aminobenzoic acid in antisolvent crystallization", *Crystal Growth and Design,* vol. 8, no. 1, pp. 37-43.

Kachrimanis, K., Braun, D.E., Griesser, U.J. 2007, "Quantitative analysis of paracetamol polymorphs in powder mixtures by FT-Raman spectroscopy and PLS regression", *Journal of pharmaceutical and biomedical analysis,* vol. 43, no. 2, pp. 407-412.

Kadam, S., van der Windt, E., Daudey, P.J. and Kramer, H.J.M. 2010, "A comparative study of ATR-FTIR and FT-NIR spectroscopy for in-situ concentration monitoring during batch cooling crystallization processes", *Crystal Growth and Design,* vol. 10, pp. 2629.

Kadam, S.S., Vissers, J.A.W., Forgione, M., Geertman, R.M., Daudey, P.J., Stankiewicz, A.I. and Kramer, H.J.M. 2012, "Rapid crystallization process development strategy from lab to industrial scale with PAT tools in skid configuration", *Organic Process Research and Development,* vol. 16, pp. 769-780.

Khamar, D., Zeglinski, J., Mealey, D., Rasmuson, A.C. 2014, "Investigating the role of solvent-solute interaction in crystal nucleation of salicylic acid from organic solvents", *Journal of the American Chemistry Society,* vol. 136, pp. 11664-11673.

Kee, N., Tan, R.B.H. and Braatz, R.D. 2009, "Selective crystallization of the metastable a-form of the L-glutamic acid using concentration feedback control", *Crystal Growth and Design,* vol. 9, no. 7, pp. 3044-3051.

Kee, N.C., Arendt, P.D., Tan, R.B.H. and Braatz, R.D. 2009, "Selective crystallization of the metastable anhydrate form in the enantiotropic pseudo-dimorph system of L-phenilalanine using concentration feedback control", *Crystal Growth and Design,* vol. 9, no. 7, pp. 3052-3061.

Kestur, U.S. and Taylor, L.S. 2013, "Evaluation of the crystal growth rate of felodipine polymorphs in the presence and absence of additives as a function of temperature", *Crystal Growth and Design,* vol. 13, pp. 4349-4354.

Khoshkhoo, S., Anwar, J. 1993, "Crystallization of polymorphs: the effect of solvent", *Journal of Physical Science,* vol. 26, pp. B90-B93.

Kim, J.W., Kim, J.K., Kim, H.S., Koo, K.K. 2011, "Application of internal seeding and temperature cycling for reduction of liquid inclusion in the crystallization of RDX", *Organic Process Research and Development,* vol. 15, pp. 602-609.

Kitamura, M. 2002, "Controlling factor of polymorphism in crystallization process", *Journal of Crystal Growth,* vol. 237–239, Part 3, no. 0, pp. 2205-2214.

Kitamura, M., Hara, T., Takimoto-Kamimura, M. 2006, "Solvent effect on polymorphism in crystallization of BPT propyl ester", *Crystal Growth and Design,* vol. 6, no. 8, pp. 1945-1950.

Kobari, M., Kubota, N. and Hirasawa, I. 2014, "A population balance model for solvent-mediated polymorphic transformation in unseeded solutions", *Crystal engineering communications,* vol. 16, pp. 6049-6058.

Kobayashi, R., Fujimaki, Y., Ukita, T., Hiyama, Y. 2006, " Monitoring of Solvent-Mediated Polymorphic Transitions Using in Situ Analysis Tools", *Organic Process Research and Development,* vol. 10, pp. 1219-1226.

Kubota, N. 2001, "Effect of impurities on the growth kinetics of crystals", *Cryst. Res. Technol.,* vol. 8, no. 10, pp. 749-769.

Kubota, N., Yokota, M. and Mullin, J.W. 2000, "The combined influence of supersaturation and impurity concentration on crystal growth", *Journal of Crystal Growth,* vol. 212, pp. 480-488.

Kubota, N., Yokota, M. and Mullin, J.W. 1997, "Supersaturation dependence of crystal growth in solutions in the presence of impurity", *Journal of Crystal Growth,* vol. 182, pp. 86-94.

Kubota, N. and Mullin, J.W. 1995, "A kinetic model for crystal growth from aqueous solution in the presence of impurity", *Journal of Crystal Growth,* vol. 152, no. 3, pp. 203-208.

Kulkarni, S.A., McGarrity, E.S., Meekes, H. and ter Horst, J.H. 2012, "Isonicotinamide self-association: the link between solvent and polymorph nucleation", *Chemical Communications,* vol. 48, pp. 4983-4985.

Kulkarni, S.A., Weber, C.C., Myerson, A.S. and ter Horst, J.H. 2014, "Self-association during heterogeneous nucleation onto well-defined templates", *Langmuir,* vol. 30, pp. 12368-12375.

Kuznetsov, V.A., Okhrimenko, T.M. and Rak, M. 1998, "Growth promoting effect of organic impurities on growth kinetics of KAP and KDP crystals", *Journal of Crystal Growth,* vol. 193, pp. 164-173.

Lang, Y., Cervantes, A.M. and Biegler, L.T. 1999, "Dynamic optimization of a batch cooling crystallization process", *Industrial and Engineering Chemistry Research,* vol. 38, pp. 1469-1477.

Langkilde, F.W., Sjoblom, J., Tekenbergs-Hjelte, L., Mrak, J. 1997, "Quantitative FT-Raman analysis of two crystal forms of a pharmaceutical compound", *Journal of pharmaceutical and biomedical analysis,* vol. 15, pp. 687-696.

Larsen, P.A., Patience, D.B. and Rawlings, J. 2006, "Manipulationg crystal size, shape, and structure", *IEEE Control Systems Magazine,* .

Leyssens, T., Baudry, C., Hernandez, M.L.E. 2011, "Optimization of a crystallization by online FBRM analysis of needle-shaped crystals", *Organic Process Research and Development,* vol. 15, pp. 413-426.

Li, Y., Chow, P.S., Tan, R.B.H. 2011, "Quantification of polymorphic impurity in an enantiotropic polymorph system using differential scanning calorimetry, X-ray powder diffraction and Raman spectroscopy", *International journal of pharmaceutics,* vol. 415, no. 1–2, pp. 110-118.

Liu, W., Wei, H., Black, S. 2009, "An investigation of the transformation of carbamazepine from anhydrate to hydrate using in situ FBRM and PVM", *Organic Process Research and Development,* vol. 13, pp. 494-500.

Liu, W., Wei, H., Zhao, J., Black, S., Sun, C. 2013, "Investigation into the cooling crystallization and transformations of carbamazepine using in situ FBRM and PVM", *Organic Process Research and Development,* vol. 17, pp. 1406-1412.

Liu, X., Sun, D., Wang, F., Wu, Y., Chen, Y. and Wang, L. 2011, "Monitoring of antisolvent crystallization of sodium scutellarein by combined FBRM-PVM-NIR", *Journal of pharmaceutical sciences,* vol. 100, no. 6.

Livingstone, D. (ed) 2009, *A practical guide to scientific data analysis*, First edn, John Wiley and Sons, Ltd.

Ma, C.Y., Wang, X.Z. 2012a, "Closed-loop control of crystal shape in cooling crystallization of L-glutamic acid", *Journal of Process Control,* vol. 22, pp. 72-81.

Ma, C.Y., Wang, X.Z. 2012b, "Model identification of crystal facet growth kinetics in morphological population balance modeling of L-glutamic acid crystallization and experimental validation", *Chemical Engineering Science,* vol. 70, pp. 22-30.

Maher, A., Croker, D., Rasmuson, A.C. and Hodnett, K. 2012, "Solution mediated polymorphic transformation: Form II to Form III piracetam in ethanol", *Crystal Growth and Design,* vol. 12, pp. 6151-6157.

Majumder, A. and Nagy, Z.K. 2013a, "Fines removal in a continuous plug flow crystallizer by optimal spatial temperature profiles with controlled dissolution", *AIChE Journal,* vol. 59, no. 12, pp. 4582-4594.

Majumder, A. and Nagy, Z.K. 2013b, "Fines removal in a continuous plug flow crystallizer by optimal spatial temperature profiles with controlled dissolution", *Process system engineering,* vol. 59, no. 12, pp. 4582-4594.

Majumder, A. and Nagy, Z.K. 2013c, "Prediction and control of crystal shape distribution in the presence of crystal growth modifiers", *Chemical Engineering Science,* vol. 101, pp. 593-602.

Mangin, D., Puel, F. and Veesler, S. 2009, "Polymorphism in processes of crystallization in solution: a practical review", *Organic Process Research and Development,* vol. 13, pp. 1241-1253.

Martens, J.H., Barg, H., Warren, M.J., Jahn, D. 2002, "Microbial production of vitamin B12", *Applied Microbiology and Biotechnology,* vol. 58, pp. 275-285.

Mattei, A., Mei, X., Miller, A.F., Li, T. 2013, "Two major pre-nucleation species that are conformationally distinct and in equilibrium of self-association", *Crystal Growth and Design,* vol. 13, pp. 3303-3307.

Mattei, A., Li, T. 2012, "Polymorph formation and nucleation mechanism of tolfenamic acid in solution: an investigation of pre-nucleation solute association", *Pharmaceutical Research,* vol. 29, pp. 460-470.

Mayer, E., Gardiner, D.J. and Hester, R.E. 1973, "Resonance Raman spectra of vitamin B12 and dicyanocobalamin", *Biochimica et Biophysica Acta,* vol. 297, pp. 568-570.

McCrone, W.C. (ed) 1965, *Polymorphism and Chemistry of the Organic Solid State,* Interscience, New York.

McPherson, A. and Gavira, J.A. 2014, "Introduction to protein crystallization", *Acta Cryst.,* vol. F70, pp. 2-20.

Minamisono, T. and Takiyama, H. 2013, "Control of polymorphism in the anti-solvent crystallization with a particular temperature profile", *Journal of Crystal Growth,* vol. 362, pp. 135-139.

Mo, Y., Dang, L. and Wei, H. 2011, "L-glutamic acid polymorph control using amino acid additives", *Industrial and Engineering Chemistry Research,* vol. 50, pp. 10385-10392.

Morissette, S.L., Soukasene, S., Levinson, D., Cima, M.J. and Almarsson, O. 2003, "Elucidation of crystal form diversity of the HIV protease inhibitor ritonavir by high-throughput crystallization", *Applied physical sciences,* vol. 100, no. 5, pp. 2180-2184.

Mukuta, T., Lee, A.Y., Kawakami, T. and Myerson, A.S. 2005a, "Influence of impurities on the solution-mediated phase transformation of an active pharmaceutical ingredient", *Crystal Growth and Design,* vol. 5, no. 4, pp. 1429-1436.

Mukuta, T., Lee, A.Y., Kawakami, T. and Myerson, A.S. 2005b, "Influence of impurities on the solution-mediated phase transformation of an active pharmaceutical ingredient", *Crystal Growth and Design,* vol. 5, no. 4, pp. 1429-1436.

Mullin, J.W. 2001, *Crystallization,* Fourth Edition edn, Butterworth Heinemann.

Murugan, N.A., Kongsted, J., Rinkevicius, Z., Agren, H. 2011, "Demystifying the solvatochromic reversal in Brooker's merocyanine dye", *Physical Chemistry Chemical Physics*, vol. 13, pp. 1290-1292.

Næs, T., Isaksson, T., Fearn, T. and Davies, T. (eds) 2004, *A user-friendly guide to multivariate calibration and classification*, NIR publications, Chichester, UK.

Nagy, Z.K., Aamir, E. and Rielly, C.D. 2011, "Internal fines removal using population balance model based control of crystal size distribution under dissolution, growth and nucleation mechanism", *Crystal Growth and Design*, vol. 22, pp. 2205-2219.

Nagy, Z.K., Braatz, R.D., 2012, "Advances and new directions in crystallization control", *Annual Review of Chemical and Biomolecular Engineering*, vol. 3, pp. 55-75.

Nagy, Z.K., Fevotte, G., Kramer, H., Simon, L.L. 2013 "Recent advances in the monitoring, modelling and control of crystallization systems", *Chemical Engineering Research and Design, ,* vol. 91, no. 10, pp. 1903–1922.

Német, Z., Kis, G.C., Pokol, G., Demeter, Á. 2009, "Quantitative determination of famotidine polymorphs: X-ray powder diffractometric and Raman spectrometric study", *Journal of Pharmaceutical and Biomedical analysis*, vol. 49, no. 2, pp. 338-346.

Nowee, S.M., Abbas, A. and Romagnoli, J.A. 2007, "Optimization in seeded cooling crystallization: a parameter estimation and dynamic optimization study", *Chemical Engineering and Processing*, vol. 46, pp. 1096-1106.

O'Brien, L.E., Timmins, P., Williams, A.C., York, P. 2004, "Use of in situ FT-Raman spectroscopy to study the kinetics of the transformation of carbamazepine polymorphs", *Journal of Pharmaceutical and Biomedical analysis*, vol. 36, no. 2, pp. 335-340.

Ono, T., ter Horst, J.H., Jansens, P.J. 2004, "Quantitative measurement of the polymorphic transformation of L-glutamic acid using in-situ Raman spectroscopy", *Crystal Growth and Design*, vol. 4, no. 3, pp. 465-469.

O'Sullivan, B., Barrett, M., Hsiao, G., Carr, A., Glennon, B. 2003, "In situ monitoring of polymorphic transitions", *Organic Process Research and Development*, vol. 7, pp. 977-982.

Parveen, S., Davey, R.J., Dent, G. and Pritchard, R.G. 2005, "Linking solution chemistry to crystal nucleation: the case of tetrolic acid", *Chemical Communications*, , pp. 1531-1533.

Pataki, H., Csontos, I., Nagy, Z.K., Vajna, B., Molnar, M., Katona, L., Marosi, G. 2012a, "Implementation of Raman signal feedback to perform controlled crystallization of carvedilol", *Organic Process Research and Development, ,* no. Polymorphism and crystallization.

Pataki, H., Markovits, I., Vanja, B., Nagy, Z.K., Marosi, G. 2012b, "In-line monitoring of carvedilol crystallization using Raman spectroscopy", *Crystal Growth and Design*, vol. 12, pp. 5621-5628.

Patel, A.D., Luner, P.E. and Kemper, M.S. 2000, "Quantitative analysis of polymorphs in binary and multi-component powder mixtures by near-infrared reflectance spectroscopy", *International journal of pharmaceutics*, vol. 206, pp. 63-74.

Poornachary, S.K., Chow, P.S. and Tan, R.B.H. 2008a, "Impurity effects on the growth of molecular crystals: Experiments and Modeling", *Advanced powder technology*, vol. 19, pp. 459-473.

Poornachary, S.K., Chow, P.S. and Tan, R.B.H. 2008b, "Effect of solution speciation of impurities on α-glycine crystal habit: A molecular modelling study", *Journal of Crystal Growth*, vol. 310, pp. 3034-3041.

Poornachary, S.K., Chow, P.S. and Tan, R.B.H. 2008c, "Influence of solution speciation of impurities on polymorphic nucleation in glycine", *Crystal Growth and Design*, vol. 8, no. 1, pp. 179-185.

Powell, A.D., Saleemi, A.N., Rielly, C.D., Nagy, Z.K. 2015, "Periodic steady-state flow crystallization of a pharmaceutical drug using MSMPR operation", *Chemical Engineering and Processing: Process Intensification*, doi:10.1016/j.cep.2015.01.002

Pratiwi, D., Fawcett, J.P., Gordon, K.C., Rades, T. 2002, "Quantitative analysis of polymorphic mixtures of ranitidine hydrochloride by Raman spectroscopy and principal components analysis", *European Journal of Pharmaceutical Sciences*, vol. 54, pp. 337-341.

Price, C.P., Grzesiak, A.L. and Matzger, A.J. 2005, "Crystalline polymorph selection and discovery with polymer heteronuclei", *Journal of American Chemical Society*, vol. 127, pp. 5512-5517.

Qamar, S., Mukhtar, S. and Seidel-Morgenstern, A. 2010, "Efficient solution of a batch crystallization model with fines dissolution", *Journal of Crystal Growth*, vol. 312, pp. 2936-2945.

Qamar, S., Noor, S. and Seidel-Morgenstern, A. 2010, " An Efficient Numerical Method for Solving a Model Describing Crystallization of Polymorphs", *Industrial and Engineering Chemistry Research*, vol. 49, pp. 4940-4947.

Qu, H., Kohonen, J., Louhi-Kultanen, M., Reinikainen, S.P. and Kallas, J. 2008, "Spectroscopic monitoring of carbamazepine crystallization and phase transformation in ethanol-water solution", *Industrial and Engineering Chemistry Research*, vol. 47, pp. 6991-6998.

Qu, H., Alatalo, H., Hatakka, H., Kohonen, J., Louhi-Kultanen, M., Reinikainen, S. and Kallas, J. 2009, "Raman and ATR FTIR spectroscopy in reactive crystallization: Simultaneous monitoring of solute concentration and polymorphic state of the crystals", *Journal of Crystal Growth*, vol. 311, no. 13, pp. 3466-3475.

Rader, R.A. 2007, "What is a generic biopharmaceutical? Biogeneric? Follow-on protein? Biosimilar? Follow-on biologic?", *BioProcess International,* , pp. 28-38.

Ramakrishna, D. (ed) 2000, *Population balances: Theory and applications to particulate systems in engineering*, Academic press Inc.

Rajeshwar, K. and Secco, E.A. 1976, "Phase transformation studies on anthranilic acid by thermal analysis, infrared absorption, and X-ray diffraction methods", *Canadian Journal of Chemistry*, vol. 54, no. 15, pp. 2509-2513.

Randolph, A.L. 1988, *Theory of particulate process*, Academic Press, San Diego, 2nd edition.

Read, E.K., Shah, R.B., Riley, B.S., Park, J.T., Brorson, K.A. and Rathore, A.S. 2010, "Process Analytical Technology (PAT) for biopharmaceutical products: Part II. Concepts and applications", *Biotechnology and bioengineering*, vol. 105, no. 2, pp. 285-295.

Reis, N.M., Liu, Z.K., Reis, C.M. and Mackley, M.R. 2014, "Hydroxypropyl methylcellulose as a novel tool for isothermal solution crystallization of micronized paracetamol", *Crystal Growth and Design,* vol. 14, pp. 3191-3198.

Rodriguez-Hornedo, N., Nehm, S.J., Seefeldt, K.F., Pagan-Torres, Y., Falkiewicz, C.J. 2006, "Reaction crystallization of pharmaceutical molecular complexes", *Molecular pharmaceutics*, vol. 3, no. 3, pp. 362-367.

Salameh, A.K., Taylor, L.S. 2006, "Physical Stability of Crystal Hydrates and their Anhydrates in the Presence of Excipients", *Journal of Pharmaceutical Sciences*, vol. 95, no. 2, pp 446-461.

Saleemi, A.N. 2011, *Strategic feedback control of pharmaceutical crystallization systems*, Doctoral thesis, Loughborough University.

Saleemi, A.N., Onyemelukwe, I.I. and Nagy, Z.K. 2013, "Effect of a structurally related substance on the crystallization of paracetamol", *Font. Chem. Sci. Eng.*, vol. 7, no. 1, pp. 79-87.

Saleemi, A.N., Nagy, Z.K. 2012, "Application of combined image analysis and process analytical technology for real time monitoring of polymorphic transformation of anthranilic acid", *UKPharmSci Conference 2012*.

Saleemi, A.N., Rielly, C.D. and Nagy, Z.K. 2012a, "Automated direct nucleation control for in situ dynamic fines removal in batch cooling crystallization", *Crystal engineering communications*, vol. 14, pp. 2196-2203.

Saleemi, A.N., Rielly, C.D. and Nagy, Z.K. 2012b, "Comparative investigation of supersaturation and automated direct nucleation control of crystal size distribution using ATR-UV/Vis spectroscopy and FBRM", *Crystal Growth and Design*, vol. 12, pp. 1792-1807.

Saleemi, A.N., Steele, G., Pedge, N.I., Freeman, A. and Nagy, Z.K. 2012, "Enhancing crystalline properties of a cardiovascular active pharmaceutical ingredient using a process analytical technology based crystallization feedback control strategy", *International journal of pharmaceutics*, vol. 430, no. 1–2, pp. 56-64.

Salvalaglio, M., Vetter, T., Giberti, F., Mazzotti, M. and Parrinello, M. 2012, "Uncovering molecular details of urea crystal growth in the presence of additives", *Journal of the American Chemical Society*, vol. 134, pp. 17221-17233.

Samad, N.A.F.A., Sin, G., Gernaey, K.V. and Gani, R. 2013, "A systematic framework for design of process monitoring and control (PAT) systems for crystallization processes", *Computers and Chemical Engineering*, vol. 54, pp. 8-23.

Samsonowicz, M., Hrynaszkiewicz, Z., Swislocka, R., Regulska, E., Lewandowski, W. 2005, "Experimental and theoretical IR, Raman, NMR spectra of 2-, 3- and 4-aminobenzoic acid", *Journal of Molecular Structure*, vol. 744-747 , pp. 345-352.

Sangwal, K. 1996, "Effects of impurities on crystal growth processes", *Progress in Crystal Growth and Characterization of Materials*, vol. 32, pp. 3-43.

Sanzida, N. 2013, *Iterative learning control of crystallization systems*, Doctoral thesis, Loughborough University.

Sanzida, N. and Nagy, Z.K. 2013, "Iterative learning control for the systematic design of supersaturation controlled batch cooling crystallisation processes", *Computers and Chemical Engineering*, vol. 59, no. 0, pp. 111-121.

Sathe, D., Sawant, K., Mondkar, H., Naik, T., Deshpande, M. 2010, "Monitoring temperature effect on the polymorphic transformation of acitretin using FBRM-Lasentec", *Organic Process Research and Development*, vol. 14, pp. 1373-1378.

Sato, K. 1993, "Polymorphic transformations in crystal growth", *Journal of Physics and Applied Physics*, vol. 26, pp. B77-B84.

Scholl, J., Bonalumi, D., Vicum, L. and Mazzotti, M. 2006, "In situ monitoring and modeling of the solvent-mediated polymorphic transformation of L-glutamic acid", *Crystal Growth and Design*, vol. 6, no. 4, pp. 881-891.

Seaton, C.C. and Parkin, A. 2011, "Making benzamide cocrystal with benzoic acid: the influence of chemical structure", *Crystal Growth and Design*, vol. 11, pp. 1502-1511.

Sebek, J., Kapitan, J., Sebestik, J., Baumruk, V., Bour, P. 2009, "L-Alanyl-L-alanine conformational changes induced by pH as monitored by the Raman optical activity spectra", *Journal of Physical Chemistry*, , no. 113, pp. 7760-7768.

Sheikholeslamzadeh, E. and Rohani, S. 2013, "Modeling and optimal control of solution mediated polymorphic transformation of L-glutamic acid", *Industrial and Engineering Chemistry Research*, vol. 52, no. 2633, pp. 2641.

Sim, G.A., Robertson, J.M. and Goodwin, T.H. 1955, "The crystal and molecular structure of benzoic acid", *Acta Crystallographica*, vol. 8, pp. 157-164.

Simon, L.L., Nagy, Z.K. and Hungerbuhler, K. 2009, "Endoscopy-based in situ bulk video imaging of batch crystallization processes", *Organic Process Research and Development*, vol. 13, pp. 1254-1261.

Simon, L.L., Reinlein, S. and Hungerbuhler, K. 2011, "Turbidity and endoscopy assisted monitoring of pseudopolymorphic transformation of citric acid", *18th International Symposium on Industrial Crystallization, ISIC 2011*.

Smith, D. 2014, *Process monitoring and control using live cell imaging for the manufacturing of cell therapies*, Doctoral thesis, Loughborough University.

Stalin, T., Rajendiran, N. 2006, "Intramolecular charge transfer associated with hydrogen bonding effect on 2-aminobenzoic acid", *Journal of Photochemistry and Photobiology*, vol. 182, pp. 137-150.

Starbuck, C., Spartalis,A., Wai,L., Wang, J., Fernandez, P., Lindemann, C.M., Zhou, G.X., Ge, Z. 2002, "Process optimization of a complex pharmaceutical polymorphic system via in situ raman spettroscopy", *Crystal Growth and Design*, vol. 2, no. 6, pp. 512-522.

Strachan, C.J., Pratiwi, D., Gordon, K.C., Rades, T. 2004, "Quantitative analysis of polymorphic mixtures of carbamazepine by Raman spectroscopy and principal component analysis", *Journal of Raman Spectroscopy*, vol. 35, pp. 347-352.

Strachan, C.J., Rades, T., Gordon, K.C., Rantanen, J. 2007, "Raman spectroscopy for quantitative analysis of pharmaceutical solids", *Journal of Pharmacy and Pharmacology*, vol. 59, pp. 179-192.

Su, W., Hao, H., Barrett, M., Glennon, B. 2010, "The impact of operating parameters on the polymorphic transformation of D-mannitol characterized in situ with raman spectroscopy, FBRM, and PVM", *Organic Process Research and Development*, vol. 14, pp. 1432-1437.

Sullivan, R.A., Davey, R.J., Sadiq, G., Dent, G., Back, K.R., ter Horst, J.H., Toroz, D. and Hammond, R.B. 2014, "Revealing the roles of desolvation and molecular self-assembly in crystal nucleation from solution: benzoic and p-aminobenzoic acid", *Crystal Growth and Design*, vol. 14, pp. 2689-2696.

Sultana, M. and Jensen, K.F. 2012, "Microfluidic continuous seeded crystallization: extraction of growth kinetics and impact of impurity on morphology", *Crystal Growth and Design*, vol. 12, pp. 6260-6266.

Sun, W., Jayaraman, S., Chen, W., Persson, K.A. and Ceder, G. 2015, "Nucleation of metastable aragonite $CaCO_3$ in seawater", *Proceedings of the National Academy of Science USA*,vol. 112, pp. 3199–3204

Susindran, V., Anthimoolam, S., Asath Bahadur, S. 2012, "Spectroscopic and thermal studies of anthranilic acid (vitamin l)-with Br and Cl", *Journal of Pharmaceutical Research,* vol. 4, no. 10, pp. 4628-4636.

Takacs-Novak, K., Avdeef, A., Box, K.J., Podanyi, B., Szasz, G. 1994, "Determination of protonation macro- and microconstant and octanol/water partition coefficient of the antiinflammatory drug niflumic acid", *Journal of Pharmaceutical, Biomedical Analysis,* vol. 12, no. 11, pp. 1369-1377.

Takacs-Novak, K., Tam, K.Y. 2000, "Multiwavelength spectrophotometric determination of acid dissociation constants Part V: microconstants and tautomeric ratios of diprotic amphoteric drugs", *Journal of Pharmaceutical, Biomedical Analysis,* vol. 21, pp. 1171-1182.

Tanoury, G.J., Hett, R., Kessler, D.W., Wald, S.A. and Senanayake, C.H. 2002, "Taking advantage of polymorphism to effect an impurity removal: development of a thermodynamic crystal form of (R,R)-formoterol tartrate", *Organic Process Research and Development,* vol. 6, pp. 855-862.

The Pharmaceutical Research and Munufacturers of America (PhRMA) and Bettelle 2014, *The U.S. biopharmaceutical industry: perspectives on future growth and the factors that will drive it*.

Threlfall, T. 2000, "Crystallization of polymorphs: thermodynamic insight into the role of solvent", *Organic Process Research and Development,* vol. 4, pp. 384-390.

Tian, F., Baldursdottir, S. and Rantanen, J. 2009, "Effect of polymer additives on the crystallization of hydrates: a molecular-level modulation", *Molecular pharmaceutics,* vol. 6, no. 1, pp. 202-210.

Tian, F., Zeitler, J.A., Strachan, C.J., Saville, D.J., Gordon, K.C. and Rades, T. 2006, "Characterizing the conversion kinetics of carbamazepine polymorphs to the dihydrate in acqueous suspension using Raman spectroscopy", *Journal of pharmaceutical and biomedical analysis,* vol. 40, pp. 271-280.

Trasi, N.S. and Taylor, L.S. 2012, "Effect of additives on the crystal growth and nucleation of amorphous flutamide", *Crystal Growth and Design,* vol. 12, pp. 3221-3230.

Trifkovic, M., Rohani, S. 2007, "Polymorphic generation through solvent selection: ranitidine hydrochloride", *Organic Process Research and Development,* vol. 11, pp. 138-143.

Tudor, A., Church, S., Hendra, P., Davies, M., Melia, C. 1993, "The qualitative and quantitative analysis of chlorpropamide polymorphic mixtures near-infrared Fourier transform Raman spectroscopy", *Pharmaceutical Research,* vol. 10, pp. 1772-1776.

U.S. Department of Health and Human Services 2004, *Guidance for Industry PAT — A Framework for Innovative Pharmaceutical Development, Manufacturing, and Quality Assurance* .

Ündey, C., Ertunç, S., Mistretta, T. and Looze, B. 2010, "Applied advanced process analytics in biopharmaceutical manufacturing: challenges and prospects in real-time monitoring and control", *Journal of Process Control,* vol. 20, pp. 1009-1018.

Van Eerdenbrugh, B. and Taylor, L.S. 2011, "Application of mid-IR spectroscopy for the characterization of pharmaceutical systems", *International journal of pharmaceutics,* vol. 417, no. 1–2, pp. 3-16.

Van Enckevort, W.J.P., van der Berg, A.C.J.F., Kreuwel, K.B.G. and Derksen, A.J. 1996, "Impurity blocking of growth steps: experiments and theory", *Journal of Crystal Growth,* vol. 166, pp. 156-161.

Vankeirsbilck, T., Vercauteren, A., Baeyens, W., Van der Weken, G., Verpoort, F., Vergote, G., Remon, J.P. 2002, "Applications of Raman spectroscopy in pharmaceutical analysis", *TrAC Trends in Analytical Chemistry,* vol. 21, no. 12, pp. 869-877.

Vekilov, P.G. 2010, "Nucleation", *Crystal Growth and Design,* vol. 10, no. Perspective, pp. 5007-5019.

Verpoort, F., Vergote, G., Remon, J. 2002, "Applications of Raman spettroscopy in pharmaceutical analysis", *Trends in analytical chemistry, ,* pp. 869-877.

Wang, I.C., Lee, M.J., Seo, D.Y., Lee, H.E., Choi, Y.K.,W.S., Kim, C.S., Jeong, M.Y. and Choi, G.J. 2011, "Polymorph transformation in paracetamol monitored by in-line NIR spectroscopy during a cooling crystallization process", *American association of pharmaceutical scientists,* vol. 12, no. 2.

Wang, X., Watcher, J.A., Antosz, F.J., Berglund, K.A. 2000, "An investigation of sovent-mediated polymorphic transformation of progesterone using in situ Raman spettroscopy", *Organic Process Research and Development,* vol. 4, pp. 391-395.

Wang, X.Z., De Anda, J.C., Roberts, K.J., Li, R.F., Thomson, G.B., White, G. 2005, "Advances in on-line monitoring and control of the morphological and polymorphic forms of organic crystals grown from solution", *KONA Powder and Particle Journal,* no. 23, pp. 69-85.

Wantha, L. and Flood, A., 2013, "Population balance modeling of the solution-mediated transformation of DL-Methionine polymorphs", *Chemical Engineering and Technology,* vol. 36, no. 8, pp. 1313-1319.

Wartewig, S., Neubert, R.H.H. 2005, "Pharmaceutical applications of Mid-IR and Raman spectroscopy", *Advanced Drug Delivery Reviews,* vol. 57, pp. 1144-1170.

Weissbuch, I., Popovitz-Biro, R., Lahav, M. and Leiserowitz, L. 1995, "Understanding and control of nucleation, growth, habit, dissolution and structure of two- and three-dimensional crystals using "tailor-made" auxiliaries", *Acta Crystallographica Section B,* vol. B51, pp. 115-148.

Weissbuch, I., Torbeev, V.Y., Leiserowitz, L., Lahav, M. 2005, "Solvent effect on crystal polymorphism: why addition of methanol or ethanol to acqueous solutions induces the precipitation of the least stable β form of glycine", *Angewandte Chemie International Edition,* vol. 44, pp. 3226-3229.

Wikstrom, H., Marsac, P.J., Taylor, L.S. 2005, "In-line monitoring of hydrate formation during wet granulation using raman spectroscopy", *Journal of Pharmaceutical Sciences,* vol. 94, no. 1 pp 209-219.

Wong, S.W., Georgakis, C., Botsaris, G.D., Saranteas, K., Bakale, R. 2008, "Online estimation and monitoring of diastomeric resolution using FBRM, ATR-FTIR, and Raman spectroscopy", *Industrial and Engineering Chemistry Research,* vol. 47, pp. 5576-5584.

Wong, S., Georgakis, C., Botsaris, G., Saranteas, K., Bakale, R. 2007, "Factors affecting on-line estimation of diastereomer composition using Raman spectroscopy", *Control Engineering Practice,* vol. 15, no. 10, pp. 1257-1267.

Wong, S.W., Georgakis, C., Botsaris, G.D., Saranteas, K., Bakale, R. 2008, "Online estimation of diastereomer composition using Raman: differentiation in High and low slurry density partial least square models", *Crystal Growth and Design,* vol. 8, no. 12, pp. 4398-4408.

Wood, W.M.L. 2001, "A bad (crystal) habit - and how it was overcome", *Powder Technology,* vol. 121, pp. 53-59.

Worlitschek, J. and Mazzotti, M. 2004, "Model-based optimization of particle size distribution in batch-cooling crystallization of paracetamol", *Crystal Growth and Design,* vol. 8, no. 5, pp. 891-903.

Wulfert, F., Kok, W.T., de Noord, O.E., Smilde, A.K. 2000, "Linear techniques for temperature-induced spectral variation in multivariate calibration", *Chemometrics and Intelligent Laboratory Systems,* , no. 51, pp. 189-200.

Wulfert, F., Kok, W.T., Smith, M.R. 1998, "Influence if temperature on vibrational spectra and consequences for the predictive ability of multivariate models", *Analytical Chemistry,* , no. 70, pp. 1761-1767.

Yang, L., Hao, H., Zhou, L., Chen, W., Hou, B., Xie, C. and Yin, Q. 2013, "Crystal structures and solvent-mediated transformation of the enantiotropic polymorphs of 2,3,5-trimethyl-1,4-diacetoxybenzene", *Industrial and Engineering Chemistry Research,* vol. 52, pp. 17667-17675.

Yang, Y. and Nagy, Z.K. 2014, "Model-based systematic design and analysis approach for unseeded combined cooling and antisolvent crystallization (CCAC) systems", *Crystal Growth and Design,* vol. 14, no. 2, pp. 687-698.

Yani, Y., Chow, P.S. and Tan, R.B.H. 2012, "Glycine open dimers in solution: new insights into α-glycine nucleation and growth ", *Crystal Growth and Design,* vol. 12, pp. 4771-4778.

Yeom, S., Yun, H. and Yang, D.R. 2013, "Optimization of temperature swing strategy for selective cooling crystallization of α-form L-glutamic acid crystals", *Korean Journal of Chemical Engineering*, vol. 30, no. 10, pp. 1836-1842.

Zapala, L., Kalembkiewcz, J., Sitarz-Palczak, E. 2009, "Studies on equilibrium of anthranilic acid in acqueous solutions and in two-phase systems: aromatic solvent-water", *Biophysical Chemistry*, vol. 140, pp. 91-98.

Zhang, P., Han, S., Zang, Y., Ford, R.C., Li, J. 2008, "Neutron spectroscopic and Raman studies of interaction between water and proline", *Chemical Physics*, vol. 345, pp. 196-199.

Zhang, Z., Wang, B., Yin, Y. and Mo, Y. 2009, "Surface-enhanced Raman spectroscopy of vitamin B12 on silver particles in colloid and in atmosphere", *Journal of Molecular Structure*, vol. 927, pp. 88-90.

Zhao, J., Wang, M., Dong, B., Feng, Q., Xu, C. 2013, "Monitoring the polymorphic transformation of imidacloprid using in situ FBRM and PVM", *Organic Process Research and Development*, vol. 17, pp. 375-381.

Zhao, Y., Yuan, J., Ji, Z., Wang, J., Rohani, S. 2012, "Combined application of in situ FBRM, ATR-FTIR, and Raman on polymorphism transformation monitoring during the cooling crystallization", *Industrial and Engineering Chemistry Research*, vol. 51, pp. 12530-12536.

Appendix

Poster and oral presentations:

- E. Simone; *How to make jeans of the right blue*; Loughborough University Conference, Loughborough, UK, March 2013 (**poster**).
- E. Simone, *Monitoring and control of polymorphic transformation in pharmaceutical crystallizations using a composite PAT array and crystallization process informatics system*; ChemEngDay, London, UK, March 2013 (**poster**).
- E. Simone, A.N. Saleemi, Z.K. Nagy, *Application of quantitative Raman spectroscopy for the monitoring and feedback control of polymorphic transformation in crystallization*; 9th European conference of Chemical engineering, the Hague, Netherlands, April 2013 (**oral presentation**).
- E. Simone, Z.K. Nagy, *Comparison and integration of signals from Raman, UV, NIR and mid-IR spectroscopy in monitoring polymorphic transformations*; What's new in fluid separation, London, June 2013 (**oral presentation**).
- E. Simone, A.N. Saleemi, Z.K. Nagy; *Application of PAT for monitoring cocrystallization and polymorphism*; AstraZeneca and Thermo Scientific seminar, Macclesfield, UK, June 2013 (**oral presentation**).
- E. Simone, A.N. Saleemi, Z.K. Nagy; *In situ monitoring of polymorphic transformations using a composite sensor array of Raman, UV, NIR, mid-IR spectroscopy, FBRM and PVM;* British association of crystal growth conference (BACG), June 2013 (**oral presentation**).
- E. Simone, A.N. Saleemi, Z.K. Nagy; *Monitoring and control of polymorphic transformation of anthranilic acid using in situ Raman, UV, NIR, PVM and FBRM*; 15th summer school of crystal growth, Gdansk, Poland, August 2013 (**poster**).
- E. Simone, A.N. Saleemi, Z.K. Nagy; *Quantitative application of Raman, UV, NIR and mid-IR Spectroscopy with PVM and FBRM in monitoring polymorphic transformations: comparison and integration of signals*; 20th International workshop of industrial crystallization, Odense, Denmark, September 2013 (**poster**).
- E. Simone, A.N. Saleemi, Z.K. Nagy. *Combined use of Raman and ATR-UV/Vis to obtain the desired polymorphic form of anthranilic acid*; EuroPACT conference, Barcelona, May 2014 (**poster**).

- E. Simone, A.N. Saleemi, Z.K. Nagy. *Solvent effect on the polymorphic outcome of a zwitterionic compound using ATR-UV/Vis and Raman*; International school of Crystallization, Granada, Spain, May 2014 (**poster**).
- W. Zhang, E. Simone, Z.K. Nagy. *Application of PAT-based feedback control strategies to improve purity and size distribution of a biopharmaceutical compound;* British Association of crystal growth conference, Leeds, UK, July 2014 (**poster**).
- E. Simone, A. Majumder, A. Borsos, Z.K. Nagy. *Model-based active polymorphic feedback control of crystallization processes. International workshop of industrial crystallization*; BIWIC 2014, Rouen, France, September 2014 (**oral presentation**).
- E. Simone, A.N. Saleemi, Z.K. Nagy. *ATR-UV/Vis signal of zwitterionic solutions: link with the polymorphic outcome in cooling crystallization*; International symposium of industrial crystallization ISIC19, Toulouse, France, September 2014 (**oral presentation**).
- E. Simone, Z.K. Nagy, *A study of the solvent effect on the polymorphic outcome of cooling crystallizations for a zwitterionic compound using UV/Vis and Raman spectroscopy*; A Transition State to the Directed Assembly of Materials Faraday Discussion, Leeds, UK, March 2015 (**poster**).
- E. Simone, Z.K. Nagy, *Effect of impurities on the crystallization of an organic compound*; ChemEngDay 2015, Sheffield, UK, April 2015 (**poster**).
- E. Simone, Z.K. Nagy, *Effect of several types of additives on the crystallization of ortho-aminobenzoic acid*; Erice Summer School of Crystallography, Erice, Italy, June 2015 (**poster presentation**).
- E. Simone, G. Steele, Z.K. Nagy, *Tailoring polymorphism of anthranilic acid using combinations of solvents and additives*; British Association of crystal growth conference, London, UK, June 2015 (**oral presentation**).
- E. Simone, G. Steele, Z.K. Nagy, *Controlling Morphology and Polymorphism of a Zwitterionic Compound (OABA) Using Different Types of Additives and Solvents*, AIChE annual meeting, Salt Lake City, US, November 2015 (**oral presentation**).
- E. Simone, Z.K. Nagy, *Application of Raman and ATR-UV/Vis Spectroscopy for a Model-Free and Model-Based Active Polymorphic Feedback Control of Crystallization Processes*, AIChE annual meeting, Salt Lake City, US, November 2015 (**oral presentation**).

- E. Simone, W. Zhang, Z.K. Nagy, *Improving Purity and Size Distribution in Biopharmaceutical Crystallization Using PAT-Based Feedback Control Strategies*, AIChE annual meeting, Salt Lake City, US, November 2015 (**poster**).

Conference proceedings:

- E. Simone, A.N. Saleemi, Z.K. Nagy; *Quantitative application of Raman, UV, NIR and mid-IR Spectroscopy with PVM and FBRM in monitoring polymorphic transformations: comparison and integration of signals*; 20th International workshop of industrial crystallization, Proc. of BIWIC 20, Odense, **2013**.
- E. Simone, A.N. Saleemi, Z.K. Nagy, *Model-based active polymorphic feedback control of crystallization processes*, 21st International workshop of industrial crystallization, Proc. of BIWIC 21, Rouen, **2014**.

Journal publications:

1 E. Simone, A.N. Saleemi, Z.K. Nagy, *Application of quantitative Raman spectroscopy for the monitoring of polymorphic transformation in crystallization processes using a good calibration practice procedure*, Chemical Engineering Research and Design (**2014**), 92 (4), 594–611. **Chapter 4**.

2 E. Simone, A.N. Saleemi, Z.K. Nagy, *Active Polymorphic Feedback Control of Crystallization Processes Using a Combined Raman and ATR-UV/Vis Spectroscopy Approach*. Crystal Growth and Design (**2014**), 14 (4), 1839–1850. **Chapter 6**.

3 E. Simone, A.N. Saleemi, Z.K. Nagy., *Raman, UV, NIR, and Mid-IR Spectroscopy with Focused Beam Reflectance Measurement in Monitoring Polymorphic Transformations*, Chemical Engineering and Technology (**2014**), 37(8), 1305-1313. **Chapter 5**.

4 E. Simone, A.N. Saleemi, Z.K. Nagy, *In Situ Monitoring of Polymorphic Transformations Using a Composite Sensor Array of Raman, NIR, and ATR-UV/vis Spectroscopy, FBRM, and PVM for an Intelligent Decision Support System*, Organic Process research and development (**2015**), 19 (1), 167–177. **Chapter 8**.

5 E. Simone, W. Zhang, Z.K. Nagy, *Application of Process Analytical Technology-Based Feedback Control Strategies To Improve Purity and Size Distribution in*

Biopharmaceutical Crystallization, Crystal Growth and Design (**2015**), 15 (6), 2908–2919. **Chapter 11**.

6 E. Simone, W. Zhang, Z.K. Nagy, *Analysis of the crystallization process of a biopharmaceutical compound in the presence of impurities using process analytical technology (PAT) tools,* Journal of Chemical Technology and Biotechnology, accepted manuscript online, DOI: 10.1002/jctb.4743. **Chapter 12**.

7 E. Simone, Z.K. Nagy. *A link between the ATR-UV/Vis and Raman spectra of zwitterionic solutions and the polymorphic outcome in cooling crystallization,* Crystal Engineering Communication (**2015**), 17, 6538-6547. **Chapter 9**.

8 E. Simone, A. Borsos, A. Majumder, Z.K. Nagy, *Systematic model identification for the active polymorphic feedback control of crystallization processes*, Submitted to Chemical Engineering and Science.

9 E. Simone, G. Steele, Z.K. Nagy, *Tailoring shape and polymorphism of anthranilic acid (OABA) using combinations of solvents and a structurally related additive,* Crystal Engineering Communication (**2015**), 17, 9370-9379. **Chapter 10**.

10 M.V. Cenzato, E. Simone, Z.K. Nagy, *A study on the effect of a polymeric additive on the crystallization of ortho-aminobenzoic acid: change in morphology and effect on polymorphism,* Submitted to the Journal of Crystal Growth.

11 A. O. Abioye; G. Tangyie Chi; E. Simone, Z.K. Nagy, *Real-time monitoring of the influence of in situ granulation on aqueous crystallization of ibuprofen in ibuprofen-cationic dextran crystanules using crystallization process informatics system (CryPRINS),* manuscript in preparation.

12 A. Klapwjck, E. Simone, Z.K. Nagy, C. Wilson, *Morphology control of succinic acid crystals using a surfactant additive,* manuscript in preparation.

Awards and prizes:

- **Best poster** within the Materials and Particle Technology category at the ChemEngDay 2013 (London, UK).
- **Best poster** award at the BIWIC 2013 held in Odense, Denmark.
- **Best poster** prize at the EuroPACT 2014 conference held in Barcelona, Spain.
- **Best poster** award at the International school of crystallization 2014 held in Granada, Spain.

- **Acceptance** for participation to the Summer school of Crystallography 2015, held in Erice (Italy).
- Engineering YES 2015 **best teamwork prize**, May 2015, Birmingham, UK.